



The  
University  
Of  
Sheffield.

## **A role for Secreted Crumbs2 in dorsal obliteration**

Christine Mary Tait

A thesis submitted in partial fulfilment of the requirements for the degree of  
Doctor of Philosophy

The University of Sheffield  
Faculty of Science  
Department of Biomedical Science

3<sup>rd</sup> April 2017

# Acknowledgements

I would like to thank Marysia for her support and encouragement, and for believing in both me and my data, when I was unsure of either.

I would like to thank my advisor Pen, whose research into Crumbs2 made my project possible, and I would like to thank my advisors David and Freek for helping me to ask wider questions. I thank my collaborators; Prof. Kate Storey for kindly welcoming me into her lab, and Dr. Raman Das for teaching me how to image timelapses in a relentlessly cheerful manner.

I would like to thank the Placzek lab, but especially Pam, Kavitha and Sarah – their unfailing support, encouragement and guidance – and their unending supplies of snacks – that got me through the last four years. The whole of ‘D-Floor’ has been a pleasure to work with, but I cannot fail to acknowledge Basudha, whose depth of knowledge about both lab and life protocols never fails to both impress and help me. Helen provided helpful conversations, tea-based moral support, and endless bike-related enthusiasm. Travis, Joe, Sara and Daniele have made the late lab days easier. Thank you to Andy, Anne-Gaelle and Matt for helpful discussions. JP’s unending positivity towards the Crumbs PCR, and his technical skills, has made a massive contribution to this project.

Thanks to all the people in my life outside of science who have supported and encouraged me, fed me beer, and who have listened politely when I talked about optimising protocols.

Thanks to James, who has been by my side through all the highs and lows of my PhD - I could not have got through the last four years without you.

For my parents, who are the hardest working people I have ever had the honour to know.

<b>Abbreviation List</b>		<b>viii</b>
<b>Abstract</b>		<b>1</b>
<b>Chapter 1: The development of the central canal of the spinal cord through dorsal obliteration</b>		<b>2</b>
1.1	Neurulation	3
1.2	Early Neurulation	3
1.3	Neural patterning and neurogenesis	5
1.4	Development of the roof plate	8
1.5	Elongation of the roof plate and formation of the dorsal glial septum	11
1.6	Central Canal formation	12
1.7	Molecular drivers of early neurulation and neurogenesis	17
1.8	Apical-Basal polarity proteins	20
1.9	The Crumbs (CRB) complex	25
1.10	The PAR complex	30
1.11	The Basal SCRIB complex	32
1.12	Alternative splicing in polarity proteins	33
1.13	Cadherins and Adherens Junctions	33
1.14	Aims	35
<b>Chapter 2: Materials and methods</b>		<b>37</b>
2.1	Collection of animal tissue	38
2.2	Gross mouse and chicken dissections	38
2.3	Histological analysis	41
2.4	Chicken embryo <i>in vivo</i> manipulations	45
2.5	<i>Ex vivo</i> experiments	48
2.6	Media	50
2.7	Imaging and Image processing	51
2.8	Molecular biology	51
<b>Chapter 3: Morphology and marker expression of the ventricular zone during dorsal obliteration of the neural tube/developing spinal cord in the mouse</b>		<b>54</b>
3.1	Introduction	55
3.2	Mouse dorsal obliteration occurs in a window between E14 and E16	55
3.3	Marker analysis of lumen-surrounding cells during dorsal obliteration	58
3.3.1	Filament proteins	58
	F-Actin	58
	Nestin	59
3.3.2	Transcription Factors	62
	SOXB1 Transcription factor family	62
	SOX1	63
	SOX2	63
	SOX3	65
	Close association between SOX-positive nuclei and dorsal Nestin+ cells	65
	Dorso-ventral patterned transcription factors	67
	PAX6	67
	NKX6.1	69
3.3.3	Junction proteins	69

ZO-1	70
3.3.4 Polarity Proteins	73
aPKC	73
CRB2	74
CRB2 association with Nestin	74
Markers analysed clearly define several distinct cell populations in the dorsal neural tube during dorsal obliteration	77
3.4 Statistical analysis of apical markers	81
3.5 Discussion	95
3.5.1 The obliteration window marks a significant change in the nature of the developing spinal cord	95
3.5.2 Structural changes during obliteration	97
3.5.3 Nestin+ cells are closely associated with strong CRB2 expression	98
3.5.4 Polarity proteins and junction complexes are downregulated in sub-dorsal VZ cells during dorsal obliteration	99
3.5.5 A model for dorsal obliteration	100
<b>Chapter 4: Dorsal Nestin+ radial glia: a role in mediating loss of neuroepithelial integrity and establishment of the funicular migratory stream</b>	<b>103</b>
4.1 Introduction	104
4.2 Prenatal dorsal Nestin+ cells have the power to drive progenitor cell delamination in an experimental model system	105
4.3 Adult dorsal Nestin+ cells have the power to drive progenitor cell delamination	110
4.4 Progenitor-delamination ability correlates with Nestin+ CRB2+ cells	115
4.5 Discussion	116
4.5.1 Dorsal Nestin-expressing Radial Glia disrupt epithelial tissues	116
4.5.2 Adult dorsal Nestin+ cells	117
<b>Chapter 5: A novel secreted isoform of <i>Crb2</i> is detected in dorsal Nestin+ radial glia and can mimic their ability to disrupt epithelial integrity</b>	<b>118</b>
5.1 Introduction	119
5.2 Database evidence for secreted isoforms of <i>Crb2</i> in mouse.	119
5.3 A potentially secreted splice variant of <i>Crb2</i> can be detected in embryonic mouse	128
5.4 A truncated splice variant of <i>Crb2</i> is detected in tissues with the ability to disrupt epithelial integrity	134
5.5 Secreted CRB2 can mimic the action of dNRG, and disrupt epithelial cells in the embryonic chick	135
5.6 Neuroepithelial cells migrate out of the neural tube after exposure to secreted CRB2	13.9
5.7 Discussion	142
5.7.1 Evidence for secreted CRB2 <i>in vivo</i>	142
5.7.2 Secreted CRB2 mediates the activity of dNRG	143
5.7.3 A model for the action of secreted CRB2 in disrupting epithelial integrity	145
<b>Chapter 6: Slice culture optimisation</b>	<b>148</b>
6.1 Introduction	149
6.2 Optimising slices and handling	151

6.3	Gross dissection	151
6.4	Plasmid injection and electroporation	153
6.5	Sectioning	153
6.6	Slice mounting	154
6.7	Imaging	158
6.8	Media optimisation	158
6.8.1	Media composition and purpose	159
6.8.2	Media tested in this optimisation	161
6.9	Results	165
6.10	Conclusion	166
<b>Chapter 7: Live imaging supports my model of dorsal obliteration</b>		<b>170</b>
7.1	Introduction	171
7.2	Elongate dorsal cells/dNRG	172
7.3	Dynamic sub-dorsal cells	173
7.4	Active dorsal migration of cell nuclei on dNRG	176
7.5	Do sub-dorsal cells extend a process that fasciculates on early dNRG pioneers?	177
7.6	Other cell processes interact dynamically with the dorsal midline	184
7.7	Medio-lateral radial glia	184
7.8	Discussion	189
<b>Chapter 8: Discussion</b>		<b>193</b>
8.1	Summary of Results	194
8.2	On-going/future studies	296
8.3	Is dorsal obliteration a late part of neurulation?	203
	Roof plate and dNRG cells	203
	Wider action of secreted CRB2?	204
	Conserved mechanism?	206
8.4	Additional factors are likely to contribute to dorsal obliteration	207
8.5	Dorsal obliteration and formation of adult central canal	209
8.6	Regeneration in the adult central canal	210
<b>Bibliography</b>		<b>213</b>
<b>Appendix</b>		<b>233</b>

<b>Tables</b>		
1.1	Summary of Apical-basal polarity proteins across <i>Drosophila</i> , <i>C. elegans</i> and mammals	25
2.1	Primary Antibodies	44
2.2	Secondary Antibodies	45
2.3	Plasmid Table	47
2.4	PCR conditions Table	53
2.5	<i>Crb2</i> PCR primer Table	53
3.1	Frequency of Ranked apical marker intensity for Dorsal analysis	89
3.2	Frequency of Ranked apical marker intensity for Medial analysis	89
3.3	Frequency of Ranked apical marker intensity serial section analysis	89
4.1	E15 mouse transplants into HH10 chicken embryo	107
4.2	Adult mouse transplants into HH10 chicken embryo	112
5.1	Splicoforms of the mouse <i>Crb2</i> gene as annotated by ENSEMBL	124
5.2	<i>Crb2</i> -002 inferred from two ESTs	124
5.3	Notes on alignment	126
5.4	Secreted <i>Crb2</i> PCR primers	129
5.5	First round PCR sequencing data	130
5.6	Second round (nested) PCR sequencing data	133
5.7	CRB2-soaked bead transplants into the HH10-12 embryonic chicken	137
6.1	Purpose of media components	162
6.2	Antibodies used in analysis of slice culture	165
A.T1	GENSAT database interrogation	237
<b>Figures</b>		
1.1	Formation of the neural tube	4
1.2	Dorsal and ventral signalling occurs from the roof plate and floor plate respectively	7
1.3	Development of the roof plate	11
1.4	Zebrafish elongated roof plate cells	13
1.5	Postnatal spinal cord	14
1.6	Proliferation around the dorsal midline	14
1.7	Zebrafish roof plate disruption	16
1.8	Polarity complex proteins	22
1.9	Domain diversity in polarity complex proteins	23
1.10	CRB family members	24
2.1	Mouse embryonic dissection schematic	40
3.1	Embryonic mouse spinal cord morphology	57
3.2	F-actin (phalloidin label) in the mouse spinal cord	60
3.3	Intermediate filament protein – Nestin	61
3.4	The SOXB1 Family	64
3.5	Nestin and SOX2	66
3.6	Transcription factors: PAX6 and NKX6.1	68
3.7	ZO-1	72
3.8	aPKC	75
3.9	Apical Basal Polarity Proteins: CRB2	76
3.10	CRB2 Nestin	78
3.11	E15/16 mouse ventricular zone – High Power	79
3.12	Schematic of Figure 3.11	80

3.13	Comparison of normalised aPKC intensity for all sections	85
3.14	Comparison of normalised CRB2 intensity for all sections	86
3.15	Comparison of normalised ZO-1 intensity for all sections	87
3.16	Regional trends in apical marker intensities from E13 to E17	88
3.17	Lumen morphology and SOX2-expressing cells at E14-E17	96
3.18	Dorsal obliteration model	102
4.1	Schematic of mouse central canal tissue into HH10-12 chicken embryo	108
4.2	E15 mouse spinal cord transplant into HH10 chicken embryo	109
4.3	SOX2 and Nestin in Adult and E17.5 mouse Spinal cord	113
4.4	Adult mouse spinal cord transplant into HH10 chicken embryo	114
5.1	Relative positions of Crb2-001 (full length transcript) and Crb2-002 and Crb2-003 (partial transcripts)	122
5.2	High power view of Crb2-001 (full length transcript) and Crb2-002 and Crb2-003 (partial transcripts)	123
5.3	Schematic showing relative positions of ESTs making up inferred Crb2-002	124
5.4	ESTs that define Crb2-002	125
5.5	Ensemble – inferred Sequence of Transcript Crb2-002	126
5.6	<i>Crb</i> isoforms schematic	127
5.7	Location of primers	129
5.8	BLAST results of sequencing data from eye first round of PCR confirms the band is full length/transmembrane <i>Crb2</i>	130
5.9	Schematic of dissections on which PCR was run	131
5.10	PCR Schematic	132
5.11	Results from First and second round (nested) PCR	133
5.12	BLAST results of sequencing data from dorsal neural tube dissection, second round nested PCR.	134
5.13	Secreted CRB2 bead transplant into HH10 chicken embryo	138
5.14	Secreted CRB2 bead transplant into RFP-electroporated HH10 chicken embryo	141
5.15	Allan Developing Brain Atlas: <i>Crb2</i> mRNA	144
5.16	CRB2-CRB2 interactions	147
6.1	Schematic of E14/E15 mouse electroporation	152
6.2	Analysis of different media after 24 hour culture	167
7.1	Elongate Dorsal Cells 1	174
7.2	Elongate Dorsal Cells 2	175
7.3	Sub Dorsal Cells 2	178
7.4	Sub Dorsal Cells 3	179
7.5	Sub Dorsal Cells 1	180
7.6	Elongate nuclei around the dorsal midline	181
7.7	Midline-interacting cells moving dorsally	182
7.8	Possible mechanisms by which sub-dorsal cells migrate dorsally	183
7.9	Midline interacting cell 1	186
7.10	Midline-interacting cells 2	187
7.11	Radial glia	188
8.1	Models of sub-dorsal cell detachment and migration	197

A.F1	Chick transitin and SOX2	234
A.F2	Dorsally moving cells	235
A.F3	Laterally moving cells	236
<b>Movies</b>		
7.1	Elongate Dorsal Cells 1	174
7.2	Elongate Dorsal Cells 2	175
7.3	Sub Dorsal Cells 2	178
7.4	Sub Dorsal Cells 3	179
7.5	Sub Dorsal Cells 1	180
7.6	Elongate nuclei around the dorsal midline	181
7.7	Midline-interacting cells moving dorsally	182
7.9	Midline interacting cell 1	186
7.10	Midline-interacting cells 2	187
7.11	Radial glia	188
A.M2	Dorsally moving cells	235
A.M3	Laterally moving cells	236



## Abbreviation List

24h	24 hour
AJ	Adherens junction
aPKC	Atypical protein kinase C
BMP4/7	Bone morphogenic protein 4/7
Bp	Base pair
C57/B	C57 black 6 mouse strain
CD-1	CD-1 mouse strain
CDC2	Cell division control protein 42 homolog
cDNA	Complimentary deoxyribonucleic acid
Chk	Chicken
CNS	Central nervous system
CO <sub>2</sub>	Carbon dioxide
CRB1/2/3	Crumbs1/2/3
CRB2s	Secreted Crumbs2
DAPI	4',6-diamidino-2-phenylindole
Dlg	Disks large
DLX5/6	homeobox genes homologous to the distal-less (Dll) gene 5/6
DMEM	Dulbecco's modified Eagle's medium
DNA	Deoxyribonucleic acid
dNRG	Dorsal Nestin-expressing radial glial-like cells
DSHB	The Developmental Studies Hybridoma Bank
E-CAD	E (epithelial)-cadherins
E13	Embryonic Day 13, <i>etc.</i> (Used primarily for mouse)
EDTA	Ethylenediaminetetraacetic acid
EMT	Ependymal to Mesenchymal transition
EST	Expressed sequence tag
EZ	Ependymal zone
FERM	4.1 protein/ ezrin/radixin/ moesin domain
FGF	Foetal growth factor
Fig	Figure
FOXI1/2	FOXI1 forkhead box I1/2
GBX2	Gastrulation Brain Homeobox 2
GDF7	Growth Differentiation Factor 7
GFAP	Glial fibrillary acidic protein
GFP	Green fluorescent protein
GLAST	GLutamate ASpartate Transporter
GPI	glycosylphosphatidylinositol anchor
H2B	Human histone 2B
HBSS	Hank's Balanced Salt Solution
HCO <sub>3</sub>	Hydrogen carbonate
HEK 239	Human Embryonic Kidney 293 cell line
HEPES	4-(2-hydroxyethyl)-1-piperazineethanesulfonic acid
HH12	Hamilton-Hamburger embryonic stage 12 (chicken embryo)
HINGS	Heat inactivated goat serum
Hpf	hours post fertilization (zebrafish)
IgG	Immunoglobulin G
IHC	immunohistochemistry

L-15	Leibovitz's L-15 media
LGL	Lethal Giant Larvae Homolog 1
LMX1A/B	LIM homeobox transcription factor 1
MAFB	Musculoaponeurotic Fibrosarcoma Oncogene Homolog B
MDCK	Madin-Darby canine kidney cell line
mRNA	Messenger Ribonucleic acid
Mse	Mouse
MSX1	Msh homeobox 1
NCC	Neural crest cells
NEUN	Neuronal Nuclei
NKX2.2/6.1	NK2 Homeobox 2.1/6.2
NMD	Nonsense mediated decay
OCT	Optimal Cutting Temperature compound
PALS	Protein associated with Lin-7
PAR6	Partitioning Defective 6
PATJ	Protein Associated To Tight Junctions
PAX3/6/7	Paired box 3/6/7
PBS	Phosphate buffered saline
PCR	Polymerase chain reaction
PDZ	Post synaptic density protein (PSD95), Drosophila disc large tumor suppressor (Dlg1), and zonula occludens-1 protein (zo-1)
PFA	Paraformaldehyde
Rbt	Rabbit
RFP	Red fluorescent protein
RNA	Ribonucleic acid
RNAseq	Ribonucleic acid sequencing
ROCK	Rho-associated protein kinase
RP	Roof plate
Rt	Rat
SCRIB	Scribble
SHH	Sonic hedgehog
SOX1/2/3/B1	Sry-related HMG box 1/2/3/B1
TFAP2	Transcription Factor AP-2 Alpha
VZ	Ventricular Zone
XERL	Xenopus EGF-like repeat with laminin-G domain protein
ZA	Zona adherens
ZIC1-6	Zinc finger of the cerebellum 1-6
ZO-1	Zonula occludens-1

# Abstract

During normal vertebrate development, the ventricular zone (VZ) of the spinal cord reduces in size during the late prenatal period. In this process, termed dorsal obliteration, dorsal VZ progenitors move away from the VZ. Remaining ventral progenitors give rise to the ependymal zone of the adult central canal. At present, little is understood of the mechanisms that drive dorsal obliteration. Here I analyse dorsal obliteration in the prenatal mouse. I show that it occurs over a tight time-window, between E14-E17. Over this period, the dorsal midline is characterised by dorsal Nestin<sup>+</sup> radial glial (dNRG) cells that display strong apical/endfeet expression of the apical polarity proteins CRB2 and ZO-1. Concomitantly, adjacent sub-dorsal VZ cells downregulate CRB2, ZO-1 and aPKC, and their nuclei become located away from the lumen. Ectopic transplantation of dNRG into the lumen of embryonic chick neural tube causes a disruption of progenitor patterning and the appearance of ectopic progenitor cells outside the neural tube, suggesting that dNRG cells secrete a diffusible factor that can disrupt neuroepithelial integrity. Previous bioinformatics studies had suggested the existence of an isoform of CRB2 that lacks the transmembrane and intercellular domain, and so may function as a secreted variant. Using a nested PCR approach, I find evidence that a isoform of CRB2 that lacks the transmembrane domain is specifically expressed in dNRG cells. Further, a protein encoded by this splice variant (secreted CRB2) can be secreted, and, when presented ectopically to chick neural tube, can disrupt neuroepithelial integrity. I therefore propose a model for dorsal obliteration in which secreted CRB2 can outcompete or interfere with a normal homodimerisation of transmembrane CRB2, leading to the destabilisation of the CRB2 complex and apical polarity, and the consequent delamination of subdorsal VZ cells. As a first step in testing this model, I develop an *in vivo* mouse slice culture assay in which to monitor cell behaviour during dorsal obliteration in real time. These studies provide evidence that the cell bodies of sub-dorsal cells immediately adjacent to elongating roof plate cells/dorsal Radial Glia migrate dorsally, using either the dorsal Radial Glia as a scaffold, or, potentially, re-orienting their own processes along the scaffold, and migrating along these. Finally, sub-dorsal cells appear to detach from the VZ in a process that may resemble apical abscission. Together, these studies suggest that a disruption of apical polarity proteins, driven through dorsal midline-secreted CRB2, is instrumental in dorsal obliteration. I discuss this model within the context of embryonic neurulation and discuss the implications for potential of the adult spinal cord.

# **Chapter 1**

**The development of the central canal  
of the spinal cord through dorsal  
obliteration**

## **1.1 Neurulation**

The term 'neurulation' usually refers to the process by which the neural plate through bending, closing and formation of the roof plate (RP), forms the neural tube. However, a recent review has argued that such 'early' neurulation is followed by a second period of development, during which the lumen of the neural tube gives rise to the central canal, and has suggested that this should be referred to as 'late' neurulation (Korz, 2014b; Mao *et al.*, 2015). This thesis is primarily concerned with processes that occur in, and may drive, late neurulation.

## **1.2 Early neurulation**

In birds and mammals the process of early neurulation is divided into primary and secondary neurulation. Primary neurulation is characterised by the mechanism by which the neural plate - a thickened epithelium that forms over the midline of the embryo and that expresses characteristic proteins, including SOXB1 proteins - forms neural folds that bend, fold and merge to form a neural tube (Figure 1.1; (Rex *et al.*, 1997; Uchikawa *et al.*, 2011; Gilbert *et al.* 2000; Kishi *et al.* (2000)). Secondary neurulation occurs in the very caudal neural tube of birds and mammals, and is the method of neural tube formation in teleosts such as zebrafish. Secondary neurulation starts with a migration of neural plate cells to the midline, causing a thickening. The thickening then transforms into the neural stem that hollows into the neural tube.

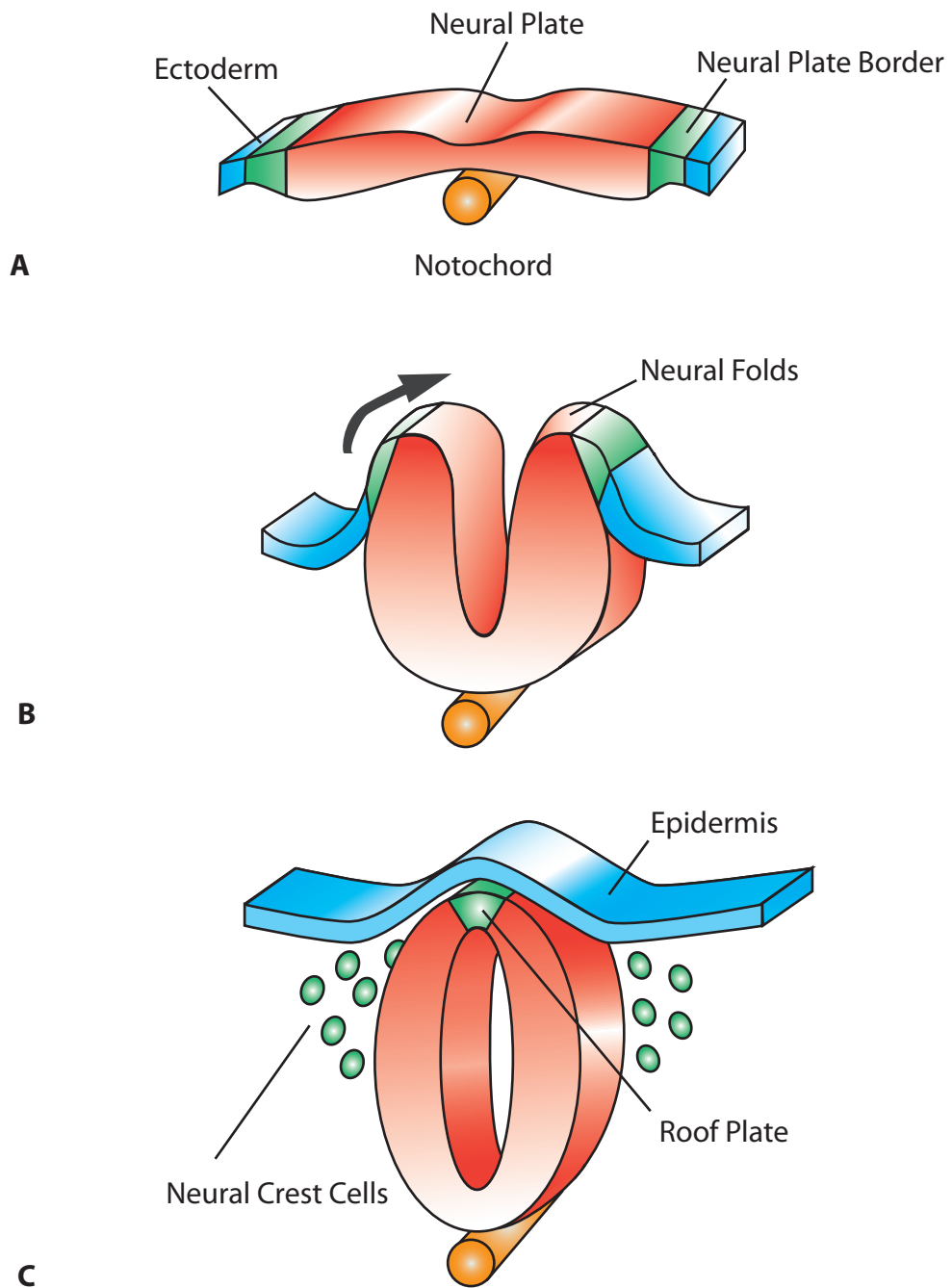


**Figure 1.1** - Formation of the neural tube. (A) The neural plate develops as a thickened epithelium overlying the notochord. Its lateral edges are bounded by neural plate border cells. (B) The neural plate bends upwards into neural folds that then fuse together to create a tube. (C) The neural tube separates from the overlying ectoderm. Cells from the neural plate border form both the roof plate at the neural tube midline and migratory neural crest cells.

### 1.3 Neural patterning and neurogenesis

The early neural tube is a bilaterally-symmetrical pseudostratified epithelium in which the basal surfaces of SOXB1-positive neural progenitor cells form the lateral edges of the neural tube and the apical surfaces are oriented towards an internal primitive lumen, or neurocoel. Neural progenitors proliferate and their nuclei undergo a stereotypic interkinetic nuclear movement in which mitosis occurs apically and S phase basally (Kosodo *et al.*, 2011; Spear and Erickson, 2012). This results in a substantial expansion in the number of neural progenitors and the initial phase of neural tube development is marked by a considerable increase in tissue size. As neural plate and neural tube formation proceed, diffusible signals emanate from posterior and anterior signalling centres, to pattern the neural tube along its anterior-posterior axis. The spinal cord thus develops from posterior parts of the neural tube.

The early posterior neural tube is further characterised by the floor plate, which forms at the ventral midline, and the roof plate, which forms at the dorsal midline (see section 1.3). These wedge-shaped glial-like cells act as signalling centres that establish dorso-ventral pattern in the neural tube. Sonic Hedgehog (SHH) deriving from the floor plate, and bone morphogenetic proteins (BMPs) and Wnts deriving from the roof plate, act antagonistically to establish a gradient of Gli transcription factors. In turn, these establish distinct dorsal-ventral identities in stem and progenitor cells (Jacob and Briscoe, 2003; Le Dreau and Marti, 2012). Dorsal domains are characterised by homeodomain transcription factors including PAX6, PAX7, while ventral domains are characterised by the homeodomain transcription factors NKX2.2 and NKX6.1 (Figure 1.2). Stem/progenitor cells throughout the ventricular zone (VZ) continue to express the SOXB1 protein, SOX2. The signature of transcription factor expression results in

stem/progenitor cells that vary, both in potential and proliferation. Thus, dorsal progenitors will give rise to dorsal commissural interneurons, while ventral progenitors will give rise to motor neurons and ventral interneurons (Figure 1.2) (Briscoe *et al.*, 2000; Jessell, 2000).

Concomitant with the formation of the wedge-shaped floor plate and roof plate, SOXB1-positive SOX9-positive neuroepithelial stem/progenitor cells begin to transform into radial glial cells, characterised by a cell body located at the ventricular zone and a long process that extends to the outer, pial surface (Kriegstein and Alvarez-Buylla, 2009). Radial glial-like cells can either self-renew, or differentiate, via progenitors, to neuronal fates. A process termed apical abscission enables differentiating cells (neurons) to become physically removed from the ventricular zone and migrate laterally along radial glial-like processes, to the mantle zone, where they undergo terminal differentiation, including axon extension (Das and Storey, 2014). In the forming spinal cord of the mouse, the initial phase of neurogenesis occurs between embryonic day E12-E18, peaking at E14 in mouse, and in chick, between E2.5-E5.5, and is followed by a period of gliogenesis (King and Munger, 1990; Rowitch, 2004). Astrocytes then oligodendrocytes are specified, peak formation of both occurring postnatally in rodents (Barry and McDermott, 2005; Sauvageot and Stiles, 2002).



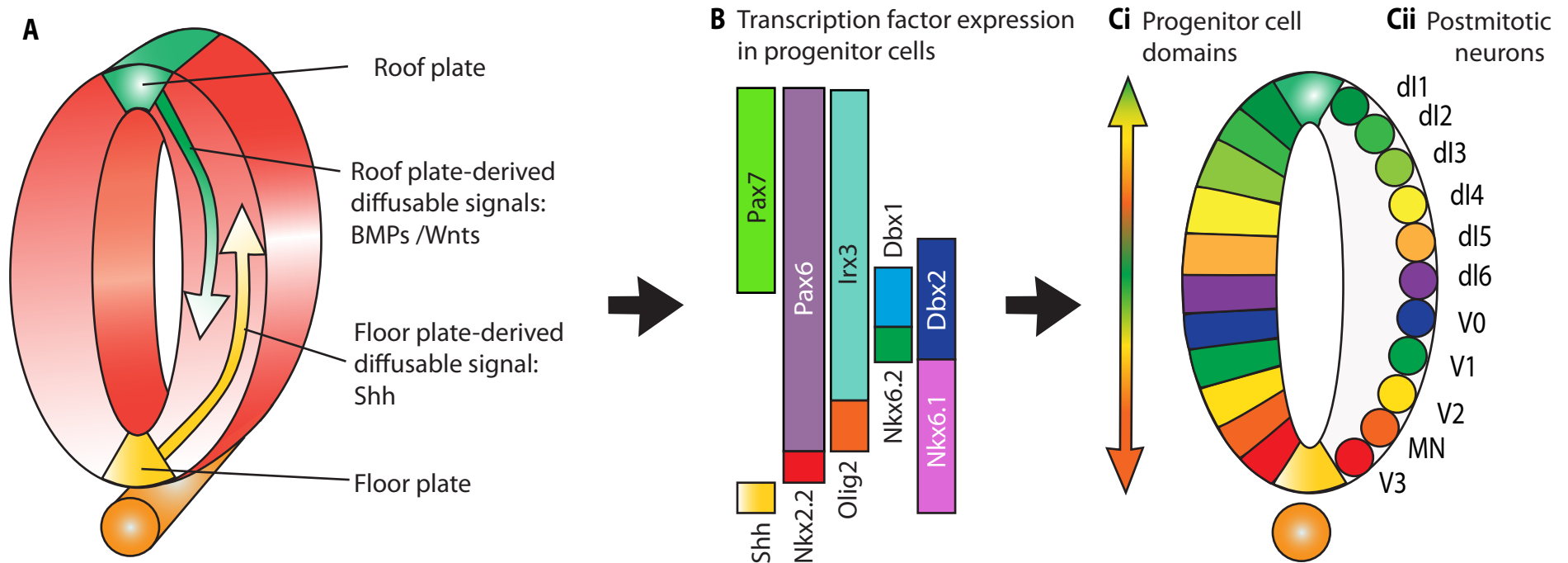


**Figure 1.2** Dorsal and ventral signalling occurs from the roof plate respectively (A). The floor plate secretes Sonic hedgehog (yellow arrow) and the roof plate secretes a wnts and Bone Morphogenetic Proteins (green arrow). Gradients of these morphogens effect domains of transcription factors (B) that in turn inform dorso-ventral progenitor identity (Ci). These progenitors then give rise to different classes of neuron (Cii). Neuron abbreviation dl - dorsal interneuron, V - ventral interneuron, MN - motor neuron.

*Adapted from: Caspary (2003), Ribes (2009), Wolpert (3rd edition)*

#### 1.4 Development of the roof plate

Roof plate cells are induced during gastrulation and initially occupy a territory termed the neural plate border, a broad territory located at the lateral edges of the neural plate (Fig. 1.1a). During neurulation, the neural plate border territory elevates as the neural plate closes to form the neural tube (Fig 1.1b and c). As a consequence, nascent roof plate cells come to reside within the dorsal aspect of the neural tube.

Studies over the last two decades have provided much insight into the genetic control of roof plate development (Simoës-Costa and Bronner, 2013). These studies show that the neural plate border contains a multi-progenitor cell population that is capable of giving rise to roof plate cells as well as neural crest cells, ectodermal placodes, epidermal cells and sensory neurons of the central nervous system (Groves and LaBonne, 2014; Simoës-Costa and Bronner, 2015). Formation of the neural plate border is closely linked to neural induction, and appears to rely on the same signals. Foetal Growth Factors (FGFs) work in concert with BMP and WNT inhibitors to activate the expression of neural genes such as the SOXB1 genes (Streit *et al.*, 2000). WNT and BMP signals originate in lateral regions of the embryo, while inhibitors of these pathways are secreted from medial regions. A balance between these signals generates a mediolateral gradient of WNT and BMP activity, and the neural plate border cells originate within a territory exposed to intermediate levels of WNT and BMP activity (Groves and LaBonne, 2014).

The output of 'intermediate' WNT and BMP signaling activity activates a particular signature of transcription factors that defines neural plate border cells. These genes, which are termed neural plate border specifiers, include *Tfap2*, *Msx1*, *Zic1*, *Gbx2*,

*PAX3/7, Dlx5/6, Gata2/3, Foxi1/2* and *Hairy2* (Khudyakov and Bronner-Fraser, 2009; Meulemans and Bronner-Fraser, 2004; Nichane *et al.*, 2008) and at least a subset appear to be directly activated by WNT and BMP signalling pathways (Garnett *et al.*, 2012). Importantly, expression of transcription factors is not uniform: this is thought to have important implications at subsequent stages, when the neural plate border becomes segregated into roof plate, premigratory neural crest and preplacodal domains (Hong and Saint-Jeannet, 2007).

The emergence of the roof plate from the neural plate border is marked by the expression of 'roof plate' specifier genes, including members of the *Lmx*, *Msx* and *Zic* families (Khudyakov and Bronner-Fraser, 2009; Meulemans and Bronner-Fraser, 2004). Their expression is thought to establish a novel state that begins to set apart emerging roof plate cells. The LIM homeodomain transcription factor *Lmx1a*, for example, is expressed in roof plate progenitors and differentiated roof plate cells in the developing spinal cord of both the chick and the mouse, where it is necessary and sufficient for caudal roof plate development (Chizhikov and Millen, 2004a) inducing expression of several roof plate components, including *MAFB*, *GDF7*, *BMP4* and *WNT1*. Fate mapping studies show that early roof plate cells are multipotent, and that single roof plate cells can either be retained as roof plate cells or can give rise to neural crest cells (Bronner-Fraser and Fraser, 1988, 1991; Bronner-Fraser *et al.*, 1991; Chizhikov and Millen, 2004b; Le Douarin *et al.*, 2004) a population of cells that undergo an epithelial to mesenchymal cell transition, and migrate away from the neural tube, ultimately differentiating to a wide array of fates, including the peripheral nervous system. Currently, it remains unclear how neural crest cells might segregate from roof plate cells. By contrast, much is known of the mechanism of neural crest specification:

Neural crest cells, it is clear, are specified under a suite of genes, termed neural crest specifiers that have a range of integrated functions. They activate an epithelial to mesenchymal transition (EMT) effector programme, which together will allow (a) neural crest cells to delaminate, (b) support their acquisition of mesenchymal properties and (c) migratory abilities, and (d) maintain the neural crest in an undifferentiated state (Bronner-Fraser and Fraser, 1988, 1991; Bronner-Fraser *et al.*, 1991). In recent years, many studies on neural crest EMT have focused on the adhesive changes that enable cells to delaminate. These studies indicate that a major driver of EMT is the direct repression of neural crest specifier genes on epithelial cadherins (Sauka-Spengler and Bronner-Fraser, 2008). In particular, downregulation of type 1 cadherins results in the dissolution of adherens junctions, allowing the segregation of single cells from the epithelium (Pla *et al.*, 2001).

Whatever the mechanism that dictates whether a cell will form a neural crest or a roof plate cell, the process of roof plate specification culminates in the expression of bona fide roof plate markers such as BMP4, BMP7, WNT1 and WNT3 (Garcia-Castro *et al.*, 2002; Liem *et al.*, 1997) that characterise a line of wedge-shaped glial-like cells that are found at the dorsal midline of the developing CNS (Chizhikov and Millen, 2004b). Along the anterior-posterior axis, the roof plate varies in width and character, and is particularly wide in the hindbrain, where distinct sub-divisions of the roof plate can be recognised through characteristic gene expression profiles (Broom *et al.*, 2012; Wilson *et al.*, 2007).

### 1.5. Elongation of the roof plate and formation of the dorsal glial septum

Studies in a wide range of species show that roof plate cells undergo a profound transformation after their initial formation. Light and electron microscopic observations in rat, mouse and cat revealed that in all species, a dramatic change in shape occurs over a 3-4 day period of prenatal life. Over this period (the 'transformation window'), roof plate cells are transformed from wedge-shaped cells, with large extracellular spaces between them, to a thin, dense septum of cells with reduced extracellular spaces between them (Altman and Bayer, 1984; Bohme, 1988; Sevc *et al.*, 2009; Snow *et al.*, 1990; Sturrock, 1981) (Figure 1.3). These studies suggested that the elongated roof plate cells contribute to the future dorsal glial septum, or dorsal funiculus, an adult structure that extends from the dorsal-most central canal to the dorsal pial surface.

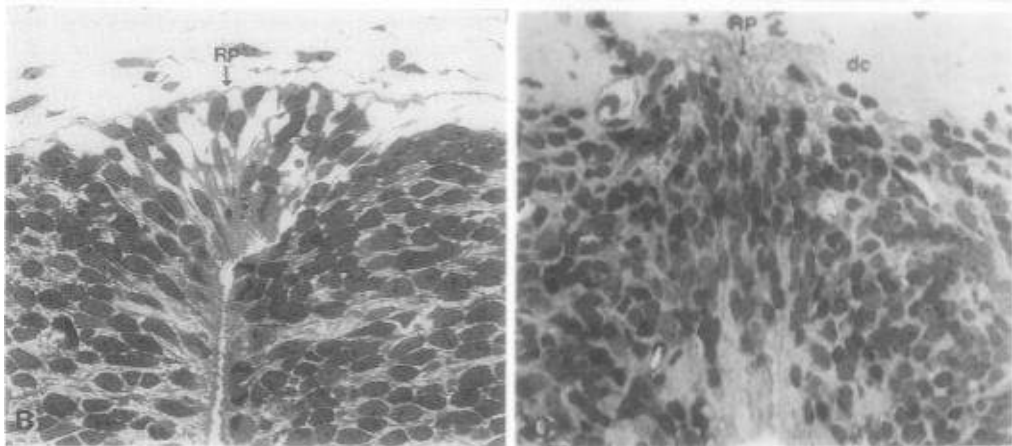


**Figure 1.3** Development of the roof plate ((Snow *et al.*, 1990) Fig 2, B and C) E13 and E15 rat roof plate showing a change from wedge-shaped to elongated roof plate cells.

Immunohistochemical analyses reveal that elongated roof plate cells express a number of markers that are traditionally associated with radial glial-like cells. These include the Glutamate transporter GLAST, Glial fibrillary acidic protein GFAP and the type VI intermediate filament marker nestin (Kondrychyn *et al.*, 2013; Sevc *et al.*, 2009; Snow *et al.*, 1990). Differentiated NeuN+ neurons are clearly absent from the region occupied by elongated roof plate cells (Sevc *et al.*, 2009). In zebrafish Notch (*mib*) mutants, anterior roof plate cells are absent, and in later embryonic life, there is no sign of anterior GFAP+ elongated roof plate cells, supporting the idea that stretched roof plate cells go on to form a stretched GFAP+ population that shares certain features with radial glial cells (Kondrychyn *et al.*, 2013). Recently, elegant studies in zebrafish have used a GFP transgenic line to analyse roof plate elongation in real time *in vivo* (Kondrychyn *et al.*, 2013). These studies confirm that wedge-shaped roof plate cells undergo a marked elongation. In fish, the transformation window occurs over the 48-66 hours post fertilisation. Elongated roof plate cells form long ventrally-directed extensions, the end-feet of which form the dorsal surface of the central canal (Figure 1.4). Dorsally, these cells extend to the pial surface (Figure 1.4).

### **1.6 Central canal formation**

At the same time that roof plate cells elongate, the primitive lumen or neurocoel of the neural tube is transformed into the central canal of the spinal cord, a process that has been termed 'dorsal obliteration' (Bohme, 1988) or late neurulation (Korzh, 2014a), and is characterised by a reduction in size of the lumen. The reduction is markedly greater dorsally, and as a result, the postnatal/adult central canal lies relatively ventrally within the adult spinal cord (Figure 1.5).

The majority of studies have suggested that the elongation of roof plate cells is intimately linked to the transformation of the primitive lumen into the central canal, and have proposed mechanisms that might link these two processes. Sevc performed BrdU analyses in rats, and showed that proliferating progenitor cells are intimately associated with elongated Nestin+ GLAST+ roof plate cells (Figure 1.6). On the basis of this observation, the authors proposed that a rearrangement and migration of radial glial cells drives the transformation of the primitive lumen into the central canal, and suggested that Nestin+ GLAST+ elongated roof plate cells act as scaffold to support the migration of radial glial cells that move dorsally from the VZ (Sevc *et al.*, 2009).

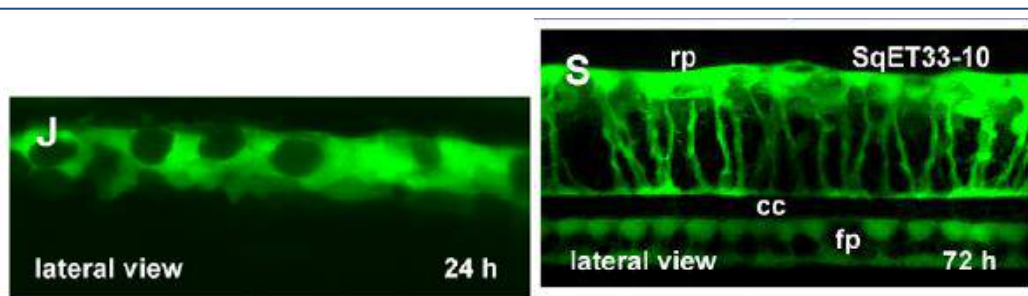
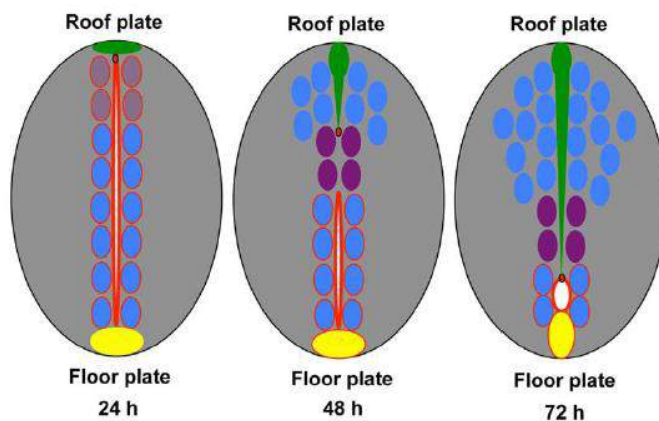


**Figure 1.4** Zebrafish elongated roof plate cells (Kondrychyn *et al.*, 2013) Figure 2 and Figure 8) (J) Roof plate from a 24h post-fertilisation embryo, (S) roof plate from a 72h post-fertilisation embryo. Long processes extend from the roof plate cells at 72h. RP – roof plate, FP – floor plate, CC – central canal.



Konrychyn describes roof plate extension in fish neural tube as a product of 'push pull' forces caused by constriction of the apical surface (red) and crowding by differentiated cells (blue).

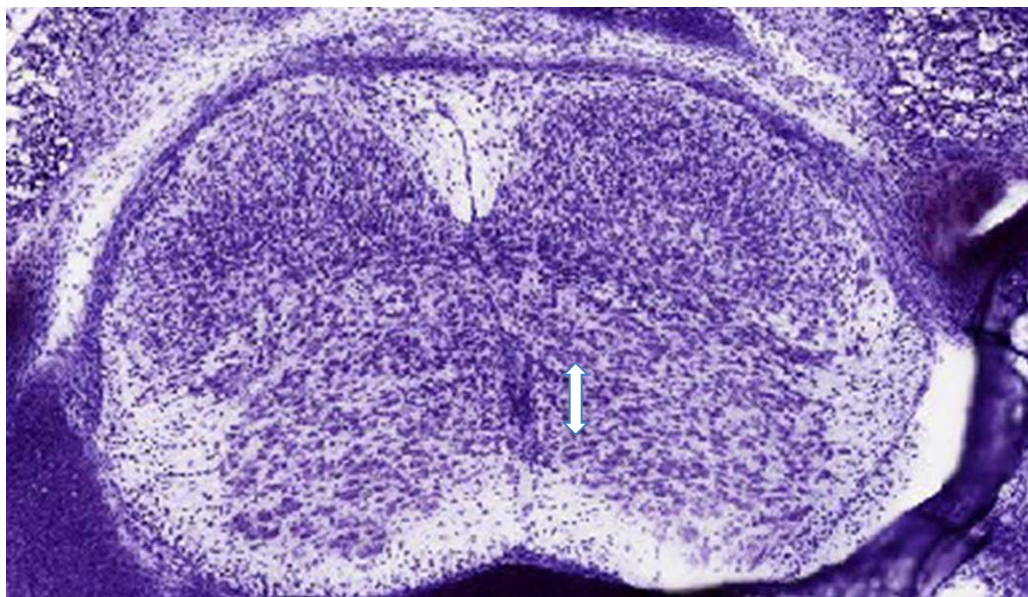


**Figure 1.5** Postnatal spinal cord. Lumen length denoted by white arrow.  
Website: © 2015 Allen Institute for Brain Science. Allen Spinal Cord Atlas [Internet]. Available from: <http://mousespinal.brain-map.org>

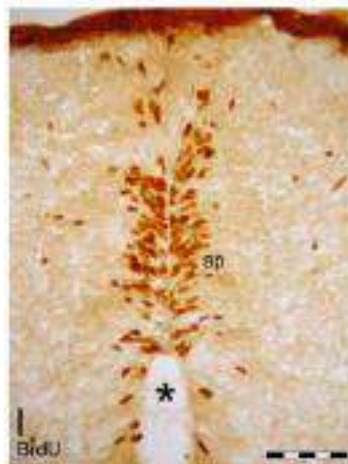


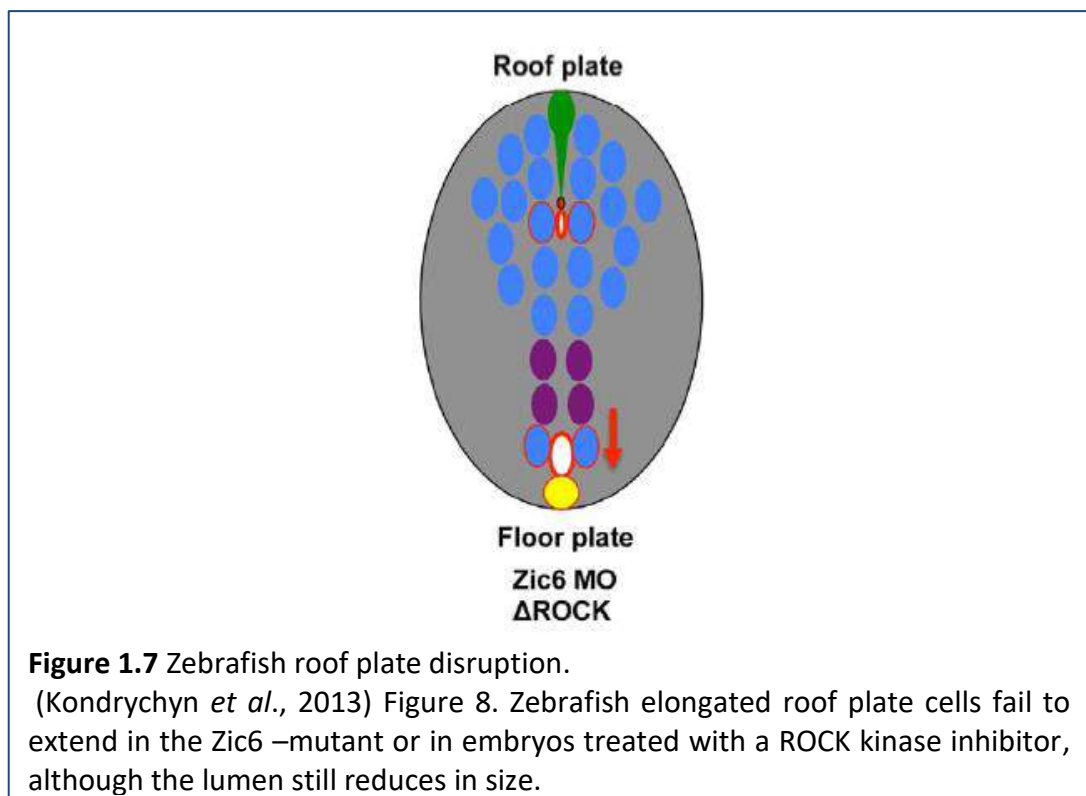
**Figure 1.6** Proliferation around the E18 Rat dorsal midline.  
(Sevc *et al.*, 2009) Figure 1.I BrdU labelling of proliferating cells reveals labelled cells along the midline close to Nestin+ GLAST+ roof plate cells.



The PAR3/PAR6/aPKC protein complex plays a key role in the establishment and maintenance of apicobasal cell polarity (see below), and studies in fish showed that central canal development is disturbed in a PARD6gamma mutant embryo. Analyses of the cells lining the neurocoel revealed that lack of PARD6gammab function leads to defects in mitotic spindle orientation during neurulation (Munson *et al.*, 2008). More recently, (Kondrychyn *et al.*, 2013) demonstrated that in this mutant, the roof plate cells fail to stretch. This again illustrates the link between roof plate cell elongation and formation of the central canal. Additionally, these studies indicate a role for cell polarity proteins in these events. Indeed, binding sites for other apico-basal polarity proteins, including those for aPKC-binding, CDC42-binding, PALS1-and CRB binding are essential for the function of PARD6 in neurocoel morphogenesis (Munson *et al.*, 2008). Furthermore, immunohistochemical studies in zebrafish show that as the lumen obliterates, the expression of apical polarity proteins in VZ cells that line the lumen changes appropriately. Thus, beta-catenin and ZO-1, which are detected in a long slit-like domain that marks the apical surface of VZ cells lining the primitive lumen become expressed in a small, round domain, shifted ventrally, that marks the apical surface of cells lining the central canal (Kondrychyn *et al.*, 2013).

The cytoskeletal actin microfilament protein, F-actin, undergoes a similar change in pattern, correlating with the rearrangement of the primitive lumen into central canal and stretching of the RP cells, and F-actin constriction has been suggested as a major driving force behind dorsal collapse (Sevc *et al.*, 2009). To date, no study has tested this directly, however, changes to the cytoskeleton have been shown to be important in the processes of roof plate elongation. In zebrafish, ZIC6 morphant roof plate cells fail to stretch (Kondrychyn *et al.*, 2013). ZIC6 has multiple roles, including regulation of

the cytoskeleton, and indeed, the cytoskeletal inhibitor of Rho-associated protein kinases (ROCK1 and ROCK2) mimics the effect of the ZIC6 morphant. This demonstrates that in zebrafish, the extension of the roof plate cytoskeleton depends on the activity of ZIC6 and Rho-associated kinase (Rock). At present it is not clear whether ZIC proteins play a similar role in other vertebrates: ZIC6 is specific to teleost fishes and homologues of this gene have not been identified in other vertebrates (Keller and Chitnis, 2007). Intriguingly, these studies suggest that the processes of roof plate elongation and dorsal obliteration are not completely interdependent: in ZIC6 morphants, or embryos treated with ROCK inhibitors, the lumen collapses normally (Figure 1.7). The idea that roof plate elongation and dorsal obliteration are integrated, but not wholly interdependent was first raised by Bohme (1988), and highlights the fact that as yet, we understand little about the mechanisms behind these two processes.



### **1.7. Molecular drivers of early neurulation and neurogenesis**

As outlined above, as dorsal obliteration proceeds, there is a change in expression of apical polarity proteins, and of F-actin. Both these components are known to play a critical role in driving early neurulation.

The ventricular zone of the early neural tube has an unusual arrangement of actin microfilaments, including F-actin, that are critical for normal neurulation (Karfunkel, 1974; Morriss-Kay and Tuckett, 1985; Sadler *et al.*, 1982; Smedley and Stanisstreet, 1986). The classically-accepted idea is that the apical constriction of neuroepithelial cells of the neural plate is driven by contraction of a network of filamentous actin (F-actin) at the apical surface, a process that includes the vimentin-positive intermediate filaments-based cytoskeleton (Li *et al.*, 2009). Several studies have approached this as the main driving force behind primary neurulation (Hildebrand and Soriano, 1999; Nagele *et al.*, 1987; Sawyer *et al.*, 2010). More recently, however, studies into the actin-severing protein, Cofilin, suggest that F-actin may play a more complex role, including distinct interactions with both apical and basal domains of neuroepithelial cells (Grego-Bessa *et al.*, 2015).

Apicobasal polarity is a cellular characteristic essential for tissue and organ morphogenesis, differentiation and homeostasis (Roignot *et al.*, 2013; Royer and Lu, 2011; St Johnston and Sanson, 2011; Yamashita *et al.*, 2010) and recent studies show that the apicobasal polarity pathway is essential for primary neurulation (Kondrychyn *et al.*, 2013). These studies show that bone morphogenetic proteins (BMPs), that derive from the surface ectoderm and roof plate, can regulate apicobasal polarity pathway components in the neural plate, including the apical components, Shroom,

CRB and PAR complexes (see below) and sub-apical adherens junctions (AJ) complexes, in a cell cycle dependent manner (Eom *et al.*, 2013). These genes are required for apical constriction (Haigo *et al.*, 2003; Hildebrand and Soriano, 1999; Lee *et al.*, 2007; Nishimura *et al.*, 2012; Nishimura and Takeichi, 2008) modulating apical junctions in the neural plate and resulting in cell and tissue shape changes that help bend, shape and close the neural tube.

Apical constriction is a cell shape change that requires the co-ordination of many distinct cell biological processes (Martin and Goldstein, 2014). These processes include the positioning of the centrosome, the contraction of actin-myosin networks, and the attachment these actin networks to cell-cell junctions, allowing co-ordinated movement within a tissue.

Although contractility and adhesion vary between cell types, there is a core of cytoskeletal and adhesion proteins that modulate forces intra- and intercellularly, and in turn drive co-ordinated processes such as apical constriction in the neural tube (Mason and Martin, 2011; Sawyer *et al.*, 2010). As in other tissues, apical constriction during vertebrate neural tube formation is associated with the positioning of the centrosome (Baker and Schroeder, 1967; Buckley and Clarke, 2014; Burnside, 1971) and with changes in cell-cell adhesion molecules, such as those found at adherens junctions (Barriga and Mayor, 2015; Miyamoto *et al.*, 2015).

As outlined in section 1.2, above, early neurulation is followed by a neurogenic period, in which neuroepithelial cells begin to generate neural progenitor cells. These migrate laterally, most likely along medio-laterally oriented neuroepithelial cell/radial glial cell

scaffolds, to the outer mantle zone where they terminally differentiate (Poluch and Juliano, 2007).

Increasing numbers of studies point to the importance of apical-basal polarity and AJ proteins as well as F-actin, in regulating the switch from symmetrically proliferative division of neuroepithelial cells to asymmetric neurogenic division of neural progenitor cells, and in promoting the events that result in lateral migration of neural progenitor cells (Kosodo *et al.*, 2004; Miyamoto *et al.*, 2015). An apical abscission event driven by changes in the actin-myosin results in the loss of apical cell membrane, and apical polarity, and mediates neuron detachment from the ventricle (Das and Storey, 2014).

In summary, apico-basal cell polarity is critical to both early neurulation and to neurogenesis, and studies are beginning to understand the mechanistic basis for apico-basal polarity proteins in regulating complex cellular behaviours, including changes in cell shape, in delamination and in migration. The finding that apico-basal polarity proteins, and F-actin undergo changes in expression as dorsal obliteration proceeds have led to the recent suggestion that similar mechanisms operate to govern early neurulation and dorsal obliteration. In turn, this has led to the suggestion that dorsal obliteration should be termed late neurulation (Korzsh, 2014a) and that the completion of this second period of central canal formation that should define the end of neurulation proper. As outlined above, however, as yet we have little mechanistic understanding of dorsal obliteration, and additional studies are needed to determine whether similar components and principles may drive early neurulation and dorsal obliteration.

## 1.8. Apical-Basal polarity proteins

Cell polarity is a fundamental regulator of many cellular processes. It plays roles in processes as diverse as differentiation, migration and molecular transport (Assemat *et al.*, 2008; Bulgakova and Knust, 2009; Gosens *et al.*, 2008; Humbert *et al.*, 2006; Kaplan *et al.*, 2009). For example, epithelial cells that line the cavities and surface of the body rely on the compartmentalization of the apical and basolateral membranes to perform an enormous variety of specialized functions. Polarity complexes are also critical in setting up and maintaining the belt-like zona adherens (ZA) or adherens junction (AJ) that separates these two compartments and is functionally important in maintaining the integrity of the epithelial sheet (Assemat *et al.*, 2008; Kaplan *et al.*, 2009; Shin *et al.*, 2006; Wang and Margolis, 2007). Together, therefore, apical and basal polarity complexes define functionally distinct plasma membrane and associated cytoplasm.

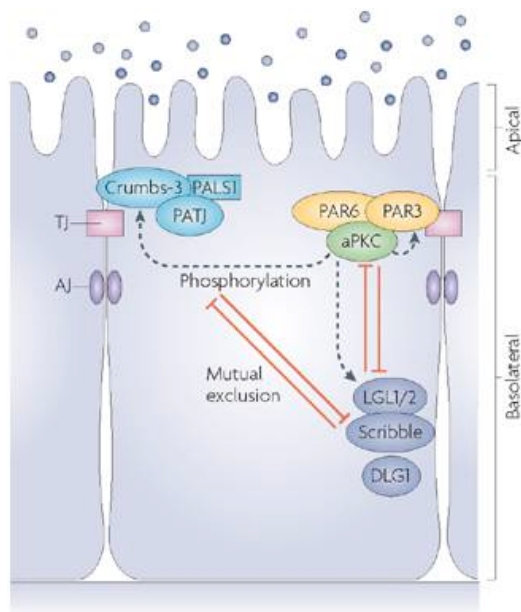
Polarity proteins fall into three complexes, each evolutionarily conserved from flies to humans (Table 1.1). Each complex has a defined localization within the cell. The apical domain hosts the CRB complex, consisting of CRB, Stardust and Discs Lost, and the PAR complex (Bazooka/PAR6/PKC) that localizes to the subapical region, while the Scribble complex (Scribble/Discs Large/Lethal Giant Larvae) localizes to the basolateral domain (Assemat *et al.*, 2008). A schematic of polarity protein interactions is provided in Figure 1.8.

Although these proteins are often discussed as if they are found in discrete complexes, the reality is that these complexes form a complicated and interconnected network. Many core members of these complexes are notable for their variety of binding/linker domains (especially PDZ, ERL1 and L27 domains, as detailed in Fig 1.9) This allows a

great deal of flexibility in binding partners, both within and between the three polarity complexes leading to an expansive functional diversity (described extensively in Assemat *et al.* (2008)).

Each complex has several core members; however, depending on tissue and developmental context, a wide variety of transient members may be bound. Additionally, these complexes are ancient and although evolutionarily conserved, they have undergone a degree of orthology. Apical-basal polarity in higher animals has a much greater degree of complexity than can be described in this brief introduction.

## Polarity complex proteins



Nature Reviews | Molecular Cell Biology

**Figure 1.8** The Crumbs (blue), Par (yellow) and Scribble complexes (purple) work in concert to define the apical-basal polarity of the cell. The apical Crumbs and Par complexes mutually antagonise the basal Scribble complex. Iden and Collard (2008)



# Domain diversity in polarity complex proteins

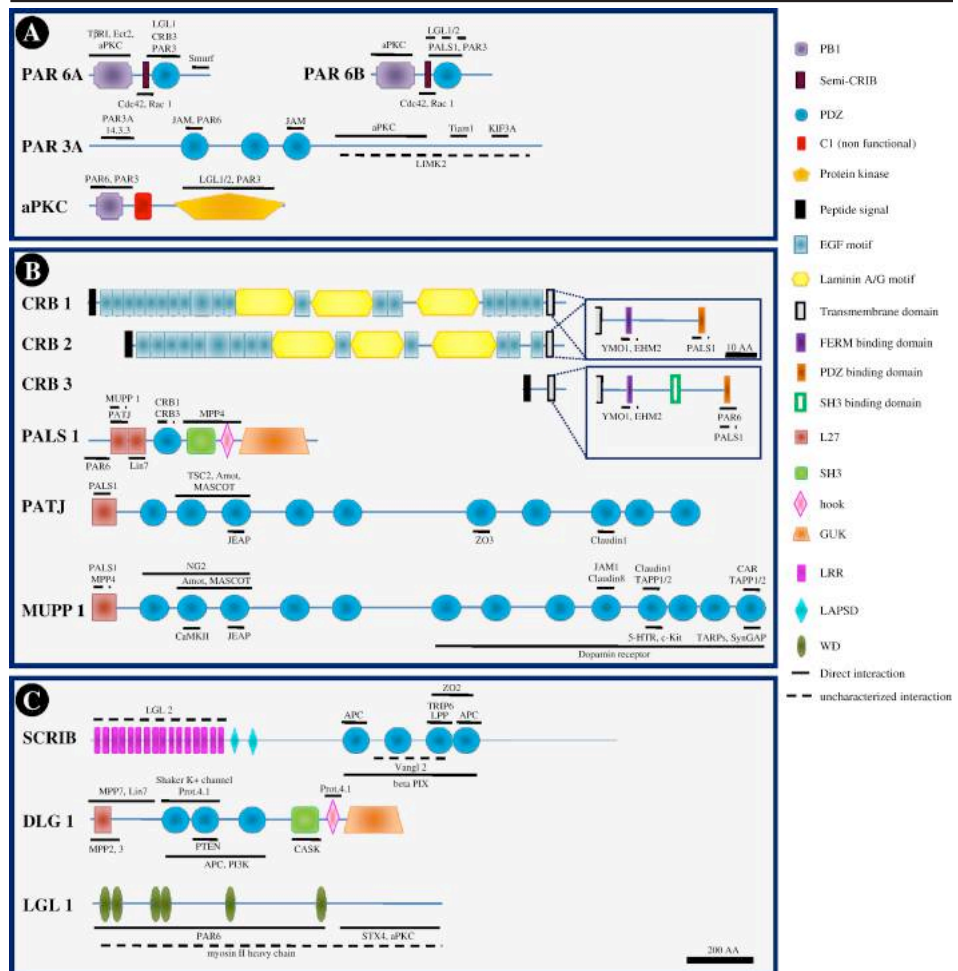


**Figure 1.9** The Crumbs, Par and SCRIB complexes contain a multitude of domain types that facilitate a wide range of interactions within and between the complexes, as well as to, for example, the cytoskeleton. Assemat et al (2008).

# Crumbs family members

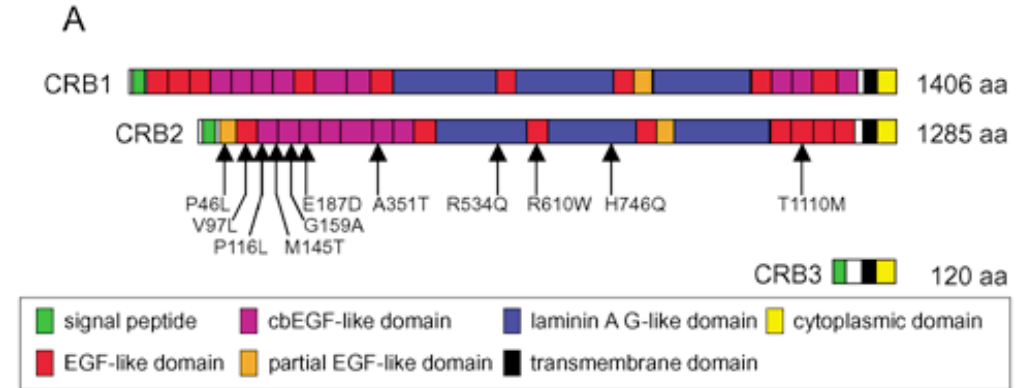


**Figure 1.10** The mammalian Crumbs family has three members. Crumbs1 (CRB1) and Crumbs2 (CRB2) have a very similar domain structure, including a very long extracellular domain. Crumbs3 (CRB3) is much smaller, and consists of only the cytoplasmic domain common to all three proteins and a signal peptide. van den Hurk (2005)

**Table 1.1** Summary of Apical-basal polarity proteins across *Drosophila*, *C. elegans* and mammals.

Polarity complex	<i>Drosophila</i>	<i>C. elegans</i>	Mammals
<b>CRB complex</b> CRB/PALS/PATJ	CRB Stardust dPATJ dLIN7	Crb1, Eat-20 TAG-117 - MPZ-1	CRB (1-3) MPP1-7/PALS INADL/PATJ/MUPP1 MPDZ/MALS
<b>PAR Complex</b> PAR3/PAR6/aPKC	Bazooka DmPAR6 DmaPKC	PAR3 PAR-6 PKC-3	PARd3/PARd3B PARD6(A,B,G) Atypical (a)PRKC/PKC
<b>Scribble complex</b> SCRIB/DLG/LGL	Scrib DLG DLGI	LET-413 DLG1 TOM1	SCRIB DLG (1-5) LLGL (1-2)

### 1.9 The CRB complex

The CRB complex was the first of the polarity complexes to be discovered in *Drosophila*, and is evolutionarily conserved from invertebrates to mammals (Assemat *et al.*, 2008; Omori and Malicki, 2006). Currently, extensive research is focused on the role of CRB genes in retinal degeneration (notably retinitis pigmentosa, (den Hollander *et al.*, 1999; Richard *et al.*, 2006), but it is becoming an increasingly important candidate for research into other diseases of epithelia, including tumourigenesis and cystic kidney diseases (Laprise, 2011; Torkko *et al.*, 2008).

The CRB complex varies in composition depending, for example, on developmental and tissue context. However several 'core members' that are always present can be identified: CRB proteins, Protein associated with Lin7-1 (PALS1, or Stardust in *Drosophila*), Lin7 and PALS1 associated tight junction protein (PATJ) (Bulgakova and Knust, 2009). CRB itself is pivotal to the functioning of the entire CRB complex. Loss of

this protein leads to degradation or delocalization of the other members (Bachmann *et al.*, 2001; Berger *et al.*, 2007; Horne-Badovinac and Bilder, 2008). The *Drosophila* Crb-mutant can be rescued by expression of the region containing a functional PDZ- and FERM- binding domain, demonstrating the importance of this cytoplasmic region to the function of the CRB complex (Wodarz *et al.*, 1993). Indeed, most studies have indicated that the cytoplasmic domain mediates the function of CRB. The exception to this is a study in zebrafish that suggests that the extracellular domain of Crb2 homodimerises and stabilizes the entire CRB complex (Zou *et al.*, 2012).

### *CRB*

Originally identified in *Drosophila*, where it is expressed during gastrulation and then in ectodermally-derived epithelia post-gastrulation (Tepass *et al.*, 1990). CRB is a type-1 transmembrane protein containing a large extracellular domain, a transmembrane domain and a small (37 amino acid) intracellular C-terminal domain. The intracellular C-terminal domain is highly conserved between orthologues. It contains highly conserved binding motifs, including the PSD-95/Discs-large/ZO-1 (PDZ)-binding motif ERLI, and the 4.1/ezrin/radixin/moesin (FERM)-binding domain that are crucial for binding to other CRB complex members (Bulgakova and Knust, 2009; Klebes and Knust, 2000; Wodarz *et al.*, 1993).

Three orthologues of CRB exist in mammals (CRB1-3) and five in zebrafish (Crb1, Crb2a/b, Crb3a/b) (Omori and Malicki, 2006). As yet, the expression patterns of CRB proteins have not been fully described in any higher model organism (Bulgakova and Knust, 2009). CRB1 and CRB2 have highly similar extracellular domains: 3 Laminin A/G

domains and 19 and 14 EGF-like domains, respectively (den Hollander *et al.*, 1999; Katoh and Katoh, 2004). CRB3 has a markedly different extracellular domain to the other CRB proteins. However, CRB3 is considered a member of the CRB complex because the transmembrane and cytoplasmic domain is highly conserved between all three mammalian CRB proteins (Gosens *et al.*, 2008; Medina *et al.*, 2002; Richard *et al.*, 2006) A schematic is provided in Figure 1.10.

Much of what is known about CRB in developing epithelia has come from studies in *Drosophila* and cell lines. CRB and other CRB complex members have been repeatedly identified as required for setting up adherens junctions and the correct localisation of E cadherin and Beta-catenin (Grawe *et al.*, 1996; Klebes and Knust, 2000; Tepass, 1996).

CRB1 has been extensively characterised in the retina, as mutations in the complex lead to retinal dystrophies including retinitis pigmentosa and Leber congenital amaurosis (den Hollander *et al.*, 1999). In mouse, mutations in CRB2 phenocopy the retinitis pigmentosa disruption as caused by CRB1 in human. Additionally, in fish, knockdown of Crb2b leads to abnormal photoreceptor cells and defects in Crb2a affects neuronal patterning in the retina (Malicki and Driever, 1999; Omori and Malicki, 2006).

CRB2 is mainly expressed in retina, brain and kidney. Studies into CRB2 have been slow owing to the embryonic lethality of the knockout in mice (Xiao *et al.*, 2011). However, the role of mutated CRB2 in retinal degeneration has been well established in mouse (as discussed above) and fish studies have shown knockdown of Crb2b result in abnormal cilia in the pronephric duct (Malicki and Driever, 1999; Omori and Malicki,

2006). In light of this, recent papers have begun to explore CRB2 as of real importance in diseases of the kidney in fish (Ebarasi *et al.*, 2015) and human (Slavotinek *et al.*, 2015). This is mirrored in clinical investigations into CRB3, where it was noted that downregulation is associated with renal cell carcinomas (Mao *et al.*, 2015). Work in the monkey brain, has implicated CRB2 in the inhibition of the Alzheimer disease associated amyloid precursor protein (Mitsuishi *et al.*, 2010).

CRB3 is widely expressed in epithelia and skeletal muscles (Lemmers *et al.*, 2004; Makarova *et al.*, 2003; Roh *et al.*, 2003). Like CRB1 and CRB2, this protein is expressed sub-apically, but in addition a isoform localises to, and is needed for the maintenance of, primary cilia in mouse and in MDCK cells (Fan *et al.*, 2007; Fan *et al.*, 2004). Additionally, knockdown of Crb3 in fish results in smaller auditory kinocilia in the inner ear (Omori and Malicki, 2006).

Although polarity is accepted as a factor in the progression of cancers, the role of the CRB complex is as yet unclear (Dow and Humbert, 2007; Khursheed and Bashyam, 2014; Wodarz and Nathke, 2007). Both over- and under-expression of CRB can lead to epithelial defects. Excessive levels of CRB in fly wing imaginal disks leads to overproliferation (Lu and Bilder, 2005). CRB3 repression has been reported in both breast cancer and tumorigenic baby mouse kidney cell lines, reported to be linked to misregulation of tight junctions (Aigner *et al.*, 2007; Karp *et al.*, 2008; Li *et al.*, 2015).

Studies into CRB2 during development of vertebrates have been slow owing to the embryonic lethality of the knockout in mice, which die at E12 due to disruption in epiblast cell polarity, disrupted EMT and endoderm and mesoderm formation (Xiao *et al.*, 2011). However, studies have implicated CRB2 as essential for neural differentiation murine embryonic stem cells and mouse brain (Boroviak and Rashbass, 2011). Unpublished studies from our collaborators (M. Maturza: PhD thesis; Rashbass lab) reveal expression of *Crb2* mRNA and protein in the apical part of VZ cells in the chick hindbrain (stage 10-17) and mouse dorsal telencephalon (E12.5-E17.5). These studies also described an atypical localisation of CRB2 in a sub-ventricular region in the dorsal telencephalon (see Chapter 4). CRB2 has also been detected in E11.5 mouse neural tissue (Lee *et al.*, 2011). CRB3 has been shown to be important for lumen formation in Madin-Darby canine kidney cells, however it is not clear whether this mechanism it utilised *in vivo* (Schluter *et al.*, 2009).

#### *PALS1/Stardust*

Stardust (Sdt) is a multiple PDZ domain MAGUK (membrane-associated guanylate kinase) protein. It is also known as PALS1 (protein associated with LIN7 1, or MPP5 (Membrane Protein, Palmitoylated 5 / MAGUK P55 Subfamily Member 5). In many cells, loss of stardust leads to a similar phenotype to loss of CRB, and in many cases these proteins appear to mutually stabilize. It has been suggested that SDT acts as a linker or scaffold with which to localize other proteins to the CRB complex. However, this cannot be the entire story, as CRB and stardust do not colocalise in every developmental stage and cell type (notably in *Drosophila* photoreceptor cells) (Berger *et al.*, 2007).

### *PATJ*

Also described as disks lost (DLT), PATJ (PALS1-associated TJ protein) is a PDZ-protein. Loss of PATJ prevents proper maintenance of CRB and Stardust within developing photoreceptor cells. Additionally, the PDZ domain of PATJ binds to PAR-6, thus connecting the two apical polarity complexes (Tepass, 2012).

### *LIN7*

Also known as Mals1, this PDZ protein has been found associated with MPP7 (a homologue of MPP5/Std) and DLG, and localizing to epithelial adherens junctions in the MDCK cell line (Bohl *et al.*, 2007). Knockout analysis suggests that this CRB complex component is less critical for viability than the others and as such, it is not always cited as a core member of the CRB complex (Bachmann *et al.*, 2001; Straight *et al.*, 2006).

## **1.10 The PAR complex**

Like the CRB complex, the PAR complex is conserved from invertebrates to vertebrates, although higher organisms often have several orthologues. The constituent members are PAR3/Bazooka, PAR6 and aPKC. This complex has been shown to localize to tight junctions of epithelial cells, play a key role in the migration of astrocytes, and interact with the WNT pathway (Gao *et al.*, 2002a; Gao *et al.*, 2002b; Sun *et al.*, 2001). At least in mammals, the interaction of all three components is critical to the establishment of apical basal polarity (Goehring, 2014; Helfrich *et al.*, 2007).



### *Atypical protein kinase C, aPKC*

Atypical protein kinase C (aPKC) has an N terminal regulatory domain, and a C terminal catalytic domain. This protein was originally identified as a binding partner of PAR3, an interaction that is critical for the asymmetric cell division during early embryogenesis in *C. elegans* (Tabuse *et al.*, 1998). aPKC interacts with the CRB complex by binding both PATJ and CRB. Several areas of research suggest that aPKC is important in the developing nervous system. In stem cells and neural progenitors, aPKC has been implicated in the regulation of primary cilia (He *et al.*, 2014). aPKC has a role in separating neural stem cells and progenitor cells through subcellular localization in chicken embryos (Ghosh *et al.*, 2008), and through the regulation of Numb distribution in *Drosophila* larvae brains (Haenfler *et al.*, 2012) and through asymmetric inheritance of both aPKC and PAR3 in fish (Alexandre *et al.*, 2010).

### *Bazooka/PAR3*

PAR3 has been shown to set up tight junctions in epithelial cells. It contains three PDZ domains, a CRIB domain, and a conserved N terminus (Kohjima *et al.*, 2002).

### *PAR6*

PAR6 contains a conserved PDZ domain and a CRIB domain (Noda *et al.* 2001). The correct apical localization of this protein is dependent upon the aPKC/PAR3 interaction. PAR6 interacts with PATJ, CRB and Stc of the CRB complex. PAR6/aPKC associates with the SCRIB complex protein DLG1 in some migrating cells, regulates Rho proteins in some migration contexts, and also interacts with RAC (Etienne-Manneville *et al.*, 2005; Gomes *et al.*, 2005; Wang *et al.*, 2003). PAR-6 can also interact with the actin cytoskeleton through association with CDC42 (Genova *et al.*, 2000).

The PAR complex, has several known interactions with the CRB complex (Nam and Choi, 2003). Most notably PAR-6 interacts with PATJ, CRB and Std, and atypical protein kinase C (aPKC) binds both PATJ and CRB. PAR-6 can also enlist additional proteins into the complex: notably, it can link the CRB complex to the actin cytoskeleton through the recruitment of CDC42 (Peterson *et al.*, 2004). Additionally, The PDZ domain of PAR6 can bind to Lethal (2) giant larvae (Lgl, part of the basolateral complex) *in vitro* (Yamanaka *et al.*, 2003). This may be part of the interaction by which Lgl negatively regulates the CRB complex.

The protein kinase aPKC colocalises with the CRB complex in embryonic epithelial cells and very early PRCs, and may serve as a link between the CRB complex and Bazooka (PAR-3 in vertebrates), thus to the phosphoinositide signaling pathway (Hong *et al.*, 2003; Nam and Choi, 2003; Sotillos *et al.*, 2004; Wodarz *et al.*, 2000). This interaction involves Bazooka being phosphorylated by aPKC, restricting it to adherens junctions and thus maintaining cell-cell adhesion (Morais-de-Sa *et al.*, 2010). These examples serve to illustrate the complexity and flexibility of the CRB and PAR complexes.

### **1.11 The Basal SCRIB complex**

The SCRIB complex maintains the basolateral domain, and consists of SCRIB, Lethal giant larvae and disks large. This complex is important for the maintenance of junctions and cell-cell contact. It interacts antagonistically with the apical PAR and CRB complexes to establish polarity and defined domains, through mechanisms including mutual antagonism. The SCRIB complex is not as well defined as the apical polarity complex, and the interactions between members has yet to be elucidated fully (Assemat *et al.*, 2008).

### **1.12 Alternative splicing in polarity proteins.**

The inter-network of interactions of polarity complex proteins, and their ability to bind to a wide variety of proteins through their complement of protein binding domains allows them to mediate complex and varied functions. However, a further level of complexity is added by the variety of splice variants undergone by many of these proteins. For example, both human CRB1 and CRB2 have been reported to encode variants that truncate the protein, so that only a putatively secreted form is translated (Katoh and Katoh, 2004; Watanabe *et al.*, 2004). Stardust is known to have at least two isoforms (Bulgakova *et al.*, 2010) and PAR3 is known to have several (Gao *et al.*, 2002b). Alternative transcripts may be the regulators of stage or tissue specific interactions. The alternative splicing of PDZ containing proteins is well described (Sierralta and Mendoza, 2004) and plays a role in the expansive functional diversity and networking of the polarity proteins. Additional regulation is effected by the precise localization of the mRNAs within the cell, which can be initiated by alternately spliced regulatory regions of the mRNA (Bachmann *et al.*, 2001; Tepass *et al.*, 1990).

### **1.13 Cadherins and Adherens Junctions**

Establishment of cell polarity in an epithelium relies upon cell-cell adhesion. Adherens junctions (AJs) are cell-cell junctions in epithelial and endothelial tissues, comprised of cadherin and catenin protein complexes. The intracellular catenin component links to the actin cytoskeleton, and the transmembrane cadherin proteins bind these proteins and extend an extracellular domain that homodimerises with the extracellular domains of cadherins on neighbouring cells Adherens junctions are a mechanism by which the actin cytoskeleton is linked between individual cells of a tissue, and so play a critical role in the integrity and stability of that tissue and forms the basis of gross tissue

dynamics, thus it is a critical component for morphogenesis of the developing embryo (Halbleib and Nelson 2006, Gul et al 2017).

Cadherins form a large family of proteins that are crucial for the calcium dependent adhesions (from which they derive their name) between animal cells (Hatta and Takeichi, 1986, Nollet *et al.*, 2000, Takeichi *et al.*, 1981). Different cadherins give rise to adherens junctions with different adhesive properties, and so a 'cadherin switch' in a subset of cells is a mechanism that often underpins tissue segregation or the initiation of a migration (Niessen and Gumbiner 2002, Takeichi 1995, Maître, L.J., and Heisenberg, C.P. 2013).

E-cadherin is the major cadherin in nonneural epithelia, and N-cadherin organizes similar AJs in neural epithelia. A switch from one type of cadherin to another is an essential change during many developmental processes. For example, as the neural plate develops into the neural tube, E cadherin is replaced by N cadherin in adherens junctions (Gartner et al, 2015; Redies and Takeichi 1996).

The epithelial to mesenchymal transition (EMT) is another important process in development in which cells depolarise and leave the epithelial sheet and become migratory. Cadherin downregulation and the subsequent loss of junction integrity is a critical first step in allowing cells to leave the epithelia. For example, neural crest cells that emigrate from the neural folds/roof plate undergo downregulation of N-cadherin in order to leave the neural tube (Taneyhill and Schiffmacher 2017). N cadherin is also downregulated in newborn neurons and intermediate progenitors after asymmetric

neurogenic division before these cells migrate away from the ventricular zone (Redies 2000).

#### **1.14 Aims**

As outlined above, we have as yet little mechanistic understanding of dorsal obliteration, and additional studies are needed to determine whether similar components and principles may drive early neurulation and dorsal obliteration. Here I set out to develop a better mechanistic understanding of dorsal obliteration, and whether it could be considered a continuum with early neurulation.

In Chapter 3 I aim to analyse and characterise the developing prenatal mouse spinal cord as it undergoes dorsal obliteration and assess whether it is a continuum with early neurulation. I will determine the time window of obliteration and analyse the characteristics of the ventricular zone cells that line the lumen using nuclear and apical markers. I will define populations of cells that may be involved in dorsal obliteration, and elucidate possible mechanisms for obliteration.

In Chapter 4 I will test whether populations of cells around the ventricular zone are able to induce embryonic cell movement or rearrangement and I will test whether this ability persists in these cells in the adult animal.

In Chapter 5 I aim to identify a component of the mechanism that may allow ventricular zone cells to encourage dorsal obliteration. I will try to demonstrate presence of the molecule *in vivo* and experimental function.

There are currently few options for imaging dynamic cell movements in embryonic mouse. In Chapter 6 I will optimise a dissection and slice culture procedure for the imaging of cells within the embryonic mouse spinal cord, and explore slice culture as a model for cell movement within the mouse spinal cord during dorsal obliteration.

In Chapter 7 I will attempt to strengthen the hypothesis derived from data generated from fixed samples in Chapters 3-5 by attempting to perform time-lapse microscopy to image dynamic cell behaviour in living tissue. These data should assess whether the inferred patterns identified are actually representative of cell migration and delamination dynamics. I will use the method developed in Chapter 6 to collect cell movement data from the time window identified in Chapter 3.

# Chapter 2

Materials and methods

## **2.1 Collection of animal tissue**

### **Mice**

Adult mice used in this study were C57/Black 6-8 weeks of age (post pubescent young adults). Sacrificed mice were anaesthetised with inhaled isoflurane (Isoflo, Abbot) before cervical dislocation. Mouse embryos (E13-E17) used were from the same colony, the dam sacrificed as before, and the embryos immersed in ice-cold Leibovitz's 15 (L-15) (Gibco) before decapitation.

Timelapse experiments were performed in collaboration with the Professor Storey Lab (University of Dundee) using CD-1 mice, killed by overdose of CO<sub>2</sub> before cervical dislocation.

### **Chicken embryos**

Chicken embryos used in this study were *Brown Bovan Gold Hen's* eggs (*Henry Stewart Farms, UK*). Fertilised eggs were held at 18°C until needed and then incubated at 37°C until the appropriate stage. Chicken embryos were killed either by dissection and immersion in ice-cold L-15 medium or by decapitation if E7+.

## **2.2 Gross mouse and chicken dissections**

### **Tissues from the adult mouse**

The decapitated mouse was pinned down and doused in 70% ethanol to improve sterility and to prevent hairs from contaminating tissue. If embryos were to be dissected from the mother then an inverse Y-shaped cut was made along the



abdomen, the uterus removed intact and placed into ice-cold L-15 for the embryos to be dissected *in vitro*.

The spinal cord was exposed by first cutting the skin from the back of the mouse, exposing the length of the spine. Then, watchmaker scissors were used to emancipate the spinal column from the ribs and muscles, before gently cutting the vertebrae in a ventro-lateral position on both sides, thus releasing the ventral portion of the vertebral column. The spinal cord was pulled out gently and placed in ice-cold L-15. Nerve roots and meninges were removed carefully with sharp forceps. Lower lumbar regions as defined by spinal cord tissue thickening.

#### **Tissues from the embryonic mouse**

The uterus was placed into ice-cold L-15, and the embryos were dissected from their placenta, yolk sacs and amnion as quickly as possible to ensure rapid cooling. Mice developed beyond E12 were decapitated immediately and quickly eviscerated. The embryos were then Theiler staged before evisceration and transfer to clean L-15. Sections were analysed from the lower lumbar/upper sacral regions as defined by limb positioning and tissue morphology (Figure 2.1).

#### **Tissue from the embryonic chicken**

Hamburger Hamilton stage 1-13 chicken embryos were dissected from the egg by cutting outside the Area Opaca, before being lifted with an egg spoon into L-15 or ice-cold 4% paraformaldehyde (PFA) (Sigma).

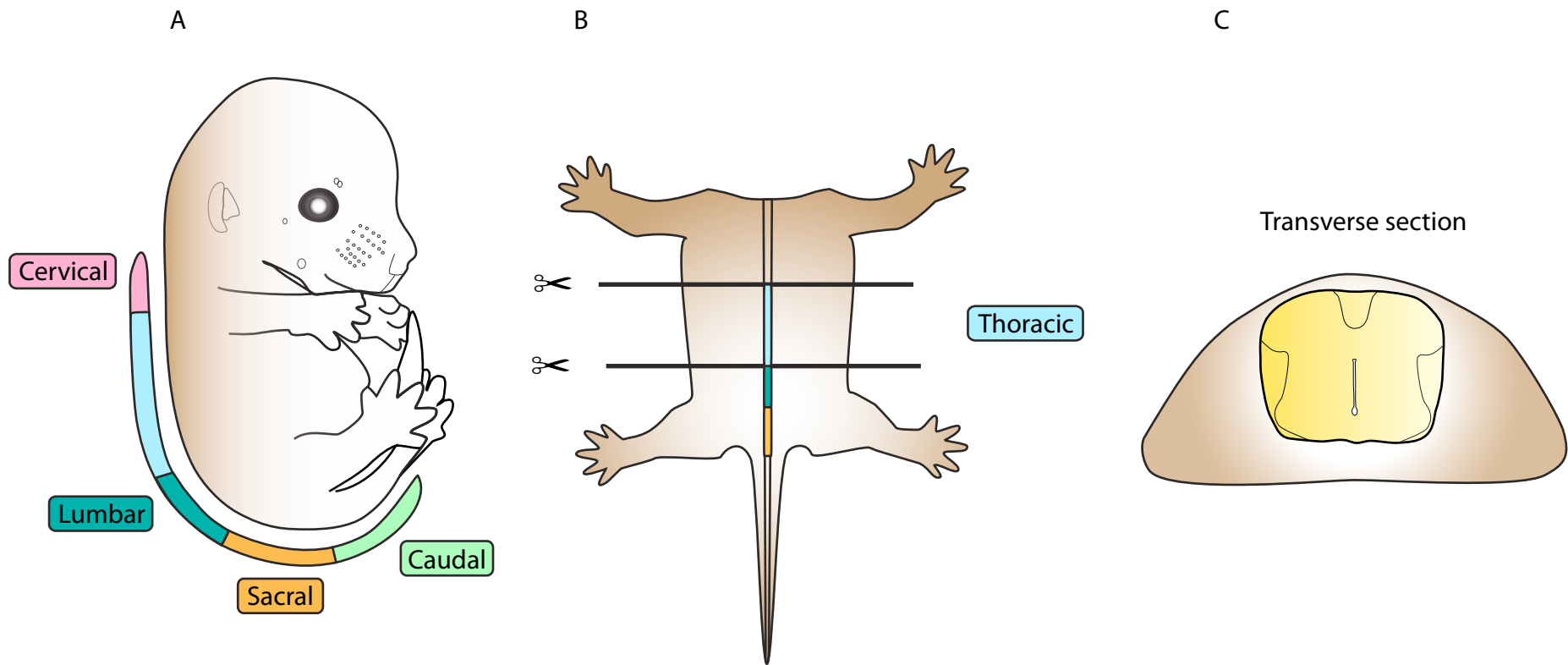


**Figure 2.1** Embryonic mouse dissection schematic

(A) depicts the embryonic mouse. The coloured line depicts the levels of the spinal cord, separated into major divisions: cervical, thoracic, lumbar and sacral. (B) shows the level at which the mouse is dissected for study, directly above and below the limbs, correlating to the thoracic spinal cord. (C) shows an idealised transverse section the lower lumbar/sacral level.

Hamburger Hamilton stage 14 to embryonic day 4.5 chicken embryos were dissected from the egg by cutting widely around the embryo, before being lifted with an egg spoon into L-15 or ice-cold 4% PFA.

Embryonic day 5+ chicken embryos were decapitated *in ovo* before being lifted into L-15, or washed in ice cold Phosphate Buffered Saline (PBS) (Sigma) before immersion in ice-cold 4% PFA. Larger embryos were eviscerated before fixation to ensure rapid cooling and effective fixation throughout the tissue.

### **2.3. Histological analysis**

#### **Fixation of tissue**

Tissues were fixed in ice-cold 4% PFA in 0.2M Phosphate Buffer (Sigma) and kept at 4°C for 2 to 24 hours. Tissue was then washed several times in ice-cold PBS.

#### **Sectioning tissue**

Sectioned tissue was used for Immunohistochemical (IHC) analysis. Fixed tissue was incubated overnight in 30% (w/v) sucrose (Sigma) solution in 0.2M Phosphate Buffer overnight at 4°C. Tissue was then embedded in Optimal Cutting Temperature compound (OCT) (VWR) and frozen on dry ice. The embedded sections were then cryosectioned to 10-30µm on a Bright cryostat and collected on Superfrost slides (SLS). The sections were then air-dried for 2 hours.

### **Immunohistochemistry on Cryosections**

Standard IHC protocol was followed for the detection of protein on cryosectioned tissue. For mouse tissue, sections were pre-incubated in a blocking and permeabilising solution comprised of PBS with 1% Heat inactivated goat serum (HINGS) (GIBCO) and 0.5% Triton-X (Sigma) for 10 minutes. For certain mouse nuclear antigens the slides were held at 90°C in Sodium Citrate Buffer (10mM Sodium Citrate (Sigma), 0.05% Tween 20 (Sigma), pH 6.0). Both chick and mouse tissue were then pre-incubated for an hour in a blocking solution comprised of PBS with 1% HINGS and 0.1% Triton-X.

The sections were then incubated with primary antibody diluted in blocking solution overnight at 4°C. The sections were rinsed well with ice-cold PBS. The next day the sections were incubated with secondary antibody for one hour at room temperature and then rinsed well with PBS. Slides were mounted with VECTASHIELD Mounting Medium with DAPI (4', 6-diamidino-2-phenylindole) (Vectorlabs) protected with glass coverslips (22x64mm No1, SLS) and sealed with clear nail varnish. Control sections were incubated only with secondary antibody to rule out non-specific labelling.

### **Whole mount Immunohistochemistry of sliced tissue**

The sliced tissues were fixed in 4% ice cold PFA for 2 hours. Slices were then incubated in blocking solution for an hour at room temperature. Slices were then incubated with primary antibody diluted in blocking solution for 40 hours at 4°C, followed by three one hour washes in ice-cold PBS (Table 2.1). The slices were then incubated with secondary antibody diluted in blocking solution, with or without DAPI for the same length of time as the primary antibody, followed by three 1-hour washes in ice-cold PBS. If the slices were to be mounted onto coverslips, VECTASHEILD (with or without

DAPI, depending on whether it was added with the secondary) may be used (Table 2.2).

**Table 2.1** Primary Antibodies. Table of antibodies used. Key: Rbt = Rabbit; Mse = Mouse; Chk = Chick; hmn = Human; Rt = Rat; Dky = Donkey; Gt = Goat; IgG = Immunoglobulin G; P = Polyclonal; M = Monoclonal. \* Phalloidin is a synthetic peptide that binds actin, rather than a true antibody.

Antibody	Animal	Type	Conc.	Source
SOX1	Rbt α Mse IgG	P	1:300	Cell signalling
SOX2	Rbt α Chk IgG	P	1:300	Abcam
SOX2	Rbt α hmn IgG	P	1:1000	Millipore
SOX3	Rbt α Mse IgG	P	1:1000	Gift from T. Edlund
PAX6	Mse α Mse IgG	M	1:50	DSHB
NKX6.1	Mse α Mse IgG	M	1:50	DSHB
Nestin (6142)	Mse α Mse IgG	M	1:300	Abcam
Transitin (eap3)	Mse α Chk IgG	M	1:50	DSHB
Laminin (I-9393)	Rbt α hmn IgG		1:200	Sigma-Aldrich
Dystroglycan (Mandag2)	Mse α hmn IgG	M	1:30	Gift from S. Winder's Lab
CRB2 (sk11)	Rbt α Mse IgG	P	1:300	Gift From P. Rashbass Lab
aPKC	Rbt α Rat IgG	P	1:300	Santa-Cruz
ZO-1	Mse α hmn IgG	P	1:300	Zymed
3B9	Mse α Mse IgG	M	1:50	DSHB
Cleaved Caspase 3	Mse α hmn IgG	P	1:500	Cell Signalling
Ki67	Mse α hmn IgG	P	1:500	Abcam
M2	Rt α Mse IgG	M	1:50	DSHB
Phalloidin 594	Peptide*	-	1:500	Thermofisher

**Table 2.2** Secondary Antibodies. Table of antibodies used. Key: Rbt = Rabbit; Mse = Mouse; Chk = Chick; hmn = Human; Rt = Rat; Dky = Donkey; Gt = Goat; IgG = Immunoglobulin G.

Antibody	Fluorophore	Conc.	Supplier
Gt $\alpha$ Mse	Alexa 594	1:500	Thermofisher
Gt $\alpha$ Mse	Alexa 488	1:500	Thermofisher
Gt $\alpha$ Rbt	Alexa 594	1:500	Thermofishergmail.
Gt $\alpha$ Rbt	Alexa 488	1:500	Thermofisher
Dky $\alpha$ Mse	Alexa 647	1:500	Thermofisher
Dky $\alpha$ Rbt	Alexa 647	1:500	Thermofisher
DAPI (4',6-Diamidino-2-Phenylindole)		1:1000	Thermofisher

## 2.4 Chicken embryo *in vivo* manipulations

### Protein-soaked bead transplantation into HH10-11 chicken embryo

Fertilised chicken eggs were incubated in an upright position at 37°C until HH10-12. The top of the egg was covered in sticky tape and a window gently cut, ensuring that the embryo and yolk remained undamaged. The inner shell membrane was removed to expose the embryo, and 20% Blue food dye (Dr. Oetker) in L-15 was injected underneath using a 30-gauge needle (Becton Dickinson) inserted at a shallow angle. The embryo was then staged using the Hamburger-Hamilton embryo staging chart. The clear vitelline membrane was then removed over the caudal neural tube into which the bead was to be transplanted. Affi-gel beads (Bio-Rad) were soaked in protein or PBS control for 24 hours before transplantation. Beads were carefully placed into the most rostral part of the open neural tube. The egg was then sealed with Parafilm (Bemis) or sticky tape before incubation at 37°C for 24 hours. Embryos

were then dissected out and fixed in ice-cold 4% PFA in 0.2M Phosphate Buffer and kept at 4°C for 2 hours. Tissue was then washed several times in ice-cold PBS to reduce the high background noise residual PFA can elicit in IHC.

### **Mouse tissue transplantation into HH10-11 chicken embryo**

The protocol for bead transplantation (above) was followed with the exception that in place of Affi-gel beads, mouse tissue was placed into the neural tube.

Freshly dissected embryonic or adult spinal cord was sliced into 400µm sections on a tissue chopper (McIlwain) and the slices placed into ice-cold L-15. Tissue to be transplanted was punched out with a pulled glass needle (1mm x 0.78, Harvard Apparatus) and mouth pipette (Sigma), before being carefully placed into the most rostral part of the open neural tube.

### **RFP Electroporation variation of transplantation into HH10-11 protocol**

The protocol for transplantation (above) was followed with the addition of an extra step.

After the inner shell membrane was removed, the embryo was electroporated with RFP plasmid (0.3µl/ml, RFP pCAGGS) mixed with a small volume of Fast Green FCF (Sigma) to make the solution visible. The plasmid mixture was drawn up into a pulled glass needle (1mm x 0.78) using a mouth pipette. The clear vitelline membrane was pierced caudal to the embryo at a low angle, and the glass needle slid into the neural tube. The plasmid mixture was then blown gently into the neural tube, after which the needle was retracted. The embryo was then subject to a current (40v, 1ms, 6 pulses)



using a BTX/Harvard Apparatus ECM 830 Square Wave Electroporator and BTX *In ovo* Genetrode™, bent L-shaped, 3 mm electrodes. Plasmid information found in (Table 2.3).

**Table 2.3** Plasmid Table. Description of plasmids used and their origin.

Plasmid	Plasmid Name/ Backbone	Description	Origin
RFP	pCAGGs	Cytoplasmic RFP	Gift from Prof. Stewart Wilson
GFP-GPI	GFP-GPI-pCAGGs	Membrane GFP	Gift from Prof. Kate Storey
RFP-H2B	pCIG-Insc-H2B-RFP	Histone RFP	Gift from Prof. Kate Storey

### **Protein-soaked bead transplantation into E4+ chicken embryo**

Fertilised chicken eggs were incubated on their sides at 37°C until the appropriate stage. The top of the egg was covered in sticky tape and a window gently cut, ensuring that the embryo and yolk remained undamaged. The inner shell membrane and the clear vitelline membrane were then removed over the area into which the bead was to be transplanted. Affi-gel beads were soaked in protein or PBS control for 24 hours before transplantation. A small incision was made carefully into the epidermal layer and beads were carefully placed securely under the layer. The egg was then sealed with Parafilm or sticky tape before incubation at 37°C for 24 hours. Embryos were then dissected out and fixed in ice-cold 4% PFA in 0.2M Phosphate Buffer and kept at 4°C for 12 to 24 hours. Tissue was then washed several times in ice-cold PBS.

## 2.5 *Ex vivo* experiments

### Mouse spinal cord slice culture for imaging on an inverted microscope

#### *Dissection*

Freshly dissected embryonic or adult spinal cord (dissections described in section 2.2) was mounted in low melting point agarose (Sigma) dissolved in Hank's Balanced Salt Solution (HBSS) (Gibco) in plastic moulds. The solidified agarose was then superglued onto chucks and sectioned at 300 $\mu$ m on a vibrating blade microtome (Leica VT1200 S). Sections were collected into ice-cold L-15.

#### *Mounting slices in collagen*

The sections could then be mounted onto imaging dishes (Fluorodish Cell Culture Dish, 35mm, 23 mm well, Poly-D-Lysine Coated, World Precision Instruments). Spots of rat-tail collagen (made in-house) were made on the imaging dish by pipetting collagen to the required diameter, and removing it with the same pipette. The thin layers of collagen left on the surface were left for 5 minutes to become tacky, ensuring that the spots do not dry out. The spinal cord slices were placed in collagen to coat the tissue, and carefully lifted out with forceps (using the collagen surface tension rather than contact between the forceps and the tissue) and placed onto the collagen spots. After ensuring that the tissue was flat against the bottom of the dish, these beds were left to set. An additional 15 $\mu$ l of collagen was then carefully added to the top, before incubation at 37°C and 5% CO<sub>2</sub> in a humidified chamber (Sanyo). When set, 3 $\mu$ l of 37°C medium was added.

### *Mouse spinal cord slice culture electroporation*

Embryonic mouse spinal cords were electroporated after evisceration, but before sectioning. The embryo was placed flat, dorsal facing upwards in ice-cold L-15. Plasmid mixed with Fast Green FCF was injected into the spinal cord lumen, caudally to the site of interest using a pulled glass needle (1mm x 0.78) until the green-coloured plasmid mixture was visible along the site of interest. The tissue was then subject to a current (100v, 1ms, 10 pulses) using a BTX/Harvard Apparatus ECM 830 Square Wave Electroporator and BTX *In ovo* Genetrode™, bent L-shaped, 3 mm electrodes. The embryo could then be mounted in agarose for Vibratoming (Please see Fig6.1 for diagram).

## 2.6 Media

### Explant medium

Optimem (Gibco)	Base medium
L-glutamine (Sigma)	1%
Pen-strep 100x (Gibco)	1%
Fetal Calf Serum (Sigma)	2.5%*

### SRN2

*Developed in the Placzek Lab*

DMEM-12 (Gibco)	Base medium
L-glutamine (Sigma)	1%
N2 100x (Gibco)	1%
B27-I 50x (Gibco)	2%
Heparin (Sigma)	0.05%

### Brachmann medium 20ml

**Brachmann, I, et al (2007) Developmental Dynamics 236:3514–3523**

DMEM (Gibco)	50%
HBSS Ca <sup>2+</sup> Mg <sup>2+</sup> free (Sigma)	25%
Fetal Calf Serum (Sigma)	25%*
Glucose (Sigma)	0.5%
L-glutamine (Sigma)	0.5%
HEPES	10mM
Pen-strep 100x (Gibco)	1%

### Dundee Media

**Developed in Professor Storey's Lab, University of Dundee**

Neurobasal (Gibco)	Base medium
Glutamax 100x (Gibco)	1%
B27 (Gibco)	2%
Fetal Calf Serum (Sigma)	10%*
Gentamycin (Gibco)	50µg/ml

\*Fetal calf serum is batch tested, and the concentration used depends on the result of the test for each application.

### *Dundee media variations*

For optimisation experiments, alternate media was made with B27 replaced with B27 without insulin (Gibco). Serum-free media was also made, and the difference made up with Neurobasal (Gibco).

## **2.7 Imaging, image processing and statistics**

### **Microscopy**

Fluorescent images were taken on a Zeiss Apotome 2 microscope with Axiovision software (Zeiss) or for high magnification images, on a Nikon Ti system running Nikon Elements AR software or a Deltavision RT system running SoftWorx. Timelapse images were taken on a Deltavision RT system.

### **Image processing**

Images were processed using Image-J (FIJI) and made into composites using Adobe Illustrator. Diagrams were made using Adobe illustrator.

### **Statistics**

Intensity data from images were extracted using Image-J (FIJI) and analysed using Excel (Microsoft).

## **2.8 Molecular biology**

### **Plasmid growth and purification**

Plasmids were introduced into Subcloning Efficiency DH5- $\alpha$  competent E. coli (Invitrogen) plated onto LB Agar (Sigma) with the appropriate antibiotic overnight. Transformed colonies were grown in LB broth (Sigma) with the appropriate antibiotic. Plasmids were purified using a Qiagen Plasmid Purification kit.

### **RNA extraction**

Tissue was dissected into RNAlater (Ambion) and RNA extracted using Trizol (Invitrogen) and Purelink RNA mini kit (Ambion). RNA was extracted into Hyclone HyPure water (GE Healthcare).

### **cDNA synthesis**

RNA was synthesized using SuperScript III First-Strand Synthesis System (Invitrogen) using 50ng/ $\mu$ l random hexamer primers supplied with the kit, and extracted into Hyclone HyPure water (GE Healthcare).

### **RT-PCR reaction**

The *Crb2s* RT-PCR reaction was performed on cDNA synthesized as described in the sections above. *Crb2* mRNA was amplified using conditions described in Table 2.4 at 20 $\mu$ M concentration. Primers described in Table 2.5 were designed to amplify full length mature *Crbs2* and mature secreted *Crb2*. A second round of PCR was then performed, designed to amplify secreted *Crb2* specifically. A GAPDH loading control was run. The reactions were run on an agarose gel with the addition of ethidium bromide (Bio-Rad) and bands of the appropriate size were excised using QiAquick Gel Extraction Kit (Qiagen) and sequenced in-house.

### **DNA electrophoresis**

Agarose gels were made using 1% ultra-pure Agarose (Invitrogen) in 1X TAE (50mM TrisHCl (Sigma), pH 8.0; 1mM EDTA (VWR International), 20mM acetic acid (Fisher Scientific), dissolved by heating in a microwave. 1 $\mu$ l Ethidium Bromide was added before the gel was poured. Loading buffer (Sigma) and deionised water was added to

each sample. Gel was run in 1X TAE at 80V. Bio-Rad DNA Mini Sub Cell GT electrophoresis kit was used for electrophoresis. The bands were visualised using a UV trans-illuminator. A 1kb or 100bp DNA ladder (New England Biolabs) was run alongside the sample.

**Table 2.4** PCR Conditions Table. First and Second (nested) round PCR conditions used in Ch5 listed stepwise.

First Reaction (Transmembrane <i>Crb2</i> )	Nested PCR (Truncated <i>Crb2</i> )
94°C for 5m	94°C for 5m
$\left( \begin{array}{l} 94^\circ\text{C for 30s} \\ 48^\circ\text{C for 30s} \\ 72^\circ\text{C for 1m 30s} \end{array} \right) \times 35$	$\left( \begin{array}{l} 94^\circ\text{C for 30s} \\ 48.8^\circ\text{C for 30s} \\ 72^\circ\text{C for 1m 30s} \end{array} \right) \times 35$
72°C for 10m	72°C for 10m
10°C hold	10°C hold

**Table 2.5** *Crb2* PCR primer table. Primers used in PCR described in Ch5.

Primer	Sequence		Exon	Tm
<b><i>Crb2</i> F</b>	TGTATGTGGGTGGGAGGTTC	[F]	Exon8	59.0
<b><i>Crb2</i> R</b>	TAACGGGAAGTCGCCAAGT	[R]	Exon10	59.0
<b>Nested F</b>	CTACAACCTCAACAGCATCC	[F]	Exon8	59.2
<b>Nested R</b>	GCTTCGGTTGGTAGACTGCC	[R]	Exon9a	58.3
<b>GAPDH</b>	AACGGGAAGCCCATCACC	[F]	-	59.7
<b>GAPDH</b>	CAGCCTTGGCAGCACCAG	[R]	-	58.0

# Chapter 3

Morphology and marker expression of  
the ventricular zone during dorsal  
obliteration of the neural  
tube/developing spinal cord in the  
mouse



### **3.1 Introduction**

The character of the neural tube varies along the rostral-caudal axis, and the progress of development magnifies these differences dramatically. The most rostral neural tube develops into the highly complex structures of the brain, whereas the caudal neural tube forms the simpler spinal cord. This difference is reflected in the stem cell niches present in either structure: the brain harbours the complex and highly active sub-ventricular and sub-granular zones in the adult, whereas the ependymal zone (EZ) of the adult spinal cord central canal is barely proliferative (for excellent reviews: Hugnot and Franzen (2011); Ihrie and Alvarez-Buylla (2011); Seri *et al.* (2004)). As outlined in the Introduction, to date only a few studies have begun to analyse the process of dorsal obliteration and the transition of the embryonic ventricular zone (VZ) to the later EZ of the central canal. None of these studies have systematically analysed the profile of cells around the lumen, nor defined the precise time over which dorsal obliteration occurs. In this chapter I describe my studies in the prenatal mouse, in which I aim to:

1. Determine the time window of dorsal obliteration.
2. Analyse the characteristics of cells that line the lumen over the period of dorsal obliteration.

### **3.2 Mouse dorsal obliteration occurs in a window between E14 and E16**

The early neural tube has a large lumen abutted by the apical side of a single layer of ventricular zone (VZ) cells. These cells proliferate and differentiate to give rise to the various spinal cord cell types present in the adult. The adult spinal cord has a much smaller lumen, and a correspondingly reduced number of ependymal zone (EZ) cells. However, the embryonic process by which the lumen reduces in size has not been

described in detail in mouse. I analysed thoracic sections from the embryonic mouse as detailed in Fig 2.1.

Initially I analysed DAPI-labelled transverse sections to compare the gross morphological changes of the lumen of the mouse neural tube from E13 onwards (Figure 3.1). At E13, early neurulation has completed and the roof plate has formed. The neural tube lumen extends almost the whole dorso-ventral length of the neural tube: the roof plate and floor plate are only a few cells deep. At E14 the roof and floor plates appear marginally thicker – particularly the roof plate. By E15 the lumen of the VZ has obliterated from the dorsal end; leaving it a third of the size that it was E13. Dorsal to the obliterated lumen, cell nuclei appear orientated and elongated in a dorsal-ventral manner and extend into the midline of a nuclei-free area (shown in high powered view, Fig 3.1 A-E'). The lumen further reduces in size dorsally by E16. DAPI-labelled cell nuclei are still detected at a midline position that extends from the dorsal lumen to the outer pia (arrows, Figure 3.1 C'-E'), through the nucleus-free area (the dorsal or posterior funiculus), although nuclei are not as obviously orientated and elongated dorso-ventrally as at E15. There is little lumen size difference between E16 and E17. Together these analyses show that there is a rapid 'window' of lumen obliteration between E14 and E16 (Schematic: Fig 3.17). Importantly, the lumen obliterates mainly from the dorsal apex, confirming that the term 'dorsal obliteration' is an appropriate term (and used hereafter). Additionally, these studies show that at the most acute stage of dorsal obliteration (E15), dorso-ventrally elongated nuclei are detected at the dorsal midline and that as the lumen decreases, the cell free territory surrounding these nuclei extends ventrally.

## Embryonic mouse spinal cord morphology

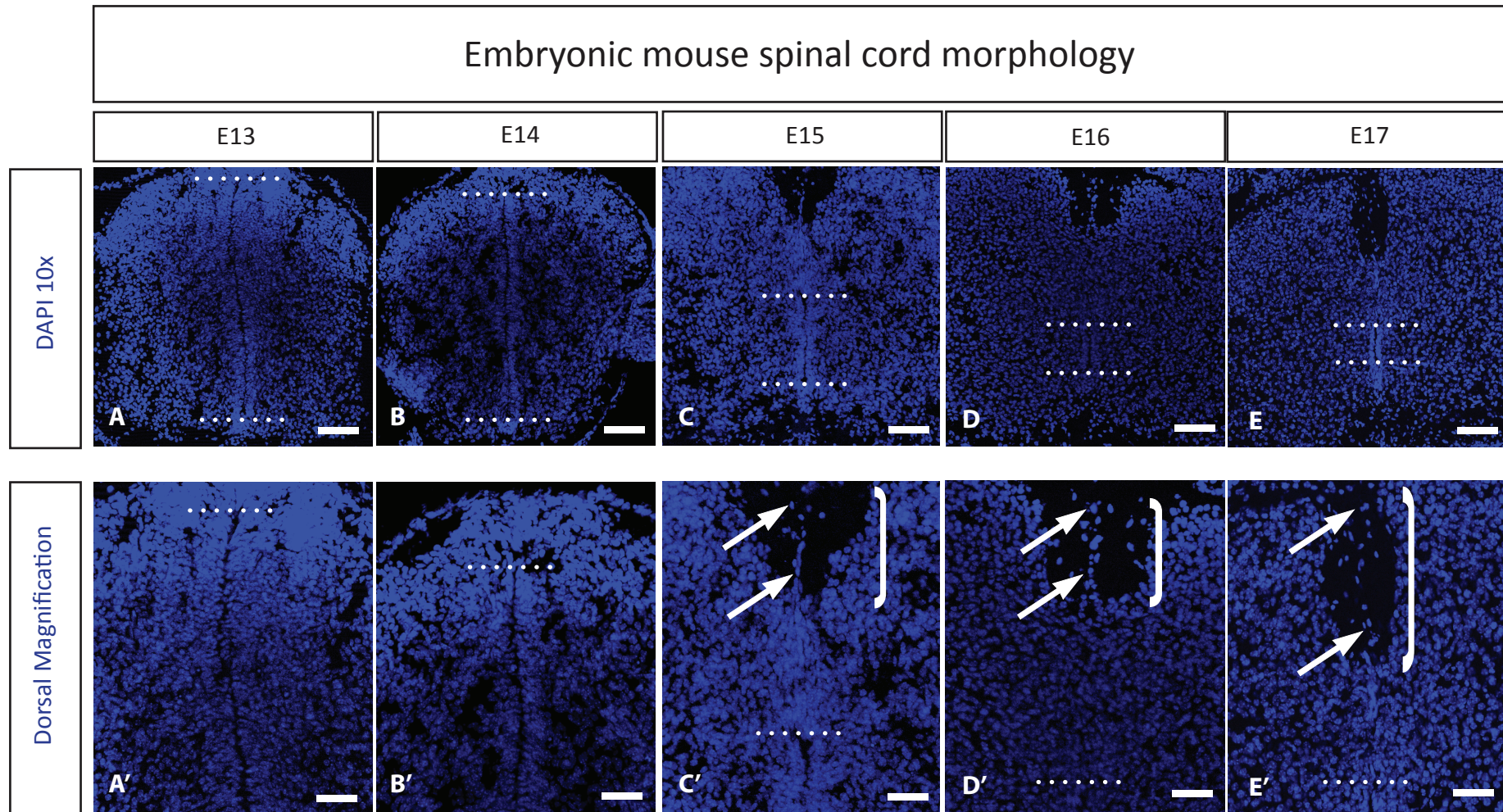


**Figure 3.1** Thoracic transverse sections. DAPI-labelled spinal cords from E13 to E17. Dotted lines mark the dorsal and ventral ends of the lumen. Brackets show the extent of the dorsal funiculus. This area is mainly nuclei-free, except for a stream of cells at the midline (arrows point to dorsal or ventral cells of this midline). Scale bar: (A-E)100 $\mu$ m (A'-E') 25 $\mu$ m.

### 3.3 Marker analysis of lumen-surrounding cells during dorsal obliteration

The pattern of expression of transcription factors, signalling and polarity proteins on cells that line the VZ has been well described at early stages, before dorsal obliteration (see Introduction). These studies show the existence of discrete radial glial populations (Malatesta *et al.*, 2008), and show that stem/progenitor cells that line the VZ can be divided into discrete populations along the dorso-ventral axis, characterised by transcription factor expression (Aigner *et al.*, 2007; Jacob and Briscoe, 2003; Jessell, 2000; Rowitch and Kriegstein, 2010). The profile of cells around the lumen at later stages, *i.e.* during and post- dorsal-obliteration, has been less well characterised (although see Fu *et al.* (2003)). Therefore, I characterised markers to elucidate the identity of lumen-surrounding cells over the period of dorsal obliteration. I reasoned that this analysis might also reveal clues as to the processes that may contribute to dorsal obliteration. Note that in the studies below I focus, in particular, on changes to cells in the dorsal part of the VZ and dorsal lumen, commenting on changes to the ventral aspect only briefly in the Discussion.

#### 3.3.1 Filament proteins

Gross morphological changes such as seen in dorsal obliteration are likely to be reflected in the cytoskeletal structure within the developing tissue. To this end, I analysed expression of F-actin (Figure 3.2) and the intermediate filament protein, Nestin (Figure 3.3).

**F-Actin:** Phalloidin labels F-actin microfilaments. At E14, prior to dorsal obliteration, F-actin is expressed in a uniform manner at the apical zone of cells throughout the VZ

(Figure 3.2 A). Additionally expression of F-actin is detected throughout the spinal cord.

Marked changes are observed by E15. At this stage, expression of F-actin in medial VZ cells is similar to that at E14, but cells at the dorsal and ventral aspect of the lumen show clear puncta of strong expression (white arrow). Additionally, while expression in most regions of the spinal cord is far weaker than at E14 (Fig 3.2 B), rope-like strands of expression are detected at the dorsal midline, extending from the dorsal aspect of the lumen to the pial surface (yellow arrows, Fig 3.2 B, C). At E17, these puncta appear to be more evenly spaced throughout cells that line the lumen (Fig 3.2 C-C'). Together these results show that F-actin undergoes a dramatic change in expression at E15, becoming strongly expressed in distinct puncta at the dorsal apex of the lumen.

**Nestin:** Nestin is a type VI filament protein. At E13 and E14, Nestin is expressed throughout the developing spinal cord on cells with radial glial morphology that extend to the lateral pial surfaces of the spinal cord (Fig 3.3, A, A' and B, B'). From E15, a pronounced change occurs. Expression of Nestin is markedly reduced in these cells, and few Nestin<sup>+</sup> processes are now detected that extend laterally. Instead, two new Nestin<sup>+</sup> populations become apparent, in cohorts of cells and cell processes that project from the ventral aspect of the lumen to the ventral pial surface and from the most dorsal aspect of the lumen to the dorsal pial surface (Figure 3.3, arrows). As the lumen obliterates over E15-E17, the dorsal processes extend, and these contacts are maintained (Fig C-E and C' to E'). The Nestin<sup>+</sup> processes of the dorsal population are restricted to the midline, *i.e.* occupy the same position as the DAPI<sup>+</sup> cell nuclei previously noted in Figure 3.1.

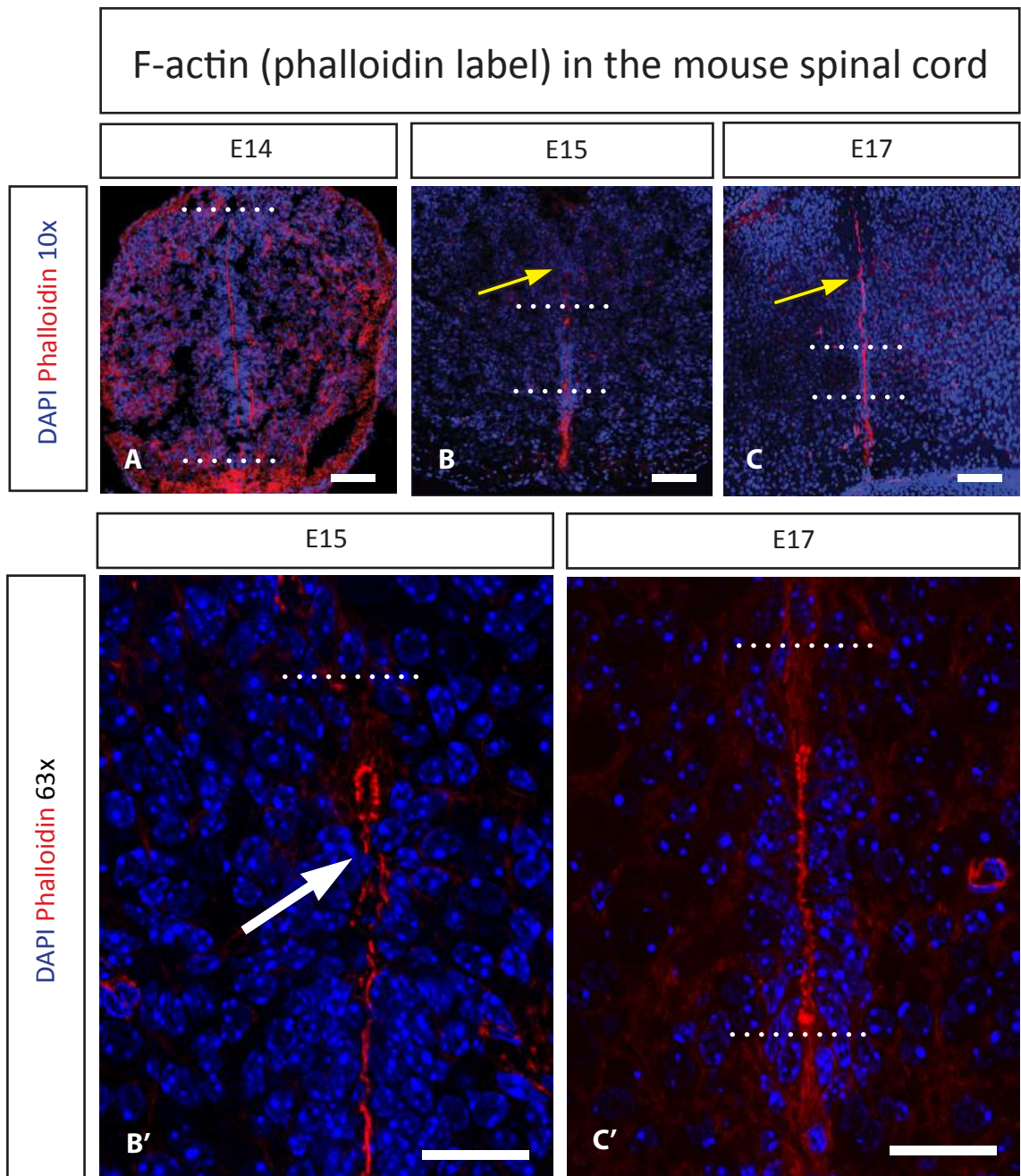


**Figure 3.2** Thoracic transverse sections. F-actin is expressed strongly around the ventricular zone at E14-E17, and also in a dorsal cable (yellow arrow) that begins to be expressed from E15 onwards (A-C). The magnified images (B'-C'') reveal that after E15, there is a gap between the DAPI-labelled nuclei of the dorsal ventricular zone cells (dotted lines) and the phalloidin labelled apical surface. At E15 (B', arrow) there are breaks in the F-actin sub-dorsally, that have disappeared by E17 (C'). Scale bars: 10x, 100 $\mu$ m; 63x, 25 $\mu$ m.

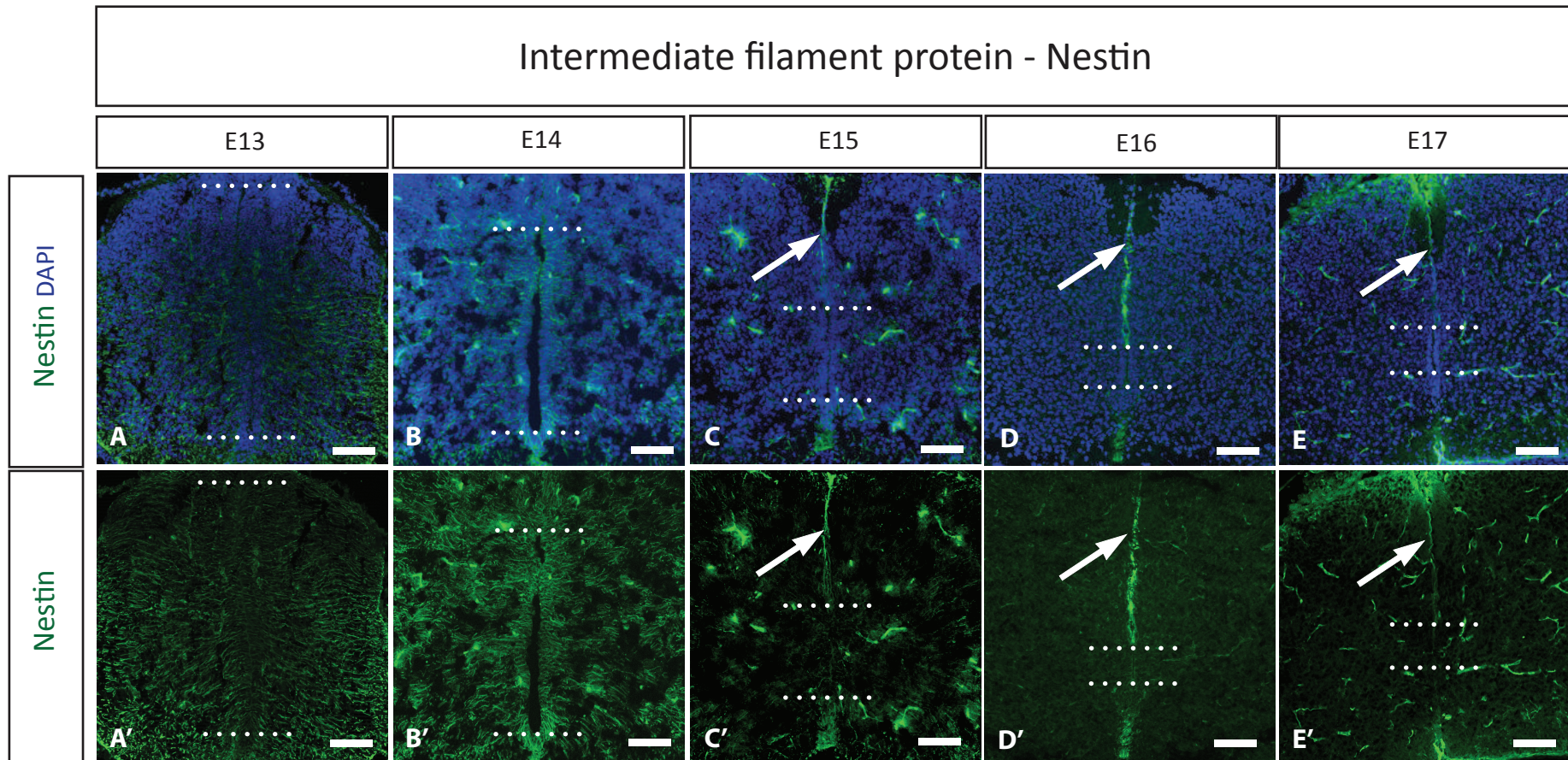


**Figure 3.3** Thoracic transverse sections. Widespread nestin expression decreases as the spinal cord develops. However, a specific cohort of nestin-expressing cells arises after E14 as dorsal obliteration proceeds (arrows). These cells have their cell bodies at the lumen (dorsal and ventral limits as interpreted from DAPI labelling marked with dotted lines) and extend long processes to the dorsal pial surface. Scale bar 100µm.

Together these analyses reveal that the dorsal VZ and the dorsal midline have distinct and high expression of cytoskeletal markers. The dorsal expression of the Nestin filament is especially interesting because it arises just before/at the window of dorsal obliteration and the lengthening Nestin+ processes correlate with the shrinkage of the lumen and with the presence of DAPI+ cell nuclei. Figures 3.11 and 3.12 show a higher power view comparing Nestin with other markers.

### **3.3.2 Transcription Factors**

Many studies have described the distinct domains of transcription factor expression along the dorsal ventral axis of the neural tube (Aigner *et al.*, 2007; Jacob and Briscoe, 2003; Jessell, 2000; Rowitch and Kriegstein, 2010). Both published studies (Fu *et al.*, 2003) and unpublished work in this lab (Chinnaiya, 2011) have demonstrated that adult spinal cord ependymal cells maintain expression of neural stem/progenitor transcription factors, but that these are in a more ventralised pattern than in the embryo. However, no studies have fully characterised the transition of markers from the embryonic to the adult state, nor the mechanism by which they become ventralised. Therefore I characterised the changes in several transcription factor families between E13 and E17.

#### **SOXB1 Transcription factor family**

The SOXB1 transcription factors are widely accepted markers of vertebrate neural stem and progenitor cells (Bylund *et al.*, 2003; Pevny and Placzek, 2005). The SOXB1 proteins comprises three evolutionarily conserved proteins (SOX1, SOX2 and SOX3) and has been demonstrated to be present in the early neural plate and neural tube; initially on neuroepithelial cells and then on VZ cells (Graham *et al.*, 2003; Pevny *et al.*,



1998; Wang *et al.*, 2006). Therefore I first analysed the changes in the expression patterns of these proteins over the period of dorsal obliteration (Figure 3.4).

**SOX1:** At E14 SOX1 is expressed in dorsal and medial VZ cells, but is weak/absent in ventral VZ cells, including the floor plate (Fig3.4 A-C). This pattern of expression persists at E15 and E16. Throughout E14-E16, scattered SOX1-positive cells are found outwith the VZ. In parts, these appear to be clustered – for instance at E16, a densely grouped lateral population is detected. Notable for consideration in my work; throughout E14-E16, SOX1-positive nuclei can be detected at the dorsal midline, *i.e.* dorsal to the obliterating lumen (high power views shown in right hand panels Fig 3.4 B', C').

**SOX2:** Through the stages analysed, E14-E16, SOX2 expression is evenly distributed throughout VZ cells, although expression is weaker in the most dorsal cells (Fig 3.4 D-F). At E15 an additional population of SOX2-positive cells is found radially out from the lateral walls. A dense population of SOX2-positive cells is also found dorsal to the obliterated lumen. Notably, these are similarly oriented and dorso-ventrally elongated to the population of DAPI+ nuclei previously noted in this region (Figure 3.4, E' arrow; high powered view). Indeed, >90% elongated nuclei appear to express SOX2, supporting that they comprise the majority of this population. By E16, fewer SOX2-positive cells are found outwith the VZ. However, a dense cluster of SOX2 cells remains dorsal to the obliterated lumen (Figure 3.4, F' arrows; high powered view). A schematic (Fig 3.17) illustrates SOX2 nuclei positions at E14-E17.

## The SoxB1 Family

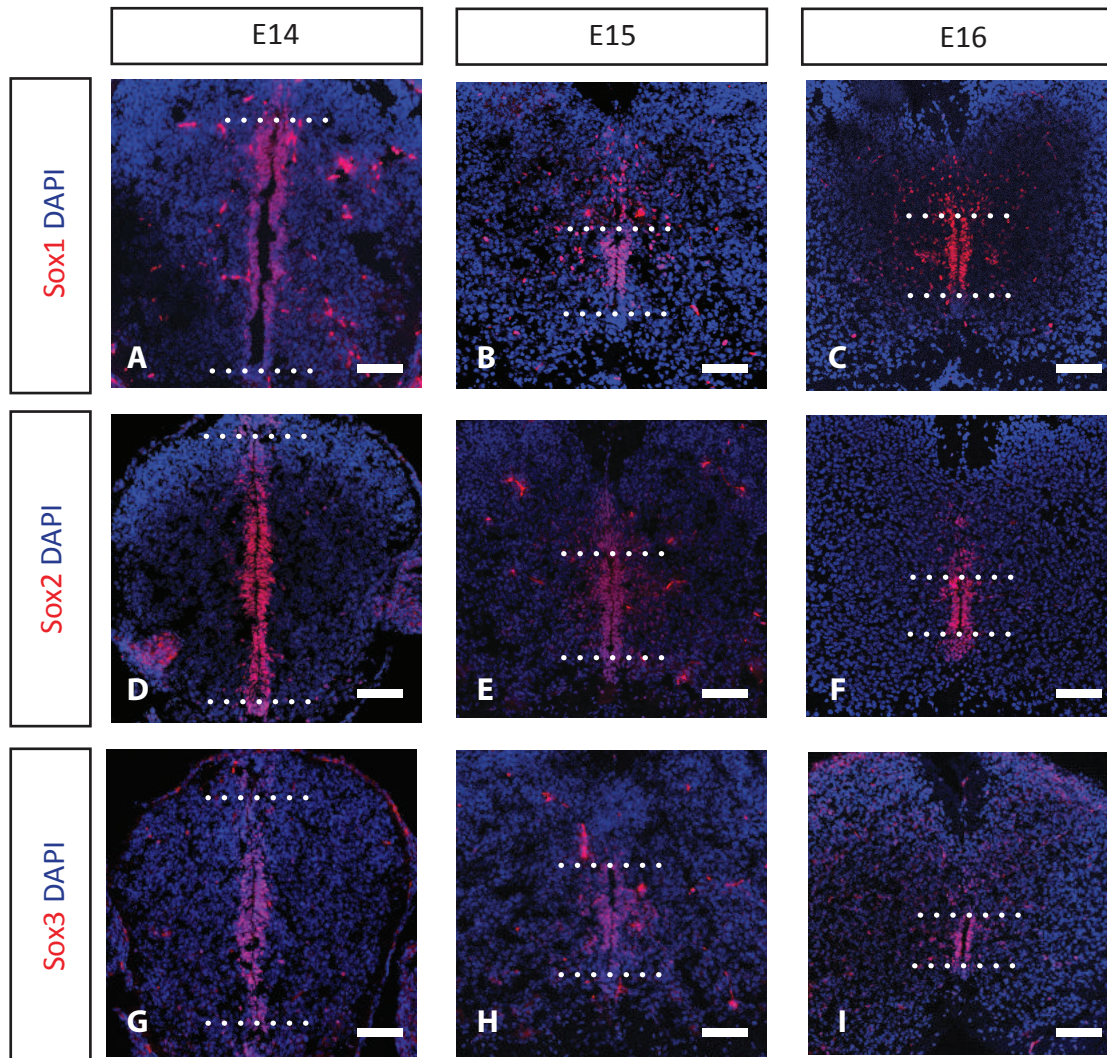
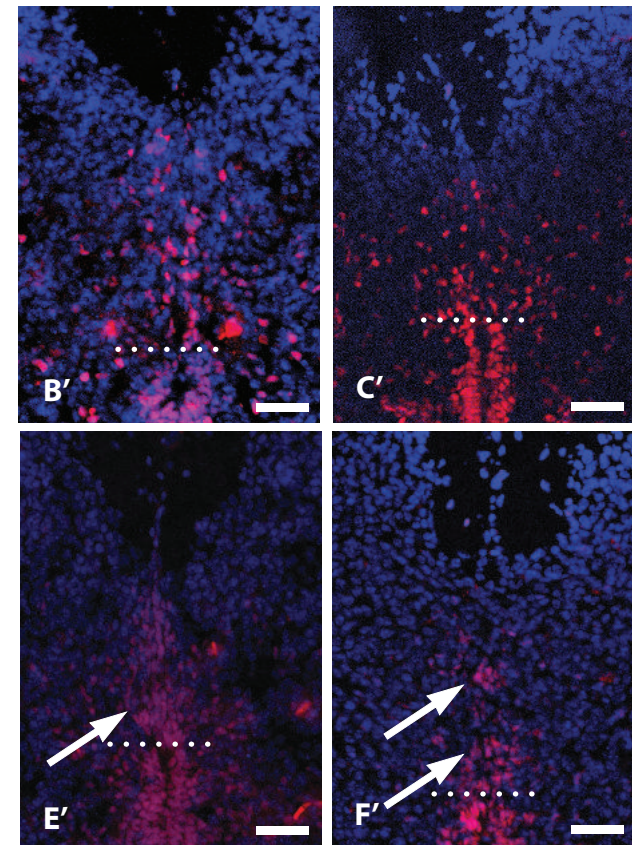


**Figure 3.4** Thoracic transverse sections. The SoxB1 family: Sox1(A-C) Sox2 (D-F) and Sox3 (G-I). Magnified images B'-F'. Lumens marked with dotted lines. Arrows/brackets point to populations of SoxB1 cells outside the lumen (See text). Scale bars: (A-I) 100µm; (B'-F') 25µm.



**SOX3:** At E14, SOX3 expression is detected throughout the VZ, although it is weaker in most dorsal/ventral cells. At E14 and E15 there is no/weak SOX3 expression in the most ventral cells (Fig3.4 G-I)). At these stages, there are a few peripheral SOX3-positive cells lateral to the VZ. As with SOX1 and SOX2, SOX3-positive nuclei can be detected dorsal to the VZ, in or close to the dorsal midline, throughout the period of dorsal obliteration. Second, over the period of dorsal obliteration, weak dorsal expression of SOXB1 declines, leaving only stronger expressing nuclei, such as are detected only ventrally at earlier stages.

#### **Close association between SOX-positive nuclei and dorsal Nestin+ cells**

Both dorsal Nestin+ cells, and oriented SOX2 nuclei are first clearly detected at E15 – *i.e.* at the time that dorsal obliteration is initiating and proceeding most rapidly. To determine whether SOXB1-positive progenitors are closely associated with dorsal Nestin+ cells through the period of dorsal obliteration, I performed double immunohistochemical analysis of Nestin and SOX2 (Figure 3.5). At E15, SOX2 expressing cells are closely associated with the processes of the dorsal Nestin+ cells. Fig 3.11 and 3.12 shows a higher power view comparing SOX2, Nestin and apical proteins at E15/6. By E16, SOX2 expressing cells associate with the dorsal Nestin+ cells in two main groups. There is a patch of SOX2 expressing cells immediately dorsal to the VZ, a gap, and then a smaller, more tightly grouped population of SOX2-positive cells dorsal to that, intercalated with Nestin+ processes. At E17, the SOX2-positive population at the dorsal midline remains clearly intercalated with Nestin+ processes (high power views Figure 3.4 H' and I').

## Nestin and Sox2

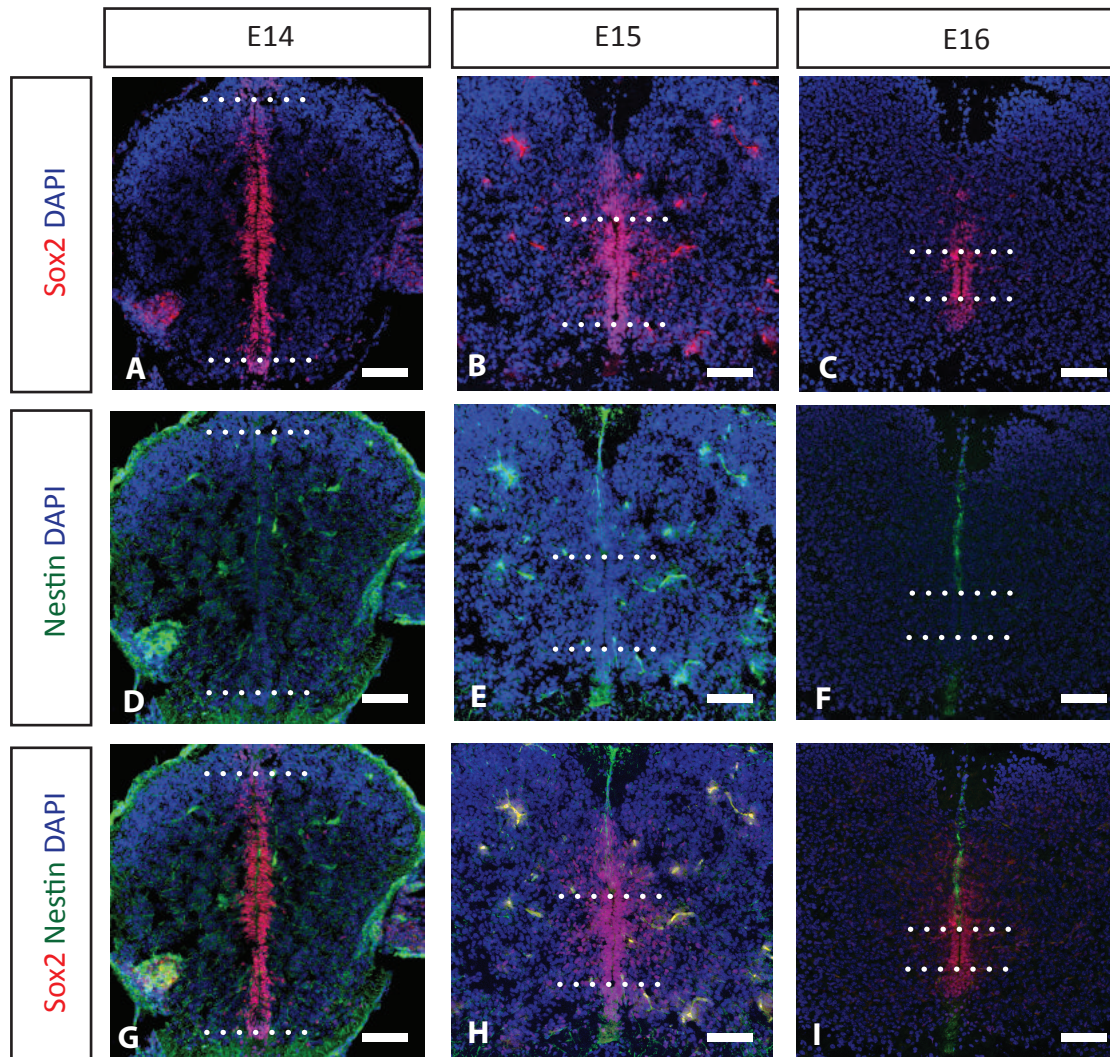
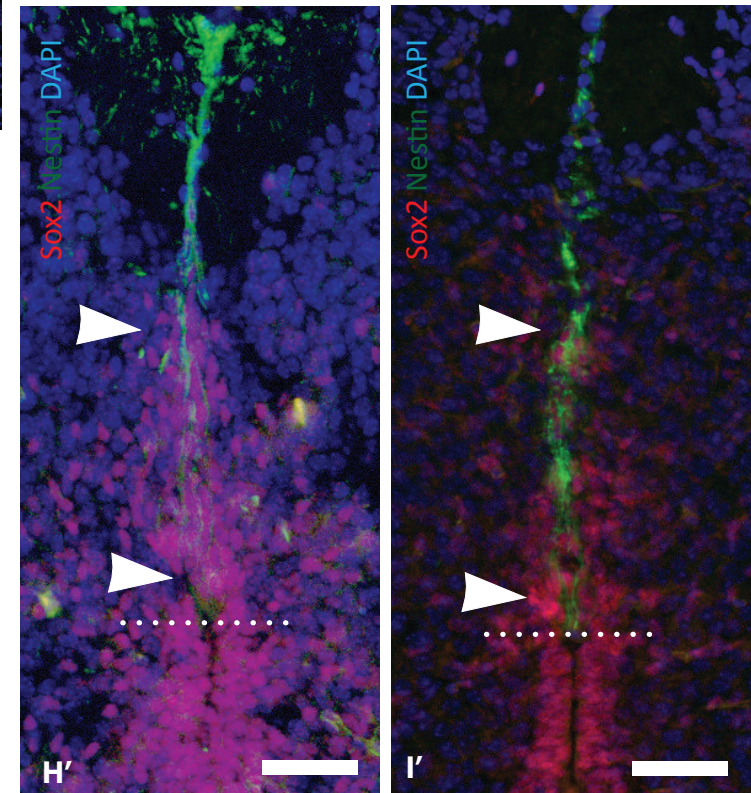


**Figure 3.5** Thoracic transverse sections. Sox2 (A-C) and Nestin (D-F) and the merged image (G-I). Magnified images of (H) and (I) are (H') and (I'). Arrowheads indicate Sox2 cells dorsal to the lumen (see text). Scale bars: 100 $\mu$ m; magnified, 25 $\mu$ m.



### **Dorso-ventral patterned transcription factors**

The morphological and SOXB1 data support the view that the VZ obliterates unevenly, reducing in particular from the dorsal aspect (Fu *et al.*, 2003). As the character of the VZ cells varies along the dorso-ventral axis (Jacob and Briscoe, 2003; Jessell, 2000; Rowitch and Kriegstein, 2010) losing progenitors unevenly from the dorsal aspect would drastically change the nature of the population persisting through development and into the adult. A previous study has tracked progenitor gene expression, and concluded that adult EZ cells are the descendants of ventral VZ cells originating from the pMN and/or p2 progenitor domains as they retain NKX6.1 (p3/pMN/p2) but not NKX2.2 (p3) expression; all other embryonic VZ domains appear to become fully depleted (Fu *et al.*, 2003; Yu *et al.*, 2013). To confirm these studies, I analysed two other transcription factors that are expressed in more restricted domains than the SOXB1 family, PAX6 and NKX6.1 (Figure 3.6).

**PAX6:** The homeobox transcription factor PAX6 has been characterised extensively at younger stages (Huettl *et al.*, 2015; Osumi *et al.*, 2008; Schwarz *et al.*, 1999; Zhang *et al.*, 2010) and classically is expressed in progenitor cells that occupy the dorsal and central part of the early neural tube, before becoming largely restricted to progenitor cells at the VZ in central regions (Pituello *et al.*, 1999; Pituello *et al.*, 1995). In keeping with this, my studies show that at both E13 and E14 PAX6 is expressed most strongly in cells in the middle third of the VZ (E13: Figure 3.6, B). By E16, however, strong expression of PAX6 is detected in the dorsal half of the VZ, where it persists at E17 (E16: Figure 3.6, B').

### Transcription factors: PAX6 and NKX6.1

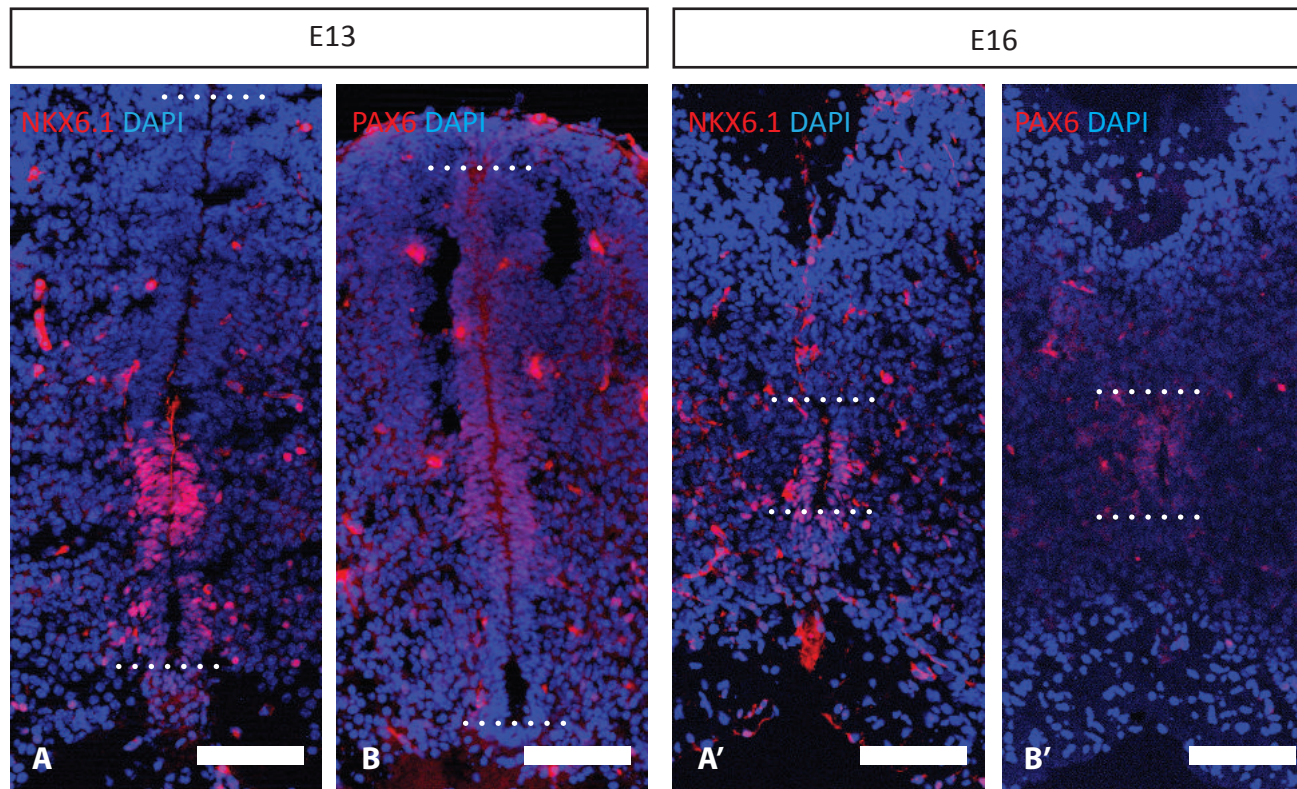


**Figure 3.6** Thoracic transverse sections. NKX6.1 is expressed in the ventral-medial ventricular zone (A, A'). PAX6 is expressed in the dorsal-medial ventricular zone (B, B'). As development progresses, these domains take up relatively larger portions of the ventricular zone. Scale bar: 100 $\mu$ m.

**NKX6.1:** The homeobox transcription factor NKX6.1 has likewise been well characterised at early neural tube stages (McMahon, 2000; Sander *et al.*, 2000). Previous studies have shown that it is expressed in cells that lie just ventral to PAX6-positive progenitors, and indeed, PAX6 and NKX6.1 have been shown to exert cross-repressive interactions on each other's expression (Briscoe *et al.*, 2000; Dichmann and Harland, 2011). In keeping with these studies, I detect strong NKX6.1 expression in the ventral third of the VZ at E13 and E14 (E13: Figure 3.6, A). Serial adjacent sections show that the dorsal boundary of NKX6.1 abuts the ventral boundary of PAX6 expression. NKX6.1 is detected most strongly in the dorsal half of this population, and is much weaker ventrally, and not detected in floor plate cells. In contrast, from E15, the dorsal boundary of NKX6.1 becomes relatively closer and closer to the dorsal lumen, so that by E16/E17, expression occupies the ventral two-thirds of the VZ (E13: Figure 3.6, A').

Together, the PAX6 and NKX6.1 data suggest that cells in the VZ become increasingly ventralised as development progresses over the dorsal obliteration window. Although there are other interpretations (see Discussion), one possibility to account for this is that dorsal-most VZ progenitors, that weakly express SOXB1 proteins and weakly express PAX6, are selectively lost in the process of dorsal obliteration.

### **3.3.3 Junction proteins**

The previous data suggest that progenitors may be lost unevenly from the dorsal aspect of the VZ. Should cells be moving away from the VZ (see later chapters that support this idea) this may be reflected in the junction complexes that maintain the

neuroepithelial integrity. To test this idea, I examined expression of ZO-1, a member of the zona occludens protein family that link tight junctions and cytoskeleton together.

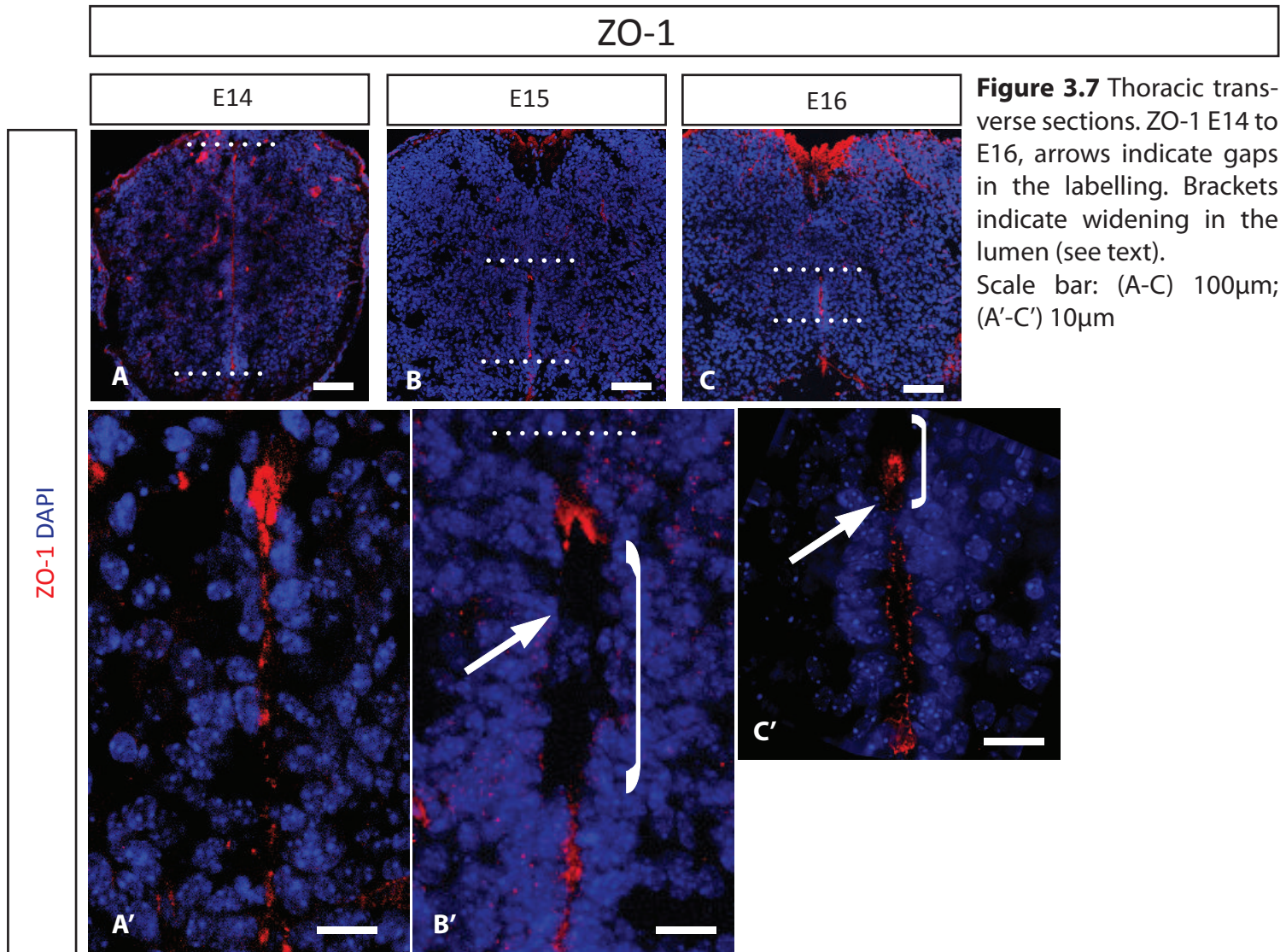
**ZO-1:** At E14 ZO-1 is localized at the apical surface of cells throughout the VZ. It is expressed in a reasonably uniform manner albeit expressed slightly more densely/strongly in cells at the most dorsal and ventral aspects, ZO-1 labelling illustrates that at this time, the lumen is present as a narrow slit throughout its dorso-ventral extent (Fig 3.7A, A'). By E15, there is a marked change in expression of ZO-1. Strong ZO-1 expression is found in cells at the most dorsal and ventral aspect of the lumen. Notably, these cells appear to be very distinct to other VZ cells, as ZO-1 labelling is not associated with a DAPI-labelled VZ-located nucleus (Fig 3.7 B,B').

Immediately below the strong ZO-1 expression, DAPI-labelled cell nuclei are detected in the upper dorsal VZ that show intriguing characteristics. First, no expression of ZO-1 is detected on these cells (arrows). Second, their nuclei appear to show a loose arrangement, and indeed, the adjacent lumen is notably wider (Fig 3.7, B' bracket) than is the case more ventrally, where DAPI-labelled nuclei continue to be arranged tightly around a slit-like lumen, and cells continue to express ZO-1. This characteristic pattern persists at E16, although the gap, marked by ZO-1 negative cells, is smaller than at E15 (Fig 3.7, C, C' and bracket).

Together, this shows 2 conclusions. First, dorsal-most cells of the lumen are distinct in character to lateral VZ cells: they do not have a nucleus that clearly lines the lumen and show strong apical expression of ZO-1. Second, VZ cells that are immediately adjacent to these show a specific loss of ZO-1, suggesting that they lose tight junction



proteins. This, together with the observation that the adjacent lumen widens suggest that such dorsally-located VZ cells undergo profound changes to their integrity at the time of dorsal obliteration.



### 3.3.4 Polarity proteins

The neuroepithelia of the developing spinal cord has clear polarity, apical at the lumen side and basal at the other. As outlined in the Introduction, apical polarity proteins have been implicated in the maintenance of epithelial integrity and in stabilising junctions, and their downregulation is a key step in allowing progenitor cells to differentiate, migrate or remodel cytoskeletal proteins (Gomez-Lopez *et al.*, 2014; Ramahi and Solecki, 2014; Singh and Solecki, 2015; Vorhagen and Niessen, 2014; Wang and Chia, 2005). There are two main apical polarity complexes: the PAR complex, and the CRB complex. Given the intriguing changes in ZO-1 expression, I therefore asked whether I could detect significant changes in expression in polarity proteins over the stages of dorsal obliteration.

**aPKC:** Atypical protein kinase C (aPKC) is a core member of the PAR polarity complex (Chen and Zhang 2013). Similar to ZO-1, at E13 and E14 aPKC expression appears even around the apical side of the VZ, although expression may be slightly stronger at the dorsal aspect (Figure 3.8A, A'). By E15, a subtle change in the pattern is detected. In particular, the loosely-arranged ZO-1-negative cells appear to downregulate aPKC (Figure 3.8, B, B' arrow). Fig 3.11 and 3.12 shows a higher power view comparing aPKC with other markers at E15/16. As noted with the ZO-1 analyses, these cells show a loose arrangement around a wider lumen. The pattern of aPKC therefore adds to the idea that dorsal progenitor cells at the VZ undergo specific changes to their integrity at a time that correlates with the rapidity of lumen size change difference during the obliteration window. The lumen at E16/E17 is less wide and has a less obvious gap in expression than E15 (Figure 3.8 C, C'; D, D')

**CRB2:** CRB is the eponymous transmembrane core protein of the CRB complex (Bulgakova and Knust, 2009). Expression profiling (Figure 3.9) shows that at E13, CRB2 is present around the apical side of VZ cells (Fig3.9 A and A'). Expression appears to be strongest in cells at the most dorsal aspect of the lumen and weaker at the most ventral region. By E15, the strong expression in dorsal-most cells is atypical: first, very strong expression persists at the apical part of the cell (*i.e.* in a similar pattern to ZO-1, Fig3.9 B and B' arrow), second, CRB2 appears to be detected in cytoplasmic regions of dorsal-most cells. Sub-dorsal VZ cells (*i.e.* potentially the ZO-1 negative population) show a very different profile of CRB2 expression over the window of obliteration. In these cells, CRB2 is not detected. However, apical expression can still be detected in more ventral VZ cells. Similar expression persists at E16-E17 although, similar to ZO-1, the extent of CRB2-negative cells at the VZ decreases (Fig3.9 C-D'')

#### **CRB2 association with Nestin**

My results show that CRB2 is expressed in an atypical manner in cells that persist at the dorsal-most VZ throughout dorsal obliteration. Previously I have shown that cells in this region express Nestin. This prompted me to perform double immunohistochemical analyses, to more rigorously compare expression of Nestin and CRB2 (Figure 3.10). At E13, CRB2 and Nestin are evenly distributed around the neural tube lumen and matter respectively (Fig 3.10 A-A''). At E15, when the lumen has obliterated and the long dorsal Nestin process is highly immunoreactive, there appears to be an overlapping area of very strong dorsal CRB2 and Nestin expression (Fig 3.10, B- B'', arrows). Fig 3.11 and 3.12 shows a higher power view comparing CRB2, Nestin and other markers at E15/6. Slight overlap between the two markers is also present at E16 . At E17, there is no overlap between the two markers (Fig 3.9 C-D'').

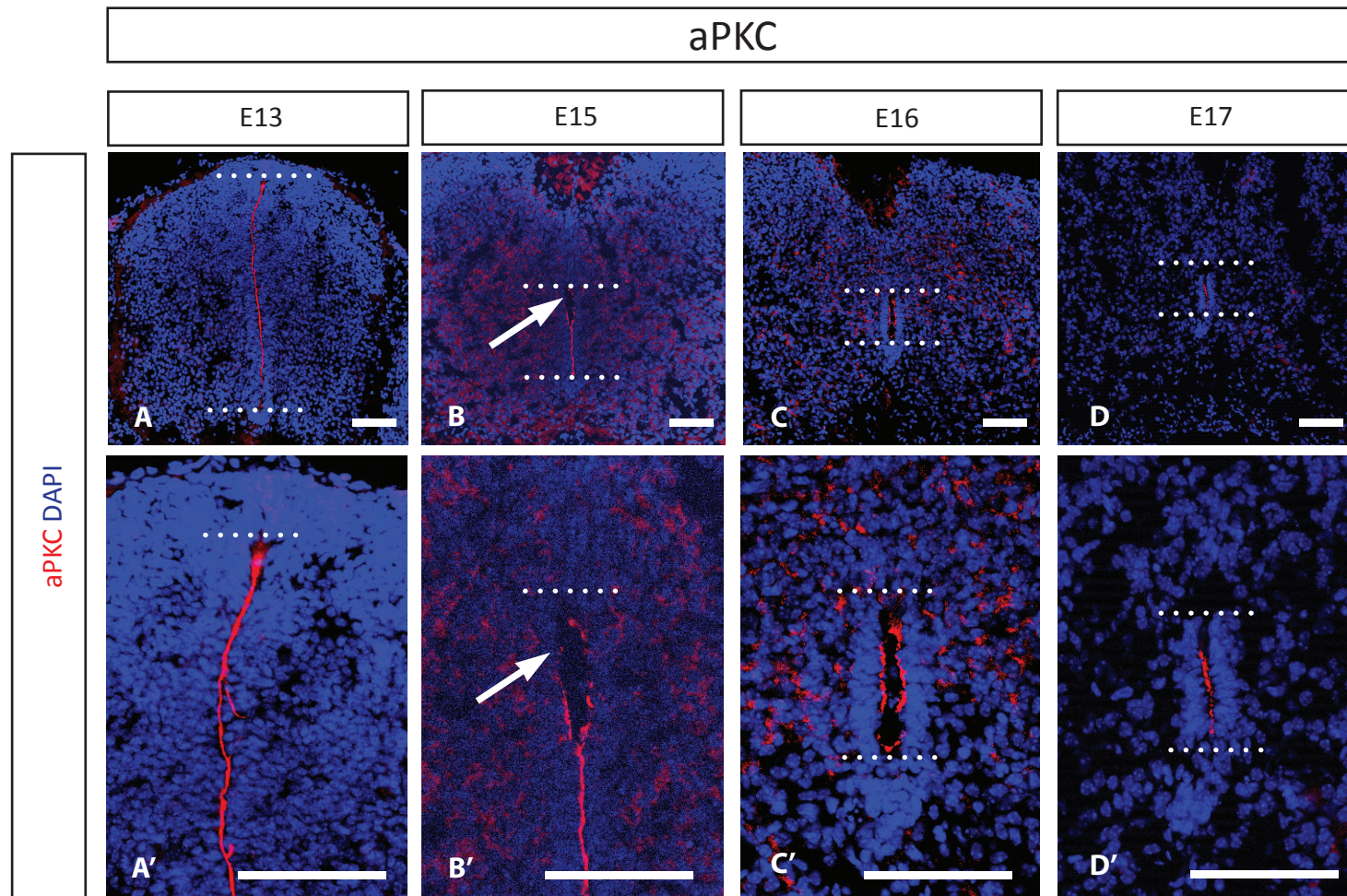


**Figure 3.8** Thoracic transverse sections. E13 to E17, arrows indicating gaps in the labelling. (A' to D') are higher magnification of (A-D) Dotted arrows marking dorsal and ventral boundaries of DAPI labelled nuclei of the lumen.

## Apical Basal Polarity Proteins: CRB2

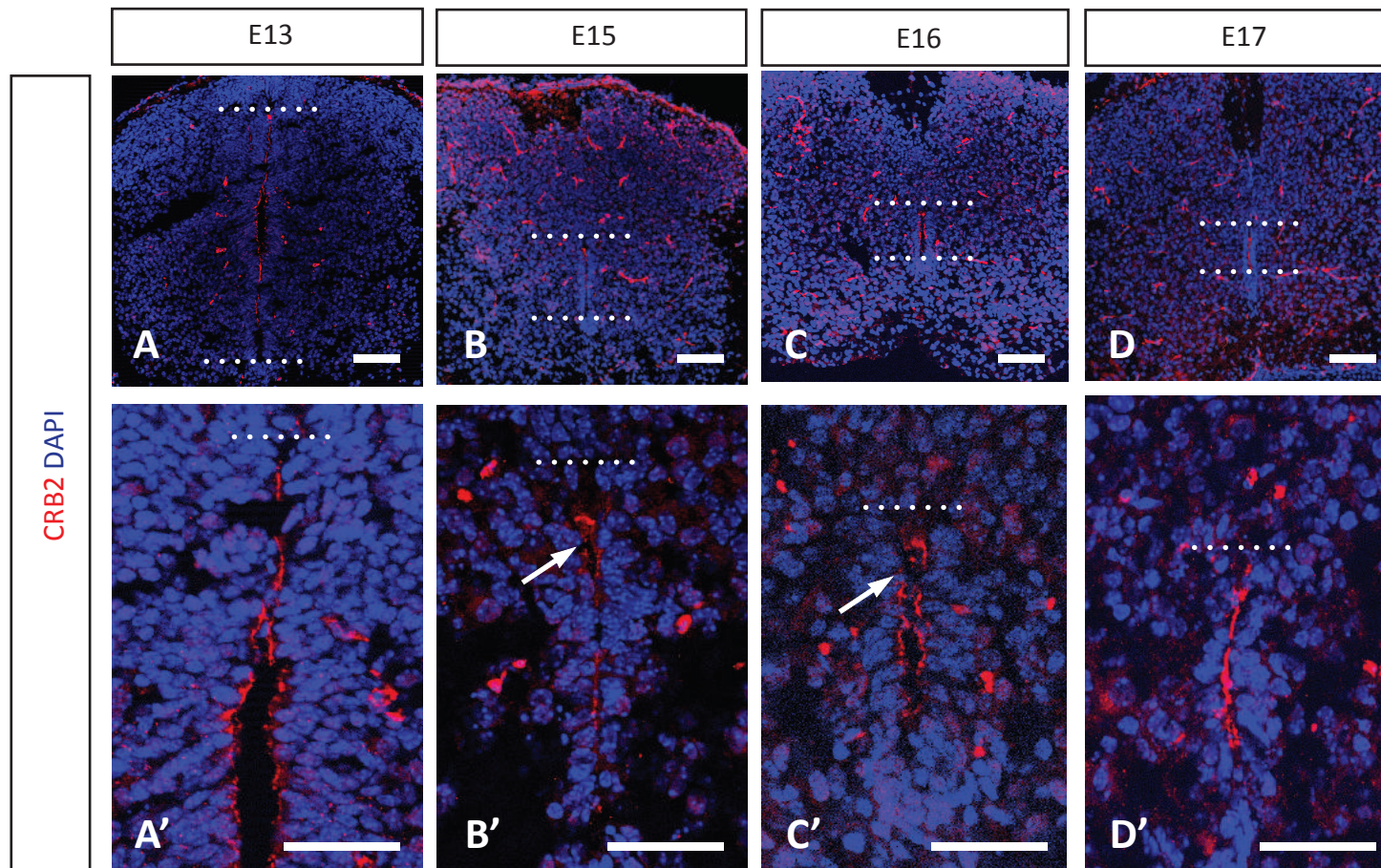


**Figure 3.9** Thoracic transverse sections. CRB2 E14 to E17, arrows indicating gaps in the labelling. Dotted arrows mark dorsal and ventral boundaries of DAPI labelled nuclei of the lumen. Scale bar: (A-D) 100 $\mu$ m, (A'-D') 50 $\mu$ m.

## **Markers analysed clearly define several distinct cell populations in the dorsal neural tube during dorsal obliteration**

A high power image of the E15/16 VZ clearly elucidates the relationship between the markers discussed above (Fig 3.11). A schematic of these images (Figure 3.12) includes nuclei traced directly from (Fig 3.11, A) so that nuclear orientation is depicted accurately. Four distinct types of cells can be described. 1) Lateral VZ nuclei are regular, closely apposed to each other and have a cuboidal shape and uniform aPKC and CRB2 expression. 2) By contrast, dorsal VZ nuclei are more rounded, more loosely arranged, and are clearly removed from the lumen. The endfeet of the dorsal Nestin-expressing Radial Glial-like cells (dNRG) are clearly visible in Fig 3.11 B (yellow arrow). These cells have extremely strong CRB2 and diffuse aPKC expression that is not confined to the apical surface, but instead appears to be either cytoplasmic or perhaps along the membranes of dorsally-reaching processes. 3) Nuclei along the dorsal midline, associated with the dNRG processes but removed from the VZ, are elongated along the dorso-ventral axis, and strongly express SOX2 (also described in Fig 3.4). Sub-dorsal VZ cells also have cuboidal nuclei as opposed to lateral VZ cells, and are loosely organised. They occupy the territory between lateral cells that express apical markers uniformly, and dorsal cells that have extremely high expression of these markers. In this region, the lumen is very wide and apical markers are both weakly and diffusely expressed.

## CRB2 Nestin

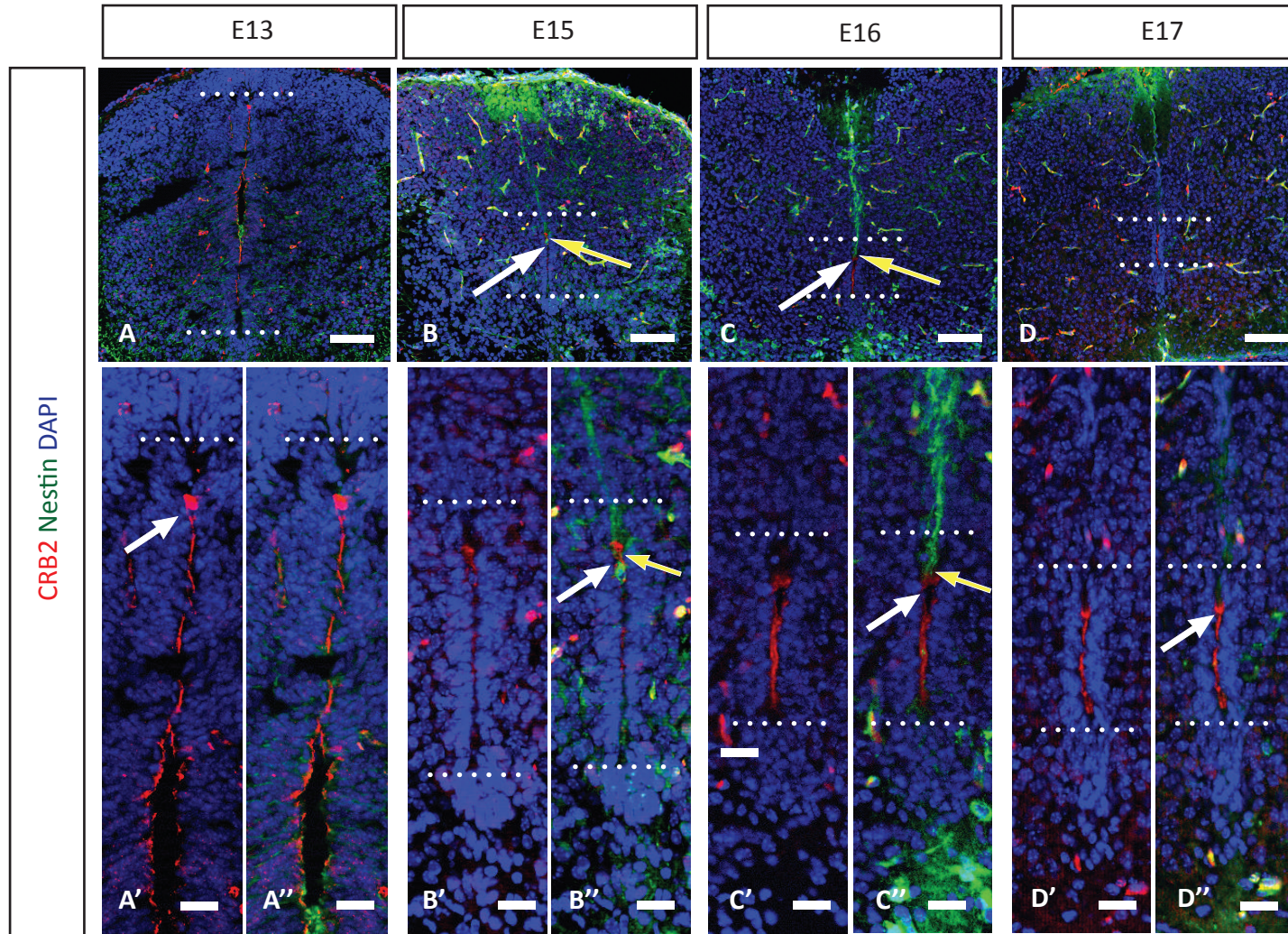


**Figure 3.10** Thoracic transverse sections. E13-E17 CRB2 and Nestin composite images (A-D). (A'-D''). Magnified image of (A-D) below (b). Yellow arrows: overlapping dorsal expression of CRB2 and Nestin. White arrows: sub-dorsal gaps in CRB2 expression (see text). Dotted arrows mark dorsal and ventral boundaries of DAPI-labelled nuclei of the lumen. Scale bar: 100µm



E15/16 mouse ventricular zone - high power

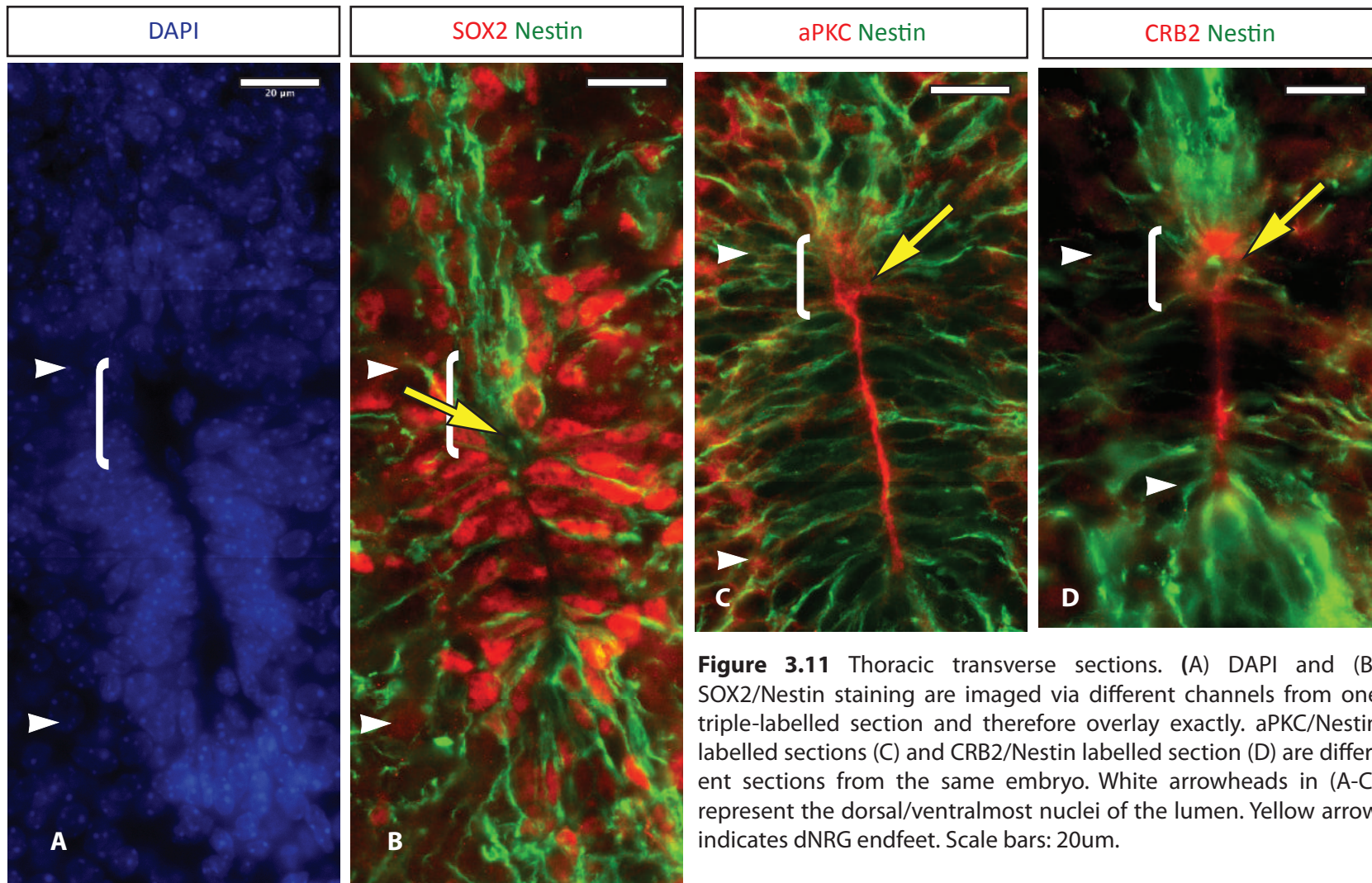


**Figure 3.11** Thoracic transverse sections. (A) DAPI and (B) SOX2/Nestin staining are imaged via different channels from one triple-labelled section and therefore overlay exactly. aPKC/Nestin labelled sections (C) and CRB2/Nestin labelled section (D) are different sections from the same embryo. White arrowheads in (A-C) represent the dorsal/ventralmost nuclei of the lumen. Yellow arrow indicates dNRG endfeet. Scale bars: 20um.

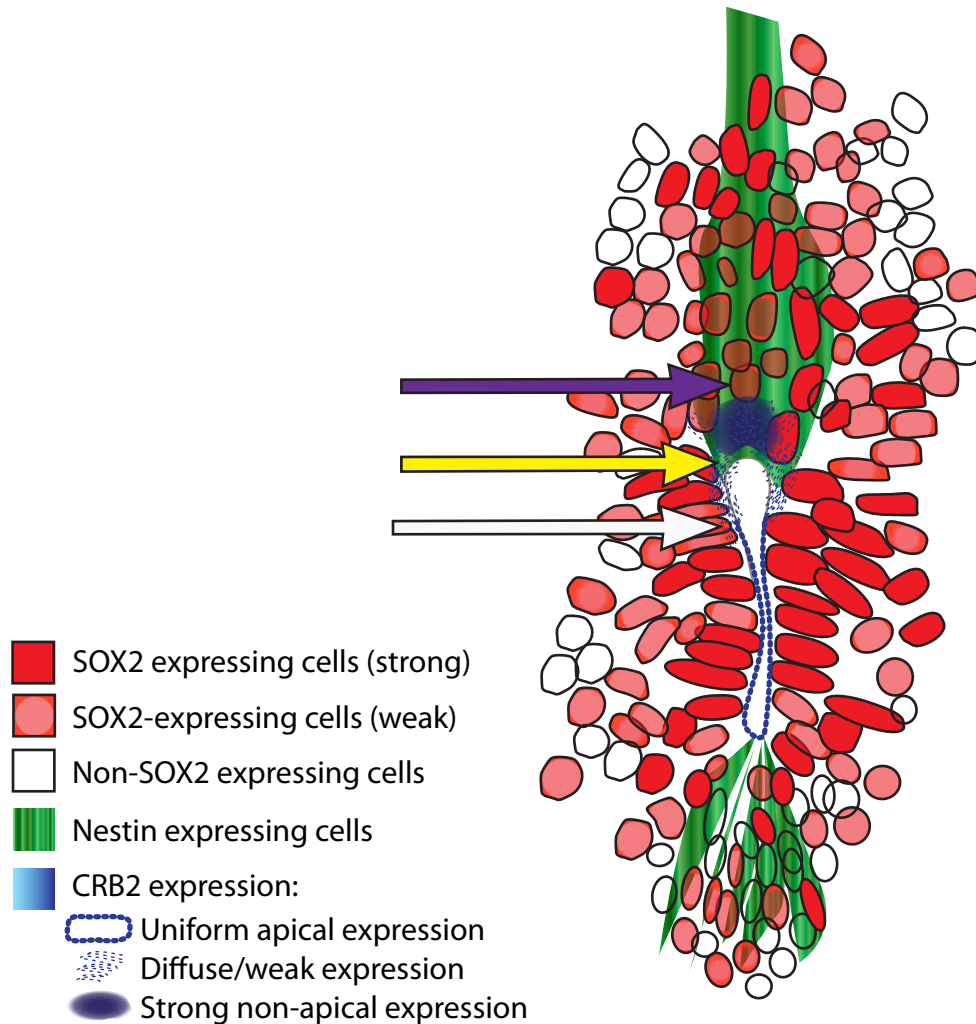


**Figure 3.12:** Schematic of SOX2/Nestin/CRB2 as imaged in Fig 3.11

Only nuclei are depicted, as cell bodies cannot be resolved. Nuclei have been traced, and therefore are an accurate representation of nuclear orientation.

Nuclei are depicted as either SOX2 negative (white), weakly (pink) or strongly expressing (red) SOX2.

Strong Nestin expression stretches dorsally from the apical surface and along the dorsal midline. The endfeet of the nestin-positive processes terminate at the apical surface (yellow arrow).

CRB2 expression is uniform around the ventral/lateral nuclei. Expression is more diffuse at the apical surface of two sub-dorsal cells (between the white and yellow arrows). The most dorsal cells have extremely strong, but diffuse, CRB2 labelling that is not restricted to the apical surface.

Most ventricular zone cell nuclei abut the lumen. Dorsally, there is a gap between the apical surface (yellow arrow) and the dorsal ventricular zone nuclei (purple arrow), likely filled with the processes of the Nestin-expressing cells. This dorsal region that is free of nuclei also exhibits strong CRB2 expression on cell processes and/or within the cytoplasm.

### **3.4 Statistical analysis of CRB2, aPKC, and ZO-1 labelling**

To determine whether the patterns of apical proteins described in this chapter visually from experimental sections were a real effect we attempted to perform a statistical analysis of these data. These imaging data were taken from several different experiments, using a variety of staining and imaging protocols that were not standardised between images. However the data were collected, each image still retains information on the apical markers with regard both their intensity and position across the lumen. Therefore, we attempted to see whether any useful data could be extracted from those images despite the fact that a direct comparison of these raw data would be inappropriate.

Previously in this Chapter we describe 'dorsal' and 'sub-dorsal' regions. The dorsal region is defined by the presence of strong nestin expression, and the sub-dorsal region is described as being directly ventral to that region; defined by a looser arrangement of nuclei and associated with a lower intensity of apical protein expression. However, these criteria are unhelpful for these tests as not all images contain nestin labelling, and apical intensity can clearly not be used to define the test area for these images.

We used FIJI to draw regions of interest (ROI) to define five adjacent regions around the lumen named; Cytoplasmic Dorsal, Dorsal, sub-dorsal region 1 (SD1), sub-dorsal region 2 (SD2), and Medial. Two 'subdorsal' regions were described as 1) the extent of the subdorsal region in which of apical intensity appeared lower varied in size and 2) in images without Nestin expression labelling we did not know the extent of the Nestin+ domain. The position and size of ROI with respect to the lumen in each image was

directly defined by the position of the “Dorsal” ROI. All ROI were placed sequentially along the lumen, with all regions being progressively more dorsal of the Dorsal ROI yet adjacent to the preceding ROI in the order SD1, SD2 and Medial, with the exception of Cytoplasmic dorsal which was immediately ventral of the Dorsal ROI. All ROI within each image were of the same area as the Dorsal ROI except for the Medial ROI which was exactly twice this area in order to capture a more representative average of the main length of the lumen. Due to variation in the size of lumen in different embryos at different stages of development, box size was determined in each image to appropriately represent the most dorsal region of the lumen as determined by a Nestin-labelled channel, then replicating box size for the other areas and a box twice the area for medial. This guide was then applied to all other images, using the dorsal-most apical labelling of the lumen surface to position the ‘dorsal’ region, then placing all boxes sequentially around it as described above. In the event that there was a clear disruption to the lumen (*e.g.* a tear), boxes were not placed adjacent to each other, but were moved to cover the next whole region of lumen. Where two apical surfaces were laterally too far apart to fit into one box the box was split into two equal halves to cover each lumen surface (both left and right) and these data across the two boxes averaged. The average pixel intensity for the relevant apical marker across the area of each ROI was measured.

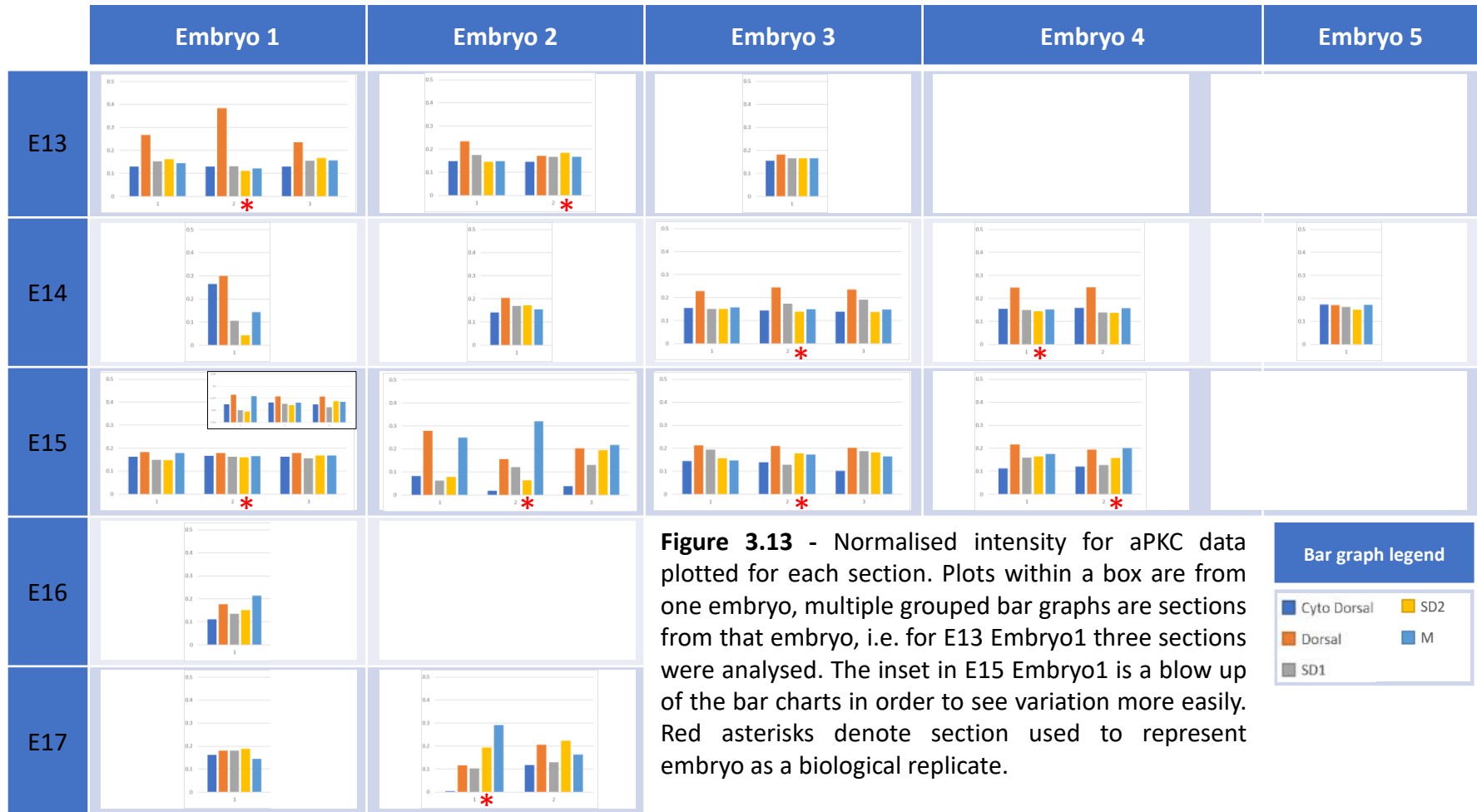
The raw average intensity values across each ROI is not directly comparable between images, so a normalisation approach was adopted so that the relative differences of average pixel intensity between ROI within images could be compared against each other on a similar scale. The normalisation method adopted was a division of each average pixel intensity of ROI from an image by the total pixel intensity (brightness)

gathered from all ROI in that image which is calculated as the sum of the average pixel intensity of each ROI multiplied by its area for all ROI from that image. This normalisation helps to take account for the differences between images by only comparing intensity data within its own image to scale, thus keeping the information on the general relationship of intensity between the regions at the cost of the absolute intensity data. The normalised data from all sections examined are displayed individually in Figures 3.13, 3.14 and 3.15 and data for each apical marker are compiled together with respect to embryonic day of development in Figure 3.16. In general, there seems to be a clear trend that Dorsal is the brightest region, cytoplasmic Dorsal as the dimmest region and that the relative brightness of the remaining three regions (SD1, SD2 and Medial) are generally more similar.

It is important to note that not all images examined are independent of each other. Indeed, several images are different sections from the same embryo (Figures 3.13, 3.14 and 3.15). A statistical analysis based on the whole dataset would not be appropriate since the test could be easily skewed by a disproportionate contribution of sections from the same embryo that is not reflective of biological replication. To address this problem, one section from each embryo was used for statistical tests (highlighted by a red asterisk in Figures 3.13, 3.14 and 3.15). The sections used for statistical testing from each embryo were those from the mid-thoracic region of the embryo. In the event that there were multiple sections from the mid-thoracic region, a section was selected at random. This procedure roughly halved the size of the dataset and took the total number of samples from aPKC from  $n=29$  to  $n=15$ , Crb2 from  $n=26$  to  $n=13$  and Zo-1 from  $n=27$  to  $n=14$ . All the biological replicate data for each marker are compiled into box and whisker diagrams that provide a general description of the

data that are similar to the equivalent charts built from the whole dataset (Figures 3.16). This observation implies that the whole datasets are not disproportionately skewed by any overrepresentation of multiple sections from any one embryo.

Given the fact that the data is not directly comparable with regard the collection methods and absolute values, it was determined that statistical tests based upon ranked average pixel intensity (from brightest to darkest within each image) were the most appropriate. Since the patterns described earlier in this chapter were not concerned with the signal intensity from the cytoplasmic dorsal region, this region was not included in the analyses. Two claims were made based on the the patterns described earlier in this chapter; firstly, that the dorsal region was usually the brightest part of the lumen and, secondly that the sub-dorsal region tended to be darker than the rest of the lumen. The first question of whether the Dorsal region tends to be brighter than the rest of the lumen can be assessed using the ranked data by asking whether the Dorsal region is the brightest region for each marker at a disproportionate frequency and tested using an exact binomial goodness of fit test. Each ROI was ranked according to its average pixel intensity against the other ROI in its image from Rank1 (brightest) to Rank4 (dimmiest). This was done for each biological replicate for each apical marker. The frequency by which each region occupied these four ranks across all time points for each marker was recorded (Table 3.1).



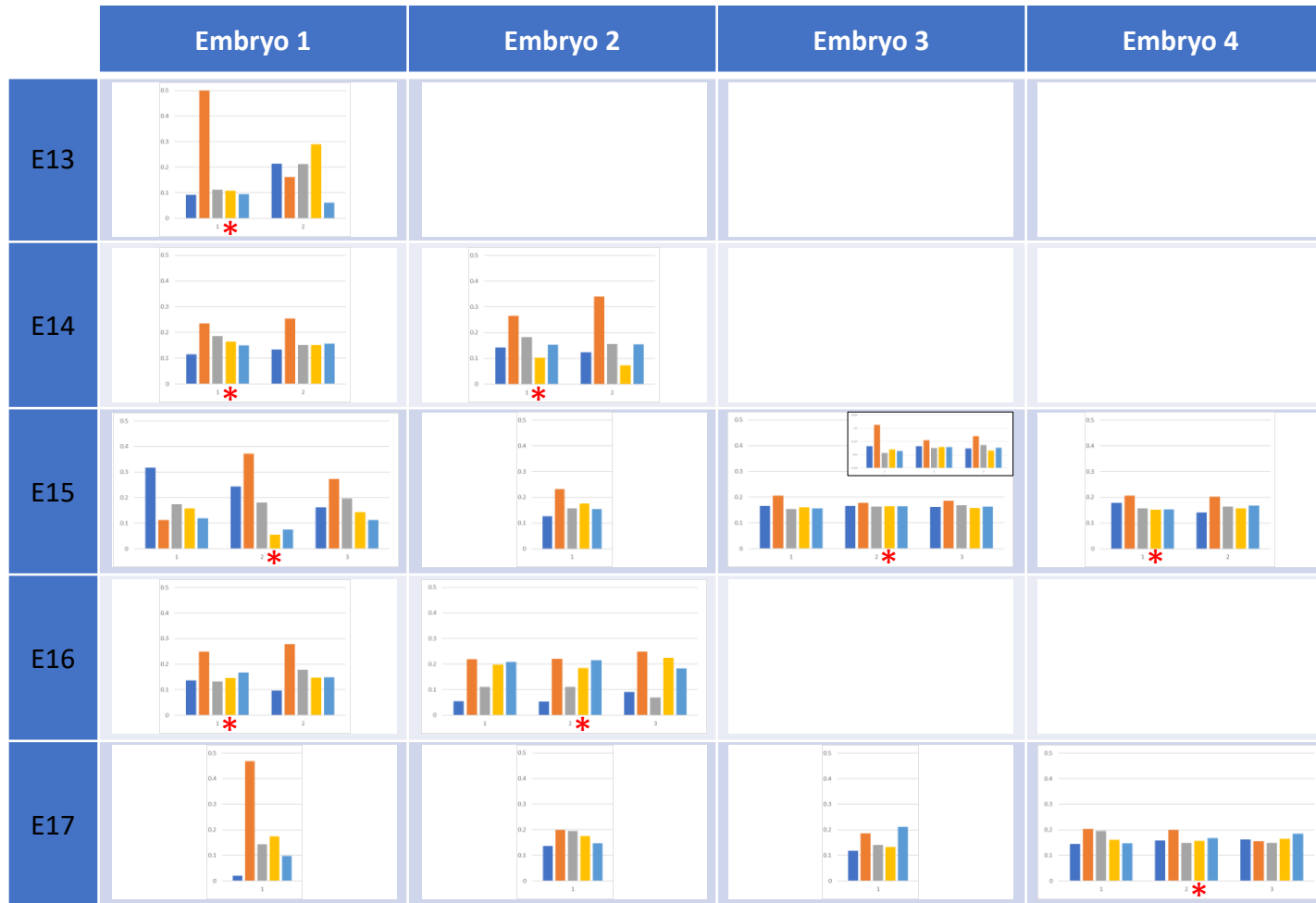


**Figure 3.14** – Normalised intensity for CRB2 data plotted for each section. Plots within a box are from one embryo, multiple grouped bar graphs are sections from that embryo, i.e. for E15 Embryo1, three sections were analysed. The inset in E15 Embryo3 is a blow up of the bar charts in order to see variation more easily. denote section used to represent embryo as a biological replicate.

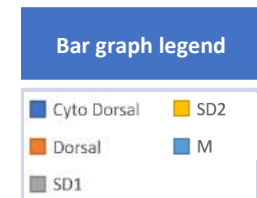






**Figure 3.15** – Normalised intensity for ZO-1 data plotted for each section. Plots within a box are from one embryo, multiple grouped bar graphs are sections from that embryo, i.e. for E16 Embryo2 six sections were analysed. The inset in E14 Embryo2 is a blow up of the bar charts in order to see variation more easily. denote section used to represent embryo as a biological replicate.

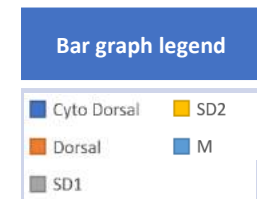




**Figure 3.16** Normalised intensity data (arbitrary units) from Cytoplasmic Dorsal, Dorsal, Sub-Dorsal1, Sub-Dorsal2 and Medial regions from all measured sections are displayed. When  $n \geq 5$ , a box and whisker charts is used. When  $n \leq 5$ , the data are represented in a bar chart, with each bar colour representing a different section. The data are divided according to embryonic day of development from E13-E17, with the two final columns displaying the data from all timepoints. The “All” column represents all sections from the dataset, regardless of timepoint whereas the “Biological replicates” column uses one section from each embryo as indicated in Figures 3.13, 3.14 and 3.15.

**Box and Whisker Legend**



	aPKC				Crb2				Zo-1			
	Dorsal	SD1	SD2	M	Dorsal	SD1	SD2	M	Dorsal	SD1	SD2	M
Rank 1	9	0	1	5	12	0	0	1	11	0	2	1
Rank 2	5	3	4	3	1	6	3	3	2	10	1	1
Rank 3	1	8	2	4	0	3	6	4	1	1	5	7
Rank 4	0	4	8	3	0	4	4	5	0	3	6	5

**Table 3.1** Each ROI was ranked according to its average pixel intensity as compared to the other ROI in its image, from Rank1 (brightest) to Rank4 (dimpest) and the rank frequencies across all biological replicates for each apical marker tallied.

	aPKC			Crb2			Zo-1		
	SD1	SD2	M	SD1	SD2	M	SD1	SD2	M
Rank1	3	4	8	6	3	4	9	3	2
Rank2	8	3	4	3	6	4	2	5	7
Rank3	4	8	3	4	4	5	3	6	5

**Table 3.2** Rank frequency data used to determine whether SD1 or SD2 is usually dimmer than the medial ROI. Three regions SD1, SD2 and Medial were ranked according to their brightness from Rank1 (brightest) to Rank3 (dimpest) and the rank frequencies across all biological replicates for each apical marker tallied.

	Zo1 E16 Embryo2			
	Dorsal	SD1	SD2	Medial
Rank 1	6	0	0	0
Rank 2	0	1	0	5
Rank 3	0	2	4	0
Rank 4	0	3	2	1

**Table 3.3** Test of inter-embryonic variation. Four regions, Dorsal, SD1, SD2 and Medial were ranked according to their brightness from Rank1 (brightest) to Rank4 (dimpest) and the rank frequencies across six serial sections from one embryo tallied.

If there were no presumed association of the apical marker to any particular region, it would be expected that the brightest region would be distributed at random among categories in accordance to experimental noise. Therefore, the null hypothesis suggests that dorsal is brightest region in one quarter of all images. For each apical marker, the dorsal region was brightest significantly frequently (exact binomial test of goodness of fit, two tailed; aPKC, 9 of 15 samples,  $p=0.00419$ ; Crb2, 12 of 13 samples  $p=5.96 \times 10^{-7}$ ; Zo-1, 11 of 14 samples  $p=4.0 \times 10^{-5}$ ).

In a similar fashion, we wanted to test whether SD1 or SD2 were generally darker than the rest of the lumen as represented by the medial ROI. For this test, the dorsal data is not relevant and so were not included. Thus, the three regions SD1, SD2 and Medial were ranked according to their brightness from Rank1 (brightest) to Rank3 (dimpest) (Table 3.2). In this scenario, there are only six possible orders in rank for these regions, and under the null hypothesis, each scenario has an equal probability. The question we are asking is whether Medial is the dimpest region less frequently than expected, since by implication if it is not the dimpest, either SD1 or SD2 must be. Under the null hypothesis that there is no association between lumen position and apical marker intensity, it is expected that the ranks be distributed randomly across these categories in accordance with experimental noise and, it is therefore expected that Medial is the dimpest region in one third of all images

For each apical marker, there was no significant deviation from the expected frequency that Medial was ranked the dimpest marker. For the marker aPKC, Medial was dimpest in three of fifteen samples, which was less frequent than the expected frequency (expected=5) but this was not significant (exact binomial test of goodness of

fit, two tailed,  $p=0.41$ ). For Crb2 Medial was ranked dimmest more frequently than expected (expected=4.33) but this was not significant (exact binomial test of goodness of fit, two tailed,  $p=0.77$ ). For ZO-1 Medial was dimmest almost exactly as frequently as expected to the nearest whole number (expected=4.67) and this is self-evidently not significant.

In almost all cases where multiple sections from a single embryo were available, the number of sections was low with the maximum number of 3 per embryo in all cases except one. For the marker ZO-1 on embryonic day 16, one embryo has data analysed from six different sections. This is the only example where there is enough data to examine whether these same patterns examined above are seen within serial sections of the same embryo. As above, the average pixel intensity was ranked for the Dorsal, SD1, SD2 and Medial regions from rank1 (brightest) to rank4 (dimmest) (Table 3.3). The null hypothesis that Dorsal should be brightest in one quarter of all images applies also in this example. In this embryo, Dorsal was ranked brightest in all six sections which is a significantly higher frequency than the expected 1.5 (exact binomial test of goodness of fit, two tailed,  $p=2.44 \times 10^{-4}$ ). Since all six sections had dorsal as the brightest region, the respective rankings of the rest of the regions would remain unchanged if the Dorsal region removed as previously so these data have not been compiled again as before, however it is possible to test whether the Medial region was dimmest as compared to SD1 or SD2 only using their rankings in Table 3.3. Again, the null hypothesis that Medial should be dimmest in one third of all samples also applies here. In this embryo, Medial was the dimmest region in one out of six sections, which is a lower frequency than the expected 2 times, but this was not significant (exact binomial test of goodness of fit, two tailed,  $p=0.671$ ).

## Statistical Conclusion and Discussion

Despite the fact that these experiments were not designed to be directly comparable with each other and are unfit for parametric testing, we have been able to apply methods that extract useful information from these images that enabled the ability to interrogate whether the patterns described visually in this chapter could be supported in a quantitative manner. The approach of average pixel intensity normalised by the total brightness across sections provides a numerical basis for comparison of trends of apical marker expression in different regions (figures 3.13-3.15) These data show that across the all markers and timepoints analysed, Dorsal was the brightest of any of the areas analysed. Expression of aPKC follows that trend at all embryonic days analysed. SD1 also appears to be less bright than Dorsal, SD2 or Medial at almost every timepoint, except E14, at which point both SD2 and Medial are less bright than this point, although SD2 is the least bright. For CRB2, Dorsal is consistently brightest. However, in general, brightness decreases more ventrally. However, At E16 SD1 appears to be least bright. ZO-1 is consistently brightest in the dorsal region. Like Crb2, the trend seems to be to become less bright ventrally. However, at E16 both SD1 and SD2 are less bright than either Dorsal or Median. Cytoplasmic dorsal is generally the least bright of all the samples. Although these normalised data provide a method by which to identify general patterns by comparing all the sections on a similar scale, it is liable that any analysis performed on these data would be misleading since it cannot account for systematic differences in data collection, such as differences in microscope detection efficiencies.

The other method applied exploited the fact that the average pixel intensity allowed for a ranking of brightness of each region within its section. These ranks could then be

tallied and allowed for a statistical interrogation of the frequency data by means of a binomial exact goodness of fit test; one of the few statistical tests that could be used to interrogate a small dataset such as this. That said, these data demonstrate that the Dorsal region of the lumen is usually the brightest region of those tested, regardless of time point for the three markers tested. Additionally, in the one case where data were available (these tests require a minimum of four sections), it could also be demonstrated that serial sections from the same embryo showed that the dorsal region was the brightest region regardless of section. It could not be demonstrated, however, that the sub-dorsal regions tended to be dimmer than the rest of the lumen for any apical marker examined. This frequency-based test on the ranked brightness of the regions is successfully able to provide some information with regard the fact that the Dorsal region is the brightest region disproportionately often and we have also found a way to address the question of whether the Sub-dorsal regions tend to be the dimmest regions.

One of the major limitations of these data is the low sample size, which limits the kind of tests that can be performed and also reduces any test's ability to reveal an underlying trend. The binomial exact goodness of fit test is an ideal candidate statistical test for these small datasets, however the questions it can answer are extremely limited and more powerful statistical tests (such as parametric tests), could be implemented on data from a more appropriately designed experiment that could better interrogate any trend. A more powerful setup for examining the patterns of apical marker expression intensity with respect to position along the lumen could be performed using a larger sample size for each timepoint, with a larger number of biological replicates as well as more sections from directly comparable positions along

the embryo's anterior-posterior axis. Sample size aside, a much more powerful test for any difference in signal intensity of an apical marker between these regions would involve a method by which the absolute intensities measured from each region could be directly compared between images. To achieve this, an experiment should be set up that uses the same staining and imaging protocols for each section. The images should be taken on the same microscope at the same magnification and at the exposure/gain settings.

Another confounding factor is that the apical surface can be either directly apposed or separated. Indeed, the apical surfaces of the medial region tended to be directly apposed, thus containing signal intensity from two apical surfaces whereas the Dorsal ROI, for example, tended to only include apical marker signal intensity from one apical surface. The major reason for this association is due to the "keyhole" like shape of the lumen. It could be reasoned then that the medial region signal intensity is generally overrepresented since there are up to twice as many apical proteins that could exist on these two apposed sheets of the lumen. On the other hand, densely packed protein from two apical surfaces may give a less bright pixel value than the sum of two separated surfaces, because of light scattering effects, saturated pixels or actual dimmer labelling because of poorer antibody penetration. This would also need to be controlled for in an ideal experimental set up.



### **3.5 Discussion**

#### **3.5.1 The obliteration window marks a important change in the nature of the developing spinal cord**

Morphological analysis of the developing mouse spinal cord between E13 and E17 has identified a window of obliteration between E14 and E16, during which the lumen undergoes a rapid decrease in size from the most dorsal aspect, resulting in a small, ventrally located lumen (Figure 3.1, Schematic: Fig 3.17). After this stage, little further size change occurs; the lumen remains a similar size into adulthood (see Chapter 4).

My analysis of the transcription factors PAX6 and NKX6.1, together with SOXB1 proteins, shows that as the VZ obliterates, the expression pattern of these markers become more dorsal. There are two potential explanations for this effect. First, it is possible that stem/progenitor cells are being lost from the VZ unevenly from the dorsal side. This idea is strongly suggested by the presence of SOX1+SOX2+ cells dorsal to the obliterated lumen. Another possibility is that VZ stem/progenitor cells are re-patterning as dorsal obliteration progresses, potentially in response to changing SHH/BMP gradients (Wilson and Maden, 2005). These possibilities could be distinguished, either through real time analyses of cell behaviour, or through lineage tracing analyses. Chapter 7 will show my studies of cell behaviour. Importantly, regardless of the mechanism, my results show that during the obliteration window, the nature and therefore potential of stem/progenitor cells that occupy the VZ/EZ of the spinal cord are fundamentally changing as obliteration occurs.

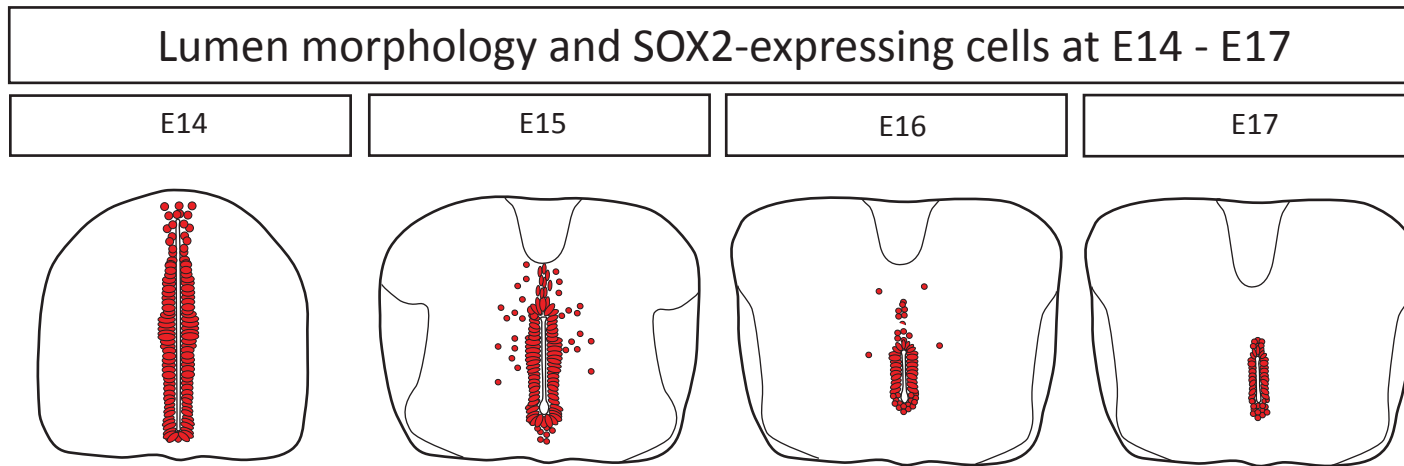


**Figure 3.17** Schematic of dorsal obliteration, showing both the reduction in lumen size as described in Figure 3.1 and position of SOX2-expressing nuclei (red) both within, and dorsal to, the ventricular zone as described in Figure 3.4.

### 3.5.2 Structural changes during obliteration

Massive structural changes such as seen in dorsal obliteration is reflected in the cytoskeletal structure of the contributing cells. My analyses of the F-actin marker phalloidin showed an intriguing pattern at the stages analysed. Between E15 and E17, that is, during and after the obliteration window, strong immunoreactivity is present along the midline both dorsal and ventral to the VZ.

F actin is known to have roles in a variety of cellular processes, including those involved in migration such as adhesion, shape change and cell protrusions. F-actin conformation varies depending on the context, and thus the unusually strong Phalloidin labelling at the dorsal midline may indicate cell behaviours unique to this dorsal region (Stricker, 2010).

The intermediate filament protein Nestin displays an interesting expression pattern. Prior to the onset of dorsal obliteration, Nestin is detected in radial glial cells that extend laterally from VZ to the pial surface. This labelling declines dramatically at E14.5, at the onset of dorsal obliteration, and concomitantly a new subset of Nestin+ cells arises at the dorsal-most VZ. As dorsal obliteration proceeds, the dorsal Nestin+ cells continue to contact both the lumen and the dorsal-most surface of the spinal cord, and extend ever-lengthening processes as the lumen obliterates.

My data show that the length of the dorsal Nestin+ cells' processes and the lumen size are negatively correlated. I then examined SOX2, a marker present early in VZ cells and then additionally in cells dorsal to the VZ. SOX2 positive cells outside the lumen are closely associated with the Nestin+ process. Long processes are a hallmark of radial

glia like cells. In the developing cortex, newborn neurons use radial glia as scaffolds to migrate (Nadarajah *et al.*, 2003). This raises the intriguing possibility that the SOX2 cells that have left the lumen use the processes of the Nestin+ cells to migrate.

### **3.5.3 Nestin+ cells are closely-associated with strong CRB2 expression**

Prior to dorsal obliteration, the polarity protein CRB2 is evenly distributed in the apical-most regions of VZ cells, and so appears evenly distributed around the lumen at E13-E14. However, over the period of rapid dorsal obliteration (E15-E16) cells in the most dorsal aspect of the VZ show stronger expression of CRB2, apically and, potentially, cytoplasmically, although the latter has not been demonstrated statistically. These cells also express high levels of apical ZO-1. There is a strong statistical association of these markers with the dorsal region, with the dorsal region being the brightest part of the lumen significantly more frequently than expected. Given that such polarity and junction complexes are crucial to the maintenance of the neuroepithelium, these analyses suggest that VZ cells at the most dorsal aspect of the developing spinal cord during the collapse window are locked tightly in the epithelium. These cells are closely-associated with the Nestin+ dorsal-most cells that appear at the same time: high power views show that the Nestin+ cells either co-express high levels of CRB2 or that Nestin+ cells immediately abut cells that express high levels of CRB2. Together, these analyses suggest that the dorsal obliteration window is characterised by the appearance of Nestin+ radial glial cells that show tight epithelial characteristics. In future I refer to these cells as dorsal Nestin+ radial glia (dNRG).

Note that since I cannot rule out the possibility that there is more than one cell type in the region occupied by Nestin+ processes, hereafter I refer to this region as the dorsal Nestin+ region.

#### **3.5.4 Polarity proteins and junction complexes may be downregulated in sub- dorsal VZ cells during dorsal obliteration**

Visual analysis of my data appears to show that dorsal obliteration is accompanied by marked changes in polarity and junction proteins, and in morphology in sub-dorsal VZ cells that immediately neighbour dNRG. Sub-dorsal VZ cells appear to downregulate apical CRB2, aPKC (a member of the PAR complex) and ZO-1 (a zona occludens protein that links tight junctions and the cytoskeleton together). Downregulation is transient, and at the end of dorsal obliteration (E17), CRB2, ZO-1 and aPKC are again detected evenly around the now-smaller VZ. The small sample size available at E17 meant that statistical analyses could not be performed to meaningfully assess this pattern and so this interpretation is not statistically supported. Therefore, this thesis will consider the possibility that the sub-dorsal region is downregulating apical proteins in the sub-dorsal area.

The transient downregulation of CRB2, ZO-1 and aPKC suggests that sub-dorsal VZ cells lose their epithelial integrity over the period of dorsal obliteration, and this possibility is supported through morphological analyses. Prior to dorsal obliteration, VZ cells that line the lateral walls of the lumen have DAPI nuclei abutted against their apical walls. However from the onset of rapid dorsal obliteration at E15, the nuclei of sub-dorsal cells are clearly removed from the apical surface. This supports the idea that sub-

dorsal VZ cells that are immediately adjacent to dNRG are more loosely held in the tissue than other ventricular zone cells.

In summary these analyses reveal that there may be changes in polarity and junction proteins concomitant with the obliteration window (E14-E16). Polarity and junction proteins show high expression in VZ cells at the most dorsal aspect of the lumen, but are specifically downregulated in sub-dorsal VZ cells. These changes are accompanied by changes in the location of nuclei of sub-dorsal VZ cells. Overall, these studies suggest that sub-dorsal cells may have reduced epithelial integrity or over the window of dorsal obliteration.

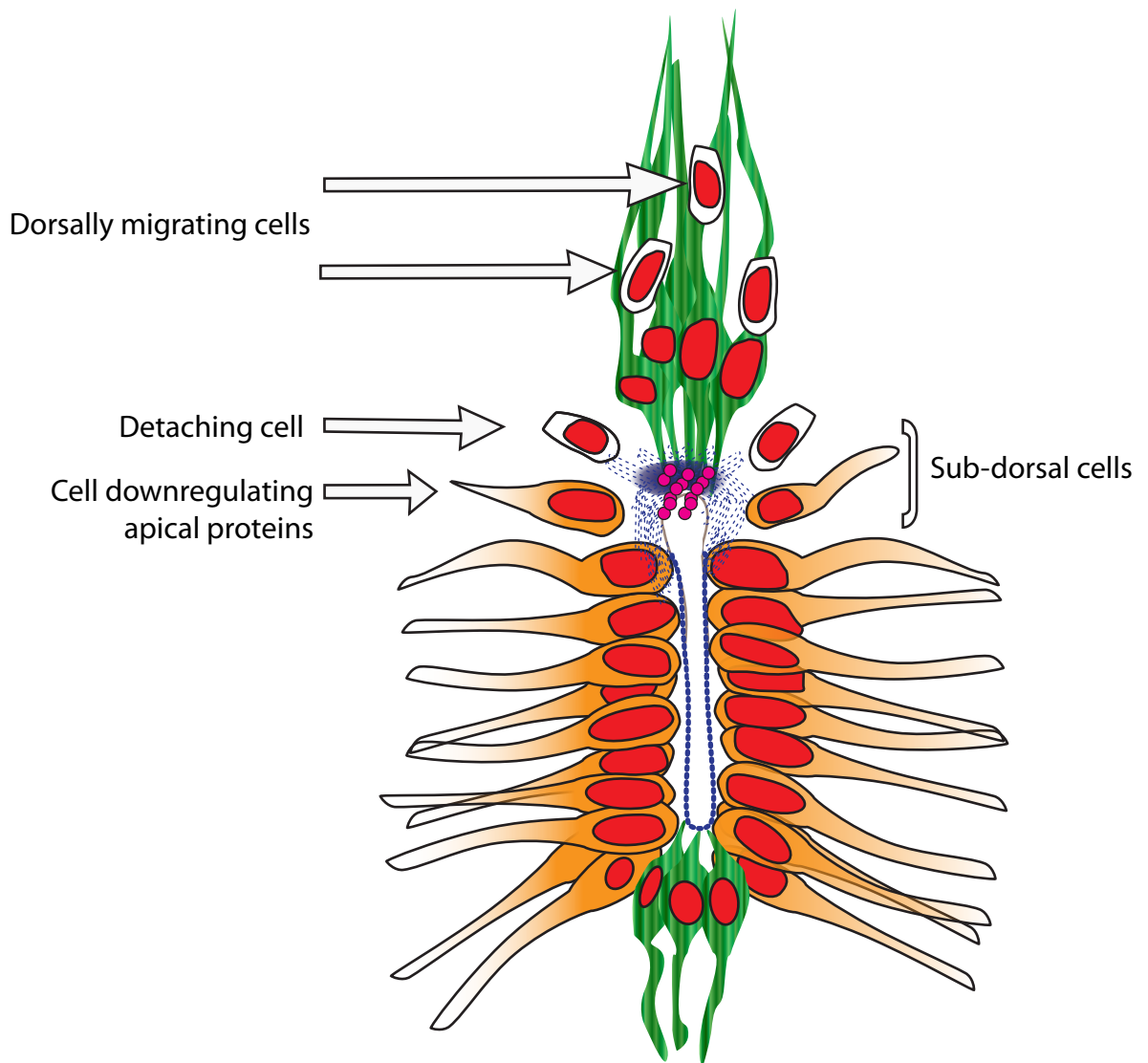
### **3.5.5 A model for dorsal obliteration**

These analyses show that the VZ of the developing spinal cord changes dramatically after E14. The timepoint between E14 and E15 marks the onset of dorsal obliteration, which decreases the size of the VZ, decreases the number of VZ cells and changes the relative position of the VZ so that it becomes ventrally located. Over this period, dNRG with lengthening dorsal projections, and strong apical expression of CRB2 and ZO-1 become apparent. At the same time, VZ cells in the sub-dorsal aspect also undergo a change, downregulating CRB2, ZO-1 and aPKC, and undergoing changes that result in their nuclei becoming located far from the lumen. Lateral VZ cells, and cells associated with the lengthening Nestin+ processes express SOX2.









Taken together, these data suggest a mechanism for collapse (Figure 3.18). The dNRG, or cells immediately adjacent to them, express a factor, or factors, that results in the downregulation of polarity and junction proteins in immediately adjacent sub-dorsal

SOX2 VZ cells. As a consequence, these lose epithelial integrity and become excluded from the VZ. These cells then use the Nestin+ long radial glial-like processes to migrate dorsally.

In the following results chapters, I aim to test this model. In particular, I first aim to ask whether dNRG (or immediately adjacent cells) have the potential to alter the neural epithelial integrity.



**Figure 3.18** The dorsal obliteration model. The dorsal NRGs (green) secrete a factor (pink) that can disrupt apical proteins. Sub-dorsal cells experience disruption/downregulation of polarity and junction proteins (blue). However, the dNRGs are protected from disruption by expression of high levels of apical proteins. The sub-dorsal cells may then detach and migrate using the dNRGs (green) as a conduit.

-  Lateral ventricular zone cells
-  SOX2 expressing cells
-  Nestin radial glia
-  Apical marker expression (aPKC, ZO-1, CRB2)
-  Regular apical expression
-  Diffuse/weak expression
-  Strong non-apical expression
-  Secreted factor



# Chapter 4

Dorsal Nestin+ radial glia: a role in mediating loss of neuroepithelial integrity and the formation of the mature central canal

#### 4.1 Introduction

In chapter 3, I described a population of Nestin<sup>+</sup> cells that arise in the most dorsal aspect of the neural tube between E13 and E14. These have radial glial-like morphology and contact both the pial surface with dorsal processes and the dorsal central canal with apical end feet, and thus we have termed them dorsal Nestin radial glia (dNRG). The dNRG extend their processes so that as the lumen obliterates, contact is always maintained at these two points. As I demonstrated in Figure 3.5, SOX2 positive cells are closely associated with the dNRG processes during dorsal obliteration. I described a model in which the lumen obliterates to form the central canal. The model suggests that dorsal Nestin<sup>+</sup> cells promote a loss of polarity and tight junctions in neighbouring SOX2 positive sub-dorsal VZ cells, causing them to delaminate from the VZ so that they are ultimately able to migrate along the dNRG processes. A prediction of this model is that dorsal Nestin<sup>+</sup> cells can cause a disruption of neuroepithelial integrity.

Given that previous studies have shown that Nestin<sup>+</sup> radial glial cells exist in a similar position in the adult spinal cord (David and Ousman, 2002; Petit *et al.*, 2011) a question that arises is whether adult Nestin<sup>+</sup> cells maintain similar characteristic properties to the Nestin<sup>+</sup> cells that I have described in the prenatal animal.

In this chapter I test whether dorsal nestin<sup>+</sup> radial glia of embryonic and adult mice have the potential to cause disruption or migration of embryonic neural progenitor cells.

## **4.2 Prenatal dorsal Nestin+ cells have the power to drive progenitor cell delamination in an experimental model system**

To investigate whether prenatal dNRG have the power to effect a delamination of neuroepithelial progenitors, I chose the embryonic chicken as a system to manipulate, as it is well-established and characterised, tractable and robust (Darnell and Schoenwolf, 2000; Davey and Tickle, 2007). My aim was to transplant prenatal Nestin+ cells into the lumen of the early chick neural tube and ask whether premature exposure of neuroepithelial cells to dNRG would lead to a loss of neuroepithelial integrity, assessed through a disruption to the position of neuroepithelial progenitor cells and a general disruption in neural tube integrity. At stage (Hamburger-Hamilton) HH10 (equivalent to an E9.5-10 mouse embryo) the embryonic chick neural tube has not fully closed at the caudal end, thus material can be placed into the U-shape cavity, exposing the apical side of VZ cells to ectopic material without damage to the surrounding tissues (Figure 4.1). At this stage the chicken embryo has not yet begun late neurulation, therefore the cell population expressing the dorsal intermediate filament translin; believed to be equivalent to Nestin (Cole and Lee, 1997; Napier *et al.*, 1999; Whalley *et al.*, 2009) has not yet developed (Appendix; Fig A.F1).

To test whether dorsal Nestin+ cells of the prenatal mouse can disrupt neuroepithelial progenitor cells of the embryonic chick neural tube, I dissected out a small area containing dNRG (see Chapter 2.5). My model predicts that only dNRG will have the power to disrupt neuroepithelial progenitors, and I therefore dissected lateral VZ cells as a control. Control lateral VZ explants, or Nestin+ cell explants were transplanted carefully in the open neural tube of the HH10 chicken embryo (Figure 4.1) and embryos were incubated at 37°C for 24 hours, until HH19-20 (equivalent to E11.5-12.5

mouse). In the first set of experiments, transverse sections were quadruply labelled with: M2 (an anti-mouse antigen) to detect the transplanted tissue; DAPI, to detect cell nuclei; dystroglycan, to label the basement membrane; and SOX2, to label progenitor cells. In a second set of experiments, transverse sections were quadruply labelled with M2, laminin (used in this instance as a marker of the basement membrane), DAPI and either NKX6.1 or PAX6. As discussed previously, NKX6.1 and PAX6 mark progenitor cells that form in distinct zones along the dorso-ventral axis (Jessell, 2000) and would therefore provide additional evidence for pattern disruption.

In the first set of experiments, control embryos, transplanted with cells lining the lateral VZ, showed an unbroken dystroglycan-labeled basement membrane. Further, strongly-labelled SOX2-positive neural progenitors were all confined to the neural tube (Figure 4.2A-A'', Table 4.1).

By contrast, embryos transplanted with dNRG showed disrupted basement membranes, as evidenced through breaks in dystroglycan expression, and cells that strongly express SOX2 were detected in an apparently ectopic position outside the neural tube (Figure 4.2B-Bi'', arrows). Furthermore, the neural tube itself appeared unusual: cell position appeared generally disrupted.

**Table 4.1** E15 mouse transplants into HH10 Chick.

<b>Tissue Transplanted</b>	<b>Disruption</b>	<b>No Disruption</b>
<b>Dorsal (6)</b>	6	0
<b>Lateral/Ventral (3)</b>	0	3

These experiments show that dNRG-transplanted embryos have a striking and significant association with the disruption of both progenitor organisation and appropriate positioning and basement membrane integrity (Fisher's exact test,  $P=0.0119$ ). These results support the idea that dNRG can disrupt neuroepithelial cell integrity.

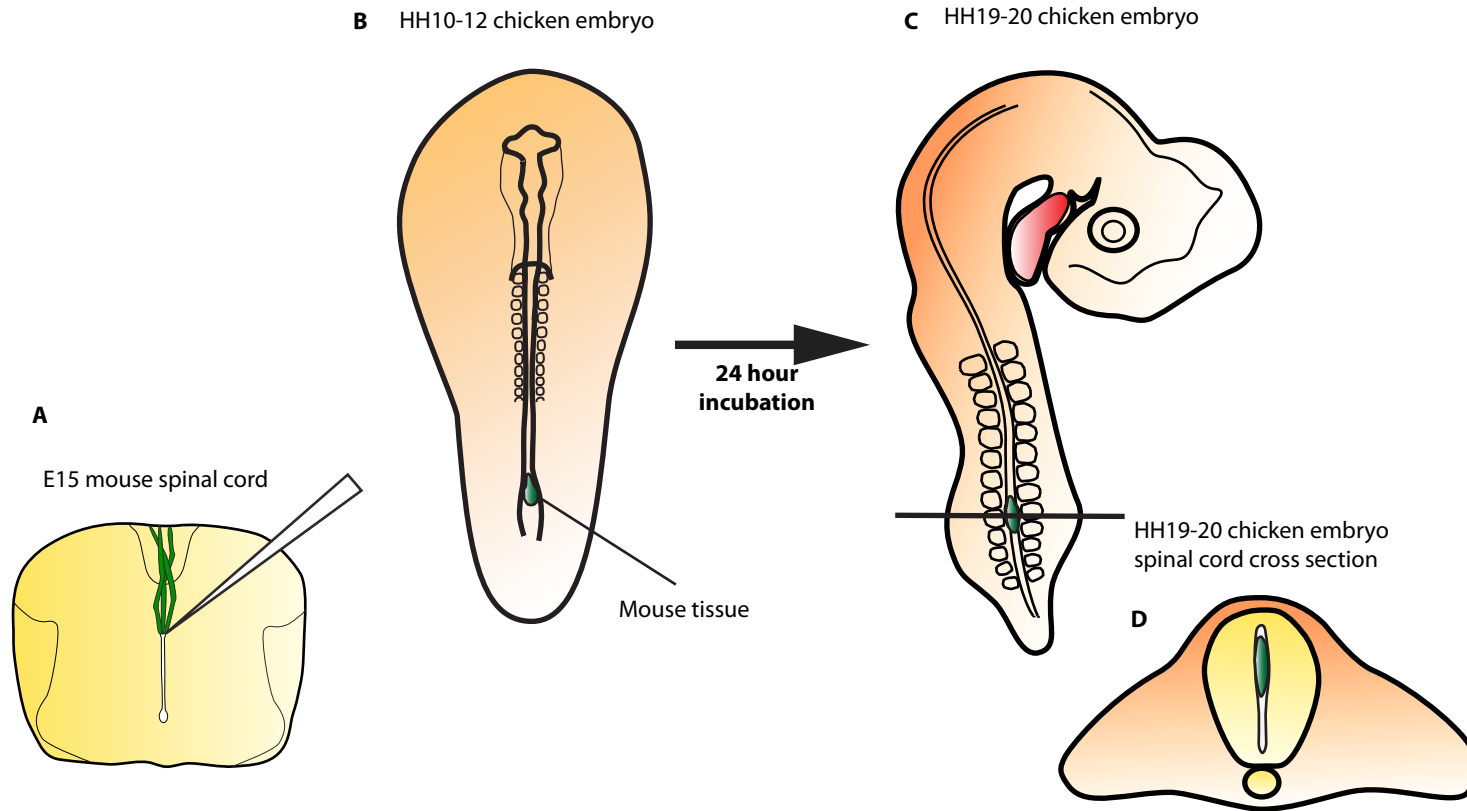
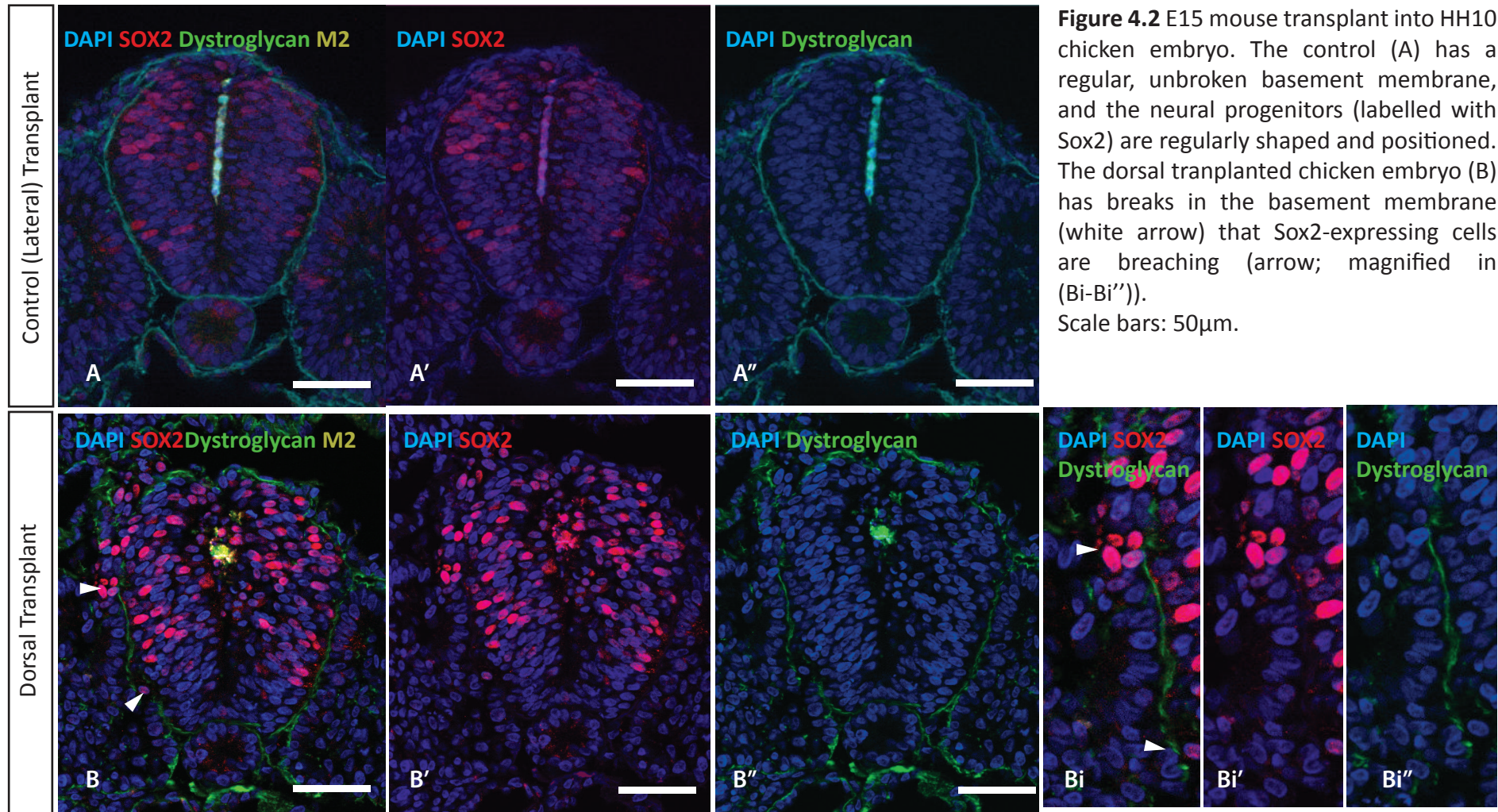


**Figure 4.1** Schematic of mouse central canal tissue into HH10-12 chicken embryo. Mouse tissue is dissected out with a fine pulled needle (A) and carefully placed in the open neural tube of a HH10-12 embryo, as rostral as possible (mouse tissue represented in green, B). The chicken embryos are then incubated for 24 hours (C). (D) represents a cross section of chicken neural tube at level of black line in (C).

## E15 mouse spinal cord transplant into HH10 chicken embryo



### **4.3 Adult dorsal Nestin+ cells have the power to drive progenitor cell delamination**

Previous studies have shown that Nestin+ cells are present in the adult spinal cord, occupying a similar position to those that I describe at the end of the dorsal obliteration window (David and Ousman, 2002; Petit *et al.*, 2011). Additional preliminary studies in our lab performed by Dr. Kavitha Chinnaiya indicated that adult Nestin+ dorsal cells may be able to induce migration of neural progenitor cells. Embryonic-like ability of adult tissue to disrupt the developing epithelia could raise the intriguing possibility that dorsal Nestin-expressing cells (a stem/progenitor marker) develop during dorsal obliteration and are maintained in the adult and may have the ability to induce delamination upon, for example, injury. To confirm these studies, I first established that I could detect similar cells.

Transverse sections of adult mouse spinal cord were triple labelled to detect DAPI, Nestin and SOX2. SOX2-expressing cells were confined to the central canal, and Nestin+ radial glial like cells, similar to those I described in the prenatal embryo, were clearly detected (Figure 4.3). As in the embryo, these cells maintain contacts at the dorsal pial surface and have end feet at the dorsal central canal. The relative size and position of the central canal and of the dorsal Nestin+ population in the adult (Fig. 4.3 C-D'') are similar to those at the end of the dorsal obliteration window at E17 (A-B'').

I then asked whether adult Nestin+ cells retain the ability to disrupt neuroepithelial progenitors, using the same assay described in Section 4.2 (and Chapter 2.4). As with the prenatal animal, I compared the effect of dorsal Nestin+ cells to that of sub-dissected lateral central canal cells. These experiments were performed in collaboration with Dr Kavitha Chinnaiya.



Chicken embryos transplanted with control tissue (adult lateral central canal) showed no disruption to neural tube integrity, with an unbroken dystroglycan-labeled basement membrane and regularly spaced neural progenitors (Fig. 4.4A-C). By contrast, chick embryos transplanted with adult dorsal neural tube tissues showed clear disruption of neural tube integrity (Figure 4.4D-G). Co-labelling with dystroglycan and SOX2 reveals breaks in the basement membrane that appear to be breached by SOX2-expressing cells (Figure 4.4F white arrowhead). Cell position irregularities are common, and frequently found next to breaks in dystroglycan, indicative of a disrupted basement membrane (Figure 4.4F, arrowhead outline,). SOX2 expressing cells are likewise detected outside the neural tube, often closely associated with basement membrane breaks (Figure 4.4F, arrowheads). These are not seen in the control transplanted embryo (Fig 4.4, C). Analysis of serial adjacent sections with NKX6.1, PAX6, or SOX2/dystroglycan, reveals similar abnormalities to those detected with prenatal Nestin+ cells). Progenitor cells, expressing NKX6.1, PAX6 or SOX2 are detected ectopically outside the neural tube, often closely associated with basement membrane breaks (not shown). Within the neural tube, the normally tight patterns of NKX6.1 and PAX6 are disrupted (arrowhead, Figure D, E), neural epithelial cells appear to show aberrant cell orientations (arrowhead, Figure 4.4 G, arrowhead). The disruption mediated by the dorsal Nestin+ graft is not limited to immediately-adjacent cells, suggesting the operation of a diffusible factor. Furthermore, the disruption is not limited to neuroepithelial cells: in several instances, the basement membrane of the notochord was disrupted, and outpocketings of notochord, or even ectopic 'mini-notochords' were observed (Figure 4.4 H). NKX6.1 cells were seen extruding from the floorplate in a bulge (Fig 4.4, J).

The disruption to the tissue-transplanted chicken embryos varies. I classified the disruption into ‘Strong’ ‘Medium’ and ‘Weak’, although these ratings are somewhat subjective. ‘Strong’ phenotypes have clear ectopic neural tube cells outside the neural tube. ‘Medium’ has internal neural tube disruption, and evidence of cells that appear to be in the process of leaving the neural tube and basement membrane disruption. ‘Weak’ characterises embryos that have only small basement membrane or minimal cell organisation disruptions, which cannot formally be excluded as sectioning artefacts. These results are shown quantitatively in Table 4.1.

**Table 4.2** Adult mouse transplants into HH10 Chick.

<b>Tissue Transplanted</b>	<b>Strong Phenotype</b>	<b>Medium Phenotype</b>	<b>Weak/ No Phenotype</b>
<b>Dorsal (9)</b>	2	5	2
<b>Lateral/Ventral (4)</b>	0	0	4

These experiments suggest two conclusions. First, that adult dorsal Nestin+ cells show the same ability as prenatal dNRG to disrupt epithelial integrity, including neuroepithelial integrity. Second, disruptions to epithelial integrity are detected at a distance, suggesting that the effect of the Nestin+ cells is mediated by a diffusible factor. These association of dorsal transplanted tissue with a disruptive phenotype are significant (Fisher’s exact test,  $p=0.0210$ ).

## SOX2 and Nestin in E17.5 and Adult mouse Spinal cord

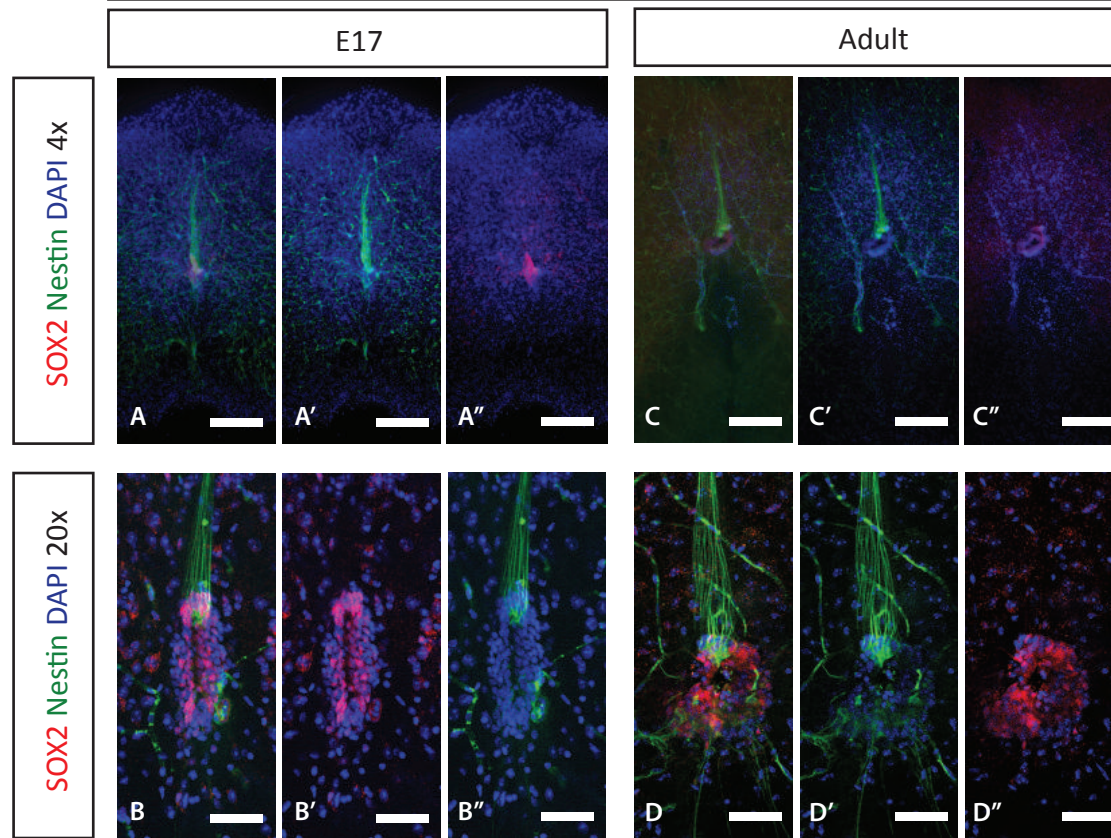
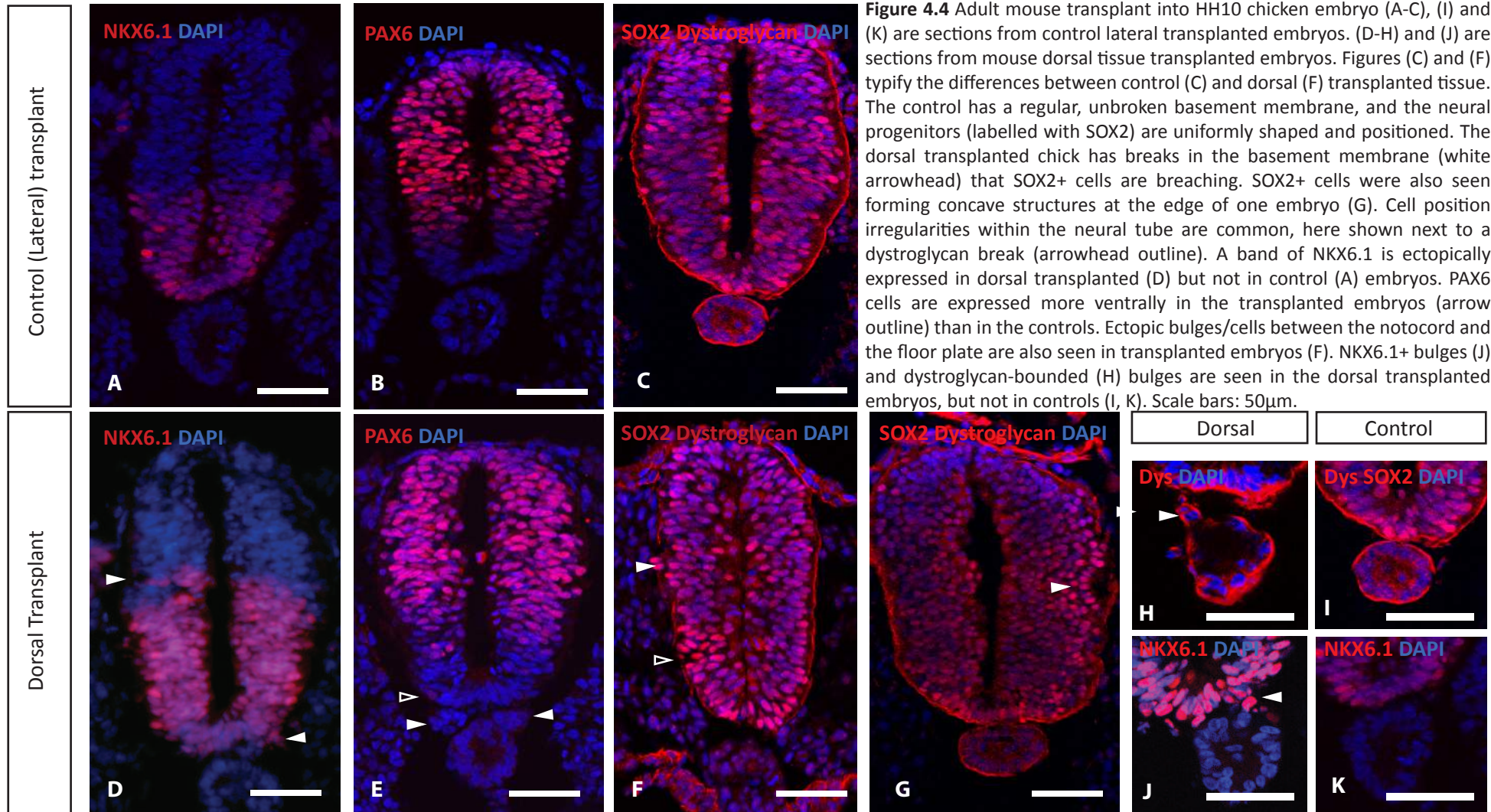


**Figure 4.3** E17 (A-B) and Adult (C-D) mouse expressing SOX2 and Nestin. In both cases, SOX2 is restricted to the central canal. The dorsal nestin end feet contact the dorsal central canal and extend long processes to the pial surface. Scale bars: 50 $\mu$ m (10x) 100 $\mu$ m (4x).

## Adult mouse spinal cord transplant into HH10 chicken embryo



#### **4.4 Progenitor-delaminating ability correlates with Nestin+ CRB2+ cells**

As I was performing these experiments, Dr Kavitha Chinnaiya performed additional grafts, the aim of which was to further assess the specificity of the effect. She wished to determine (a) whether similar populations of Nestin+ CRB-positive cells existed elsewhere in the CNS, and if so, whether these shared the ability to disrupt neuroepithelial integrity, and (b) whether, conversely, Nestin-negative regions were unable to disrupt neuroepithelial integrity. I briefly summarise these studies, as they are pertinent to later studies, outlined in Chapter 5.

A systematic analysis of the CNS, from embryonic to adult stages, revealed that Nestin+ cells with radial glial-like morphology and atypical CRB2 expression were detected in the E17.5 dorsal telencephalon. Transplantation of these cells into the HH10 chick embryonic neural tube revealed that they are extremely effective in mediating disruption of epithelial integrity. SOX2, PAX6 and NKX6.1 positive cells are detected in ectopic positions outside the neural tube. Patterning within the neural tube is highly disrupted. Labelling with an anti-SHH antibody reveals that disruptions are detected, additionally, in both floor plate and notochord: thus, ectopic, or 'mini' floor plate and notochord structures are frequently detected.

Tissues that do not express Nestin or atypical CRB2, including E17.5 ventral telencephalon, fail to disrupt the integrity of the neuroepithelium in this assay. Therefore, these studies suggest that radial glial like cells that occupy a dorsal position in the spinal cord and telencephalon express Nestin and atypical CRB2, and that these cells specifically secrete a diffusible factor that disrupts epithelial integrity, including neuroepithelial integrity.

## **4.5. Discussion**

### **4.5.1. Dorsal Nestin radial glia disrupt epithelial tissues**

In this chapter, I set out to ask, first, whether prenatal dNRG show an ability to disrupt neuroepithelial integrity, and second, whether adult dorsal Nestin+ cells maintain this function. My analyses show that both embryonic and adult dorsal transplants clearly have an ability to cause neural progenitor disruption when transplanted into chicken neural tube. A range of phenotypes is detected, but consistently basement membrane disruption is seen and progenitor cells are disorganised. Within the neural tube, progenitor domains are disrupted and cells are mis-oriented. Progenitor cells that appear to breach the disrupted neuroepithelium are detected, and are even found outside of the apparent confines of the neural tube. Interestingly, disruption is not limited to the neural tube, nor to tissue immediately adjacent to the transplant (as assayed when cryosectioned, 24 hours after transplantation). Bulges are detected in notochord, and 'mini-notochords' are detected. This raises the possibility that the disruption is caused by a factor that can act over a long distance, such as a secreted protein. My experiments cannot rule out the possibility that the ectopic cells arise due to a switch in fate. However, two pieces of evidence suggest this is unlikely. First, ectopic 'mini-notochords' are associated with smaller endogenous notochords, suggesting that the mini-structures arise from the endogenous structure. Second, neural progenitors that are detected outside the neural tube are invariably associated with breaks in adjacent basement membrane. The most prosaic interpretation of these results is that dNRG secrete a long-range diffusible factor that disrupts epithelial junctions, allowing cells to move away from their neighbours. I suggest that cells of similar character (neural progenitors, for instance, or notochord) re-form small structures with homologous cells, resulting in for example mini-notochords. This would

suggest that cell adhesion molecules that mediate 'like-like' interactions are not entirely downregulated. This, together with the fact that ectopic cells do not appear to change their morphology suggests that the effect I observe is distinct from a standard epithelial to mesenchymal cell transition (Clay and Halloran, 2010; Kerosuo and Bronner-Fraser, 2012).

Overall, then, in this experimental model, my results provide support for the idea that dNRG are able to disrupt neuroepithelial integrity.

#### **4.5.2 Adult dorsal Nestin+ cells**

Although I have not formally proved that the dorsal Nestin+ cells detected in the adult are the same population as those dNRG I described in the prenatal animal, two lines of evidence from my studies suggest that they are. First, the overall position and dorso-ventral length, both of the central canal and of the Nestin+ radial glial cells, are similar at E17 and in the adult (Figure 4.3). Second, adult Nestin+ cells retain the ability to disrupt neuroepithelial cells. Therefore, I tentatively suggest that the completion of dorsal obliteration marks the onset of the 'adult' central canal, and that the Nestin+ cells that form in dorsal obliteration persist in the dorsal midline, where they are maintained into adulthood.

If this model is correct, a number of questions arise. First, can a diffusible factor be identified, that derives specifically from dNRG, and mediates a similar effect, and does it operate to mediate dorsal obliteration?

# Chapter 5

A novel truncated isoform of CRB2 is detected in dorsal Nestin+ radial glia and can mimic their ability to disrupt epithelial integrity



## 5.1 Introduction

My observations show that in mouse, dorsal obliteration occurs over a tight time-window, between E13 and E17, and is associated with a disruption in junction and apical polarity proteins in sub-dorsal Ventricular Zone (VZ) cells (Chapter 3). Sub-dorsal VZ cells lie immediately adjacent to dorsal Nestin<sup>+</sup> radial glia (dNRG) (Chapter 3) and my experimental evidence suggests that these are capable of disrupting neuroepithelial progenitors, causing them to 'delaminate' from the neuroepithelium (Chapter 4). The dNRG can exert this effect at a distance. Based on these results, I hypothesised that dNRG may be the source of a secreted signal that is capable of disrupting apical polarity proteins in local VZ cells, allowing sub-dorsal VZ cells to delaminate (Figure 5.1). I described in Chapter 3 that expression of CRB2 appears atypical in dNRG, and appears punctate. Furthermore, in Chapter 4, I showed a correlation in Nestin<sup>+</sup>/atypical CRB2<sup>+</sup> cells and epithelial-disrupting ability. These observations, together with previous data that suggests the existence of a secreted form of CRB2 in humans (described below), and evidence that CRB can play a role in epithelial-to-mesenchymal cell transitions (described below) led me to ask whether secreted CRB2 might mediate the action of the dNRG. In this chapter I describe the detection and characterisation of a novel truncated isoform of *Crb2* that may encode a secreted protein, and an experimentally made secreted CRB2 whose profile and action fit this model.

## 5.2 Database evidence for secreted isoforms of CRB2 in mouse

The vast majority of studies into the role of CRB proteins, including CRB2, focusses on the full-length transmembrane protein. As outlined in the Introduction, however, bioinformatic studies of cDNA derived from human brain and a human NTERA-2

embryonic carcinoma cell line neuronal precursor cell line have shown that human *Crb2* can be spliced into both full length and truncated isoforms (Katoh and Katoh, 2004). Truncated transcripts generate a protein that does not contain the transmembrane or intracellular domains and, therefore, is potentially secreted. In support of this idea, transfection of a GFP-tagged version of Xerl (the *Xenopus* homologue of CRB2) into *Xenopus* embryos shows that after lysing the embryos, Xerl protein can be found in the soluble fraction (Kuriyama and Kinoshita, 2001; Kuriyama *et al.*, 2003) while immunohistochemical analyses in embryos suggest a diffuse pattern *in vivo*, suggestive of a secreted protein. Finally, an unpublished bioinformatics study in the Rashbass lab suggests that a similar secreted splice variant may exist in the mouse (Murtaza, 2012). The Rashbass lab made a secreted CRB2 construct and added His and V5 tags. When stably cloned into a mammalian expression vector, and transfected into HEK 293 cells, the resulting protein is secreted. (Murtaza, 2012). None of these studies, however, have proved whether CRB2 exists as a secreted protein *in vivo*, or whether a secreted variant exists in mouse.

Large online databases are a rich source of expression data that becomes extremely useful when paired with biological context. To begin to address whether I could find evidence for a secreted variant of mouse CRB2, I first interrogated the ENSEMBL mouse genome assembly (images downloaded June 2015). Ensembl annotates three CRB2 transcripts on the forward strand of chromosome 2: *Crb2-001*, *Crb2-002* and *Crb2-003* (Fig 5.1). Of these, *Crb2-001* is a full-length, 6.4kb transcript, covering 13 exons that encode transmembrane *Crb2* (Figures 5.1, 5.2 and Table 5.1). By contrast, *Crb2-002* and *Crb2-003* are partial/processed transcripts (Figures 5.1, 5.2 and Table 5.1) for which there is no *in vivo* expression or functional data. *Crb2-003* covers a part

of intron 11-12, exon 12 and part of exon 13 (Figure 5.1, Figure 5.2). Crb2-002 is an assembled sequence (Tables 5.2, 5.3, Figures 5.3, 5.4 and 5.5) that has been inferred from a cDNA sequencing project in mouse brain that revealed two Expressed Sequence Tags (ESTs), both of which contained intron 9-10 spliced into the sequence. These ESTs are of different lengths, overlap, and extend from exon 8-10 or 9-10 (detailed in Figures 5.3, 5.4 and 5.5). The assembled sequence therefore predicts a transcript that covers a part of exon 8, exon 9, an intronic sequence and a part of exon 10 and is predicted to be 1.1kb (Fig. 5.2).

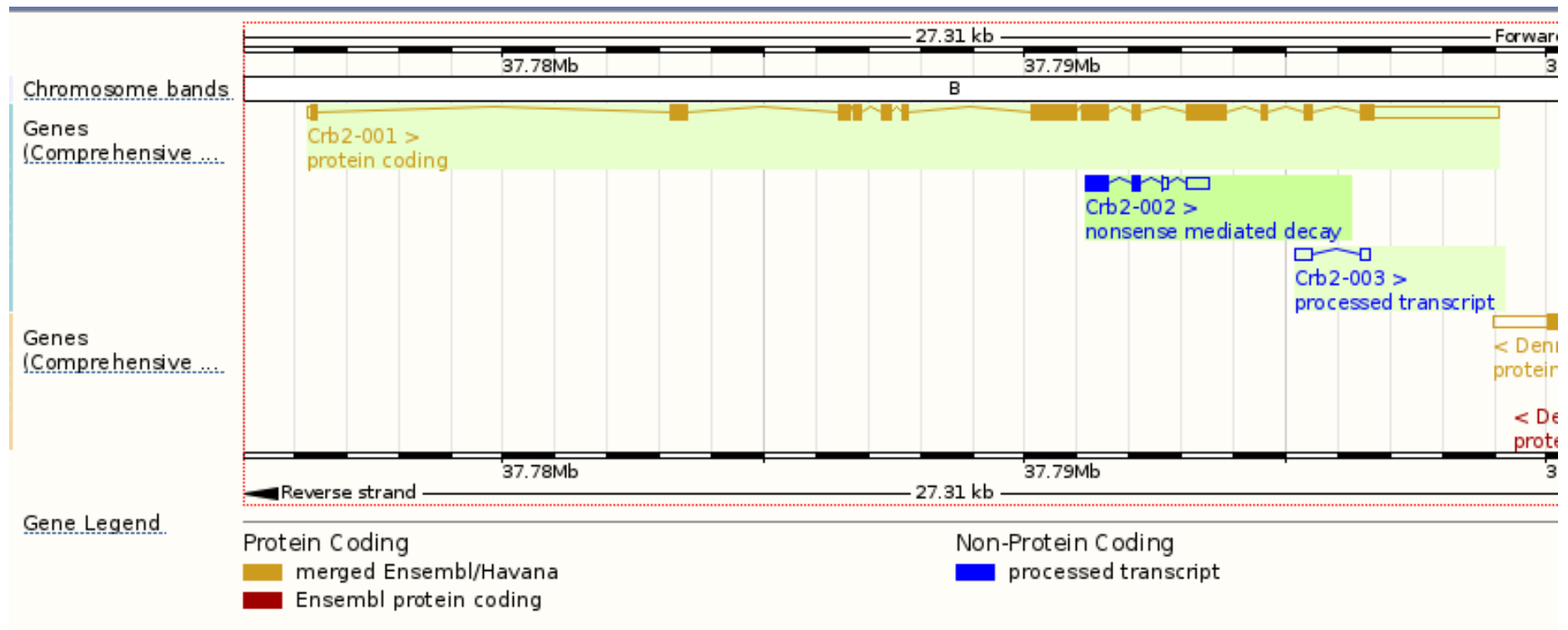


**Figure 5.1** Relative positions of Crb2-001 (full length transcript) and Crb2-002 and Crb2-003 (partial transcripts). The mouse *Crb2* gene is encoded on the forward strand of chromosome 2: 37,776,249-37,799,103. Ensembl annotates three transcripts. Crb2-001 is protein coding for the transmembrane ‘*Crb2*’ protein, the expression and function of which is well characterised in the literature. Crb2-002 and Crb2-003 are processed transcripts for which there is no *in vivo* expression or function data. Image downloaded from Ensembl October 2015

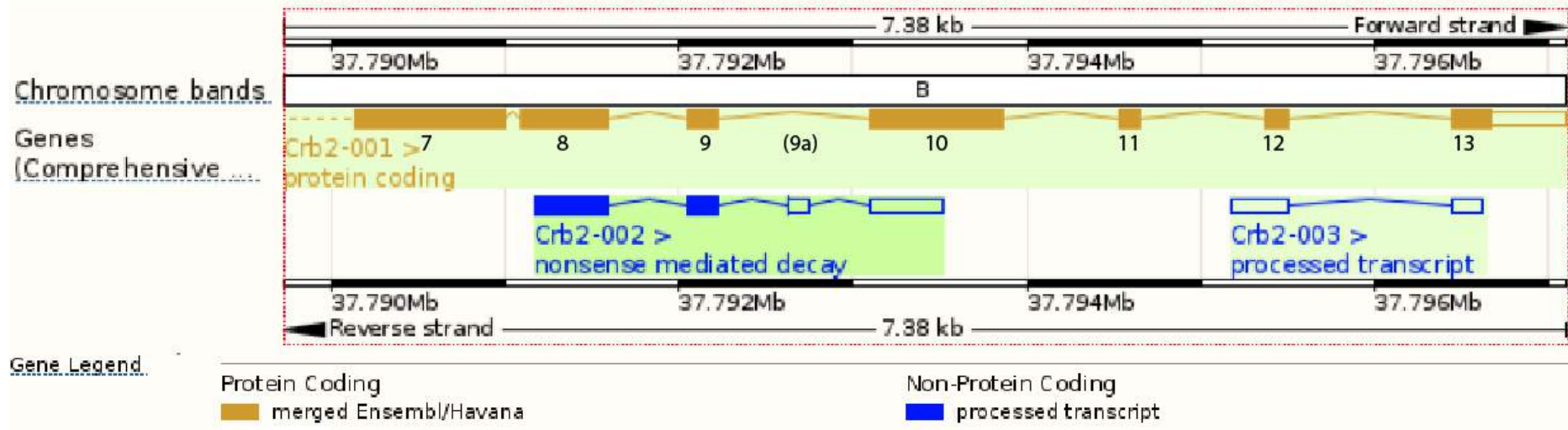


**Figure 5.2** High power view of Crb2-001 (full length transcript) and Crb2-002 and Crb2-003 (partial transcripts)

The mouse *Crb2* gene is encoded on the forward strand of chromosome 2: 37,776,249-37,799,103. Ensembl annotates three transcripts. Crb2-001 is protein coding for the transmembrane ‘*crb2*’ protein, the expression and function of which is well characterised in the literature. Crb2-002 and Crb2-003 are processed transcripts for which there is no *in vivo* expression or function data.

Crb2-001 is shown from exon 7 to exon 13 (the final exon). Crb2-002 contains exons 8-10, and additionally a part of intron9-10 spliced in. Crb2-003 covers exon 12 and 13.

Image downloaded from Ensembl October 2015

**Table 5.1** Isoform of the mouse *Crb2* gene as annotated by Ensembl.

Mouse <i>Crb2</i> : Ensembl transcripts					
Chromosome 2: 37,776,249-37,799,103					
Name	Transcript Type	Exons	bp	AA	Source
<b>Crb2-001</b>	Full length	13	6372	1282	Ensembl: ENSMUST00000050372
<b>Crb2-001</b>	Partial	4	1132	(107)	Ensemble: ENSMUST00000137693
<b>Crb2-003</b>	Partial	2	502	-	Ensembl: ENSMUST00000137693

The full-length transcript covers 13 exons. Crb2-002 covers exons 8 (partial), exon 9, intron9-10, and exon 10 (partial). Exon Crb2-003 covers part of intron 11-12, exon 12 and part of exon 13. Ensembl, accessed April 2015

**Table 5.2** Crb2-002 inferred from two ESTs.

Mouse <i>Crb2</i> -002 – EST evidence			
Accession number	Length	Exons	Source
<b>CB246995.1</b> <b>GI: 28368639</b>	778 bp	8 (partial), 9, intron9-10, 10 (partial)	C57BL/6 Embryo E12.5dpc whole brain
<b>CD355110.1</b> <b>BQ771048</b> <b>GI:21979524</b>	652 bp	9 (partial), intron9-10, 10 (partial)	C57BL/6 Embryo E12.5dpc whole brain

Source ESTs for the inferred transcript Crb-002. Ensembl, accessed April 2015

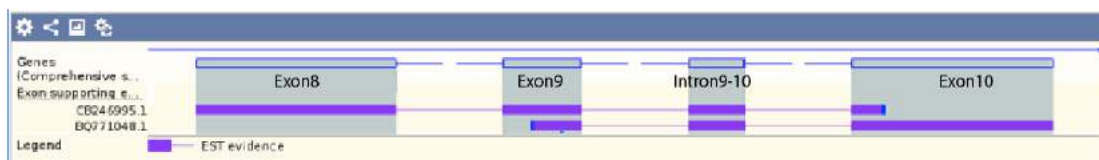


**Figure 5.3** Schematic showing relative positions of ESTs making up inferred transcript Crb2-002. Blue outlined boxes (top) refer to Crb2-002 (full sequence shown– Figure 5.4). Purple boxes refer to EST evidence (see also Table 5.2; Figure 5.3). Ensembl, accessed April 2015

## Figure 5.4 ESTs that define Crb2-002

The sequence of transcript Crb2-002 is derived from evidence from two ESTs. Bases 1-778 are covered by bases 1-778 of GenBank gi:28368639. Bases 481-1132 are covered by bases 1-652 of GenBank gi:21979524  
Retrieved from Ensembl July 2015

**GenBank Acc: CB246995**  
**GenBank gi: 28368639**  
**778bp**  
**Exons: exon8 (partial), 9, intron9-10, exon10 (partial)**  
**<http://www.ncbi.nlm.nih.gov/nucest/gi|28368639>**

GTCATTTTTCTCCGCACCCGCGAACCTGCCGGCCTGTTGCTCCAGTTTGCCAATGAT  
TCAGTTGCGAGCCTGACTGTGTTCCTGAGTGAGGGCCAGATCCGGGCTGAGGGGCTGGGT  
CACCTGCTGTGGTCCCTCCCTGGGCGCTGGGATGATGGACTCCCCACTTGGTGATGCTC  
AGCTTTGGGCCTGACCAGCTGCAGGACCTGGGCCAGCGGCTGTATGTGGGTGGGAGGTT  
TACCTGATGACACCCAGCTCTGGGGTGGGCCCTTCCGAGGCTGTCTCCAGGACCTACAA  
CTCAACAGCATCCACCTCCCCTTCTTCTCTTCCCCGATGGAGAACTCAAGTTGGCCCAGT  
GAACTGGAAGCTGGCCAGTCCCAACCTCACCCAGGGTTGTGTCTCTGAGGACACGTGC  
AATCCCAATCCCTGTTTTCAATGGTGGCACGTGCCACGTACCTGGAATGACTTCTACTGC  
ACCTGCTCCGAGAACTTACGGGGCCACCTGTGCCCAGCAGCGATGGTGCCCCAGGCAG  
CCATGCCTGCCTCCTGCCACCTGTGAGGAGGTTCCAGATGGCTTTGTGTTTTAGGGACTA  
TGGATATGGGCCCCTACACCCCATTTGTTGGGTGCTAGGGATGGAACCCANAGCCTCCTA  
CAAGCTAGGCAGTCTACCAACCGAAGCTACTCTGCCAGCCTTACAGAAGGTGTGGCCGAG  
GCCACGTTCCGCGAGGGCCCTCCTGCTGTGTTACAGGCCACAACGTGTCTCATCGCTC

**GenBank Acc: BQ771048**  
**GenBank gi: 21979524**  
**652bp**  
**Exons: exon9 (partial), intron9-10, exon10 (partial)**  
**<http://www.ncbi.nlm.nih.gov/nucest/GI:21979524>**

CTGCTCCGAGAACTTACGGGGCCACCTGTGCCCAGCAGCGATGGTGCCCCAGGCAG  
CCATGCCTGCCTCCTGCCACCNTGTGAGGAGGTTCCAGATGGCTTTGTGTTTTAGGGACTA  
TGGATATGGGCCCCTACACCCCATTTGTTGGGTGCTAGGGATGGAACCCAAAGCCTCCTA  
CAAGCTAGGCAGTCTACCAACCGAAGCTACTCTGCCAGCCTTACAGAAGGTGTGGCCGAG  
GCCACGTTCCGCGAGGGCCCTCCTGCTGTGTTACAGGCCACAACGTGTCTCATCGCTC  
AGCGGGCTCACCTGGCCTTCCGCACGCGGACTCCGAGGCTGGGCTACTGCGCGCCGTC  
TCCGCCGAGGTGCCCACTCCAATATCTGGTTGGCGGTGCGCAACGGCTCGCTGGCAGGA  
GATGTGGCGGGTTTCGGTGCTGCCCGCGCCCGGGCCGCGGCTGGCCGACGGCGCCTGGCAT  
CGCGTGCGCCTAGCCCGGGAGTTCCACAGGCCGCTGCCTCGCGCTGGCTGCTGTGGCTG  
GACGGCGCGGCGACACCCGTGGCCTTGCACGGCTTGGGCGGCGACCTGNGCTTTCTGCAG  
GGTCCGGGTGCAGTGCCTCTGCTACTGGCTGAGAATTCACGGGCTGCCTGGGC

Alternating exons are marked black and blue. Unlike the sequence of the transmembrane version of Crb2, these ESTs both contain intron9-10 (underlined). The 5' end of the transcript has not been collected, so it is impossible to tell the start site of this transcript from this dataset. Nucleotides common to both sequences are in bold.

**Figure 5.5: Ensemble - inferred Sequence of Transcript Crb2-002**

```

0001 NNGTCATTTTTTCCCTCCGCACCCGCGAACCTGCCGGCCTGTTGCTCCAGTTTGCCAATGAT
0059 TCAGTTGCGAGCCTGACTGTGTTTCCCTGAGTGAGGGCCAGATCCGGGCTGAGGGGCTGGGT
0119 CACCCTGCTGTGGTCCCTCCCTGGGCGCTGGGATGATGGACTCCCCCACTTGGTGATGCTC
0179 AGCTTTGGGCCTGACCAGCTGCAGGACCTGGGCCAGCGGCTGTATGTGGGTGGGAGGTTC
0239 TACCCTGATGACACCCAGCTCTGGGGTGGGCCCTTCCGAGGCTGTCTCCAGGACCTACAA
0299 CTCAACAGCATCCACCTCCCCTTCTTCTCTTCCCCGATGGAGAACTCAAGTTGGCCCAGT
0359 GAACTGGAAGCTGGCCAGTCCCTCCAACCTCACCCAGGGTTGTGTCTCTGAGGACACGTGC
0419 AATCCCAATCCCTGTTTTCAATGGTGGCACGTGCCACGTACCTGGAATGACTTCTACTGC
0479 ACCTGCTCCGAGAACTTCACGGGGCCACCTGTGCCAGCAGCGATGGTGCCCCAGGCAG
0539 CCATGCCTGCCTCCTGCCACCTGTGAGGAGGTTCCAGATGGCTTTGTGTTTTAGGGACTA
0599 TGGATATGGGCCCCCTACACCCCATTTGTTGGGTGCTAGGGATGGAAACCAAGCCTCCTA
0659 CAAGCTAGGCAGTCTACCAACCGAAGCTACTCTGCCAGCCTTACAGAAGGTGTGGCCGAG
0719 GCCACGTTCCGCGAGGGCCCTCCTGCTGTGTTTACAGGCCACAACGTGTCTCATCGCTC
0779 AGCGGGCTCACCCCTGGCCTTCCGCACGCGCGACTCCGAGGCTGGGCTACTGCGCGCCGTC
0839 TCCGCCGCAGGTGCCCACTCCAATATCTGGTTGGCGGTGCGCAACGGCTCGCTGGCAGGA
0899 GATGTGGCGGGTTTCGGTGCTGCCCCGCGCCCGGGCCGCGCTGGCCGACGGCGCCTGGCAT
0959 CGCGTGCGCCTAGCCCGGGAGTTCCCACAGGCCGCTGCCTCGCGCTGGCTGTGGCTG
1019 GACGGCGCGGGCGACACCCGTGGCCTTGCACGGCTTGGGCGGCGACCTGGGCTTTCTGCAG
1079 GGTCCGGGTGCAGTGCCCTCTGCTACTGGCTGAGAACTTACGGGCTGCCTGGGC

```

Crb2-002 is an assembled sequence (figure 5.3) that has been inferred from a cDNA sequencing project in mouse brain that revealed two ESTs, both of which contained intron9-10 spliced into the sequence. These ESTs are of different lengths, overlap and extend from exon 8-10, or 9-10 (detailed in figure 5.3).

Retrieved from Ensembl July 2015

**Table 5.3** Notes on alignment. There are some discrepancies between the EST sequences that make up Crb2-002, summarised here. Number given as a nucleotide identifier 'N123', refers to number within that sequence. Bold **CATGN** refer to nucleotide sequence. Where an unidentified nucleotide 'N' has occurred in one EST, sequence of Crb2-002 has referred to either the other EST sequence, or to the full mRNA/genomic sequence marked (\*).

GI:28368639	GI:21979524	Crb2-002
Between N559/560	N80 N	Between N559/N560
N649 N	N170 A	N649 A
-	N588 N	N1067 <b>G*</b>
-	N634/N635	N1114 <b>C*</b>



As described in section 5.1 (above) bioinformatic analyses of human Crb2 suggests that a secreted variant may be produced from an isoform that includes exons 1-10 and additionally intron 10-11, raising the possibility that the addition of part of intron 9-10 in the mouse Crb2-002 transcript could encode the C-terminal of a homologous secreted variant of CRB2. Henceforth intron 9-10 is referred to as exon 9a when it is included in a processed transcript.

Sequence analysis of Crb2-002 suggests that the addition of intron 9-10 as an exon (exon 9a) would introduce a premature STOP codon and produce a polypeptide that does not possess the transmembrane domain (Figure 5.6). Together this bioinformatic data suggests that in mouse, CRB2 may exist as a secreted protein, as well as a transmembrane protein.

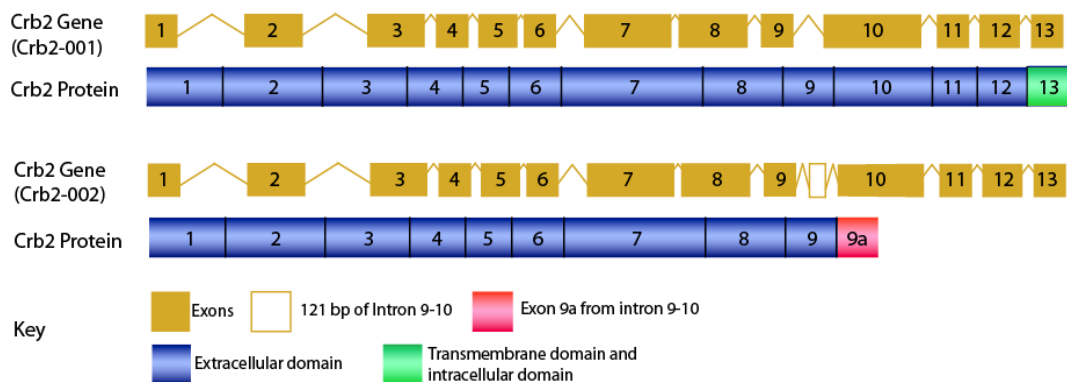


**Figure 5.6** *CRB* isoforms schematic. Schematic of the full-length transmembrane *CRB2* Crb2-001 and the truncated version (Crb2-002). As only a partial transcript of Crb2-002 (exons 8-10) has been detected by sequencing studies, it is unknown how much of exons 1-7 would be included in the protein.

### **5.3 A potentially secreted splice variant of CRB2 can be detected in embryonic mouse**

Currently, there is no antibody against secreted CRB2, so I took a Polymerase Chain Reaction (PCR) approach to the detection of this isoform.

Exon 9a is 121bp long, and contains repetitive and palindromic sequences, suggesting that it might be difficult to design primers. Indeed, I made three attempts to design primers against exon 9a (not shown) and used these in an attempt to clone truncated *Crb2* from a range of tissues, including the dorsal spinal cord and the eye (positive control) (van der Hurk *et al*, 2005). None of these experiments resulted in successful detection of a secreted *Crb2* isoform in any tissue sampled. I therefore adopted a nested PCR approach, working in collaboration with J. P. Ashton.

In order to detect a processed transcript that contained exon 9a, we first designed primers against exon 8 and exon 10 (Table 5.4, Crb2F and Crb2R; Figure 5.7), which should, in theory, anneal with transcripts of both full-length *Crbs2* and truncated *Crbs2*, to amplify the region contained between exon 8 and exon 10. Internal nested primers against exon 8 and exon 9a were designed (Table 5.4, Nested F and Nested R; Figure 5.7) that, in theory, specifically anneal to secreted Crb2, and a second round of PCR was run on the whole reaction from the first round of PCR. A house-keeping gene, Glyceraldehyde 3-phosphate Dehydrogenase (GAPDH), was also run as a loading control.

**Table 5.4 *Crb2* PCR primers**

Primer	Sequence		Exon	Tm
<i>Crb2</i> F	TGTATGTGGGTGGGAGGTTC	[F]	Exon 8	59.0
<i>Crb2</i> R	TAACGGGAAGTCGCCAAGT	[R]	Exon 10	59.0
<i>Nested</i> F	CTACAACTCAACAGCATCC	[F]	Exon 8	59.2
<i>Nested</i> R	GCTTCGGTTGGTAGACTGCC	[R]	Exon 9a	58.3
<i>GAPDH</i>	AACGGGAAGCCCATCACC	[F]	-	59.7
<i>GAPDH</i>	CAGCCTTGGCAGCACCAG	[R]	-	58.0

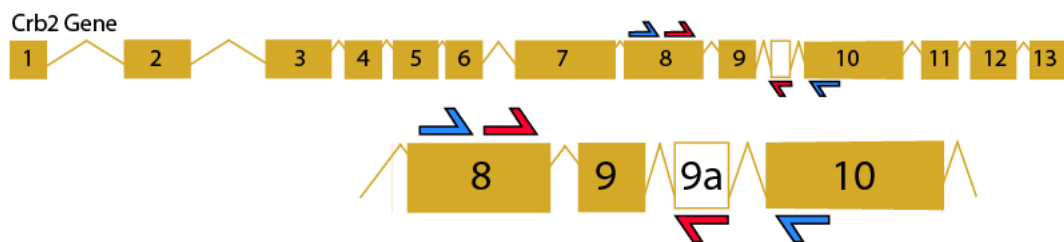


**Figure 5.7** Location of primers. Full gene and ‘zoomed in’ view provided. *Crb2*F and *Crb2*R (first round PCR primers) shown in blue. Nested primers (second round PCR) shown in red.

mRNA was prepared from adult eye (a tissue known to express *Crb2* (van den Hurk *et al.*, 2005), transcribed into cDNA and was then subject to PCR. Bands of ~820 bases and ~940 bases were detected indicative of the sequence without (full-length, transmembrane) and with exon 9a (truncated) respectively. Bands were excised and submitted for sequencing (Table 5.5; Figure 5.9). A second round of PCR was performed on the whole PCR reaction using nested primers, including a primer specifically against exon 9a. This revealed a band of ~400bp (Figure 5.10) that, when excised and sequenced, proved to encode the truncated *Crb2*. This provides proof of principle that the nested primers can detect the putatively secreted variant. In addition, these experiments suggest that a secreted variant of CRB2 may be made in the adult eye.

**Table 5.5** First Round PCR sequencing data

Sequence aligns with exon8-exon10 of Crb2 (Figure 5.8); alternating exons in blue/black

First round PCR - From Eye cDNA
<p> <span style="color: blue;">NNNNNNNNNNNNNNNNNNNNNNGGNNANTNNNTTGGCCCNGTG</span>  <span style="color: blue;">AACTGGAAGCTGGCCAGTCCTCCAACCTCACCCAGGGTTG</span>  <span style="color: blue;">TGTCTCTGAGGACACGTGCAAT</span> <span style="color: black;">CCCAATCCCTGTTTCAAT</span>  <span style="color: black;">GGTGGCACGTGCCACGTCACCTGGAATGACTTCTACTGCA</span>  <span style="color: black;">CCTGCTCCGAGAACTTCACGGGGCCCACCTGTGCCAGCA</span>  <span style="color: black;">GCGATGGTGGCCAGGCAGCCATGCCTGCCTCCTGCCACC</span>  <span style="color: blue;">TGTGAGGAGGTTCCAGATGGCTTTGTGTNTNAGTTTGTGT</span>  <span style="color: blue;">CCTGNNTGCTGGGTACGGAAGATGGTTAGAGATCCCTTAN</span>  <span style="color: blue;">GGTTTATGGGATGNTGGGTGGTGGACCANGAATGCCAACA</span>  <span style="color: blue;">NCCCAATATGGTGGGTACTGCATTCTGAGAAACACTCT</span>  <span style="color: blue;">TANGGAAGGTGAGCATATGCTGGGGTTTCTAAGGCNACTT</span>  <span style="color: blue;">CAAGGGAGCCACAGGANAGGAAGGAGTGTGAGGCATGTGT</span>  <span style="color: blue;">GANGTTTTAAAGTTCCTATGGACAGCTGANACACANGGTT</span>  <span style="color: blue;">ACTAANNNTGCTGCNNNNNNANNATTTGANNCCCACCNNN</span>  <span style="color: blue;">TNNCTCANNNNCCANGGGNNNNNANGNTGNTCNGGCTAGN</span>  <span style="color: blue;">CNGNNTCNNNTNNNNCNNANGGNGATNNNGNNNNNAN</span>  <span style="color: blue;">NNGTGANNNNCCTGNNTCNNNNNNNNNNNNNTNNNGNANN</span>  <span style="color: blue;">ATGNNNNNNNNCCNNNNNNNNNTNNNNNNNNNGNTNNN</span>  <span style="color: blue;">NATGGNNNNNNNNNNNNNTNCNNNCNNNNN</span> </p>

PREDICTED: Mus musculus crumbs homolog 2 (Drosophila) (Crb2), transcript variant X2, misc\_RNA  
 Sequence ID: [ref|XR\\_866014.1|](#) Length: 3272 Number of Matches: 1

Range 1: 2489 to 2727		<a href="#">GenBank</a>	<a href="#">Graphics</a>	<a href="#">Next Match</a>	<a href="#">Previous Match</a>
Score	Expect	Identities	Gaps	Strand	
438 bits(237)	2e-119	238/239(99%)	0/239(0%)	Plus/Plus	
Query 30	TTGGCCCNGTGA	ACTGGAAGCTGGCCAGTCCTCCAACCTCACCCAGGGTTGTGTCTCTGA	89		
Sbjct 2489	TTGGCCCAGTGA	AACTGGAAGCTGGCCAGTCCTCCAACCTCACCCAGGGTTGTGTCTCTGA	2548		
Query 90	GGACACGTGCAATCCCAATCCCTGTTTCAATGGTGGCACGTGCCACGTCACCTGGAATGA	149			
Sbjct 2549	GGACACGTGCAATCCCAATCCCTGTTTCAATGGTGGCACGTGCCACGTCACCTGGAATGA	2608			
Query 150	CTTCTACTGCACCTGCTCCGAGAACTTCACGGGGCCCACCTGTGCCAGCAGCGATGGTG	209			
Sbjct 2609	CTTCTACTGCACCTGCTCCGAGAACTTCACGGGGCCCACCTGTGCCAGCAGCGATGGTG	2668			
Query 210	CCCCAGGCAGCCATGCCTGCCTCCTGCCACCTGTGAGGAGGTTCCAGATGGCTTTGTGT	268			
Sbjct 2669	CCCCAGGCAGCCATGCCTGCCTCCTGCCACCTGTGAGGAGGTTCCAGATGGCTTTGTGT	2727			

**Figure 5.8** BLAST results of sequencing data from eye first round PCR (Table 5.5) confirms that the band is full length/transmembrane Crb2  
 Queried with <http://blast.ncbi.nlm.nih.gov/Blast.cgi>

I then used the same nested PCR approach on spinal cord dissected from E14.5 (*i.e.* the onset of dorsal obliteration). I hypothesised that the truncated isoform will be present in the region harbouring Nestin+ elongated RP cells, but not in lateral VZ cells. Therefore, I dissected these regions (Figure 5.9) and performed a PCR as for the eye on each sample. Bands of 820 base pairs, indicative of the transmembrane protein were obtained from both dorsal and lateral tissues. Bands representing transmembrane *Crb2* were not always visible, however sequencing confirmed the existence of the expected sequence.

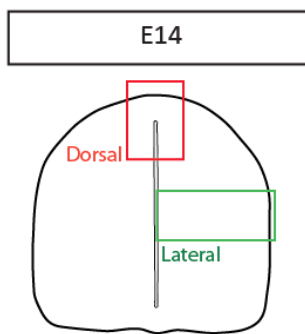
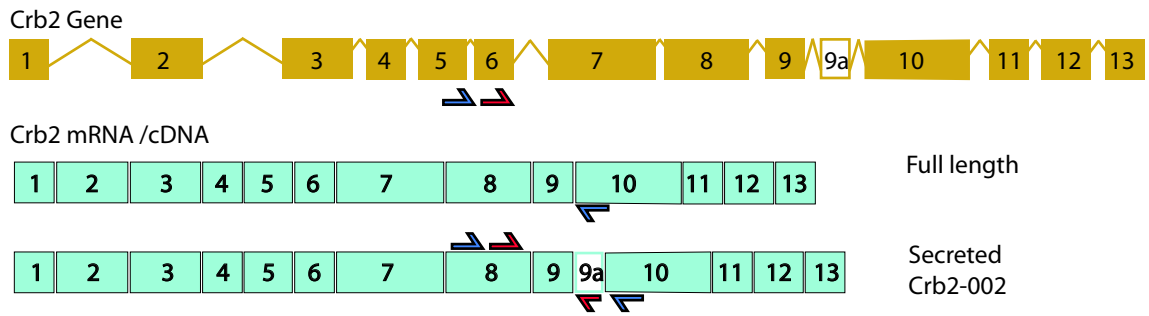


**Figure 5.9** Schematic of spinal cord dissections. The dorsal and lateral dissections for PCR are highlighted in red and green, respectively.

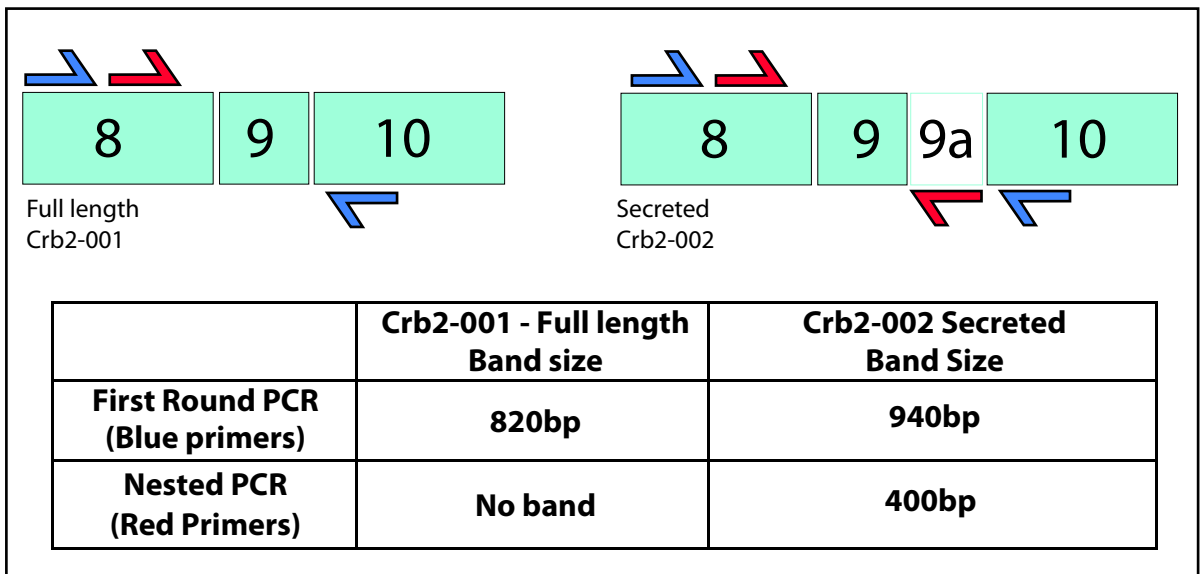
In the first round of PCR, a band of 940 bases and in the second round of PCR a band of 400 bases (indicative of the truncated slice variant) was detected in dorsal tissue, but not in lateral tissue (Figure 5.11). Sequence analysis of the band confirmed that this was the truncated variant of *Crb2* (Table 5.6). A schematic of the PCR process is provided in figure 5.10.

**Figure 5.10** The PCR approach to detecting secreted Crb2

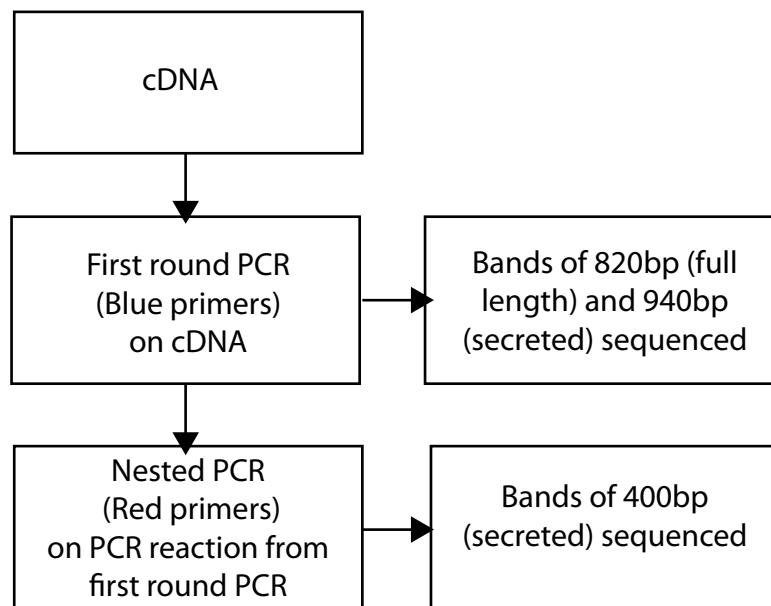
Overview of Crb2 mRNA/cDNA targeted by PCR



Location of First and Second round (nested) primers used in PCR



Overview of PCR protocol



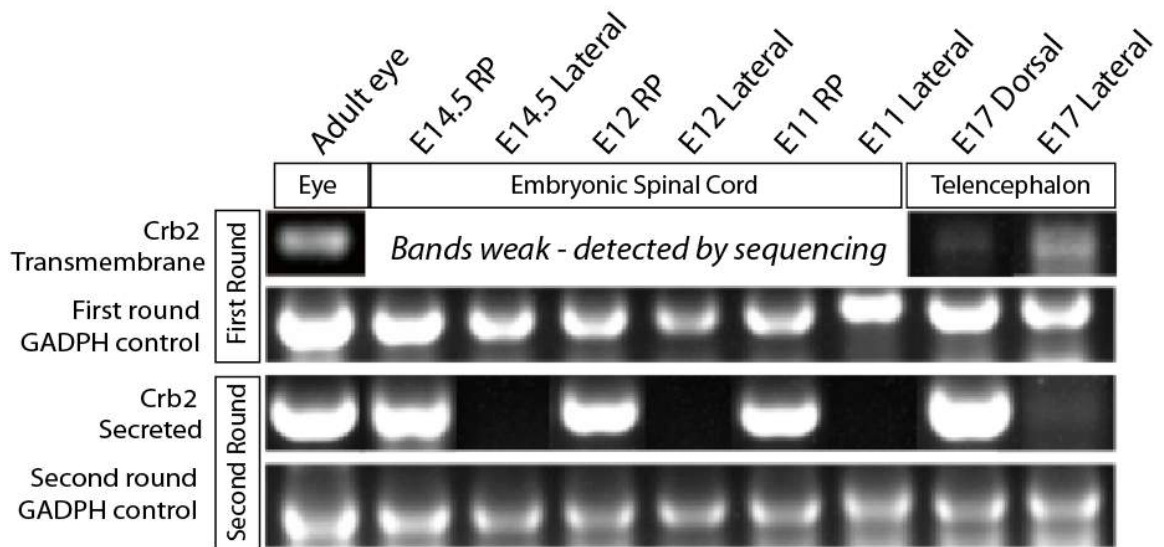


**Figure 5.11** Results from First and second round (nested) PCR Transmembrane *Crb2* is present in all samples tested. The *Crb2* band (820bp) is not always seen on the gel, but can always be detected by sequencing. The 940bp band that corresponds to truncated *Crb2* is often too faint to see in the first round of PCR (not shown). However, robust 400bp bands are seen after the second round/nested PCR. When sequenced, they contain exon 9a. *Gadph* controls are present and strong in both rounds of PCR for all samples.

**Table 5.6** Second round (nested) PCR sequencing data  
Sequence aligns with exon8-exon9a of *Crb2*-002 (Figure 5.12); alternating exons are blue/black. Exon9a is underlined.

Second round PCR – From E14 Mouse dorsal dissection
<p> NNNNNNNCNNNNGGNNANTCNNTTGNNCCNGTGA ACTGGA  AGCTGGCCAGTCCTCCAACCTCACCCAGGGTTGTGTCTCT  GAGGACACGTGCAATCCCAATCCCTGTTTCAATGGTGGCA  CGTGCCACGTCACCTGGAATGACTTCTACTGCACCTGCTC  CGAGAACTTCACGGGGCCACCTGTGCCAGCAGCGATGG  TGCCCCAGGCAGCCATGCCTGCCTCCTGCCACCTGTGAGG  AGGTTCCAGATGGCTTTGTGT<u>TTTANGGACTATGGATATG</u>  GGCCCCTACACCCATTTGTTGGGTGCTAGGGATGGAACC  CAAAGCCTCCTACAAGCTAGGCAGTCTACCNACCGAAGN </p>

UI-M-F10-cdy-m-24-0-UI.r1 NIH\_BMAP\_F10 Mus musculus cDNA clone IMAGE:6836257 5', mRNA sequence.  
 Sequence ID: [gb|CB246995.1](#) Length: 778 Number of Matches: 1

Range 1: 357 to 684 [GenBank](#) [Graphics](#) ▼ Next Match ▲ Previous Match

Score	Expect	Identities	Gaps	Strand
595 bits(322)	6e-167	325/328(99%)	0/328(0%)	Plus/Plus
Query 31	GTGAACTGGAAGCTGGCCAGTCCCTCCAACCTCACCCAGGGTTGTGTCCTGAGGACACGT			90
Sbjct 357	GTGAACTGGAAGCTGGCCAGTCCCTCCAACCTCACCCAGGGTTGTGTCCTGAGGACACGT			416
Query 91	GCAATCCCAATCCCTGTTTCAATGGTGGCAGTGCCACGTCACCTGGAATGACTTCTACT			150
Sbjct 417	GCAATCCCAATCCCTGTTTCAATGGTGGCAGTGCCACGTCACCTGGAATGACTTCTACT			476
Query 151	GCACCTGCTCCGAGAACTTCACGGGGCCACCTGTGCCAGCAGCGATGGTGCCCCAGGC			210
Sbjct 477	GCACCTGCTCCGAGAACTTCACGGGGCCACCTGTGCCAGCAGCGATGGTGCCCCAGGC			536
Query 211	AGCCATGCCTGCCTCCTGCCACCTGTGAGGAGGTTCCAGATGGCTTTGTGTTTANGGAC			270
Sbjct 537	AGCCATGCCTGCCTCCTGCCACCTGTGAGGAGGTTCCAGATGGCTTTGTGTTTANGGAC			596
Query 271	TATGGATATGGGCCCTACACCCATTTGTTGGGTGCTAGGGATGGAACCCAAAGCCTCC			330
Sbjct 597	TATGGATATGGGCCCTACACCCATTTGTTGGGTGCTAGGGATGGAACCCANAGCCTCC			656
Query 331	TACAAGCTAGGCAGTCTACCNACCGAAG 358			
Sbjct 657	TACAAGCTAGGCAGTCTACCAACCGAAG 684			

**Figure 5.12** BLAST results of sequencing data from dorsal neural tube dissection, second round nested PCR. BLAST search confirms that sequence from the 400bp band contains exon9a and is the same sequence as Crb2-002. The BLAST search retrieves Crb2-002 as well as both ESTs (ESTs detailed in Table 5.2). Alignment between the PCR product sequence and EST CB246995.1 shown above.

#### 5.4 A truncated splice variant of *Crb2* is detected in tissues with the ability to disrupt epithelial integrity

I next hypothesised that I would be able to detect the putative secreted, truncated form of *Crb2* in tissues that, in Chapter 4, I had identified as being able to disrupt neuroepithelial integrity. To this end, I subdissected dorsal, or lateral VZ tissue from E11 spinal cord and E17 telencephalon, extracted mRNA from each, and subjected each to the nested PCR approach. These studies revealed that after round 2, a band indicative of truncated *Crb2* was detected only in E17 dorsal telencephalon, and spinal cord roof plate (Figure 5.11). Sequence analysis confirmed that these bands were mRNA that could encode truncated *Crb2* (not shown).



Together these experiments provide evidence that a truncated, putatively secreted isoform of *Crb2* does exist in mouse *in vivo* as it does in human, (Katoh and Katoh, 2004), albeit that the exact splice event is not identical to that in human, and we have no evidence that it is translated.

### **5.5 Secreted CRB2 can mimic the action of dNRG, and disrupt epithelial cells in the embryonic chick**

I therefore next set out to ask whether secreted CRB2 can mimic the action of dNRG, and disrupt epithelial cells in the embryonic chick assay described in Chapter 4. Previously, the Rashbass lab had constructed a HEK 293 cell line that produced a V5- and His-tagged truncated CRB2 (encoded from Exons 1-9a) that was secreted by the cell line into the medium (M. Murtaza thesis). The protein could be detected (via the His and V5 tags) in the media of transfected cells. Both Western blot analysis and liquid chromatography-electrospray ionization (LC-ESI) mass spectrometry were used to confirm that the secreted protein was a CRB2-related protein of the correct size. I soaked affigel beads in purified protein obtained from these cells, or control PBS (see Materials and Methods), and then transplanted secreted CRB2-soaked beads, or control beads into the HH10-12 embryonic chicken neural tube. The aim was to test the effect this secreted protein has upon chicken progenitors, asking if it mimics the effect of the Nestin+ elongated RP cells. After transplantation, embryos were incubated a further 24hrs, then analysed with the same markers used in Chapter 4. In addition, expression of ZO-1 was analysed, to address whether secreted CRB2 would cause a disruption of tight junctions.

Analysis of serial adjacent sections with NKX2.1/laminin, PAX6/laminin, SOX2/dystroglycan, or ZO-1 reveals that secreted CRB2 beads cause similar abnormalities to those detected with Nestin<sup>+</sup> elongated RP cells (Figure 5.13). Progenitor cells, expressing SOX2 or NKX6.1 or are detected ectopically outside the neural tube (Fig 5.13 E and G), often closely associated with basement membrane disruption (arrowheads Figure 5.13 E). Within the neural tube, the normally tight pattern of NKX6.1 is disrupted (not shown). CRB2 and ZO-1 appear to show breaks in the apical expression (Fig 5.13, F and H, arrowhead). Additionally, there appear to be ectopic floor plate and notochord in some transplanted embryos (Fig 5.13 I and K).

By contrast, embryos transplanted with control PBS-soaked beads appeared normal, with an unbroken dystroglycan-labeled or laminin-labelled basement membrane, and normally-patterned SOX2-positive and NKX6.1-positive or neural progenitors confined to the neural tube (Figure 5.13 A-D, I-J).

As disruption to the tissue-transplanted chicken embryos varies in severity. I classified the disruption into 'Strong' 'Medium' and 'Weak', although these ratings are somewhat subjective. 'Strong' phenotypes have clear ectopic neural tube cells outside the neural tube. 'Medium' has internal neural tube disruption, and evidence of cells that appear to be in the process of leaving the neural tube and basement membrane disruption. 'Weak' characterises embryos that have only small basement membrane or minimal cell organisation disruptions, which cannot formally be excluded as sectioning artefacts. These results are shown quantitatively in Table 5.7 and it is demonstrable that the secreted CRB2-soaked bead has a significant association with a strong or medium disruptive phenotype as opposed to the control (Fisher's exact test,  $p=0.042$ ).

Together these results support the idea that secreted CRB2 can disrupt neuroepithelial cell integrity, and suggests that it mediates this function in Nestin+ cells.

**Table 5.7** CRB2s-soaked bead transplants into the HH10-12 embryonic chicken

<b>Tissue Transplanted</b>	<b>Strong Phenotype</b>	<b>Medium Phenotype</b>	<b>Weak/No Phenotype</b>
<b>Secreted CRB2 soaked beads (25)</b>	10	5	10
<b>PBS soaked beads (4)</b>	0	0	4

## Secreted CRB2 bead transplant into HH10 chicken embryo

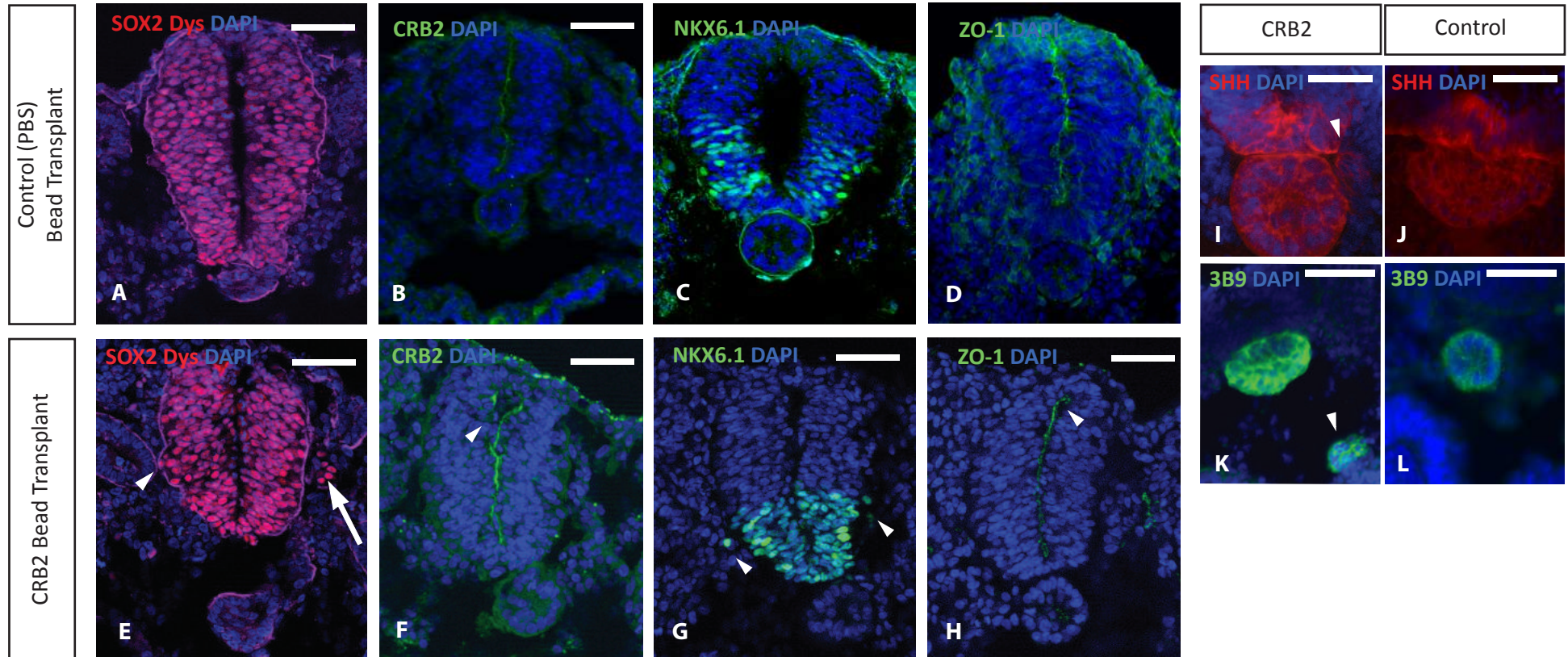


**Figure 5.13** Thoracic transverse sections. The PBS-soaked bead control (A) has a regular, unbroken basement membrane (Dystroglycan, red), and the neural progenitors (labelled with SOX2; nuclear, red) are regularly shaped and positioned. The Secreted CRB2-soaked bead transplanted chicken embryo (E) has bulges of cells either side both within the confines of the basement membrane (arrowhead) and ectopically outside the neural tube (arrow). SOX2<sup>+</sup> progenitors within the neural tube appear disorganised in the CRB2-transplanted embryo (E) The disruption shown in (E) is mirrored by breaks in the apical CRB2 labelling (F' arrowhead) and ectopic NKX6.1 cells (G arrowheads) and breaks in apical ZO-1 labelling (H, arrowhead). (E-H) are serial sections. Occasionally ectopic floorplate-like (I, arrow) or ectopic notochord-like (K, arrow) structures are observed. Scale bars: 50 $\mu$ m, except in (I) and (J), which are 25 $\mu$ m.

## 5.6 Neuroepithelial cells migrate out of the neural tube after exposure to secreted CRB2

As described above, secreted CRB2-soaked beads frequently led to the appearance of ectopic PAX6 and NKX6.1-expressing cells, some of which appeared to be located immediately adjacent to, but outside, the neural tube (Figure 5.13, arrowheads). To provide direct proof that such progenitors had originated within the neural tube (rather than being non-neural progenitor cells provoked, by secreted CRB2, to undergo a change in fate), I coupled bead-transplantation experiments with electroporation studies. As described in the Material and Methods, RFP was electroporated into the neural tube of an HH10-12 chicken embryo, followed immediately by transplantation of secreted CRB2-soaked (or control) beads. The RFP construct used is not neural specific, but at the low concentrations of plasmid used, and with targeted electroporation, it is unlikely that RFP+ cells outside the neural tube were unintentionally electroporated. This would allow me to determine whether progenitors found outside the neural tube had migrated out of the neural tube, rather than undergone a fate change. Some ectopic cells appear to express SOX2 more weakly than those in the *in situ*, it may be that cells are down-regulating SOX2 as they leave the neural tube.

The PBS-soaked bead control (Figure 5.14, A-C) has a regular, unbroken basement membrane, and the neural progenitors (labelled with SOX2) are regularly shaped and positioned within the neural tube. Although there are RFP-expressing cells outside the neural tube, these are not SOX2-expressing cells. The secreted CRB2-soaked bead transplanted chicken embryo has RFP+ SOX2 expressing colabelled cells outside the

neural tube boundary (Figure 5.14 D-I, arrows) accompanied by basement membrane breaks.

In conclusion, secreted CRB2 can provoke a disruption to the integrity of the neuroepithelium that is sufficient to allow neural progenitors to escape from the confines of the neural tube.

Secreted CRB2 bead transplant into RFP-electroporated HH10 chicken embryo

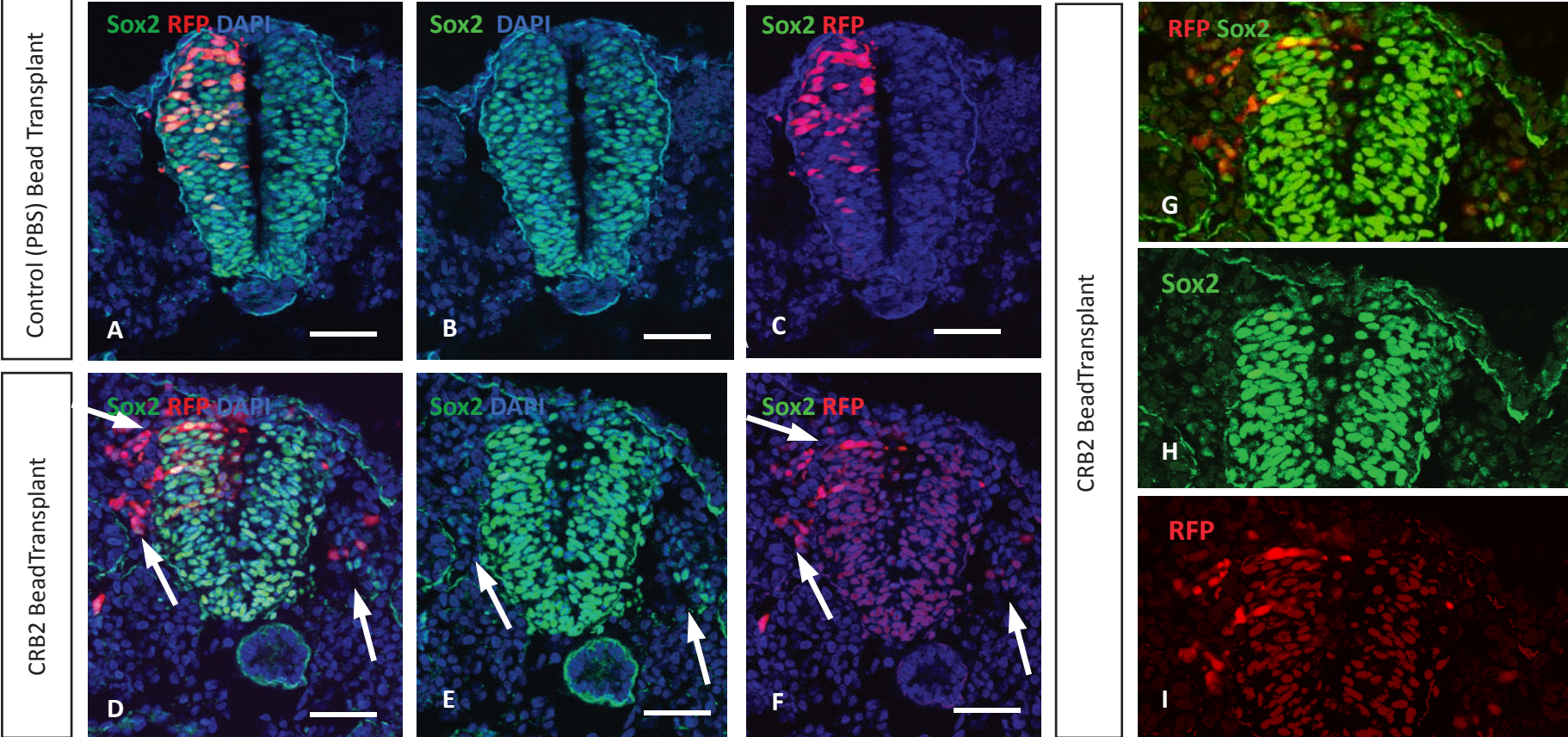


**Figure 5.14** Thoracic transverse sections. The PBS-soaked bead control (A-C) has a regular, unbroken basement membrane, and the neural progenitors (labelled with SOX2) are regularly shaped and positioned. Although there are RFP+ cells outside the neural tube, these are not SOX2-expressing cells. The Secreted CRB2-soaked bead transplanted chicken embryo (B) has RFP+ SOX2 expressing colabelled cells outside the neural tube boundary (arrows). Images (G-H) is the same CRB2 transplanted embryo, shown magnified and without DAPI for clarity. Scale bar: 50µm.

## 5.7 Discussion

In this chapter I asked (1) whether I can find evidence for a isoform of CRB2 that lacks the transmembrane domain *in vivo*, and so may function as a secreted variant; (2) whether a secreted protein encoded by this splice variant and overexpressed in a cell line is biologically active; and (3) whether secreted CRB2 can disrupt neuroepithelial integrity in a similar manner to transplantation of the dorsal Nestin-positive region.

### 5.7.1 Evidence for secreted CRB2 *in vivo*

Bioinformatic analyses suggest that *Crb2* is alternatively spliced, and that one of the isoforms includes a truncated transcript, Crb2-002. Recent annotations (Ensembl, June 2015) agree with our interpretation that a STOP codon is introduced by the addition of intron 9-10. My immunohistochemical analysis revealed that CRB2 has an atypical distribution in the dorsal most VZ, leading to the question: does the presence of secreted CRB2 explain the atypical expression pattern of *Crb2* in the dorsal VZ?

My PCR results suggest that it might, and show that truncated *Crb2* transcript exists *in vivo* in the mouse. While large-scale exome sequencing projects are powerful, they may pick up transcriptional noise due to aberrant or non-processed transcripts. However, my repeatable PCR results, and the specific regionalisation of those transcripts to dorsal spinal cord and dorsal telencephalon suggest that an isoform of CRB2 that lacks the transmembrane domain, and is therefore likely to be a secreted protein if translated, is transcribed as an mRNA. The addition of *Crb2* exon 9a in the mouse would lead to a frameshift, allowing the translation of a premature stop codon. If translated this isoform would cause truncated protein, consisting of only the extracellular part of CRB2 – a putatively secreted protein. In support of this idea,



transfection of an artificially created isoform into HEK 293 cells results in the appearance of a novel band of between 110 and 180kD in the medium (Miturza, 2011). Furthermore, my studies show that such conditioned medium contains secreted CRB2 that can disrupt neuroepithelial integrity.

### **5.7.2 Secreted CRB2 mediates the activity of dNRG**

A number of lines of evidence suggest that *in vivo*, secreted CRB2-expressing cells are either dNRG or are closely associated with them. First, my PCR data suggests that there is strict regionalisation of the truncated transcript, and therefore probably the secreted protein. Second, the profile of *Crb2* in the Allan Brain Atlas mRNA data (probe against Exon13 of the transmembrane isoform, thus detecting only the full-length mRNA) confirms unusually high expression of *Crb2* in a region close to Nestin processes in the early postnatal (4 day) mouse, a pattern that is not seen in the 56-day-old adult. No embryonic data was available (Fig. 5.15). Third, the immunohistochemical studies that I described in Chapter 3 showed close, or even co-localisation of Nestin expression and atypical *Crb2* expression, particularly strong in, or around, the endfeet of the dorsal Nestin+ cells.

Together with the observation that transplanting beads soaked in secreted CRB2 results in a similar phenotype to that of transplanted mouse dorsal Nestin cells, my results suggest that secreted secreted CRB2 mediates an ability of dorsal Nestin cells to disrupt neuroepithelial integrity.

Allan Developing Brain Atlas: *Crb2* mRNA

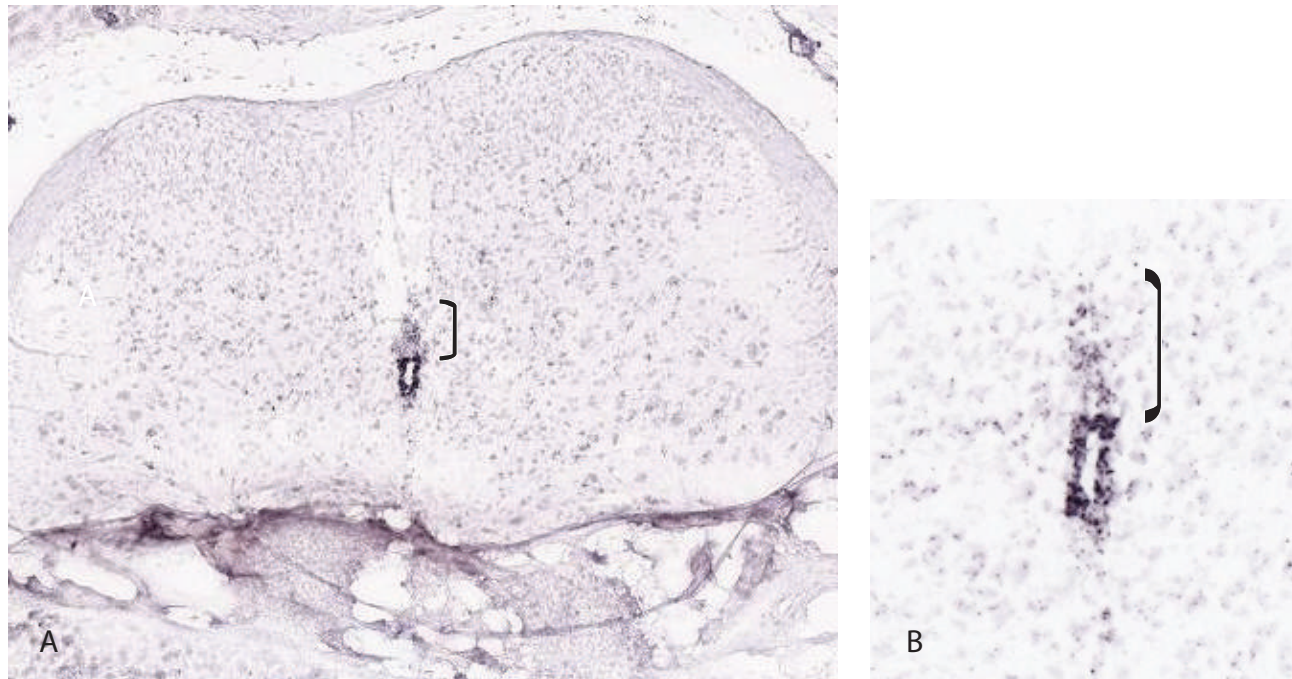


**Figure 5.15** Allan Brain Atlas: *Crb2* *in situ* analysis of a 4 day old mouse spinal cord. Strong labelling around the central canal is seen. Dorsal to the central canal, there is a line of punctate expression (bracket). magnified view in (B).

Allan Developing Brain Atlas: <http://mousespinal.brain-map.org/imageseries/show.html?id=100021981>

If this is the case, why can I detect the isoform of truncated CRB2 in roofplate cells at E11/E12, a time when roof plate cells do not have the ability to disrupt neuroepithelial integrity? A possible explanation is that translation of the isoform into a functionally active protein is delayed until the start of dorsal obliteration. In support of this, atypical CRB2 expression is not detected before E15.

The disruptions that I detected after transplanting secreted CRB2 are greater than those detected after transplantation of Nestin positive cells. Why might this be? A likely possibility is that secreted CRB2-loaded beads release much more protein into the embryo than is physiologically relevant. In support of this idea, analysis of RNA sequencing data (available from Ensembl: not shown) suggests that, although this transcript can be processed from neural tissue, there is not a strong RNAseq signature, suggesting that secreted CRB2 is present in the dorsal neural tube at very low levels. This agrees with my experience, in that roofplate samples from around 40 embryos are needed to detect truncated *Crb2* mRNA in my hands.

### **5.7.3 A model for the action of secreted CRB2 in disrupting epithelial integrity**

The intracellular domain of transmembrane CRB2 acts as a scaffold for the CRB complex, and thus is a crucial for its familiar function as a polarity protein (Rashbass and Skaer, 2000). Studies in zebrafish suggest that the extracellular domain of CRB2 homodimerises, and that homodimerisation stabilises the entire CRB2 complex (Zou *et al.*, 2012). This leads to the interesting possibility that secreted CRB2 may be able to compete or interfere with the homodimerisation of transmembrane CRB2. This would lead to the destabilisation of the CRB complexes, and thus of apical polarity. As loss of polarity is a major step in allowing cell delamination from an epithelium, this would

provide a mechanism for secreted CRB2 to mediate the effects we observe *in vivo* (Figure 5.16).

In conclusion, in this chapter I have presented evidence for the possible presence of secreted CRB2 during the dorsal obliteration window, shown that secreted CRB2 can mediate epithelial delamination and suggested a possible mechanism by which it might regulate cell polarity. However, I have not presented evidence that secreted CRB2 operates in this manner to mediate dorsal obliteration. In Chapters 6 and 7, I present studies that will, in future, allow me to address this question.

## CRB2-CRB2 interactions

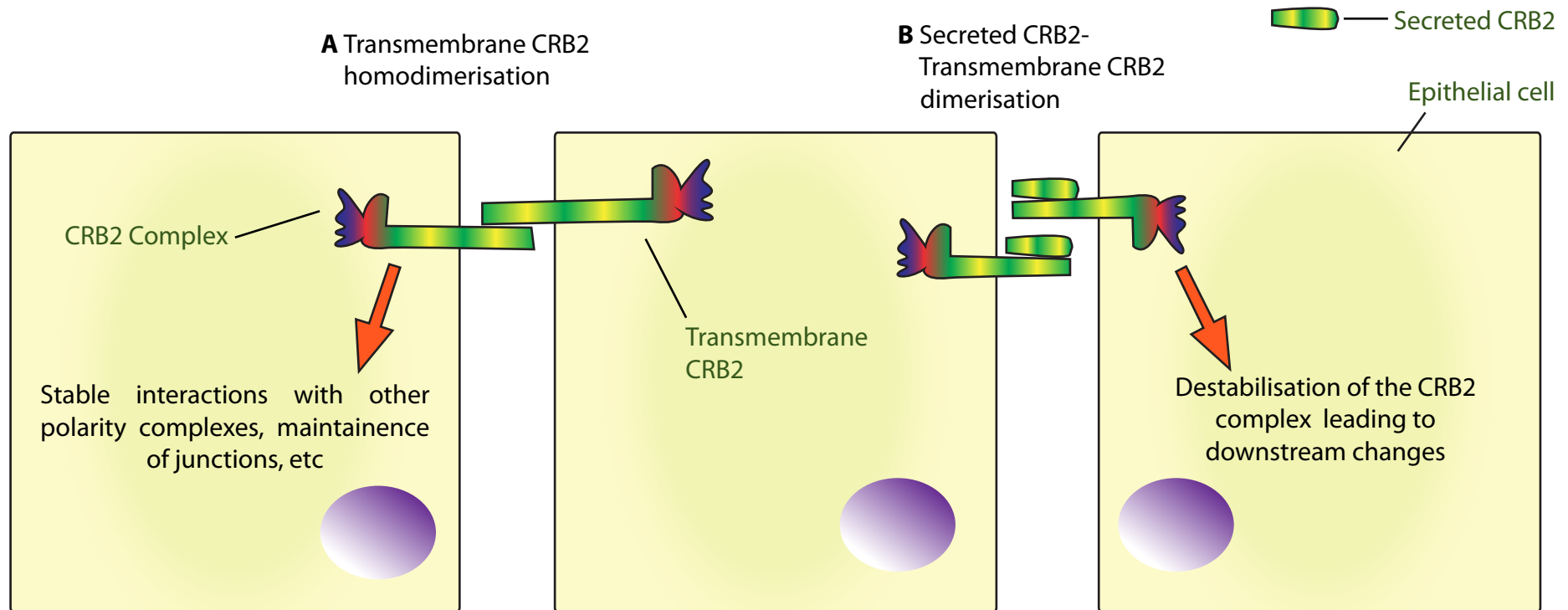


**Figure 5.16** CRB2-CRB2 interaction (A) has been shown to stabilise polarity in epithelia through homophilic binding of the long extracellular domain; Zou (2011). Secreted CRB2 has the same sequence as the extracellular domain of Transmembrane CRB2 and thus they may dimerise (B). Secreted CRB2-Transmembrane CRB2 dimerisation may destabilise the epithelia by preventing the stabilising homodimerisation of transmembrane CRB2.

# Chapter 6

## Slice culture optimisation

## 6.1 Introduction

I reasoned that in order to be able to address whether secreted CRB2 is indeed playing a role in disrupting the integrity of sub-dorsal Ventricular Zone (VZ) cells, I would need to develop a robust model in which I could dynamically visualise the cellular processes that occur in dorsal obliteration. Dorsal obliteration occurs along the dorsal-ventral axis, through the centre of the tissue, and *in vivo* and *ex utero* cultures are not suitable for imaging this process. I considered whether to develop a model using an alternative species, but ruled out these possibilities: the chicken embryo undergoes dorsal obliteration over E7-E12 (Appendix 1), a time when the embryo is large and tissue is too dense to image through. The zebrafish is transparent and transgenic lines that express markers suitable for imaging spinal cord development are available. However, zebrafish undergo a process that is broadly similar to secondary neurulation and are therefore not necessarily a suitable model in which to examine dorsal obliteration of the type examined in this thesis (Schmidt *et al.*, 2013). I therefore set out to develop a mouse slice culture system in which to dynamically follow dorsal obliteration.

Organotypic slice cultures are rapidly gaining popularity as a technically easier, more accessible and more ethical alternative to working *in vivo*, and have been utilised for multiple studies in rodents and other organisms. Advances in microscopy and the availability of electroporatable plasmids that express both cell type-specific and general reporters have allowed slice culture to become a way of live imaging previously inaccessible tissues. The main challenge of working with slice cultures is controlling the environment so that the tissue behaves in a reproducible way relevant to normal processes occurring in the animal. For instance, *in situ* tissue receives molecular and mechanical signals from surrounding tissues, and the effect when these

are removed is unknown. This is especially true for developing tissues undergoing stretching morphogenesis, and in the case of the neural tube, clearly developing along the rostro-caudal and dorso-ventral axes. Additionally, composition of media has a profound effect upon the behaviour of slices in culture, and it has become clear that the media needs to be optimised specifically for aspects assayed, tissue type and age. An additional challenge comes through sectioning, which clearly causes trauma to the tissue: indeed, neural slice culture has been used as an assay for injury response. Collectively, this means that published papers report optimised protocols for a particular type and age of tissue, and each procedure is optimised for a particular read out, for example, electrophysiology of neurons.

Live imaging of developing tissue comes with additional challenges. Not only does a tissue and age-specific culturing regime need to be developed to keep the tissue healthy over an extended period of time, but it must be cultured in a way that is amenable to imaging, and imaged in such a way that minimises phototoxicity (Dailey *et al.*, 2011). These limitations notwithstanding, slice culture has proved a useful and informative tool to study neural cell behaviour in detail.

Relatively few papers have described slice cultures and imaging in the developing nervous system, and the majority of these are focussed on the brain. However, more recently, embryonic spinal cord *ex vivo* cultures have been established in chick (Das and Storey, 2014; Tubby *et al.*, 2013), in mouse (Brachmann and Tucker, 2011) and in rats (Pakan and McDermott, 2014). For timelapse experiments, Brachmann and Das used widefield microscopy to image developing neurons, and McDermott used two-photon microscopy.



This chapter describes the slice culture protocols that I developed to allow me to perform subsequent *in vivo* imaging during the obliteration window (E14-E16) of embryonic mice (described in Chapter 7). Several of the optimisation steps were worked out in collaboration with Dr. Raman Das (University of Dundee).

## **6.2 Optimising slices and handling**

The first hurdle in slice culture is that embryonic mouse slices are accustomed to the mother's stable internal body temperature and the constant supply of nutrients and oxygen. In order to slow tissue degradation, the tissue was held on ice whenever possible during the procedure, kept in cold medium when working under the microscope, and the room temperature steps kept as short as possible. Ideally, tissue should go from uterus to incubator in under an hour, certainly not more than 90 minutes.

## **6.3 Gross dissection**

The uterus was dissected out into L-15 on ice and the embryos dissected out from membranes quickly, before decapitation and evisceration. The embryos were then transferred to new L-15 on ice. Embryos were taken individually into a fresh dish of L-15 and the back flattened by snipping any tissue under tension with watchmaker scissors (figure 6.1). Subsequent to dissection, each step required optimisation, as detailed below.

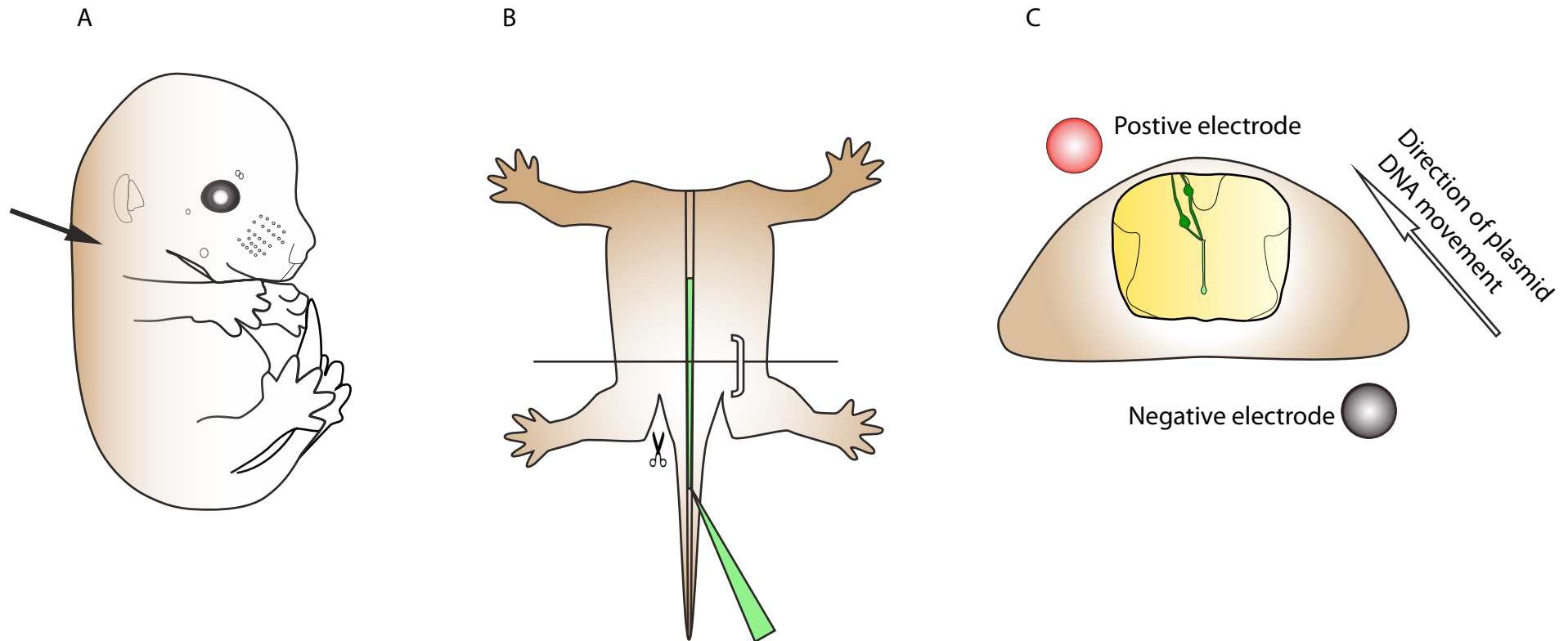


**Figure 6.1** Schematic of E14/E15 mouse electroporation.

(A) depicts the embryonic mouse. The arrow shows the point and angle at which it is decapitated. After evisceration, the mouse is laid out in an open book conformation (B). The area that sections are to be taken from is depicted by the bracket. A glass pipette is used to inject plasmid into the spinal cord, caudal to the area of interest (B; green). The line in (B) represents the cross-section shown in (C). Electrodes are placed above (positive) and underneath (negative) the embryo, and a current run through the spinal cord at an angle to specifically targets the plasmid towards dNRG (position of electrodes shown in cross section (C)).

#### **6.4 Plasmid injection and electroporation**

In initial studies I followed the standard protocol in our lab; cutting embryos into 400 $\mu$ m slices, then dropping DNA into the lumen and placing electrodes either side of whole slices to electroporate. However, the precision of electroporation proved difficult to control, and the cut surface was often also electroporated which obscured examination of otherwise well-electroporated target cells.

In collaboration with Dr. Raman Das, I therefore developed an alternative protocol, electroporating the entire intact spinal cord. This method proved to be much more efficient and precise. To maintain consistency with my previous analyses, I targeted the lumbar spinal cord, injecting DNA using a pulled glass needle into the most caudal point of the sacral region, where the lumen is easily accessible (Fig6.1B). Fast green/plasmid mix was mouth pipetted into the lumen until the green was seen rostral to the region of interest. Electrodes were placed so that the negative electrode was under/ventral to the embryo and the positive electrode was over the top/dorsal. (Fig6.1C). The electrodes were angled so that current flowed precisely through the location to be targeted. After the neural tube was electroporated, excess tissue was trimmed to allow ease of mounting. Tissue immediately surrounding the neural tube tissue was kept *in situ*, as it may be providing signals important to maintain tissue health and integrity.

#### **6.5 Sectioning**

I first attempted to section tissue on a tissue chopper, reasoning that tissue choppers have the advantage of throughput (tissue processed under a minute). However, even at the gentlest setting, the morphology of the delicate embryonic tissue became

damaged, and it proved difficult to control the regularity of slice size as the tissue moves around slightly as it is being processed.

Vibratome sectioning proved to be a much slower, but much gentler method. Multiple tissues were mounted in a mould, encapsulated in agarose and set at room temperature (around 5 minutes). Blocks were superglued onto chucks. The brand of superglue proved to be important, as some types did not set strongly or quickly. Loctite proved to be an optimal brand.

The vibratome tank was filled with ice-cold PBS, or L-15. Ice packs were placed either side of the tank to keep it as cold as possible. Sections were collected from the tank using an egg spoon/number 5 forceps and placed in L-15 on ice. Tissue was sectioned at low speed and largest amplitude, using a fresh razor blade each experiment. 300µm proved to be the optimal thickness for sections: thinner sections were fragile to handle and tended not to survive well in culture. Thicker sections had too much out of focus light and a higher chance of cells moving out of focus when imaging,.

## **6.6 Slice mounting**

For high-resolution imaging prior to culture, slices were embedded in a 3-dimensional substrate and then mounted on a microscopy grade dish, as close to the glass bottom as possible. Dishes were Poly-D-Lysine Coated Fluorodish Cell Culture Dishes, 35mm, (Das and Storey, 2014). I compared two different mounting substrates; rat tail-derived collagen and Matrigel . The former is an established method for mounting tissues and explants. It is easy to use and inexpensive, however, it is not chemically defined and therefore may have batch-specific effects.. The latter is a fibroblast-derived

extracellular matrix compound that has been increasing in popularity as a versatile and manipulatable substrate.

Matrigel-mounted slices appeared to survive slightly better than collagen mounted slices. However, the slices were much more difficult to mount accurately as Matrigel sets extremely quickly, more so when not kept on ice. This made accurate orientation under the microscope (both dorso-ventral, and position relative to the bottom of the dish) very difficult. Working with Matrigel was slow, frustrating and ultimately led to relatively few slices mounted. However, it should be noted that the speed of substrate setting, the slightly better health of the tissue and the growing popularity of Matrigel in published papers makes this substrate a candidate for further optimisation in future applications.

When mounting in collagen (in collaboration with Dr. Raman.Das), I initially followed the procedure described in Das and Storey (2014), optimised for chick spinal cord slices. Slices were transferred onto a 20-30ul bed of collagen, using a Pasteur pipette, and the slice then orientated and pushed flat against the dish bottom with forceps. However, this protocol was not optimal for the more delicate mouse slices that tended to split at the roof plate especially at E13-E14. Further, successfully transferred slices were difficult to push flat onto the bottom of the dish without damaging the tissue. Additionally, there was a high number of unimagable slices due to tissue not being close enough to the bottom of the dish, either because the slices were not flush with the bottom, or because they had begun to float as the collagen set. A high number (60-70%) of collagen beds detached as I carried the plate from the incubator to the imaging facility.

I therefore optimised the collagen mounting. Collagen was made immediately prior to mounting. 15-20 $\mu$ l beds were pipetted into the dish, then drawn back up with the same pipette leaving only a very thin layer of collagen on the imaging dish, the 'collagen disc'. The collagen in the pipette was then deposited onto another dish, the 'coating dish'. Slices to be mounted (usually 5 or 6) were carefully separated from the agarose (still immersed in L-15), lifted out using Number 5 forceps, and immersed into the collagen on the coating dish. Lifting the tissue in this manner could damage the tissue both directly by the forceps themselves but also when passing the sample through the meniscus of the surrounding media. However, damage could be limited by allowing the tissue to rest naturally on one of the forceps' prongs (rather than picking it up by 'tweezing' it) or by picking it up in a drop of L-15 suspended between the arms of the forceps (much harder to achieve). Transferring the tissue by pipette (silicone-coated, collagen-coated, glass or standard pipette) led to high losses, as the tissue is sticky and often tears at the midline.

In the time taken to transfer slices into the coating dish, the collagen discs became sticky. It was important not to leave the time between these steps too long (*i.e.* each imaging dish was prepared individually, rather than in batches) as if the collagen disc dried out completely the collagen bed placed on top was more likely to detach. Slices were then lifted out from the collagen of the coating plate, and placed into the collagen discs of the imaging plate. To do this, slices were nudged towards the top of the collagen and then lifted out, using surface tension to transfer a blob of collagen without the slice coming into contact with the forceps. It was generally best to keep the coating dish under the microscope, and the imaging dish to the side of the microscope where side-light made the collagen discs obvious. I found that transferring

the slices in this manner led to higher successful rates of transfer, as opposed to swapping the dishes under the microscope, or moving between two microscopes.

In all cases, prior to transfer, imaging dishes were labelled before use, and a large black mark made at the back of the dish walls. Labelling was carried out while the dish was still mostly in the wrapper, to decrease the chance of fingerprints or dirt on the imaging surface. The imaging dishes were immediately placed into a larger dish lined with microscope tissue, and were only taken out to image. This ensured that no small scratches or dirt on the glass of the imaging dishes impaired the imaging quality. When all slices were transferred, the imaging dish was orientated so that the black mark was at the top of the dish. Each slice was then orientated so that the ventricles of each slice were parallel, and the dorsal edges of the slices were pointing towards the top of the dish. This ensured that the plate could be easily orientated for imaging, and that each slice within the dish was at the correct orientation.

The collagen-embedded slices were left to set. This was carried out at room temperature so as not to disturb the orientation of the slices when transferring them to the incubator. Another layer, approximately 10 $\mu$ l, was placed on top of each bed. The slices were then left to set at 37°C. When set, 3ml of 37°C media was added. The slices were kept in a 37°C 5% CO<sub>2</sub> humidified incubator. As far as practical, the slices were protected from sharp knocks and shocks (*e.g.* closing the incubator door carefully), as mouse tissue is sensitive to this sort of trauma. Slices were left for 12+ hours to recover and for the fluorescent proteins to be expressed.

This protocol is quick and effective. In my hands, compared to the protocol used by Das *et al*, I found that I had considerably fewer losses due to slices being damaged when transferred by pipette or when pushed down to the bottom of the collagen bed, ~100% success of slices correctly placed in order to be imaged, and ~100% of collagen beds remaining attached to the plate when carried.

### **6.7 Imaging**

Imaging was carried out on a Deltavision Core microscope system, using a 20x oil or dry lens. Images were captured using a Xenon light source and a CoolSnap HQ2 cooled CCD camera (photometrics). Thirty to forty optical sections (exposure time, 10-50 milliseconds for each channel, 512x512 pixels, 2x2 binning) spaced 1.5 $\mu$ m apart were imaged for each slice at 10-minute intervals over 24 hours. Images were deconvolved and maximum intensity projections of Z-stacks were made using SoftWorx imaging software (Applied Precision). A bright-field reference image was acquired at each time point and this was used to determine the position of the apical surface. Slices were kept in a WeatherStation environmental chamber at 37°C with 5% CO<sub>2</sub>, with a dampened tissue placed in the chamber to keep the dish humidified.

### **6.8 Media optimisation**

Selecting appropriate media is a critical task in slice culture. It feeds the tissue, keeps it healthy, and provides extrinsic signals that can *e.g.* tip the balance of differentiation and proliferation. As described in section 6.2, many studies have been carried out on slice culture, and each has optimised media in order to carry out those specific studies. I used these protocols as a basis therefore, and carried out optimisation in order to obtain the best data from my slices.



The first question that needs to be addressed is the readout by which the media is going to be judged. In this case, I looked for media that would maintain an intact ventricular zone, as analysed by SOX2, Crb2 and ZO-1, would not cause an expansion of the dorsal Nestin population and would not promote unusual proliferation or apoptosis. As previously discussed, slice culture can be used as an injury model, characterised by an expansion of Nestin positive cells, the depletion of the ventricular zone of SOX2 progenitors and the increase of SOX2 cells intercalated with the Nestin-positive processes. I aimed use the media that would best maintain the tissue in a normal rather than injury state.

### **6.8.1 Media composition and purpose**

#### **Components of media**

Much of the information on this section was taken from the extensive *Cell Culture Media: A Review* (<http://dx.doi.org/10.13070/mm.en.3.175>) last modified: 2015-08-02; original version: 2013-03-05. Accessed August 2015, additional information was taken from manufacturer datasheets.

#### *Basal media*

Basal media can be either artificial (composition specified) or natural (biological fluids, exact composition not known, batch variability). While natural media can be very useful, reproducibility is an issue. Therefore, artificial media is preferred in many situations. Defined artificial media is prepared with nutrients, vitamins, salts, serum proteins, carbohydrates *etc*, and composition varies depending on intended application.

### *Buffering systems*

Culture pH can have a huge impact on the viability of cells and tissue. Buffering can be achieved by 'natural buffering' in which the  $\text{CO}_3/\text{HCO}_3$  of the medium is balanced by  $\text{CO}_2$  gas in the air, usually by maintaining cultures in a 5-10%  $\text{CO}_2$  incubator. This system can become alkaline quickly (within minutes) in air, thus it is important to include an indicator, such as phenol red and work quickly, Alternately, HEPES can be used, which maintains strict buffering between pH 7.2-7.4, does not require  $\text{CO}_2$  buffering but can be toxic at high concentrations for some types of cells. Additionally, HEPES has been shown to greatly increase cytotoxicity of media exposed to fluorescent light (Zegler *et al.*, 1985). Phenol Red is often present in commercial media, where it functions both as a pH buffer and an indicator, allowing cultures to be visually monitored and infections *etc* to be easily identified. However, phenol red can mimic the effects of hormones such as oestrogen and interfere with other elements of metabolism.

### *Serum*

Serum is derived from the blood of foetal calves, collected from the fluid remaining after the blood coagulates. As such, it is a complex mix of factors. Although extremely useful in keeping cells healthy in culture, it has the caveat that different batches will have different compositions and concentrations thereof, all of which are unknown. Serum also has buffering ability.

### *Antibiotics*

Antibiotics inhibit the growth of bacteria and fungus, however, they can also interfere with the normal function of certain cell types.

### *Other elements*

Serum free media are usually made with the addition of inorganic salts, carbohydrates, proteins/peptides, fatty acids/lipids, vitamins, trace elements and amino acids, which would otherwise be supplied by serum.

## **6.8.2 Media tested in this optimisation**

Four types of media were tested: 'Brachmann' as described in Brachmann and Tucker (2011) 'Dundee' as described in Das and Storey (2014); SRN2, a medium developed in our lab to support neural-derived cells, and explant media, a standard media we use for culturing explants (Dale *et al.*, 1997; Dale *et al.*, 1999; Vesque *et al.*, 2000)

The components of media tested in this optimisation are as follows:

**Brachmann media:** DMEM, HBSS Ca<sup>2+</sup>Mg<sup>2+</sup> free, Fetal Calf Serum, Glucose, L-glutamine, HEPES, Pen-strep

**Dundee media:** Neurobasal, Glutamax, B27, Fetal Calf Serum, Gentamycin

**Explant medium:** Optimem, L-glutamine, Pen-strep, Fetal Calf Serum

**SRN2:** DMEM-12, L-glutamine, N2, B27-I, Heparin

**Table 6.1 Purpose of media components**

Component	Purpose
<b><i>Basal medium</i></b>	
DMEM	<p>Dulbecco's modified Eagle's medium is a nutrient rich medium. Originally developed to support cells in culture, thus geared towards the promotion of rapid cell division of somatic cells. Contains no proteins or growth promoting agents, therefore usually used with serum. Uses a sodium bicarbonate buffer system, therefore needs incubated with CO<sub>2</sub>. Widely used in both murine and chicken cell/tissue culture.</p>
DMEM F12	<p>Dulbecco's Modified Eagle Medium (DMEM): Nutrient Mixture F12 (Ham's) (1:1). Ham's F-12 was formulated as a nutrient rich media. Serum free versions include HEPES buffer.</p>
Neurobasal	<p>Developed to meet the different nutrient needs of embryonic neurons in culture. Developed by noting that neurons in DMEM:F12 had higher viability than DMEM, and thus optimising the concentrations of the F12 components for neural maintenance (removing for example, excitatory amino acids glutamate and aspartate). Generally used with B27.</p> <p>(Brewer <i>et al.</i>, 1993)</p>
OptiMEM	<p>Serum free growth factor/insulin-containing medium. Contains HEPES and Sodium Bicarbonate buffering. Contains various additives that allow a reduced volume of serum to be used.</p>

HBSS	Hanks Balanced Salt Solution. No buffering. Also contains D-Glucose.
<b>Serum</b>	
FBS	Fetal Bovine Serum (Also, FCS: Fetal Calf Serum). Cheap additive containing a complex range of nutrients and growth factors. Good for maintaining healthy tissue generally – but has the caveat that there can be massive variation between batches and the composition of the serum is generally unknown.
<b>Energy and nitrogen</b>	
D-glucose	Glucose is very soluble and chemically stable in normal physiological solutions and media. Approximately 5.5mM D-glucose approximates normal blood sugar levels <i>in vivo</i> . Usually present in Basal Media.
L-glutamine	L-glutamine is a particularly notable additive to media, as it supplies nitrogen for NAD, NADPH and nucleotides, and can be metabolised for energy. However this essential amino acid is unstable, and is converted to ammonia when degraded, which can be toxic.
Glutamax	Glutamax is a more stable alternative to L-glutamine, and may be preferred for long term cultures.
<b>Other components</b>	
Heparin	Heparan sulfate is a polysaccharide component of the extracellular matrix. It can modify tissue responses to other factors, e.g. it stabilises FGF binding to receptors and can

	influence neurite outgrowth (Kinnunen <i>et al.</i> , 1996; Ornitz <i>et al.</i> , 1992)
B27	Supplement developed for growth/maintenance of neurons. With or without insulin. Insulin-containing versions may promote over-differentiation in neural slice culture (Placzek lab, unpublished)
N2	Serum substitute, developed for growth/maintenance of neural cells
Antibiotics	Penicillin-Streptomycin or Gentamycin was used. Gentamycin is stronger and broader spectrum.

## 6.9 Results

Slices were cultured for 24 hours in appropriate media and then cryosectioned at 20-30µm, before analysis with various antibodies (Fig 6.2).

**Table 6.2** Antibodies used in analysis of slice culture.

Antibody	Purpose
Nestin	Labels dorsal Nestin cells
SOX2	Marker of the ventricular zone
CRB2	Apical polarity marker
ZO-1	Apical junction complex marker
Cleaved Caspase	Apoptosis marker
KI67	Proliferation marker

The criteria that the media was tested on included the maintenance of the ventricular zone, apical surface and with a normal distribution of Nestin.

Control freshly fixed spinal cord slices labelled with SOX2, NESTIN and CRB2 were provided for comparison with cultured slices (Fig6.2, A-C). Of the four media tested, only Brachmann and Dundee had a normal looking ventricular zone, although SOX2-expressing cells were more dispersed dorsally than in an intact embryo (Fig 6.2, Ai-Di, Aii and Dii). Explant media lost the SOX2-positive cells around the ventricular zone entirely (Fig6.2, Aiii), those SOX2-expressing cells were localised entirely around the dorsal neural tube. Nestin also displayed an unexpected and unusual upregulation around the ventricular zone (Fig 6.2, Bii). SRN2 Media showed an increased dorsal upregulation of nestin and dorsal localisation of SOX2-expressing cells (Fig6.2, Aiv-Biv), a pattern that is seen in unhealthy tissue (tissue in any media shows this distribution if not processed quickly enough).

Of all the media tested, only Brachmann media showed good Crb2 apical expression (Fig6.2, Ci). Other media showed strong dorsal expression of Crb2, and SRN2 displayed an unusual dorsal nuclear pattern of this marker (Fig6.2, Cii-Civ).

Cleaved Caspase 3 is an apoptotic marker. SRN2 displayed large amounts of apoptosis, and explant media the least (Fig6.2, Div and Diii). Dundee and Brachmann media displayed similar levels of apoptosis, but dying cells were more concentrated around the ventricular zone in Brachmann media (Fig6.2, Dii and Di).

### **6.10 Conclusion**

While mice are the experimental animal of choice in many fields of biology and as such have been extensively genetically and systemically characterised, few techniques for *in vivo* live imaging are available, and those that are have extensive technical and often ethical issues. Imaging the developing nervous system is a prime example of this issue: although some live imaging of adult mouse brain and spinal cord have been carried out, the techniques used often involve invasive and complicated surgery (Hillman, 2007; Lichtman and Fraser, 2001). Similar issues arise in imaging the development of *in utero* mouse embryos. While progress has been made imaging non-invasively, these techniques are suitable for resolution at the morphological/structural level, but are not yet suitable for live cell tracking (Larina *et al.*, 2012; Norris *et al.*, 2013).



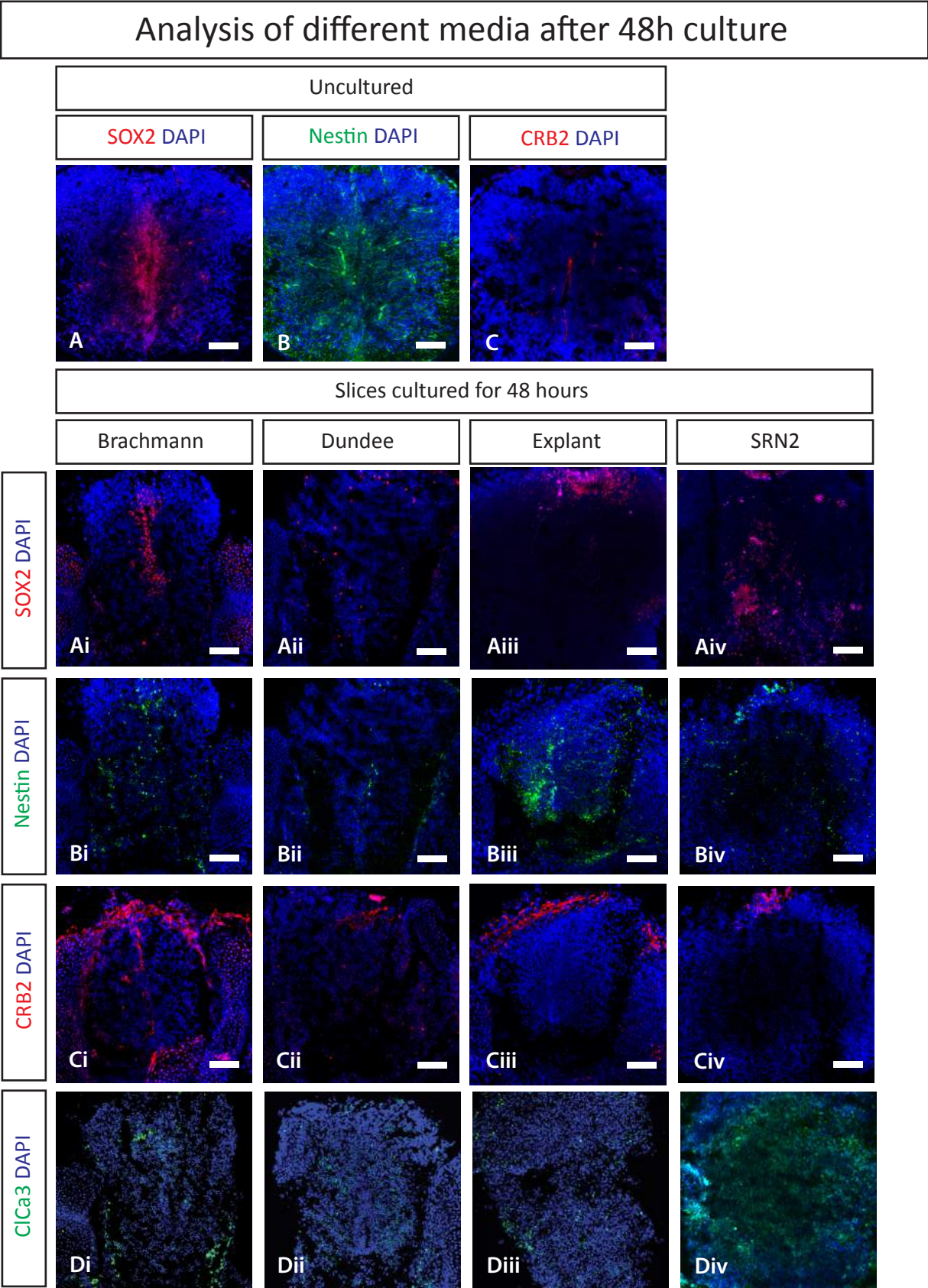


**Figure 6.2** Effects of different types of media on cultured embryonic mouse spinal cord. (A-C) is freshly fixed and labelled tissue. (Ai-Div) Culture of embryonic spinal cord was trialled with four media; Brachmann (Ai-Di), Dundee (Aii-Dii), Explant (Aiii-Diii) and SRN2 (Aiv-Div). SOX2 (A-Aiv) and Nestin (B-Biv) were used to assay ventricular zone progenitor maintenance; CRB2 (C-Civ), the integrity of the apical surface; and cleaved caspase 3 (ClCa3), (Di-Div) the levels of apoptosis. Scale bar: 100µm.

Alternative methods of live imaging include *ex vivo/ex utero* systems, in which an entire organ or embryo is cultured and imaged. Although this bypasses the ethical implications of chronically wounded animals, the technical difficulties of imaging structures beyond the surface of the organ remain. Whole embryos have been cultured successfully in rolling systems, although after E11 the embryo becomes too large to remain viable in culture (Garcia *et al.*, 2011; Kalaskar and Lauderdale, 2014; Piliszek *et al.*, 2011).

A third alternative is to use another species more amenable to live imaging. Chicken embryos have been a mainstay of developmental science for decades, and techniques have been developed to allow beautiful *in ovo* imaging (Kulesa *et al.*, 2010) The translucent embryos of the zebrafish, and the expansion and ease of genetic manipulation allowing the development of reporter lines in this species has led to a wealth of high resolution imaging of developmental processes (Renaud *et al.*, 2011).

It was noted that even with the most optimal culturing conditions, the health of the cultured tissue depended on the speed at which the embryo was processed and transferred into the incubator.

Either Dundee or Brachmann media is the most suitable for culturing. Arguably Brachmann media has a more normal distribution of apical markers and possibly dorsal SOX2-positive cells, however, there is a greater proportion of dying cells in the ventricular zone. Dundee media has acceptable levels of apoptosis, mainly in the alar/basal plates, outside the ventricular zone.

However, it must be addressed that these slices were cultured without imaging. Phototoxicity is a real issue for the types of timelapse imaging that this chapter is optimising for, used in Chapter 8. The addition of HEPES in Brachmann media may increase cytotoxicity upon exposure to fluorescent light. All data taken together, Dundee media was chosen for the timelapse imaging.

# Chapter 7

Live imaging supports my model of  
dorsal obliteration

## 7.1 Introduction

As outlined in Chapter 6, I developed a slice culture system for analysing spinal cord over the obliteration window. In this chapter I will describe studies in which I performed real time imaging of cells and nuclei in such slice cultures. The experiments described in this chapter were performed in collaboration with Dr. Raman Das and Prof. Kate Storey, using an adaptation of a protocol (Das and Storey, 2014) first described for analysis of cell behaviour in early chick neural tube. Briefly, I co-electroporated H2B-RFP (to label cell nuclei) and GPI-GFP (to label cell membranes) into mouse spinal cord slices taken from either E13, E14 or E15 embryos, targeting small groups of cells in and adjacent to the dorsal Ventricular Zone (VZ). I opted for a semi-random electroporation of cells in and around the dorso-lateral lumen. The aim was to test the hypotheses that (a) elongated roof plate cells are present at the dorsal-most midline and (b) sub-dorsal cells immediately adjacent to these detach. Thus I aimed to capture examples of elongated roof plate/dNRG and detaching VZ cells. In addition, I expected to image a variety of other cells in their vicinity. Electroporated slices were incubated for up to 24 hours to allow recovery and expression of the transiently transfected plasmids, and slices were imaged for 24-48 hours.

Ages of embryos at start of imaging are given in the format 'E13+24h'. This is to indicate that the embryo was sacrificed at E13.5, was electroporated and left to recover for 24h, and then imaged. In theory, this would approximate to a starting point for imaging of an E14 embryo.

My live imaging studies reveal that cells in and around the dorsal VZ show several distinct morphologies and behaviours, these include potential examples of elongate

roof plate cells/cells with dNRG-morphology at the dorsal midline and sub-dorsal cells whose cell body appears to detach.

## **7.2 Elongate dorsal cells/dNRG**

I captured examples of elongated cells at the dorsal midline. These cells have a distinctively dorsal to ventral orientation, and appear to be static – *i.e.* their cell body does not move over the course of the culture period/imaging. Below I describe two cells imaged in two slice cultures taken from different embryos.

The first is a midline-situated cell imaged for 1140 minutes in a (E14+24h) slice culture, in which the dorsal midline is relatively short (Fig 7.1, Movie 7.1 Elongate Dorsal Cells 1 Movie). The morphology of the cell changes subtly over the imaging period from wedge-shaped to cuboidal and then to wedge shaped/radial glial shape. Throughout this period the nucleus stays in the dorsal-most region of the cell *i.e.* close to the pial surface. This cell resembles the elongated roof plate cells in mouse/dorsal radial glia described in zebrafish (Kondrychn *et al*, 2009). Although it is difficult to determine the precise location of the lumen, the position and shape of this cell support the idea that it is a roof plate cell that transits between wedge-, elongated and radial-glial shapes (note in the text below I refer to this cell as an elongated roof plate cell). This cell remains stably in position, in contrast to immediately adjacent cells (described below).

In support of the idea that roof plate cells transit to dNRG, imaging of a second slice culture in which the midline is much longer (E14+24h, Fig 7.2, Movie 7.2 Elongate Dorsal Cells 2 Movie) reveals a cell at the dorsal midline that displays dNRG morphology (referred to hereafter as a dNRG cell). The cell has a rounded nucleus and

both dorsal and ventral processes. This cell remains stably in position, in contrast to adjacent cells that are more dynamic, both cytoplasmically and in the shape/position of their nuclei (described below).

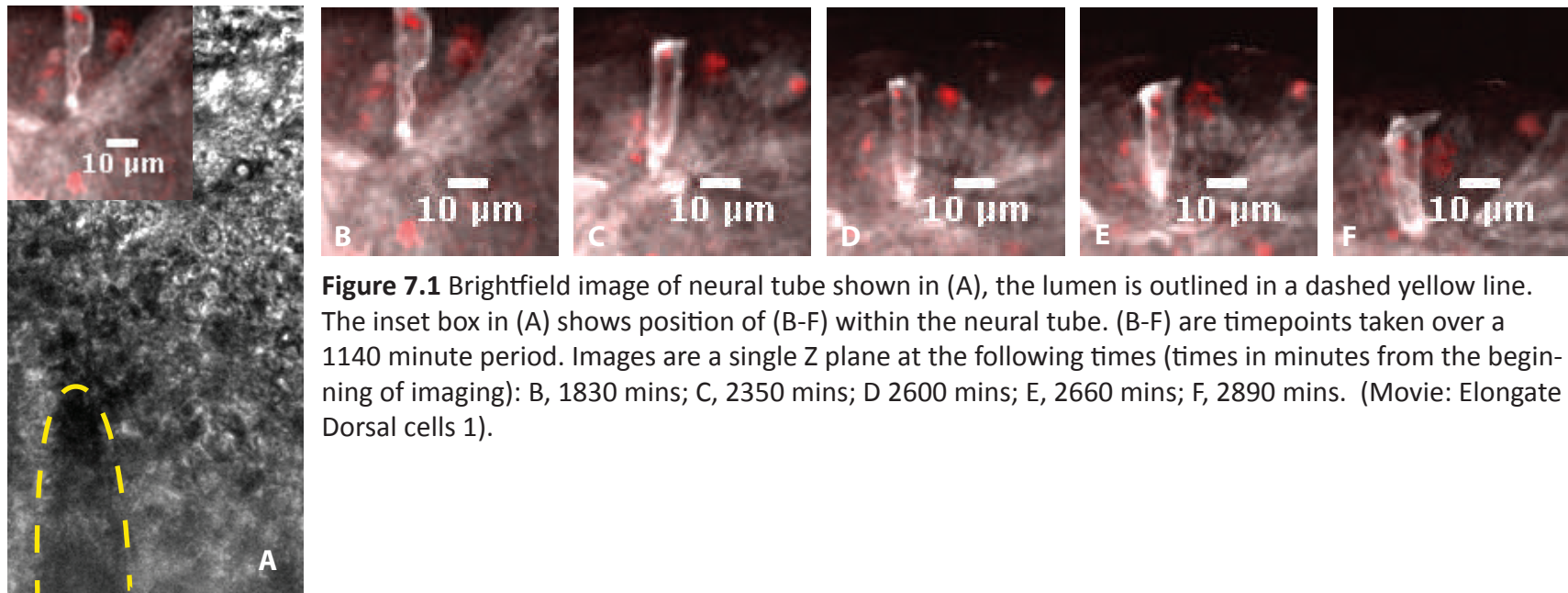
It is notable that neither of these cells has a cell body directly abutting the lumen. This agrees with my findings from static images in Chapter 3, showing that the nucleus of dNRG cells is distant from the apical surface.

### **7.3 Dynamic sub-dorsal cells**

In the first (E14+24h) slice culture described above, cells on either side of the elongated roof plate cell display wedge-shaped appearances at the start of the imaging period, and project diagonally to the pial surface with mirror symmetry to each other. Both cells are slightly out of focus in the (E14+24h) slice culture described in Fig 7.1, and I therefore refocused on each side. This reveals that wedge-shaped cells immediately adjacent to elongated midline roof plate cells are dynamic and display behaviour suggestive of their extrusion.

Left of the midline, two thinly-wedged/elongated cells are labelled that appear to have an apical contact at/close to the VZ and a basal contact at the pial surface. Over the course of the imaging period, both cell bodies appear to move dorsally, away from the lumen, and both cells then break their ventral process (Fig7.3, Movie 7.3: Sub Dorsal Cell 2). As the cell bodies detach from the VZ, the nuclei appear to move rapidly towards the pial surface.

## Elongate dorsal cells 1





## Elongate dorsal cells 2

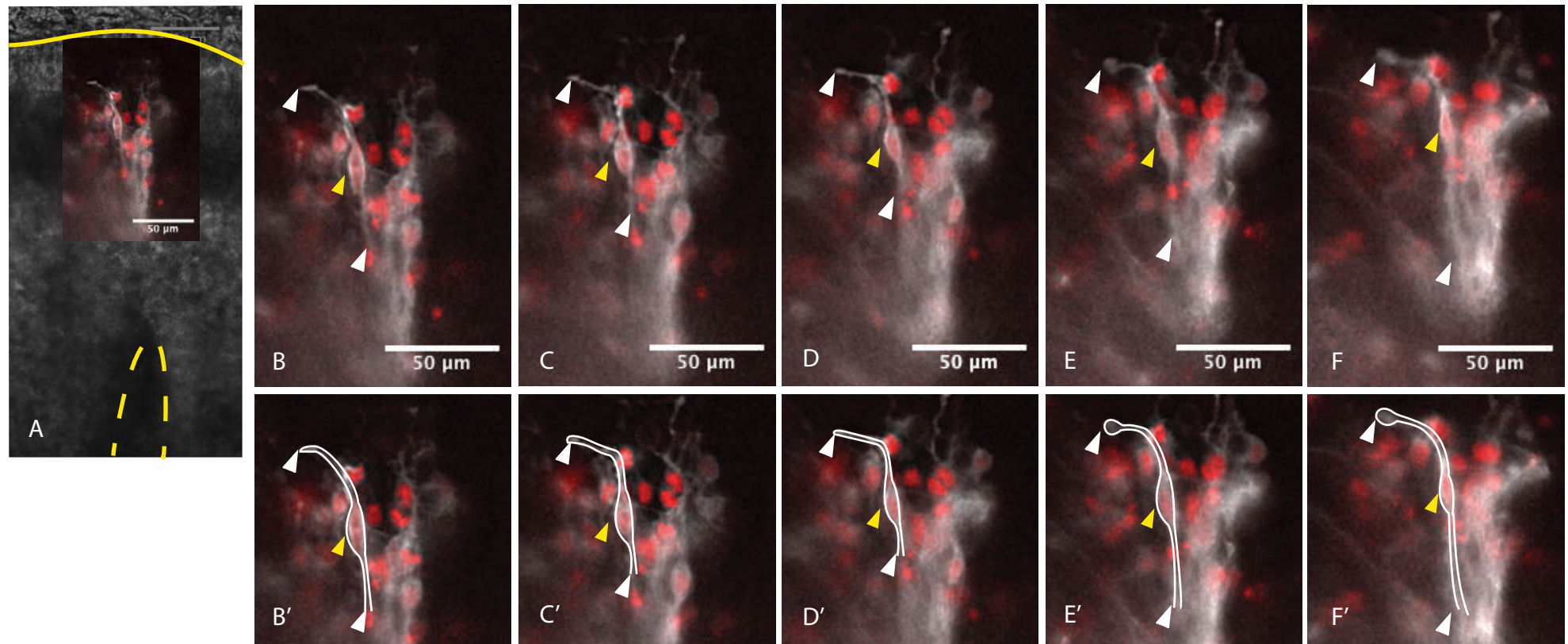


**Figure 7.2** Brightfield image of neural tube shown in (A). Outline of neural tube is shown in a yellow unbroken line, and the lumen is outlined in a dashed yellow line. The white box in (A) shows position of (B-F) within the neural tube. (B-F) are timepoints taken over 700 minutes demonstrating that the cell shown with arrows does not move substantially over this time period. Images are a single Z plane at the following times (times in minutes from the beginning of imaging): B, 250 mins; C, 320 mins; D 420 mins; E, 500 mins; F, 700 mins. The cell body (yellow arrowhead) and the dorsal/ventral processes of the cell (white arrowhead) can be followed. (B'-F') are the same images as (B-F) cropped and with the elongate cell outlined. It should be noted that the ventral process of this cell is not always clearly defined due to out of focus light. The white arrow therefore depicts the most ventral part of the process clearly attributed to that cell, and the process is likely to continue further ventrally than can be resolved. Images are a single Z plane. (Movie - Elongate dorsal cells 2).

In a slightly different field of focus (again, imaging to the left of the midline), three cells appear to detach (Fig 7.4 and Movie 7.4: Subdorsal Cells 3 Movie). The first cell to detach appears to have a ventral process angled towards the lumen and another dorsally. The ventral process is lost before the cell rounds up. The second cell to detach also appears to have a dorsal process that the cell loses. The final cell to detach clearly moves its nucleus dorsally before it detaches the dorsal process and rounds up.

Right of the midline are two cells that lie close to the elongate dorsal midline roof plate cell (Fig 7.5 and Movie 7.5: Subdorsal Cell 1 Movie). One cell is directly behind the elongated roof plate cell, so is difficult to resolve in any detail, however, it clearly rounds up. The second clearly has a cell body far from its ventral attachment..

Of eight cells (six sub dorsal) convincingly moving dorsally, five are seen to detach. Both these cells appear to undergo an event possibly similar to apical abscission (Das and Storey, 2014). Since this was a slice culture from an (E14+24h) embryo, I conclude that I have captured cell extrusion at the very onset of the dorsal obliteration process.

#### **7.4 Active dorsal migration of cell nuclei on dNRG**

In the second (E14+24h) slice culture, I find evidence for an active dorsal migration of cell nuclei in close proximity to dNRG cells. Intermingled with the GFP+ processes in the midline of the embryo described in 'Fig 7.2, Movie 7.2 Elongated Dorsal Cells 2' are elongated nuclei that clearly move dorsally, relative to the static dNRG. As the nuclei move dorsally, they round up (Fig 7.6, Movie 7.6, Elongate Nuclei). Frequently, the nuclei move laterally once they are close to the pial surface. These observations confirm and extend the static images I showed in Fig 3.4, in which I detect SOXB1-

positive cell bodies that are intermingled with dNRG and are elongated and orientated dorso-ventrally. These live imaging studies support the idea that a dorsal movement of cell bodies nuclei drives dorsal obliteration.

### **7.5 Do sub-dorsal cells extend a process that fasciculates on early dNRG pioneers?**

In the example described above, I was unable to resolve the shape of the cells whose nuclei moved dorsally, since they were intimately intermingled with dNRG cells. However, in a slice culture from a 3<sup>rd</sup> embryo, (E13+24h), in which the midline is relatively long, I obtained preliminary evidence that suggests that sub-dorsal cells may extend a dorsal process that projects closely along the dNRG scaffold, and that the cell body migrates along this as it detaches from the lumen. This evidence is shown in Fig7.7 and Movie 7.7 (E13+24h; Movie: Midline interacting cell Moving; 1100 minutes). In this example there appear to be two closely associated cells to the left of the midline. Both cells extend highly dynamic dorsal and ventral processes that project parallel to the midline. The cell bodies of both cells move dorsally along their own processes, coming to rest at/near the pial surface (Fig 7.7, white arrowheads). Both cells died at the same time (Fig7.7, G; not shown in movie). The ventral process of at least one of these cells is angled towards the lumen (blue arrowheads). Unfortunately the resolution is insufficient to determine whether this process does end at the lumen, or to which cell it belongs.

Nonetheless, this preliminary evidence raises the possibility that later-emerging sub-dorsal cells may extend processes towards the midline/pial surface, potentially along the dNRG scaffold and that they use their own processes as a dorsal conduit (Figure 7.8: schematic).

## Two Subdorsal cells 2

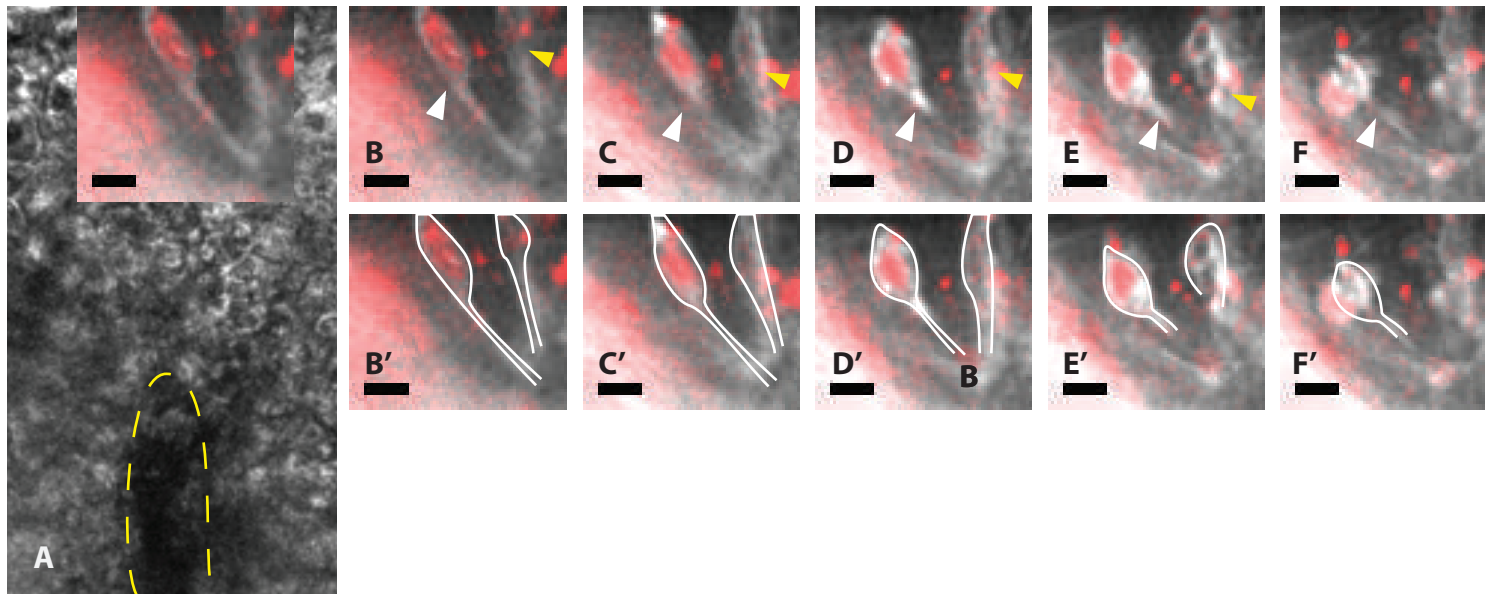


**Figure 7.3** Brightfield image of neural tube shown in (A), the lumen is outlined in a dashed yellow line. Yellow arrowhead denotes right hand cell behind the wedge-shaped cell that detaches in (F). White arrowhead shows left hand cell that begins to detach in (D) however, this cell appears to retain a thin ventral process until the end of imaging. (B'-F') are the same images as (A-F) but with the two cells outlined. Images are a single Z plane. (Movie: Two Sub Dorsal Cells 2). Times in minutes from the beginning of imaging): B, 260 mins; C, 300 mins; D 360 mins; E, 421 mins; F, 560 mins

### Sub dorsal cells 3

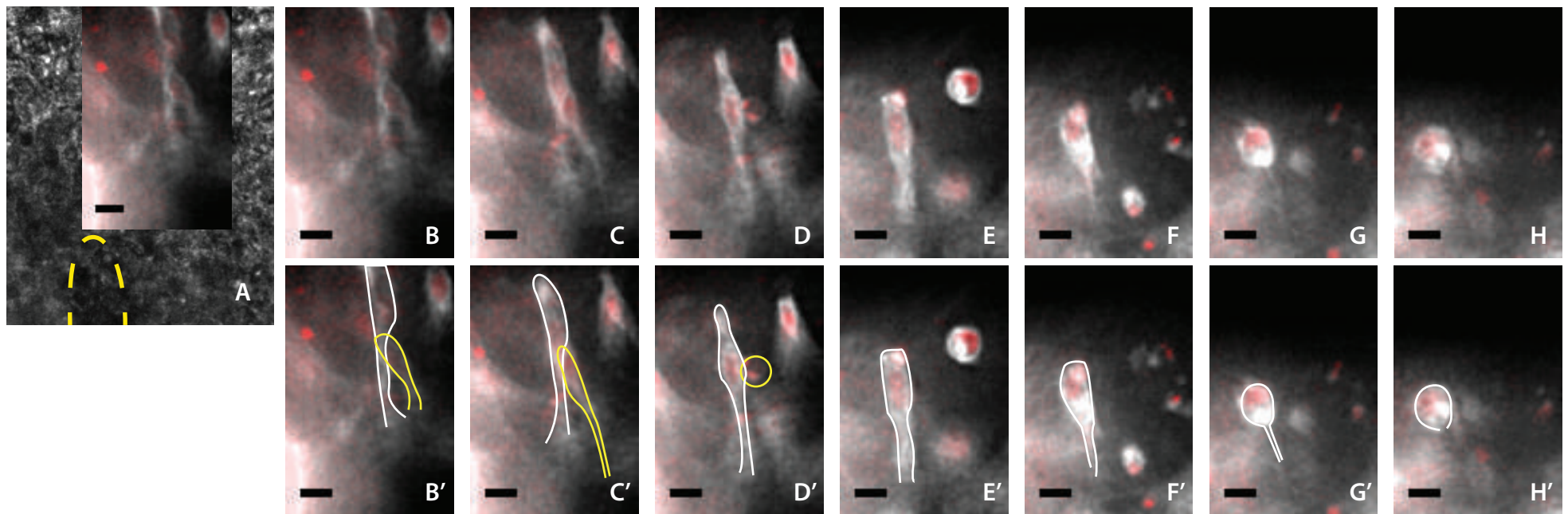
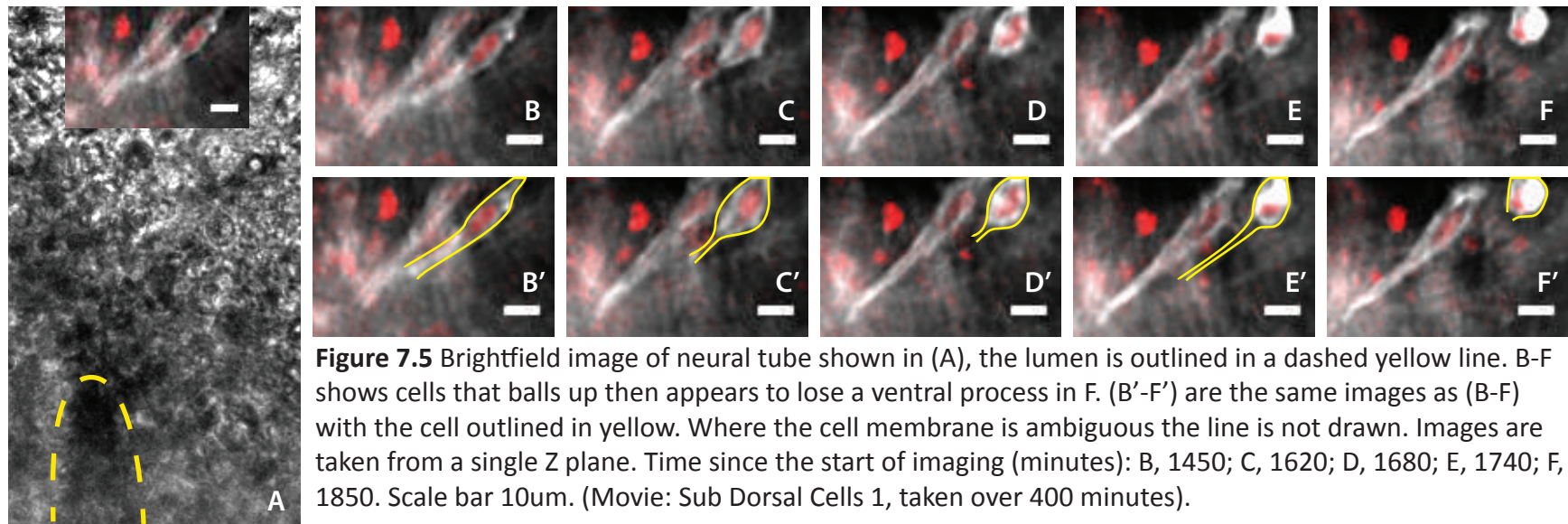


**Figure 7.4** Brightfield image of neural tube shown in (A), the lumen is outlined in a dashed yellow line. Two detaching cells are visible. (B'-H') are the same images as (B-H), with two cells outlined. The left hand cell outlined in white rounds up in (G) and may detach the process by (H). The right hand cell outlined in yellow rounds up at (D'). Images are a single Z plane. Times from start of imaging (minutes): B, 1110; C, 1380; D, 1540; E, 2030; F, 2250; G, 2500; H, 2650. Sub Dorsal Cells 3 Movie; 1530 minutes.

### Sub dorsal cells 1



## Elongate nuclei around the dorsal midline

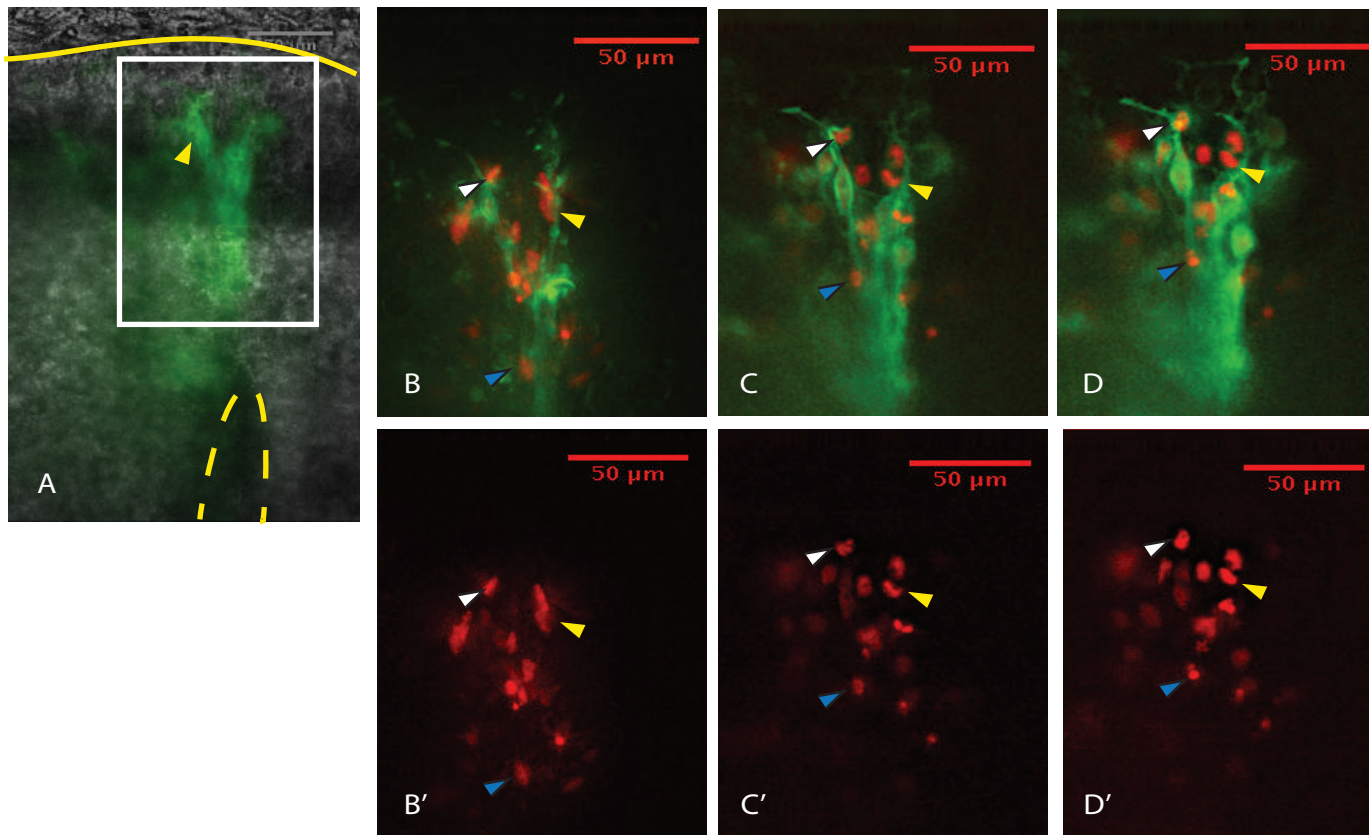


**Figure 7.6** Brightfield image of neural tube shown in (A). Outline of neural tube is shown in a yellow unbroken line, and the lumen is outlined in a dashed yellow line. The white box shows position of (B-D) within the neural tube. (B-F) show GFP-membrane and RFP-nuclear labelled cells. (B'-D') shows RFP-nuclear labelled only. Arrowheads follow select cells that begin with elongated nuclei and round up. Imaged over 1000 minutes Images taken from a single Z plane (Elongate Nuclei movie). Timepoints (minutes since the start of imaging) (B) 304; (C) 314, (D) 335

### Midline-interacting cells moving dorsally

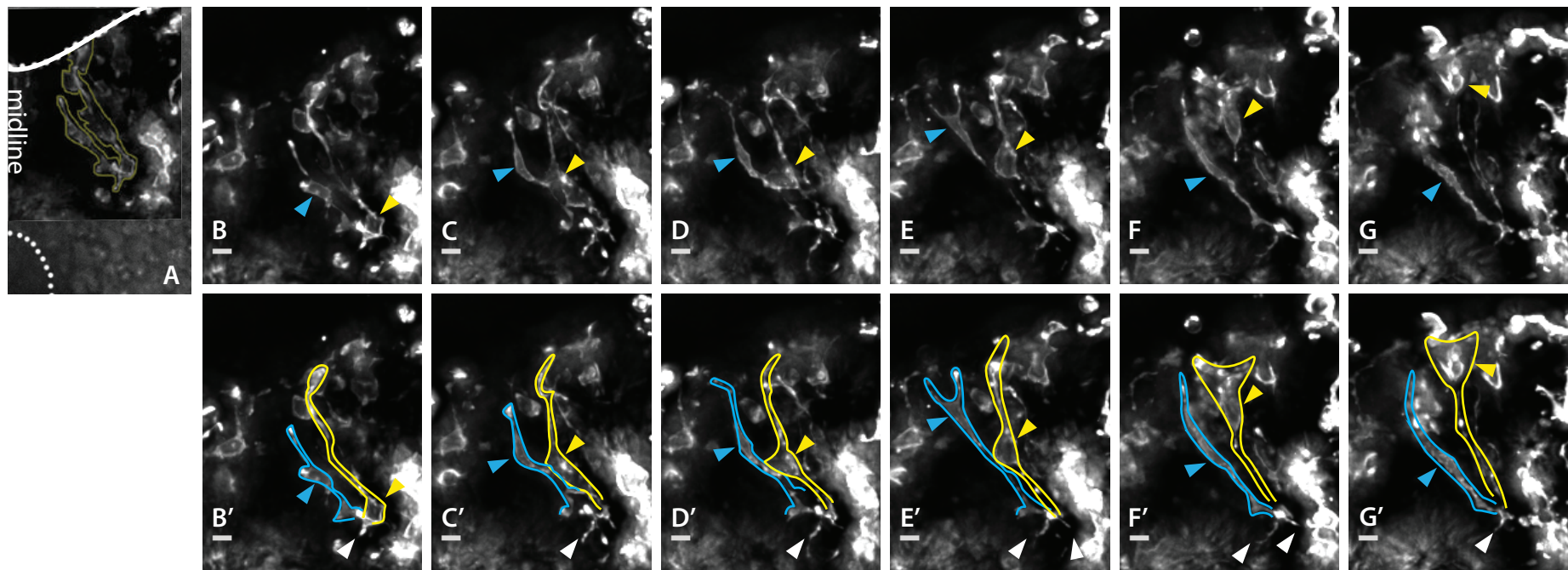


**Figure 7.7** Brightfield image of neural tube shown in (A). Outline of neural tube is shown in a white unbroken line, the lumen is marked with a dotted line, and the approximate position of the midline is marked in text. The yellow outline in (A) shows two closely connected cells. (B'-G') are the same images as (B-G) except that the left hand cell is outlined in blue, and the right hand cell is outlined in yellow. Where the cell outline is ambiguous the line has not been drawn. Yellow and blue arrows mark the cell bodies. White arrows mark ventral processes that may belong to either of these cells. Images taken from a single Z plane. Time since start of imaging (minutes): B , 1550; C, 1840; D, 1920; E, 2020; F, 2250; G, 2490. Movie taken over 1110 minutes. (Movie: Midline interacting cell 1).



## Possible mechanisms by which sub-dorsal cells migrate dorsally

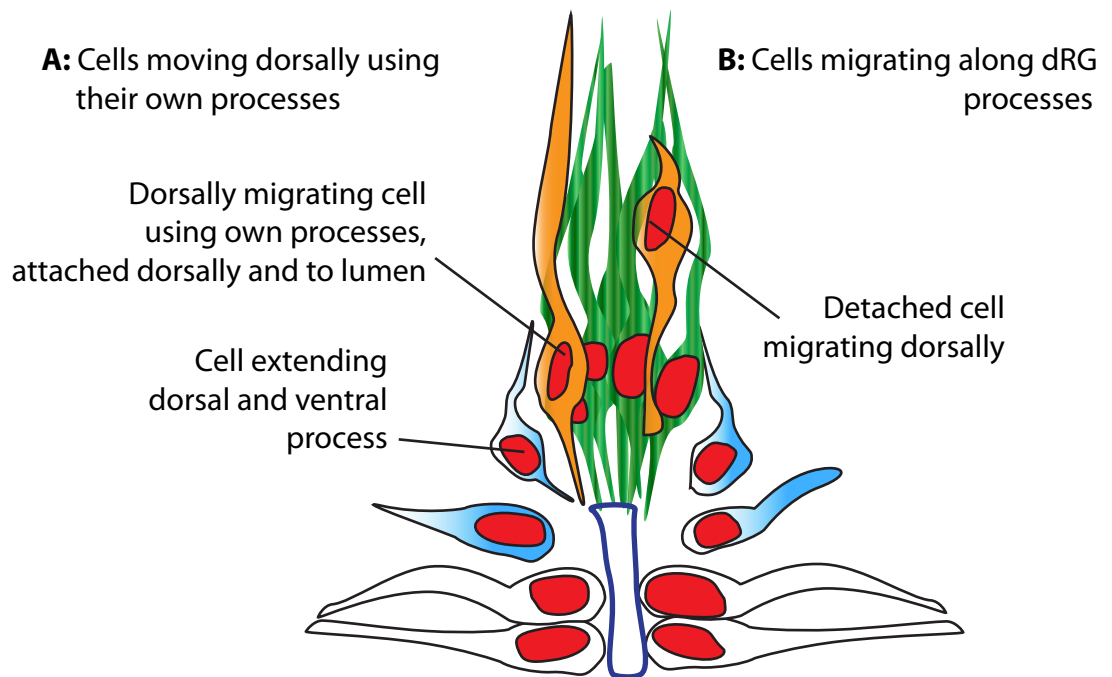
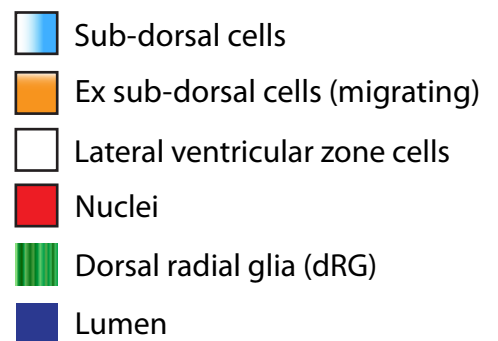


**Figure 7.8** Models of migration

Sub-dorsal cells may migrate by either (A) extending processes dorsally and moving their cell body along these extensions. They may retain ventral contact with the lumen. Alternatively, (B) Cells may detach and migrate along the dorsal processes of neighbouring cells, e.g. dRG cell to migrate dorsally.



## **7.6 Other cell processes interact dynamically with the dorsal midline**

In addition to these cell behaviours, my live imaging revealed other cells that interact dynamically with the dorsal midline. In a 4<sup>th</sup> (E14+24h) slice culture, a cell whose cell body is situated in the VZ below the dorsal midline reaches out a process that appears to contact the dorsal midline, and then retracts this process (Fig 7.9, Movie 7.9: Midline interacting cell 1; 5510 minutes (note on the opposite side of the lumen, a more dorsally located cell appears to detach). A second behaviour seen in cells close to the midline is described in: Fig 7.10 (Movie 7.10: Midline interacting cells 2). These cells (probably nascent neurons) migrate dorsally towards the pial surface, or laterally towards the midline. The dorsally reaching cell retracts slightly. The midline-approaching cell sharply angles dorsally at a certain point. (Embryo E14+24hours; Movie shot over 1010 minutes). Taken together, it appears clear that cells are attracted to the dorsal midline/pial surface close to the dorsal midline, and explore them by extending processes towards it. This could indicate the presence of a chemoattractant. The sharp turn of the cell in Fig. 7.10 could suggest either the physical barrier posed by the roof plate, or a chemorepellant factor.

## **7.7 Medio-lateral radial glia**

Finally, in a slice culture imaged at (E15+24h), I obtained evidence that medio-lateral radial glial persist beyond E15. In Chapter 3 I described that Nestin expression declines in medio-lateral radial glia from around E13 (Figure 3.3). My live imaging studies reveal that medio-lateral radial glia nonetheless persist beyond this stage (Fig. 7.11 and Movie 7.11). Thus, at E15+24h I detect medio-lateral radial glial cells that are distributed evenly along the VZ. They appear to have cell bodies (arrow outlines) located at or near the VZ and lateral processes reaching to the pial surface. They are

similar to E16 rat spinal cord radial glia as described by McDermott *et al* (2006). Like the rat cells described in this paper, this cell population has cytoplasmic thickening along the processes (yellow arrowhead). Interkinetic nuclear migration is not detected in these cells, possibly either because proliferation has slowed in radial glia at this embryonic stage, or because these cells represent or are becoming a post mitotic glial population. However, the cells are dynamic: one cell clearly extends then retracts processes halfway along its apical-basal process (white arrowhead). There is a wide band of tissue at the dorsal midline (visible both in the brightfield image and the RFP image) that is likely to be composed of dNRG, but these are not electroporated. (Figure 7.11; Glial Processes Movie).

Midline interacting cell 1

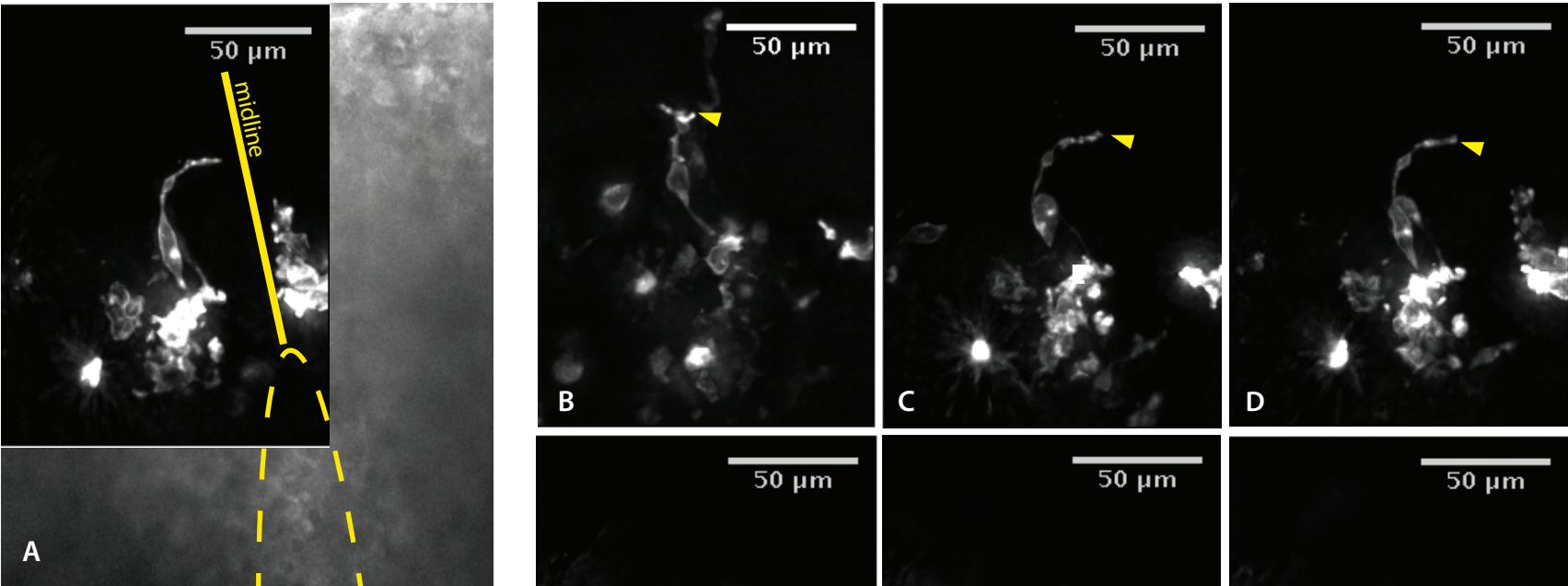


**Figure 7.9** Brightfield image of neural tube shown in (A), the lumen is outlined in a dashed yellow line. (B-G) are timepoints taken over 2510 minutes. Yellow arrows denote the end of the dorsal process. Time from start of imaging (minutes): B, 1240; C, 1740; D, 1910; E, 2430; F, 2790; G, 3120. (Movie: Midline interacting cell 1). Images takeb from a single Z plane.

## Midline-interacting cells 2

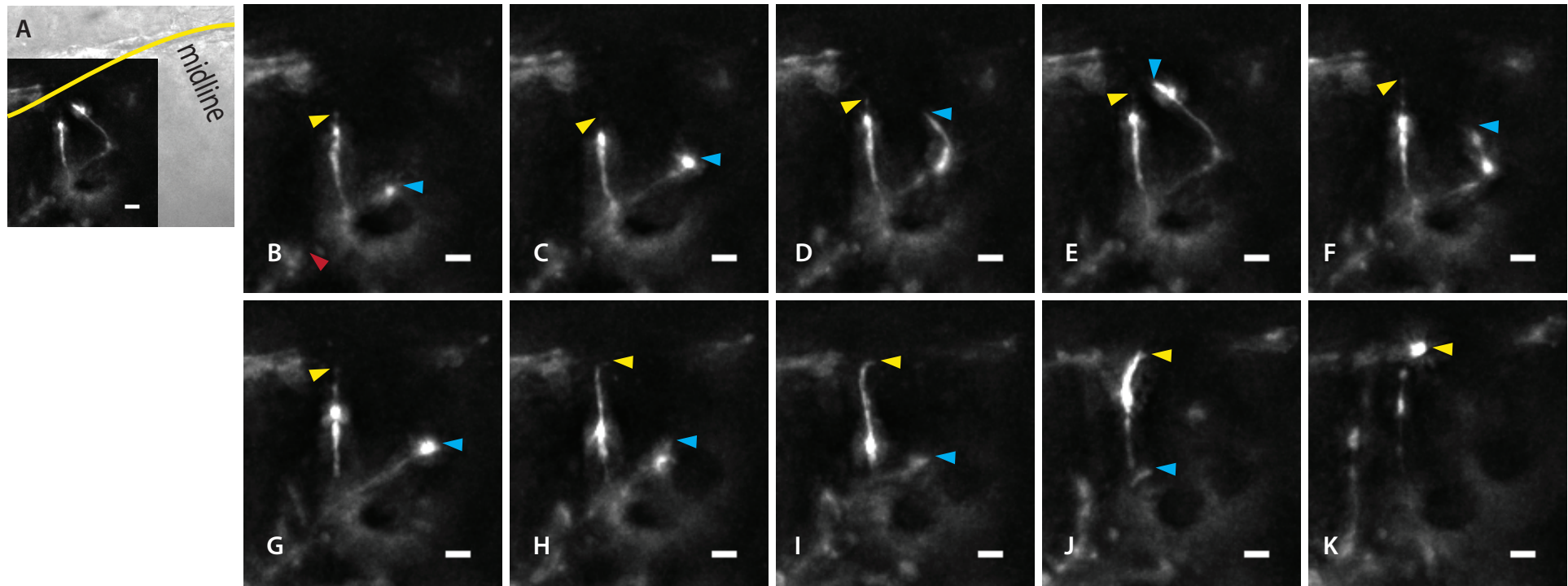


**Figure 7.10** Brightfield image of neural tube shown in (A). Outline of neural tube is shown in a yellow unbroken line, the approximate position of the midline is marked in text. (B-K) shows a cell (marked with blue arrowheads) that extends towards the midline, then angles sharply dorsally. The red arrowhead in (B) shows the most ventral identifiable part of this cell. Another cell extends and then retracts a process dorsally (yellow arrowheads indicate tip of process). This cell also demonstrates some dynamic, bright cytoplasmic thickening. Images and movie are 9 Z-slices (18 $\mu$ m) as the processes are not all at the same focus. Time since the beginning of imaging (minutes): B, 1780; C, 1940; D, 1950; E, 1960; F, 1969; G, 1972; H, 1977; I, 1979; J, 1983; K, 1985. (Movie: Midline interacting cell 2, 870 minutes).

## Radial Glia

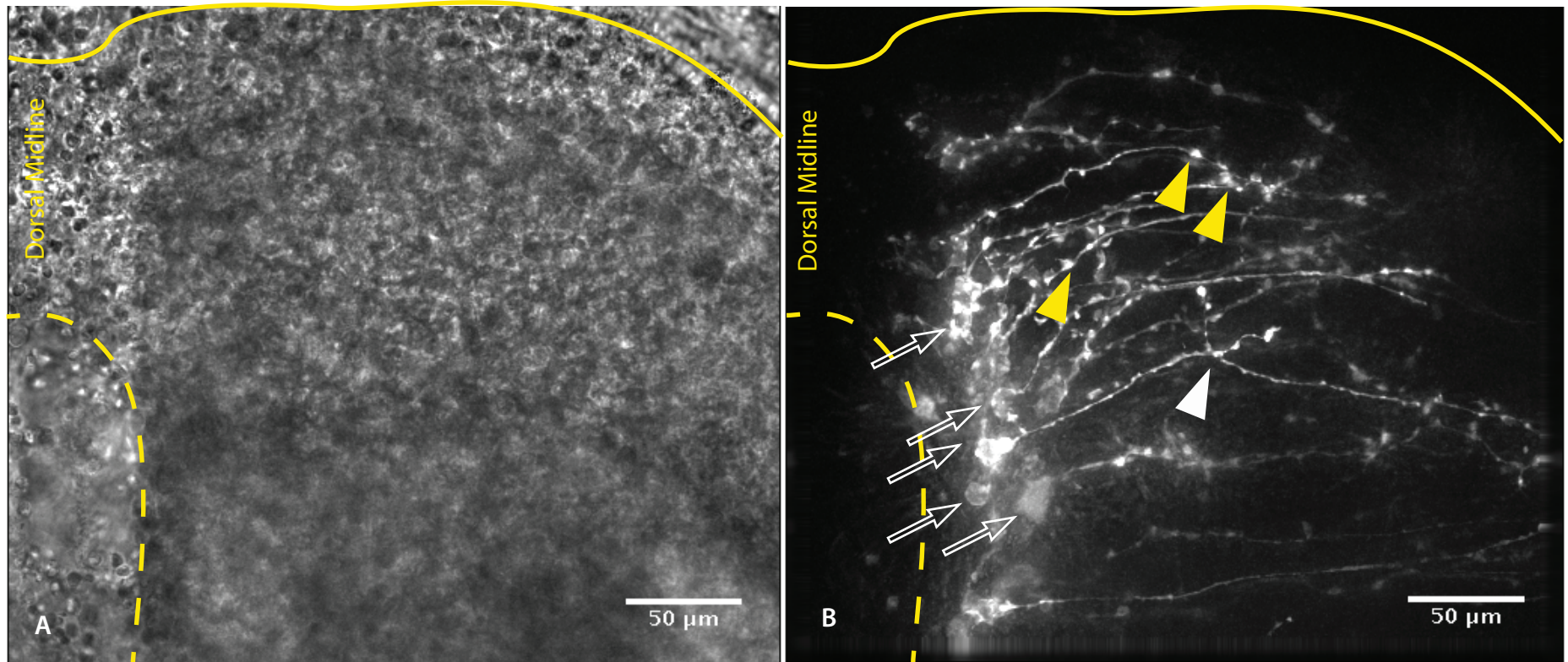


**Figure 7.11** Brightfield image of neural tube shown in (A). Outline of neural tube is shown in a yellow unbroken line, and the lumen is outlined in a dashed yellow line. Some cytoplasmic thickenings are denoted by yellow arrowheads. White arrow outlines indicate some of the basally located cell bodies. White arrowhead indicates glial process that has two additional shorter processes that extend then retract. As the cell bodies and processes are not all in the same plane, (B) and the movie are a Z projection of 31 Z sections (62μm) Imaged over 1400 minutes (Movie: Glial Processes).

## 7.8 Discussion

Live imaging is a technique that is growing in popularity as the tools developed have become more sophisticated. The previous chapters of this thesis have asked specific questions of dead and static tissue. From this, I developed a model for dorsal obliteration as detailed in Figure 3.18 that predicts that subdorsal VZ cells migrate dorsally, using the dNRG cell processes as a conduit. Here, I tested this prediction by asking whether I could capture cells moving dorsally away from the VZ in living tissue. In line with my dorsal obliteration model, I find evidence that cells break away from the subdorsal VZ and migrate away. In addition, these studies suggest additional details of the model (discussed below). However, before doing so, I will comment more generally on the slice cultures.

Any *ex vivo* system, including slice culture, has to be viewed with a degree of caution: the data needs to be interpreted carefully; with the acceptance that culture itself will cause a response within the tissue. However, my slice culture conditions closely recapitulated those developed by Das and Storey, and shown to closely mimic spinal tissue *in vivo* (Das and Storey, 2014). Moreover, in my slices, I detected cells that I would expect in a healthy spinal cord, including medio-lateral radial glia (Fig 7.11) and dorsal commissural neurons (not shown). This gives me confidence that the spinal cord slices are healthy and that the new cell behaviours that I describe are representative of those found in the developing embryo.

In large part our studies on spinal cord development are informed through static analyses of transcription factor expression that suggest a rather static picture. My

studies suggest that the developing spinal cord is a highly dynamic tissue, composed of moving, tactile and responsive cells.

My studies provide evidence that elongated cells situated at the dorsal midline are non-mobile, compared to their neighbours. In Figure 7.1, I describe a wedge-shaped/elongated cell at the dorsal midline in an (E14+24h) slice culture. The dorsal funiculus, and hence this cell, are shorter than expected for E14+24 hours, however, I believe this is due to the precise rostro-caudal position of the slice. Comparison of this slice with another of the same age that has a longer midline (Fig 7.2) reveals that in the more developed slice, the midline is occupied by a cell with long dorsal and ventral processes. These cells share the same property of being relatively immobile when compared to neighbouring cells and of having nuclei far removed from their ventral extreme. I suggest that the first cell represents a roof plate cell, classically described as 'wedge shaped', and the second, a more mature dNRG cell.

Cells closely associated with these dorsal midline cells are sub-dorsal cells. In the less mature slice, I capture extrusive behaviours. Thus I detect that the wedge-shaped midline roof plate cell sits next to several cells that appear to break away by detaching from a ventral process then rounding up and moving dorsally (Figs 7.3, 7.4, 7.5). In the more mature slice I did not capture active extrusion. However, cells around the dNRG midline cell were highly active: their nuclei are seen to both change from an elongated to a rounded shape (reminiscent of SOXB1 data in Fig3.4) and to move dorsally.



My model states that cells break away from the VZ subdorsally and use the dNRG to migrate. The cell behaviour observed adjacent to the wedge-shaped and the elongate glial-like dorsal cells fits with this model.

In addition, I captured other cell behaviours that may add a more complex detail to the model. In a slice culture from an older embryo (E15+24h), I observe that cells with a dorso-ventral process extend parallel to the dNRG and that their cell bodies use their own process as a conduit. This raises the possibility that detaching cells re-polarise from medio-lateral to dorso-ventral, and extend a dorso-ventral process along a dNRG scaffold. In development, early neurons called 'pioneers' lay down an axonal scaffold 'followers' fasciculate on the pioneers. Future studies are required to test whether a similar process operates in dorsal obliteration, and whether the dNRG provide an attractant that supports a re-orientation of the detaching VZ cell. (Hidalgo and Brand, 1997).

As discussed above, I observed that cells appear to detach their process before rounding up/migrating dorsally. In some instances, the detaching process appears to be under some tension (for example, see the cell marked with the yellow arrowheads in Fig 7.4 (Sub Dorsal Cell 3). This suggests that the cells are actively migrating away, and perhaps have to overcome a force/threshold in order to detach. It is impossible to confirm from this data, but interesting to speculate that the mechanism may be similar to apical abscission described by Das and Storey (2014) in which loss of proteins binding nascent neurons to the VZ are suddenly lost, allowing the cells to migrate away. Local disruption of apical polarity (and thus epithelial integrity) by secreted CRB2

may be a contributory mechanism to allowing an already mechanically stressed cell to be released from the lumen.

In addition, I captured other unexpected cell behaviours. These include several cells extending processes, bent towards the midline then retracting. The directionality of the processes suggests that there may be a chemoattractant towards which the cell processes migrate, and a more localised repellent that causes retraction. Future studies are required to test these ideas.

# Chapter 8

## Discussion

## 8.1 Summary of Results

In this thesis I set out to understand the mechanistic basis for formation of the central canal in the mouse. Previous studies have suggested that central canal formation occurs through dorsal obliteration, a process that is intimately linked to lengthening roof plate cells (Altman and Bayer, 1984; Bohme, 1988; Kondrychyn *et al.*, 2013; Sevc *et al.*, 2009; Snow *et al.*, 1990; Sturrock, 1981). However at present little is known about the mechanism that drives dorsal obliteration or that links roof plate cells with this process. My studies reveal a potential contributory mechanism. In Chapter 3, I show that during dorsal obliteration, ventricular zone (VZ) cells that lie immediately adjacent to Nestin-positive dRG cells may be undergoing a change in apico-basal polarity proteins, downregulating CRB2, ZO-1 and aPKC. Analysis of static images suggests that these cells are poorly integrated into the VZ, suggesting that they may be detaching from the lumen. In Chapter 4, I provide evidence of that cells are capable of disrupting neuroepithelial cell integrity during early neurulation. In Chapter 5, I show that dorsal nestin-expressing radial glia or closely associated cells synthesise a mRNA that can encode for a truncated isoform of the apical polarity protein, CRB2, and that an experimentally synthesised secreted protein product of that truncated mRNA can likewise disrupt neuroepithelial cell integrity during early neurulation. This is the first *in vivo* demonstration of a CRB2 isoform that is potentially secreted. Although we do not have an antibody that specifically detects the secreted CRB2 isoform, immunohistochemical analysis using an antibody that detects the transmembrane CRB2 isoform shows that cells show unusual expression of CRB2 over the period of dorsal obliteration, with strong apical labelling and diffuse non-apical labelling (Chapter 3). Previous studies have suggested that Crb2 can play a role in epithelial to mesenchymal cell transition (Karp *et al.*, 2008; Varelas *et al.*, 2010) and additional

studies in zebrafish suggest that CRB2 can bind homophilically (Zou *et al.*, 2012). Together with my observations, these findings raise the possibility that secreted CRB2 plays a role in dorsal obliteration. I hypothesise that secreted CRB2 is secreted locally from dorsal Nestin+ Radial Glia (dNRG), that it binds homophilically to transmembrane Crb2 on immediately adjacent cells, and downregulates or disrupts apico-basal polarity, hence allowing VZ stem/progenitor cells to delaminate from the VZ epithelium. To begin to be able to test this model, I set out to develop live imaging of mouse spinal cord slices. I describe how I developed a slice culture system, in which VZ cell integrity is maintained (Chapter 6) and describe its use in beginning to analyse dorsal obliteration *in vivo* (Chapter 7). My studies in Chapter 7 appear to support the relationship between wedge-shaped and elongated roof plate cells. They reveal that dorsal RG cells extend a process ventrally towards the lumen, supporting static reports in mouse and live imaging in fish. They confirm static studies in rat, suggesting that dorsal RG cells act as a barrier, preventing cells/cell processes/axons from crossing. They provide evidence that subdorsal VZ cells can detach from the VZ, and move dorsally. Finally, they suggest a model in which early-detaching dorsal VZ cells migrate along dorsal RG processes but in which later-detaching VZ cells re-polarise, extend a process along the dorsal RG and move their cell body dorsally along this process. The components of this model are summarised in Figure 8.1.

Below, I first describe ongoing/future studies that will allow me to further test my hypothesis. I then discuss the broad questions that arise from these studies. In particular, I discuss my experiments within the context of neurulation. I then suggest why I think that if translated into a protein, secreted CRB2 may be only part of a complex array of signals that effect dorsal obliteration. Finally, I discuss the

implications of dorsal obliteration for studies in the adult spinal cord, both in healthy tissue and injured tissue.

## **8.2 On-going/future studies**

### ***Statistical analysis of markers***

In chapter 3 we attempted a statistical demonstration of the labelling pattern that we had described around the lumen: for apical proteins dorsal was very strong, a sub dorsal population was weak and the lateral ventricular zone was more even, and the intensity lay somewhere in-between. Our Statistical analysis does not support this interpretation, but the sample size analysed was too small, and the data collected in a way that did not allow good statistical analyses. One of the major limitations of these data is the low sample size, which limits the kind of tests that can be performed and also limits any test's ability to reveal an underlying trend. However, more powerful statistical tests (such as parametric tests) could be implemented on data from a more appropriately designed experiment that could better interrogate any trend. A more powerful setup for examining the patterns of apical marker expression intensity with respect to position along the lumen could be performed using a larger sample size for each timepoint, with a larger number of biological replicates as well as more sections from directly comparable positions along the embryo's anterior-posterior axis. Sample size aside, a much more powerful test for any difference in signal intensity of an apical marker between these regions would involve a method by which the absolute intensities measured from each region could be directly compared between images. To achieve this, an experiment should be set up that uses the same staining and imaging protocols for each section. The images should be taken on the same microscope at the same magnification and at the exposure/gain settings.

## Models of sub-dorsal cell detachment and migration

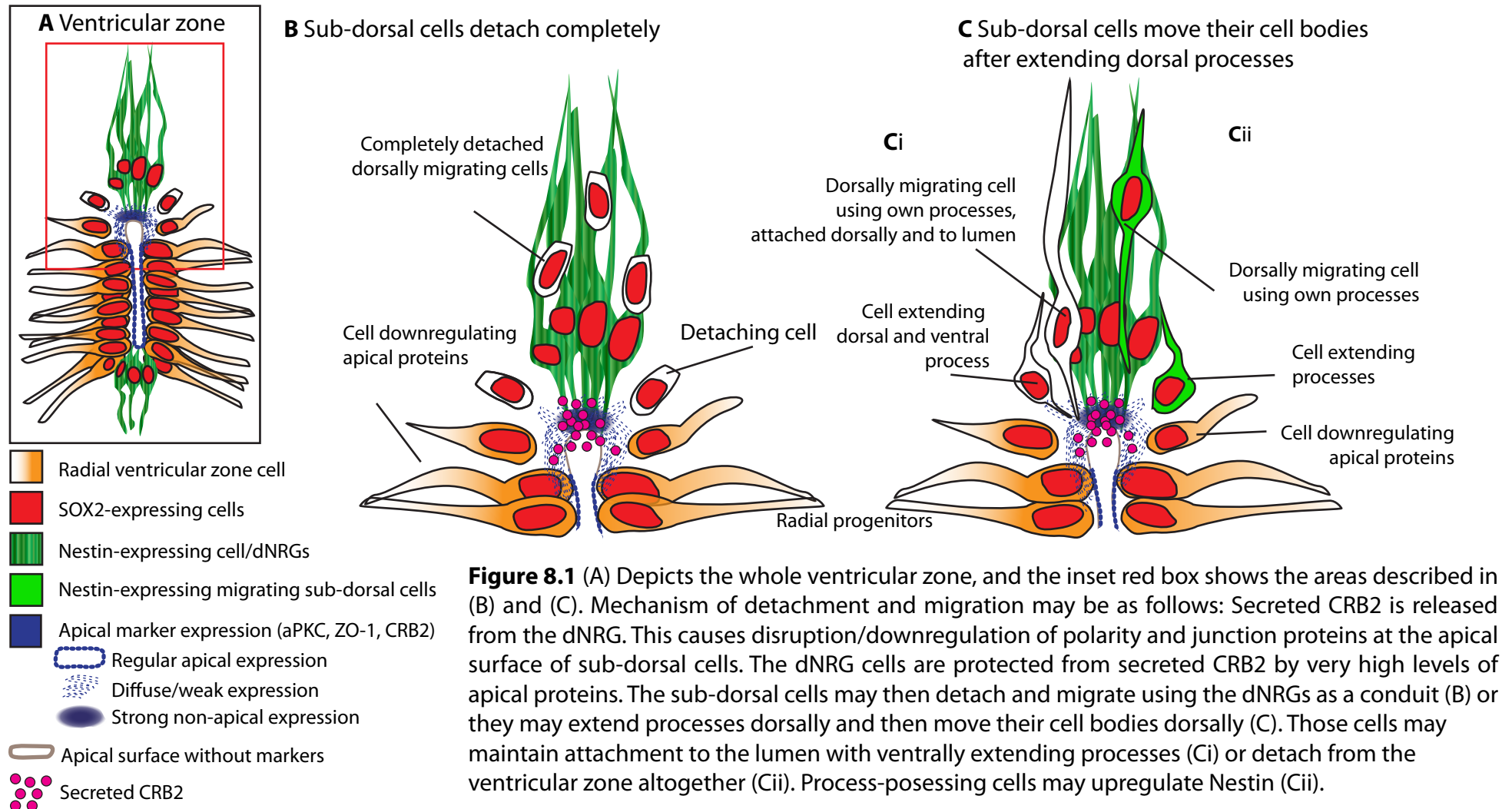


**Figure 8.1** (A) Depicts the whole ventricular zone, and the inset red box shows the areas described in (B) and (C). Mechanism of detachment and migration may be as follows: Secreted CRB2 is released from the dNRG. This causes disruption/downregulation of polarity and junction proteins at the apical surface of sub-dorsal cells. The dNRG cells are protected from secreted CRB2 by very high levels of apical proteins. The sub-dorsal cells may then detach and migrate using the dNRGs as a conduit (B) or they may extend processes dorsally and then move their cell bodies dorsally (C). Those cells may maintain attachment to the lumen with ventrally extending processes (Ci) or detach from the ventricular zone altogether (Cii). Process-possessing cells may upregulate Nestin (Cii).

### ***Determination of the function and mechanism of truncated Crb2/secreted CRB2***

One major issue with these data is that we have not been able to show that a secreted CRB2 exists *in vivo*. From the mRNA, a truncated *Crb2* construct has been made that produces a secreted CRB2 in a cell line *in vitro*, and this protein has an effect under experimental conditions. Secondly, the truncated *Crb2* mRNA has been detected in the dorsal Nestin-expressing region of the neural tube, but not in lateral ventricular zone cells, consistent with disruption data from the transplantation experiments. Therefore it seems possible that secreted CRB2 exists *in vivo* and has a biological effect.

The truncated *Crb2* transcript is formed from the splicing in of a premature stop codon. Premature truncation of a transcript can trigger the Nonsense Mediated mRNA Decay (NMD) pathway, a surveillance mechanism that ensures that mRNAs containing premature stop codons, introduced by mutation, errant transcription or unproductive pre-mRNA splicing, are degraded before translation occurs. Although widely cited as a mechanism for 'quality control' of aberrant mRNAs, the role of NMD as a posttranscriptional regulator is well established. It has been estimated that 5-30% of genes produce transcripts that are predicted to be targets of nonsense mediated decay (Lykke-Andersen and Jensen, 2015). However, although it is agreed that NMD events conserved and present in bacteria to higher organisms, its mechanisms vary broadly and are not well understood in any model (reviewed extensively in Brogna, *et al.* 2016; Karousis *et al.*, 2016).

Many genes appear to be regulated at the pre-translation level by alternative splicing in which transcription switches between the production of translated and NMD-destroyed isoforms. (Lykke-Andersen and Jensen, 2015; Hamid and Makeyev 2014;



McGlincy and Smith, 2008). Alternatively Spliced Nonsense Mediated mRNA decay (AS-NMD) may be of particular relevance to neural development, as transcriptomic profiling has identified many tissue-specific splicing events, the largest proportion of which originates from neural tissues. For example, AS-NMD mediates regulation of mouse synaptic protein PSD-95, a widely used postsynaptic marker for glutamatergic synapses in rodent and human (Castle *et al.*, 2008, Pan *et al.*, 2008 and Wang *et al.*, 2008).

The mechanism of NMD has not been reliably solved, and prediction of transcripts subject to NMD is unreliable: not all premature stop codons trigger NMD (Hurt *et al* 2013). Recent work in *Drosophila* has highlighted the complexity of gene regulation – noting that four classic pseudogenes containing a premature stop codon were, in fact, transcriptionally active in neurons, thus earning them the title ‘pseudo-pseudogenes’ (Prieto-Godino *et al*, 2016).

For this study, although we have detected the truncated *Crb2* transcript, we have not detected the protein and so we have no formal evidence that the transcript is translated. As the truncated transcript contains a premature stop codon, it may well be subject to AS-NMD. However, as presence of a stop codon is not unambiguously the trigger of NMD, it is worth considering that the truncated *Crb2* escapes degradation and is translated into a secreted protein *in vivo*.

The presence of the truncated *Crb2* transcript raises the interesting point that it may be negatively regulating the levels of full-length CRB2 protein at the transcriptional level, *i.e.* a switch to transcribing the truncated *Crb2* transcript that is then destroyed

means that there are less full length *Crb2* transcripts to be translated. This would reduce the levels of CRB2 – either in the highly CRB2-expressing dorsal nestin cells, or perhaps as a mechanism to reduce CRB2 in the sub-dorsal cells.

Whatever mechanism is present, steps should be taken to elucidate whether a functional molecule, whether a secreted protein or negatively regulating mRNA, is present. The protein could perhaps be detected by synthesis of a secreted isoform-specific antibody, although previous attempts have been unsuccessful.

However, due to the transplantation disruption data of both tissue and experimentally synthesised protein, and indeed the ability to synthesise a biologically active protein *in vitro* it is the favoured hypothesis of this writer that truncated *Crb2* is translated into a secreted protein.

### **Other markers**

These studies have not addressed that the widespread downregulation of polarity markers and junctional proteins without any balancing mechanism is likely to lead to tissue disintegration and epithelial instability. The possible model described in this thesis does not suggest that the neuroepithelium loses epithelial integrity completely. However, loss of polarity and junction proteins may be permissive to the migration of cells away from the lumen. We have not investigated that mechanism in any detail in this thesis. It is possible that the downregulation or degradation of polarity proteins in membranes left behind when cells undergo an apical abscission mechanism, such as in newborn neurons (Das and Storey, 2015) leads to lower intensity of labelling of these proteins in the sub-dorsal ventricular zone. These studies have not investigated any

biomechanical mechanisms. It was noted in the live imaging data that some cells appeared to detach their apical process from the ventricle and retract it rapidly (data not shown). It would be interesting to see if cells under mechanical stress were more sensitive to downregulation of polarity/junctional protein downregulation, which could perhaps act as a permissive mechanism for allowing cells to leave the ventricular zone. Furthermore, there are many important protein complexes that we have not investigated, such as adherens junctions, that should be studied in order to come to a conclusive picture of dorsal obliteration.

### **Functional studies**

My functional studies to date have used chick neural tube to test whether dNRG cells/secreted CRB2 protein will induce progenitor cells to delaminate. In both cases, delamination is detected, and was accompanied by downregulation of apical (ZO-1, CRB2, aPKC) proteins, internal disorganisation within the neural tube, and SOX2/PAX6/NKX6.1-expressing progenitors outside the neural tube. Although this assay has been informative, it relies on the analysis of static images. If time allowed, I would have liked to develop further assays, such as described below:

#### ***Development of a cell-based assay***

A cell-based assay will allow finer analysis of the action of secreted CRB2 *ex vivo*. I predict that secreted CRB2 can bind to transmembrane CRB2, disrupt polarity and thus the epithelial integrity. Rat retinal pigment epithelium cells and Madin-Darby canine kidney cells both express CRB2 and form an epithelial monolayer in culture. I predict that adding secreted CRB2 to a culture of these cells would disrupt the epithelial sheet.

I would then be able to test the prediction that secreted CRB2 is able to disrupt CRB2-expressing epithelia, and live image the disruption in real time. Secondly, as the secreted CRB2 has a V5 and a His tag, it should be possible to analyse where secreted CRB2 binds to these cells, and test the prediction that it binds to the extracellular domain of transmembrane CRB2.

***Further tests of slice cultures: Can secreted CRB2 promote premature dorsal obliteration in an ex vivo slice culture assay?***

My model predicts that secreted CRB2 allows cells to detach from the ventricular zone. Addition of secreted CRB to slice culture may allow me to see more/premature dorsal movement of cells in comparison to untreated cultures. Addition of secreted CRB2 may have two possible outcomes: 1) an increased number of cells leaving the ventricular zone, from along the dorsal-ventral axis in a random manner or 2) an increase in the number of cells leaving/premature migration from the dorsal ventricular zone. This experiment will provide some information about how rate-limiting secreted CRB2 is. It is possible that all cells in the ventricular zone are primed to leave/can be induced to leave by the presence of secreted CRB2 or the resulting disruption to apical polarity. This would certainly mirror some of the effects seen when transplanting dorsal radial glial cells into E10-12 chicken embryos. However, the mouse spinal cord post E13 has developed to withstand the presence of secreted CRB2 (for example high levels of polarity proteins at the endfeet of the dNRG) therefore, cells may leave the VZ prematurely, but in a regulated way. It is likely that cells leaving the ventricular zone is regulated by a large number of factors, such as mechanical tension, chemoattraction and cell-surface interactions, and a number of these may need to be in place before a cell can leave the VZ.

### ***Blocking the action of secreted CRB2***

Blocking the action of secreted CRB2 could be very informative. As no antibody exists against secreted CRB2, other strategies would have to be used. One way of knocking secreted CRB2 down is to electroporate a gene-skipping oligo. This short length of nucleotides would be designed to sit across the splice site of exon 9a, thus preventing the transcription of the truncated/secreted isoform. This could then be electroporated into slice culture. The ideal experiment would be to electroporate the construct into in utero mouse spinal cords, but this would be technically difficult.

### **8.3 Is dorsal obliteration a late part of neurulation?**

Recently it has been argued that dorsal obliteration should be considered part of late neurulation. My studies suggest that cellular processes that are apparent in dorsal obliteration are very common to cellular processes that occur in early neurulation. My studies therefore support this idea.

### **Roof plate and dNRG cells**

The appearance of roof plate cells and their wedging is thought to be vital to the bending of neural plate and its progression to neural tube *i.e.* therefore key to early neurulation (Ornitz *et al.*, 1992; Snow *et al.*, 1990). Studies in rat (Snow *et al.*, 1990) and fish (Kondrychyn *et al.*, 2013) suggest that, subsequent to their appearance of wedged-shaped cells, roof plate cells elongate, and then transit further to a radial glial-like cell. My work confirms and extends these studies. Double labelling with GFP-GPI membrane and a RFP-H2B nuclear reporter shows elongated roof plate cells at E13.5, and radial glial like cells at E14 whose cell bodies and nuclei do not directly abut the

lumen. At E13.5, the nucleus is in the more basal part of the cell; at E14.5, the cell body sits midway between lumen and pia, and sends processes to each. This mirrors my immunohistochemical analysis of Nestin/CRB2 that reveals a gap between the dorsal apical surface and dorsal nuclei (yellow arrowhead Fig 3.10).

How similar might dNRG be to radial glial cells that extend laterally? At earlier stages of neurulation, Nestin+ radial glial extend from lumen to pial surface throughout the developing neural tube (Figure 3.3). They play a critical role in neurogenesis first, acting as a stem like cells that can support neurogenesis, and second, their processes providing a scaffold for early-born neurons to migrate laterally. However, expression of Nestin diminishes from E14, after which neurogenesis also declines. My *in vivo* imaging studies show that radial glia persist at this stage (Fig 7 11). From E14, and concomitant with the loss of Nestin from radial glia, I see Nestin expression on dRG cells, and my model predicts that progenitors will move along them. This raises possibility that Nestin itself is important in some way for conducting progenitors/neurons. It is interesting to note that as the dRG cells develop long processes, the long rostral to caudal afferent axons in the dorsal funiculus begin to develop.

#### **Wider action of secreted CRB2?**

My model suggests that sub-dorsal VZ cells may delaminate, then move dorsally along radial glia. My model suggests that this delamination may be mediated by secreted CRB2. But might secreted CRB2 be playing a similar role at earlier times in neurulation? secreted *Crb2* mRNA can be detected in E11.5, well before the onset of dorsal obliteration. It is possible that secreted CRB2 is present as a translated protein at or

before this stage. We hypothesise that roof-plate cells are the source of secreted CRB2, cells that come from the same population of cells that give rise to the multipotent neural crest cell lineage. Could a population of secreted CRB2 – expressing cells be involved in the delamination of neural crest cells? Conversely, could roof plate cells be protected from the effects of secreted CRB2 and so selectively maintained in the dorsal spinal cord?

One hypothesis to explain the segregation of neural tube and neural crest cells suggests that, in fact, all cells in the early roof plate acquire the potential to delaminate and migrate, but this potential is mobilized only in the subset of these cells that will become neural crest cells (Gammill and Bronner-Fraser, 2002). The remaining dorsal midline cells never access their delamination or migratory potential and are retained as roof plate cells. The nature of this activation of the delamination or migratory potential remains completely unknown at present, but it has been postulated to occur at the post-transcriptional level and/or to be linked to changes in cytoskeletal and cell-adhesion complexes.

Finally, it is interesting to speculate whether secreted CRB2 playing a role in cell delamination more widely, both in health and disease. It is widely accepted that disrupted polarity and the interlinked mechanisms of *e.g.* epithelial to mesenchymal transition are critical to the progression of many cancers. It would be interesting to investigate whether secreted CRB2 plays a role in regulating cancers. CRB2 has not been well characterised in cancers, but the closely related family member CRB3 has been implicated in diseases: loss has been implicated in tumorigenicity in epithelial cell lines (Aigner *et al.*, 2007; Karp *et al.*, 2008; Li *et al.*, 2015). Defects in CRB1/CRB2 can

cause retinopathies (den Hollander *et al.*, 1999; van den Hurk *et al.*, 2005). Both of these homologues have large, and very similar, extracellular domains. Some of the mutations in *Crb1* in human retinal diseases are in the large extracellular domain, suggesting that this domain does have a role in maintaining epithelial integrity. Additionally, the extracellular domain of CRB2A in zebrafish has been reported to homophilically bind and stabilise the CRB complex (Zou *et al.*, 2012). It is easy to imagine a misregulation of secreted versions of CRB1 or CRB2 that could allow cells to aberrantly leave the epithelia.

### **Conserved mechanism?**

My studies show that the truncated *Crb2* transcript does exist in mouse, as it does in human, but that the exact splice event is not identical. The human equivalent of truncated *Crb2* is created by a splicing event that includes intron 10a after exon 10 (Katoh and Katoh, 2004): note this sequence was interpreted from cDNA derived from NTERA2 neuronal precursor cells, treated with RA for 5 weeks to induce neural differentiation and then with a mitotic inhibitor). Therefore, the splicing site itself is likely to be of less significance than the resulting truncating mutation that leads to an extracellular domain-only protein. The function of this truncated protein, and importantly, the functional sites of this protein are unknown. Presumably, any truncating mutation could occur anywhere between the functional sites of the truncated protein and the C-terminus of the large extracellular domain.

These studies have not provided bioinformatic evidence that a similar splicing event occurs in chicken. However, the lack of an obvious homologous splicing event in chicken does not disprove the existence of a similar secreted protein: bioinformatic studies



depend on the depth and completeness of sequencing projects, and to date, chicken mRNA/ESTs have been less intensively sequenced than mouse. Two incidences of exon 9a-containing ESTs were described in the mouse, both originating from the same sequencing study. It is possible that sequencing studies have not picked up the chicken equivalent of this presumably rare transcript. There is considerable homology between the first half of the chicken and mouse exon structure that then becomes more divergent towards the C-terminus of the protein. This suggests that it is perhaps the N terminus that is functionally important, and the region of the mammalian truncating splicing event is less so. Additionally, a truncated version of chicken CRB2 may be spliced by some alternative mechanism to the mammalian genes. Therefore, despite the lack of bioinformatic evidence for a truncated chicken CRB2, it is reasonable not to dismiss the possibility of its existence.

#### **8.4 Additional factors are likely to contribute to dorsal obliteration**

Studies into neural crest cell formation are beginning to define the complex biological steps that a cell follows – including delamination, epithelial-to-mesenchymal transition and then migration. My model suggests that dorsal obliteration will require complex steps and signals. Here I have focused on a potential role for secreted CRB2, potentially in delamination. But other signals could be important, for instance for a putative re-polarisation of detaching VZ cells or in their migration.

GENSAT is a useful resource that catalogues neural expression of a large number of different molecules in mouse through both *in situ* hybridisation and GFP-tagged transgenic techniques. Mining through the database reveals many factors that are

expressed in interesting patterns during the obliteration window. I have listed the most relevant in the Appendix (Appendix A.T1).

Interesting hits include members of the BMP family, a family of signalling ligands that have been shown to play varied role in cell proliferation, migration and axon guidance (Bragdon *et al.*, 2011). GDF10/BMP3b, for instance, is expressed strongly in the dorsal midline and the dorsal funiculus. This protein has been implicated in excessive proliferation during cancer development (Dai *et al.*, 2005), and overexpression attenuates cell proliferation, transformation, migration/invasion, and EMT (Cheng *et al.*, 2015). GDF10/BMP3b has also been linked to regulation of glial behaviour by sonic hedgehog in the cerebellum (Mecklenburg *et al.*, 2014). Likewise, a second member of the BMP family, BMP1, has previously been shown to be expressed in the premigratory neural crest and transiently in migrating cephalic neural crest cells (Marti, 2000). It seems highly likely that either, or both, may play a part in the dorsal obliteration phenotype.

ZIC2 is a C2H2-type zinc finger transcription factor that is present in the dorsal midline and dorsal horn at E15. It is required for early neurulation (Nagai *et al.*, 2000), neural crest formation and hindbrain patterning during neurulation (Elms *et al.*, 2003), and eye development (Bhansali *et al.*, 2014). Given its role in early neurulation, it might play a role in later aspects of neurulation, including dorsal obliteration. Conditional studies would be required to test this.

CX3CL1 is a large cytokine protein that is detected at E15 in the dorsal midline and dorsal horn. It has been linked to normal eye development, and is misregulated during

retinal degeneration in a mouse model of retinitis pigmentosa (Zieger *et al.*, 2014). CX3CL1 is constitutively expressed in several regions of the CNS, released both by neuronal and astrocytic cells, and is reported to mediate neuron-microglial interactions, stimulating microglial cell migration but reducing basal neuronal movement (Lauro *et al.*, 2006).

### **8.5 Dorsal obliteration and formation of adult central canal**

My studies into late neurulation shed light into the formation of the central canal and development of the dorsal glial septum. A number of studies have examined the characteristics of cells that line the adult central canal. The lateral walls are largely made up of lumen-contacting cuboidal ependymocytes and tanycytes. Lineage-tracing studies with retroviral constructs show that these derive from stem/progenitor cells that line to embryonic VZ (Fu *et al.*, 2003; Spassky *et al.*, 2005). Adult ependymocytes/tanycytes express markers that are detected in embryonic stem and progenitors, including SHH, NKX6.1 and PAX6, but in a pattern that appears relatively ventralised, *i.e.* supporting a model in which dorsal-most VZ progenitors are lost during dorsal obliteration, so that only ventral VZ cells persist around the lumen into adulthood (Fu *et al.*, 2003; Yu *et al.*, 2013). The ventral floor of the central canal is lined by radial glial cells (Petit *et al.*, 2011). And, pertinent to my work, the dorsal-most part of the central canal is occupied by the end-feet of cells termed dorsal ependymoglia (Fiorelli *et al.*, 2013; McDermott *et al.*, 2005; Sabourin *et al.*, 2009). The body of these cells is situated close to the lumen of the central canal, and they extend a long process to the pial surface. Studies have termed this region the dorsal glial septum (Bohme, 1988). The dorsal population of Nestin+ ependymoglia that persist in adulthood are thus similar in morphology, position and character to the dNRG that I

describe at the end of late neurulation, and it seems likely that they are the same cells, or are linearly-related to them.

### **8.6 Regeneration in the adult central canal**

In future my work may inform studies into the regenerative potential of the adult spinal cord. Unlike lower vertebrates such as eels and lizards, mammals have a very poor ability to repair spinal cord damage (Stenudd *et al.*, 2015). Injury generally leads to production of only glial and oligodendrocyte lineages, and the formation of a glial scar. Thus, much current work is centred on a better understanding of potential stem cells that may persist in the adult spinal cord.

In recent decades, much evidence has accumulated to show that neural stem cells exist in the central nervous system into adulthood, and are capable of giving rise to new cells, including neurons and astrocytes. In the brain, neural stem cells have been described in the sub ventricular zone (SVZ) of the lateral ventricles, the sub granular zone (SGZ) of the dentate gyrus and the hypothalamus (Alvarez-Buylla *et al.*, 2002; Broom *et al.*, 2012; Doetsch *et al.*, 1999; Jin *et al.*, 2001). *In vivo* lineage-tracing studies, and *ex vivo* neurospherogenic assays, provide evidence for multipotent self-renewing neural stem cells that can give rise to new neurons (Deleyrolle and Reynolds, 2009) By contrast, the adult spinal cord appears to have little/no ability to generate new neurons, and currently there is much debate about whether an adult stem cell exists around the central canal of the adult spinal cord, where it resides and how plastic it might be (Hugnot, 2011; Hugnot and Franzen, 2011; Peretto and Bonfanti, 2015; Zou *et al.*, 2012).

Three lines of evidence suggest that ependymocytes that line the lateral walls of the central canal are unlikely to be an active neural stem cell. They undergo some proliferation in the early postnatal animal, but not in the adult. Similarly, in mice, SOX4 is expressed in proliferating ependymocytes in young animals but not adults, supporting the idea that a character change in maturing ependymocytes diminishes their potential (Sabourin *et al.*, 2009). Further, in contrast to the SVZ and the SGZ, the adult central canal has a scant sub-ependymal layer. Instead, GFAP+SOX2 astrocytes, Olig2+ oligodendrocyte progenitors, and NeuN neurons are closely apposed to ependymocytes. Together, these studies suggest that in the normal healthy animal, ependymocytes in the adult spinal cord are not actively proliferative, gliogenic or neurogenic. Potentially, this relates to dorsal obliteration. My model suggests that dorsal VZ stem/progenitors detach from the sub-dorsal VZ. In the embryo, such progenitors are likely to be more plastic than ventral progenitors (which are confined through the action of SHH). Thus, it is possible that ependymocytes that remain around the central canal have restricted potential. Future studies are needed to test this, and to understand the fate of the detached VZ cells.

Other studies nonetheless suggest that stem/progenitor cells persist, and can be activated through a number of events, including injury and exercise. Evidence for this largely derives from analysis of the neurospherogenic potential of adult spinal cord cells *ex vivo*, and from lineage-tracing studies *in vivo*. Analysis of different regions of the adult mouse central canal shows that the dorsal region (harbouring Nestin+ RG, and potentially detached VZ cells) has a much higher proportion of neurosphere forming cells than the ventral/lateral central canal (harbouring ependymocytes) or the parenchyma, in keeping with rat studies that suggest a higher proliferative potential of

dorsal ependymocytes in the early postnatal animal (Sabourin *et al.*, 2009). This raises the intriguing possibility that either the dNRG cells may be a stem-like population, or that detached SOX2+ progenitors persist as a stem-like population.

Previous studies in the lab support these ideas, showing that in an adult mouse 'injury-slice model', the dNRG cell population expands and is associated with increased numbers of intermingled SOX2+ progenitors (Chinnaiya, 2011). The ability of the adult Nestin+ cells to induce neural migration upon transplantation into a host chicken embryo (chapter 4) may indicate a mechanism that mediates the release of neural cells upon injury. The transplanted tissue is injured by the process of dissection, and there is likely to be signals that the nestin cells or the host tissue can recognise. This may prime the host tissue to be sensitive to secreted CRB2, or perhaps more likely, induces the dNRG to secrete secreted CRB2 that then permits neural cells to migrate. Future studies are needed to investigate this further.

It is interesting to speculate on the extent to which the processes that occur in dorsal obliteration and the development of the dNRG might be re-awakened in adults, and the extent to which they can affect repair and homeostasis of the adult spinal cord.

# Bibliography

Aigner, K., Dampier, B., Descovich, L., Mikula, M., Sultan, A., Schreiber, M., Mikulits, W., Brabletz, T., Strand, D., Obrist, P., Sommergruber, W., Schweifer, N., Wernitznig, A., Beug, H., Foisner, R., Eger, A., 2007. The transcription factor ZEB1 (deltaEF1) promotes tumour cell dedifferentiation by repressing master regulators of epithelial polarity. *Oncogene* 26, 6979-6988.

Alexandre, P., Reugels, A.M., Barker, D., Blanc, E., Clarke, J.D., 2010. Neurons derive from the more apical daughter in asymmetric divisions in the zebrafish neural tube. *Nat Neurosci* 13, 673-679.

Altman, J., Bayer, S.A., 1984. The development of the rat spinal cord. *Adv Anat Embryol Cell Biol* 85, 1-164.

Alvarez-Buylla, A., Seri, B., Doetsch, F., 2002. Identification of neural stem cells in the adult vertebrate brain. *Brain Res Bull* 57, 751-758.

Assemat, E., Bazellieres, E., Pallesi-Pocachard, E., Le Bivic, A., Massey-Harroche, D., 2008. Polarity complex proteins. *Biochim Biophys Acta* 1778, 614-630.

Bachmann, A., Schneider, M., Theilenberg, E., Grawe, F., Knust, E., 2001. *Drosophila* Stardust is a partner of Crumbs in the control of epithelial cell polarity. *Nature* 414, 638-643.

Baker, P.C., Schroeder, T.E., 1967. Cytoplasmic filaments and morphogenetic movement in the amphibian neural tube. *Dev Biol* 15, 432-450.

Barriga, E.H., Mayor, R., 2015. Embryonic cell-cell adhesion: a key player in collective neural crest migration. *Curr Top Dev Biol* 112, 301-323.

Barry, D., McDermott, K., 2005. Differentiation of radial glia from radial precursor cells and transformation into astrocytes in the developing rat spinal cord. *Glia* 50, 187-197.

Berger, S., Bulgakova, N.A., Grawe, F., Johnson, K., Knust, E., 2007. Unraveling the genetic complexity of *Drosophila* stardust during photoreceptor morphogenesis and prevention of light-induced degeneration. *Genetics* 176, 2189-2200.

Bhansali, P., Rayport, I., Rebsam, A., Mason, C., 2014. Delayed neurogenesis leads to altered specification of ventrotemporal retinal ganglion cells in albino mice. *Neural Dev* 9, 11.

Bohl, J., Brimer, N., Lyons, C., Vande Pol, S.B., 2007. The stardust family protein MPP7 forms a tripartite complex with LIN7 and DLG1 that regulates the stability and localization of DLG1 to cell junctions. *J Biol Chem* 282, 9392-9400.

Bohme, G., 1988. Formation of the central canal and dorsal glial septum in the spinal cord of the domestic cat. *J Anat* 159, 37-47.



- Boroviak, T., Rashbass, P., 2011. The apical polarity determinant Crumbs 2 is a novel regulator of ESC-derived neural progenitors. *Stem Cells* 29, 193-205.
- Brachmann, I., Tucker, K.L., 2011. Organotypic slice culture of GFP-expressing mouse embryos for real-time imaging of peripheral nerve outgrowth. *J Vis Exp*.
- Bragdon, B., Moseychuk, O., Saldanha, S., King, D., Julian, J., Nohe, A., 2011. Bone morphogenetic proteins: a critical review. *Cell Signal* 23, 609-620.
- Brewer, G.J., Torricelli, J.R., Evege, E.K., Price, P.J., 1993. Optimized survival of hippocampal neurons in B27-supplemented Neurobasal, a new serum-free medium combination. *J Neurosci Res* 35, 567-576.
- Briscoe, J., Pierani, A., Jessell, T.M., Ericson, J., 2000. A homeodomain protein code specifies progenitor cell identity and neuronal fate in the ventral neural tube. *Cell* 101, 435-445.
- Brogna, S., McLeod T., Petric., M, 2016, The Meaning of NMD: Translate or Perish. *Trends in Genetics* 395–407.
- Bronner-Fraser, M., Fraser, S.E., 1988. Cell lineage analysis reveals multipotency of some avian neural crest cells. *Nature* 335, 161-164.
- Bronner-Fraser, M., Fraser, S.E., 1991. Cell lineage analysis of the avian neural crest. *Development Suppl* 2, 17-22.
- Bronner-Fraser, M., Stern, C.D., Fraser, S., 1991. Analysis of neural crest cell lineage and migration. *J Craniofac Genet Dev Biol* 11, 214-222.
- Broom, E.R., Gilthorpe, J.D., Butts, T., Campo-Paysaa, F., Wingate, R.J., 2012. The roof plate boundary is a bi-directional organiser of dorsal neural tube and choroid plexus development. *Development* 139, 4261-4270.
- Buckley, C., Clarke, J., 2014. Establishing the plane of symmetry for lumen formation and bilateral brain formation in the zebrafish neural rod. *Semin Cell Dev Biol* 31, 100-105.
- Bulgakova, N.A., Knust, E., 2009. The Crumbs complex: from epithelial-cell polarity to retinal degeneration. *J Cell Sci* 122, 2587-2596.
- Bulgakova, N.A., Rentsch, M., Knust, E., 2010. Antagonistic functions of two stardust isoforms in *Drosophila* photoreceptor cells. *Mol Biol Cell* 21, 3915-3925.
- Burnside, B., 1971. Microtubules and microfilaments in newt neuralation. *Dev Biol* 26, 416-441.

Bylund, M., Andersson, E., Novitsch, B.G., Muhr, J., 2003. Vertebrate neurogenesis is counteracted by Sox1-3 activity. *Nat Neurosci* 6, 1162-1168.

Castle J.C., Zhang C., Shah J.K., Kulkarni A.V., Kalsotra A., Cooper T.A., Johnson J.M., 2008, Expression of 24,426 human alternative splicing events and predicted cis regulation in 48 tissues and cell lines. *Nat Genet* 40: 1416–1425

Cheng, C.W., Hsiao, J.R., Fan, C.C., Lo, Y.K., Tzen, C.Y., Wu, L.W., Fang, W.Y., Cheng, A.J., Chen, C.H., Chang, I.S., Jiang, S.S., Chang, J.Y., Lee, A.Y., 2015. Loss of GDF10/BMP3b as a prognostic marker collaborates with TGFBR3 to enhance chemotherapy resistance and epithelial-mesenchymal transition in oral squamous cell carcinoma. *Mol Carcinog*.

Chinnaiya, K.a., 2011. A comparative analysis of the ventricular zone/ependymal layer in the embryonic and adult mouse spinal cord. University of Sheffield.

Chizhikov, V.V., Millen, K.J., 2004a. Control of roof plate formation by Lmx1a in the developing spinal cord. *Development* 131, 2693-2705.

Chizhikov, V.V., Millen, K.J., 2004b. Mechanisms of roof plate formation in the vertebrate CNS. *Nat Rev Neurosci* 5, 808-812.

Clay, M.R., Halloran, M.C., 2010. Control of neural crest cell behavior and migration: Insights from live imaging. *Cell Adh Migr* 4, 586-594.

Cole, G.J., Lee, J.A., 1997. Immunocytochemical localization of a novel radial glial intermediate filament protein. *Brain Res Dev Brain Res* 101, 225-238.

Dai, J., Keller, J., Zhang, J., Lu, Y., Yao, Z., Keller, E.T., 2005. Bone morphogenetic protein-6 promotes osteoblastic prostate cancer bone metastases through a dual mechanism. *Cancer Res* 65, 8274-8285.

Dailey, M.E., Marrs, G.S., Kurpius, D., 2011. Maintaining live cells and tissue slices in the imaging setup. *Cold Spring Harb Protoc* 2011, pdb top105.

Dale, J.K., Vesque, C., Lints, T.J., Sampath, T.K., Furley, A., Dodd, J., Placzek, M., 1997. Cooperation of BMP7 and SHH in the induction of forebrain ventral midline cells by prechordal mesoderm. *Cell* 90, 257-269.

Dale, K., Sattar, N., Heemskerk, J., Clarke, J.D., Placzek, M., Dodd, J., 1999. Differential patterning of ventral midline cells by axial mesoderm is regulated by BMP7 and chordin. *Development* 126, 397-408.

Darnell, D.K., Schoenwolf, G.C., 2000. The chick embryo as a model system for analyzing mechanisms of development. *Methods Mol Biol* 135, 25-29.

Das, R.M., Storey, K.G., 2014. Apical abscission alters cell polarity and dismantles the primary cilium during neurogenesis. *Science* 343, 200-204.

Davey, M.G., Tickle, C., 2007. The chicken as a model for embryonic development. *Cytogenet Genome Res* 117, 231-239.

David, S., Ousman, S.S., 2002. Recruiting the immune response to promote axon regeneration in the injured spinal cord. *Neuroscientist* 8, 33-41.

Deleyrolle, L.P., Reynolds, B.A., 2009. Identifying and enumerating neural stem cells: application to aging and cancer. *Prog Brain Res* 175, 43-51.

den Hollander, A.I., ten Brink, J.B., de Kok, Y.J., van Soest, S., van den Born, L.I., van Driel, M.A., van de Pol, D.J., Payne, A.M., Bhattacharya, S.S., Kellner, U., Hoyng, C.B., Westerveld, A., Brunner, H.G., Bleeker-Wagemakers, E.M., Deutman, A.F., Heckenlively, J.R., Cremers, F.P., Bergen, A.A., 1999. Mutations in a human homologue of *Drosophila crumbs* cause retinitis pigmentosa (RP12). *Nat Genet* 23, 217-221.

Dichmann, D.S., Harland, R.M., 2011. Nkx6 genes pattern the frog neural plate and Nkx6.1 is necessary for motoneuron axon projection. *Dev Biol* 349, 378-386.

Doetsch, F., Caille, I., Lim, D.A., Garcia-Verdugo, J.M., Alvarez-Buylla, A., 1999. Subventricular zone astrocytes are neural stem cells in the adult mammalian brain. *Cell* 97, 703-716.

Dow, L.E., Humbert, P.O., 2007. Polarity regulators and the control of epithelial architecture, cell migration, and tumorigenesis. *Int Rev Cytol* 262, 253-302.

Ebarasi, L., Ashraf, S., Bierzynska, A., Gee, H.Y., McCarthy, H.J., Lovric, S., Sadowski, C.E., Pabst, W., Vega-Warner, V., Fang, H., Koziell, A., Simpson, M.A., Dursun, I., Serdaroglu, E., Levy, S., Saleem, M.A., Hildebrandt, F., Majumdar, A., 2015. Defects of CRB2 cause steroid-resistant nephrotic syndrome. *Am J Hum Genet* 96, 153-161.

Elms, P., Siggers, P., Napper, D., Greenfield, A., Arkell, R., 2003. Zic2 is required for neural crest formation and hindbrain patterning during mouse development. *Dev Biol* 264, 391-406.

Eom, D.S., Amarnath, S., Agarwala, S., 2013. Apicobasal polarity and neural tube closure. *Dev Growth Differ* 55, 164-172.

Etienne-Manneville, S., Manneville, J.B., Nicholls, S., Ferenczi, M.A., Hall, A., 2005. Cdc42 and Par6-PKCzeta regulate the spatially localized association of Dlg1 and APC to control cell polarization. *J Cell Biol* 170, 895-901.

Fan, S., Fogg, V., Wang, Q., Chen, X.W., Liu, C.J., Margolis, B., 2007. A novel Crumbs3 isoform regulates cell division and ciliogenesis via importin beta interactions. *J Cell Biol* 178, 387-398.

Fan, S., Hurd, T.W., Liu, C.J., Straight, S.W., Weimbs, T., Hurd, E.A., Domino, S.E., Margolis, B., 2004. Polarity proteins control ciliogenesis via kinesin motor interactions. *Curr Biol* 14, 1451-1461.

Fiorelli, R., Cebrian-Silla, A., Garcia-Verdugo, J.M., Raineteau, O., 2013. The adult spinal cord harbors a population of GFAP-positive progenitors with limited self-renewal potential. *Glia* 61, 2100-2113.

Fu, H., Qi, Y., Tan, M., Cai, J., Hu, X., Liu, Z., Jensen, J., Qiu, M., 2003. Molecular mapping of the origin of postnatal spinal cord ependymal cells: evidence that adult ependymal cells are derived from Nkx6.1+ ventral neural progenitor cells. *J Comp Neurol* 456, 237-244.

Gammill, L.S., Bronner-Fraser, M., 2002. Genomic analysis of neural crest induction. *Development* 129, 5731-5741.

Gao, L., Joberty, G., Macara, I.G., 2002a. Assembly of epithelial tight junctions is negatively regulated by Par6. *Curr Biol* 12, 221-225.

Gao, L., Macara, I.G., Joberty, G., 2002b. Multiple splice variants of Par3 and of a novel related gene, Par3L, produce proteins with different binding properties. *Gene* 294, 99-107.

Garcia, M.D., Udan, R.S., Hadjantonakis, A.K., Dickinson, M.E., 2011. Live imaging of mouse embryos. *Cold Spring Harb Protoc* 2011, pdb top104.

Garcia-Castro, M.I., Marcelle, C., Bronner-Fraser, M., 2002. Ectodermal Wnt function as a neural crest inducer. *Science* 297, 848-851.

Garnett, A.T., Square, T.A., Medeiros, D.M., 2012. BMP, Wnt and FGF signals are integrated through evolutionarily conserved enhancers to achieve robust expression of Pax3 and Zic genes at the zebrafish neural plate border. *Development* 139, 4220-4231.

Genova, J.L., Jong, S., Camp, J.T., Fehon, R.G., 2000. Functional analysis of Cdc42 in actin filament assembly, epithelial morphogenesis, and cell signaling during *Drosophila* development. *Dev Biol* 221, 181-194.

Ghosh, S., Marquardt, T., Thaler, J.P., Carter, N., Andrews, S.E., Pfaff, S.L., Hunter, T., 2008. Instructive role of aPKCzeta subcellular localization in the assembly of adherens junctions in neural progenitors. *Proc Natl Acad Sci U S A* 105, 335-340.

Gilbert S. F. *Developmental Biology*. (2002) 7th ed. Sunderland, MA: Sinauer Associates; 2003

Goehring, N.W., 2014. PAR polarity: from complexity to design principles. *Exp Cell Res* 328, 258-266.

Gomes, E.R., Jani, S., Gundersen, G.G., 2005. Nuclear movement regulated by Cdc42, MRCK, myosin, and actin flow establishes MTOC polarization in migrating cells. *Cell* 121, 451-463.

Gomez-Lopez, S., Lerner, R.G., Petritsch, C., 2014. Asymmetric cell division of stem and progenitor cells during homeostasis and cancer. *Cell Mol Life Sci* 71, 575-597.

Gosens, I., den Hollander, A.I., Cremers, F.P., Roepman, R., 2008. Composition and function of the Crumbs protein complex in the mammalian retina. *Exp Eye Res* 86, 713-726.

Graham, V., Khudyakov, J., Ellis, P., Pevny, L., 2003. SOX2 functions to maintain neural progenitor identity. *Neuron* 39, 749-765.

Grawe, F., Wodarz, A., Lee, B., Knust, E., Skaer, H., 1996. The *Drosophila* genes *crumbs* and *stardust* are involved in the biogenesis of adherens junctions. *Development* 122, 951-959.

Grego-Bessa, J., Hildebrand, J., Anderson, K.V., 2015. Morphogenesis of the mouse neural plate depends on distinct roles of cofilin 1 in apical and basal epithelial domains. *Development* 142, 1305-1314.

Groves, A.K., LaBonne, C., 2014. Setting appropriate boundaries: fate, patterning and competence at the neural plate border. *Dev Biol* 389, 2-12.

Gärtner, A., Fornasiero, E.F., Dotti, C.G., (2015) Cadherins as regulators of neuronal polarity. *Cell Adh Migr.* 9(3): 175–182.

Gärtner, A., Fornasiero, E.F., Munck, S., Vennekens, K., Seuntjens, E., Huttner W.B., Valtorta F., Dotti, C.G., (2012) N-cadherin specifies first asymmetry in developing neurons. *EMBO J.* Apr 18; 31(8):1893-903.

Haenfler, J.M., Kuang, C., Lee, C.Y., 2012. Cortical aPKC kinase activity distinguishes neural stem cells from progenitor cells by ensuring asymmetric segregation of Numb. *Dev Biol* 365, 219-228.

Haigo, S.L., Hildebrand, J.D., Harland, R.M., Wallingford, J.B., 2003. Shroom induces apical constriction and is required for hinge point formation during neural tube closure. *Curr Biol* 13, 2125-2137.

Halbleib JM, Nelson WJ. Cadherins in development: cell adhesion, sorting, and tissue morphogenesis. *Genes Dev* 2006; 20:3199-214

Hamid F.M., Makeyev E.V., 2014, Emerging functions of alternative splicing coupled with nonsense-mediated decay. *Biochem Soc Trans* 42: 1168–73.

He, Q., Wang, G., Wakade, S., Dasgupta, S., Dinkins, M., Kong, J.N., Spassieva, S.D., Bieberich, E., 2014. Primary cilia in stem cells and neural progenitors are regulated by neutral sphingomyelinase 2 and ceramide. *Mol Biol Cell* 25, 1715-1729.

Helfrich, I., Schmitz, A., Zigrino, P., Michels, C., Haase, I., le Bivic, A., Leitges, M., Niessen, C.M., 2007. Role of aPKC isoforms and their binding partners Par3 and Par6 in epidermal barrier formation. *J Invest Dermatol* 127, 782-791.

Hidalgo, A and Brand AH; 1997. Targeted neuronal ablation: the role of pioneer neurons in guidance and fasciculation in the CNS of *Drosophila*. *Development*. 124(17):3253-62.

Hildebrand, J.D., Soriano, P., 1999. Shroom, a PDZ domain-containing actin-binding protein, is required for neural tube morphogenesis in mice. *Cell* 99, 485-497.

Hillman, E.M., 2007. Optical brain imaging in vivo: techniques and applications from animal to man. *J Biomed Opt* 12, 051402.

Hong, C.S., Saint-Jeannet, J.P., 2007. The activity of Pax3 and Zic1 regulates three distinct cell fates at the neural plate border. *Mol Biol Cell* 18, 2192-2202.

Hong, Y., Ackerman, L., Jan, L.Y., Jan, Y.N., 2003. Distinct roles of Bazooka and Stardust in the specification of *Drosophila* photoreceptor membrane architecture. *Proc Natl Acad Sci U S A* 100, 12712-12717.

Horne-Badovinac, S., Bilder, D., 2008. Dynein regulates epithelial polarity and the apical localization of stardust A mRNA. *PLoS Genet* 4, e8.

Huettl, R.E., Eckstein, S., Stahl, T., Petricca, S., Ninkovic, J., Gotz, M., Huber, A.B., 2015. Functional dissection of the Pax6 paired domain: Roles in neural tube patterning and peripheral nervous system development. *Dev Biol*.

Hugnot, J.P., Franzen, R., 2011. The spinal cord ependymal region: a stem cell niche in the caudal central nervous system. *Front Biosci (Landmark Ed)* 16, 1044-1059.

Humbert, P.O., Dow, L.E., Russell, S.M., 2006. The Scribble and Par complexes in polarity and migration: friends or foes? *Trends Cell Biol* 16, 622-630.

Ihrie, R.A., Alvarez-Buylla, A., 2011. Lake-front property: a unique germinal niche by the lateral ventricles of the adult brain. *Neuron* 70, 674-686.

Jacob, J., Briscoe, J., 2003. Gli proteins and the control of spinal-cord patterning. *EMBO Rep* 4, 761-765.

Jessell, T.M., 2000. Neuronal specification in the spinal cord: inductive signals and transcriptional codes. *Nat Rev Genet* 1, 20-29.

Jin, K., Minami, M., Lan, J.Q., Mao, X.O., Batteur, S., Simon, R.P., Greenberg, D.A., 2001. Neurogenesis in dentate subgranular zone and rostral subventricular zone after focal cerebral ischemia in the rat. *Proc Natl Acad Sci U S A* 98, 4710-4715.

Kalaskar, V.K., Lauderdale, J.D., 2014. Mouse embryonic development in a serum-free whole embryo culture system. *J Vis Exp*.

Kaplan, N.A., Liu, X., Tolwinski, N.S., 2009. Epithelial polarity: interactions between junctions and apical-basal machinery. *Genetics* 183, 897-904.

Karfunkel, P., 1974. The mechanisms of neural tube formation. *Int Rev Cytol* 38, 245-271.

Karp, C.M., Tan, T.T., Mathew, R., Nelson, D., Mukherjee, C., Degenhardt, K., Karantza-Wadsworth, V., White, E., 2008. Role of the polarity determinant crumbs in suppressing mammalian epithelial tumor progression. *Cancer Res* 68, 4105-4115.

Katoh, M., Katoh, M., 2004. Identification and characterization of Crumbs homolog 2 gene at human chromosome 9q33.3. *Int J Oncol* 24, 743-749.

Keller, M.J., Chitnis, A.B., 2007. Insights into the evolutionary history of the vertebrate *zic3* locus from a teleost-specific *zic6* gene in the zebrafish, *Danio rerio*. *Dev Genes Evol* 217, 541-547.

Kerosuo, L., Bronner-Fraser, M., 2012. What is bad in cancer is good in the embryo: importance of EMT in neural crest development. *Semin Cell Dev Biol* 23, 320-332.

Khudyakov, J., Bronner-Fraser, M., 2009. Comprehensive spatiotemporal analysis of early chick neural crest network genes. *Dev Dyn* 238, 716-723.

Khursheed, M., Bashyam, M.D., 2014. Apico-basal polarity complex and cancer. *J Biosci* 39, 145-155.

King, E.D., Munger, B.L., 1990. Myotome and early neurogenesis in chick embryos. *Anat Rec* 228, 191-210.

Kinnunen, T., Raulo, E., Nolo, R., Maccarana, M., Lindahl, U., Rauvala, H., 1996. Neurite outgrowth in brain neurons induced by heparin-binding growth-associated molecule (HB-GAM) depends on the specific interaction of HB-GAM with heparan sulfate at the cell surface. *J Biol Chem* 271, 2243-2248.

- Kishi, M., Mizuseki, K., Sasai, N., Yamazaki, N., Shiota, K., Nakanishi, S., Sasai, Y., (2000) Requirement of Sox2-mediated signaling for differentiation of early *Xenopus* neuroectoderm. *Development*, 127, 791–800
- Klebes, A., Knust, E., 2000. A conserved motif in Crumbs is required for E-cadherin localisation and zonula adherens formation in *Drosophila*. *Curr Biol* 10, 76-85.
- Kohjima, M., Noda, Y., Takeya, R., Saito, N., Takeuchi, K., Sumimoto, H., 2002. PAR3beta, a novel homologue of the cell polarity protein PAR3, localizes to tight junctions. *Biochem Biophys Res Commun* 299, 641-646.
- Kondrychyn, I., Teh, C., Sin, M., Korzh, V., 2013. Stretching morphogenesis of the roof plate and formation of the central canal. *PLoS One* 8, e56219.
- Korzh, V., 2014a. [Neurulation continues: the parade commander is...apical constriction]. *Ontogenez* 45, 240-249.
- Korzh, V., 2014b. Stretching cell morphogenesis during late neurulation and mild neural tube defects. *Dev Growth Differ* 56, 425-433.
- Kosodo, Y., Roper, K., Haubensak, W., Marzesco, A.M., Corbeil, D., Huttner, W.B., 2004. Asymmetric distribution of the apical plasma membrane during neurogenic divisions of mammalian neuroepithelial cells. *EMBO J* 23, 2314-2324.
- Kosodo, Y., Suetsugu, T., Suda, M., Mimori-Kiyosue, Y., Toida, K., Baba, S.A., Kimura, A., Matsuzaki, F., 2011. Regulation of interkinetic nuclear migration by cell cycle-coupled active and passive mechanisms in the developing brain. *EMBO J* 30, 1690-1704.
- Kriegstein, A., Alvarez-Buylla, A., 2009. The glial nature of embryonic and adult neural stem cells. *Annu Rev Neurosci* 32, 149-184.
- Kulesa, P.M., Bailey, C.M., Cooper, C., Fraser, S.E., 2010. In ovo live imaging of avian embryos. *Cold Spring Harb Protoc* 2010, pdb prot5446.
- Kuriyama, S., Kinoshita, T., 2001. Xer1, a novel CNS-specific secretory protein, establishes the boundary between neural plate and neural crest. *Int J Dev Biol* 45, 845-852.
- Kuriyama, S., Ueda, A., Kinoshita, T., 2003. Xer1 is a secreted protein required for establishing the neural plate/neural crest boundary in *Xenopus* embryo. *J Exp Zool A Comp Exp Biol* 296, 108-116.
- Laprise, P., 2011. Emerging role for epithelial polarity proteins of the Crumbs family as potential tumor suppressors. *J Biomed Biotechnol* 2011, 868217.



- Larina, I.V., Syed, S.H., Sudheendran, N., Overbeek, P.A., Dickinson, M.E., Larin, K.V., 2012. Optical coherence tomography for live phenotypic analysis of embryonic ocular structures in mouse models. *J Biomed Opt* 17, 081410-081411.
- Lauro, C., Catalano, M., Trettel, F., Mainiero, F., Ciotti, M.T., Eusebi, F., Limatola, C., 2006. The chemokine CX3CL1 reduces migration and increases adhesion of neurons with mechanisms dependent on the beta1 integrin subunit. *J Immunol* 177, 7599-7606.
- Le Douarin, N.M., Creuzet, S., Couly, G., Dupin, E., 2004. Neural crest cell plasticity and its limits. *Development* 131, 4637-4650.
- Le Dreau, G., Marti, E., 2012. Dorsal-ventral patterning of the neural tube: a tale of three signals. *Dev Neurobiol* 72, 1471-1481.
- Lee, A.P., Brenner, S., Venkatesh, B., 2011. Mouse transgenesis identifies conserved functional enhancers and cis-regulatory motif in the vertebrate LIM homeobox gene *Lhx2* locus. *PLoS One* 6, e20088.
- Lee, C., Scherr, H.M., Wallingford, J.B., 2007. Shroom family proteins regulate gamma-tubulin distribution and microtubule architecture during epithelial cell shape change. *Development* 134, 1431-1441.
- Lemmers, C., Michel, D., Lane-Guermonprez, L., Delgrossi, M.H., Medina, E., Arsanto, J.P., Le Bivic, A., 2004. CRB3 binds directly to Par6 and regulates the morphogenesis of the tight junctions in mammalian epithelial cells. *Mol Biol Cell* 15, 1324-1333.
- Li, P., Mao, X., Ren, Y., Liu, P., 2015. Epithelial cell polarity determinant CRB3 in cancer development. *Int J Biol Sci* 11, 31-37.
- Li, Y.C., Bai, W.Z., Sakai, K., Hashikawa, T., 2009. Fluorescence and electron microscopic localization of F-actin in the ependymocytes. *J Histochem Cytochem* 57, 741-751.
- Lichtman, J.W., Fraser, S.E., 2001. The neuronal naturalist: watching neurons in their native habitat. *Nat Neurosci* 4 Suppl, 1215-1220.
- Liem, K.F., Jr., Tremml, G., Jessell, T.M., 1997. A role for the roof plate and its resident TGFbeta-related proteins in neuronal patterning in the dorsal spinal cord. *Cell* 91, 127-138.
- Lu, H., Bilder, D., 2005. Endocytic control of epithelial polarity and proliferation in *Drosophila*. *Nat Cell Biol* 7, 1232-1239.
- Lykke-Andersen S1., Jensen TAH1. 2015, Nonsense-mediated mRNA decay: an intricate machinery that shapes transcriptomes. *Nat Rev Mol Cell Biol* 11, 665-77

Makarova, O., Roh, M.H., Liu, C.J., Laurinec, S., Margolis, B., 2003. Mammalian Crumbs3 is a small transmembrane protein linked to protein associated with Lin-7 (Pals1). *Gene* 302, 21-29.

Malatesta, P., Appolloni, I., Calzolari, F., 2008. Radial glia and neural stem cells. *Cell Tissue Res* 331, 165-178.

Malicki, J., Driever, W., 1999. oko meduzy mutations affect neuronal patterning in the zebrafish retina and reveal cell-cell interactions of the retinal neuroepithelial sheet. *Development* 126, 1235-1246.

Mao, X., Li, P., Ren, Y., Li, J., Zhou, C., Yang, J., Liu, P., 2015. Cell polarity protein CRB3 is an independent favorable prognostic factor for clear cell renal cell carcinoma. *Int J Oncol* 46, 657-666.

Marti, E., 2000. Expression of chick BMP-1/Tolloid during patterning of the neural tube and somites. *Mech Dev* 91, 415-419.

Martin, A.C., Goldstein, B., 2014. Apical constriction: themes and variations on a cellular mechanism driving morphogenesis. *Development* 141, 1987-1998.

Mason, F.M., Martin, A.C., 2011. Tuning cell shape change with contractile ratchets. *Curr Opin Genet Dev* 21, 671-679.

McDermott, K.W., Barry, D.S., McMahan, S.S., 2005. Role of radial glia in cytotogenesis, patterning and boundary formation in the developing spinal cord. *J Anat* 207, 241-250.

McGlinchy N.J., Smith C.W., 2008, Alternative splicing resulting in nonsensemediated mRNA decay: what is the meaning of nonsense? *Trends Biochem Sci* 33:385–393

McMahan, A.P., 2000. Neural patterning: the role of Nkx genes in the ventral spinal cord. *Genes Dev* 14, 2261-2264.

Mecklenburg, N., Martinez-Lopez, J.E., Moreno-Bravo, J.A., Perez-Balaguer, A., Puelles, E., Martinez, S., 2014. Growth and differentiation factor 10 (Gdf10) is involved in Bergmann glial cell development under Shh regulation. *Glia* 62, 1713-1723.

Medina, E., Lemmers, C., Lane-Guermonprez, L., Le Bivic, A., 2002. Role of the Crumbs complex in the regulation of junction formation in *Drosophila* and mammalian epithelial cells. *Biol Cell* 94, 305-313.

Meulemans, D., Bronner-Fraser, M., 2004. Gene-regulatory interactions in neural crest evolution and development. *Dev Cell* 7, 291-299.

Mitsuishi, Y., Hasegawa, H., Matsuo, A., Araki, W., Suzuki, T., Tagami, S., Okochi, M., Takeda, M., Roepman, R., Nishimura, M., 2010. Human CRB2 inhibits gamma-secretase

cleavage of amyloid precursor protein by binding to the presenilin complex. *J Biol Chem* 285, 14920-14931.

Miyamoto, Y., Sakane, F., Hashimoto, K., 2015. N-cadherin-based adherens junction regulates the maintenance, proliferation, and differentiation of neural progenitor cells during development. *Cell Adh Migr* 9, 183-192.

Morais-de-Sa, E., Mirouse, V., St Johnston, D., 2010. aPKC phosphorylation of Bazooka defines the apical/lateral border in *Drosophila* epithelial cells. *Cell* 141, 509-523.

Morriss-Kay, G., Tuckett, F., 1985. The role of microfilaments in cranial neurulation in rat embryos: effects of short-term exposure to cytochalasin D. *J Embryol Exp Morphol* 88, 333-348.

Munson, C., Huisken, J., Bit-Avragim, N., Kuo, T., Dong, P.D., Ober, E.A., Verkade, H., Abdelilah-Seyfried, S., Stainier, D.Y., 2008. Regulation of neurocoel morphogenesis by *Pard6* gamma b. *Dev Biol* 324, 41-54.

Murtaza, M.a., 2012. The role of *Crumbs2* in neural development. University of Sheffield.

Nadarajah, B., Alifragis, P., Wong, R.O., Parnavelas, J.G., 2003. Neuronal migration in the developing cerebral cortex: observations based on real-time imaging. *Cereb Cortex* 13, 607-611.

Nagai, T., Aruga, J., Minowa, O., Sugimoto, T., Ohno, Y., Noda, T., Mikoshiba, K., 2000. *Zic2* regulates the kinetics of neurulation. *Proc Natl Acad Sci U S A* 97, 1618-1623.

Nagele, R.G., Hunter, E., Bush, K., Lee, H.Y., 1987. Studies on the mechanisms of neurulation in the chick: morphometric analysis of force distribution within the neuroepithelium during neural tube formation. *J Exp Zool* 244, 425-436.

Nam, S.C., Choi, K.W., 2003. Interaction of *Par-6* and *Crumbs* complexes is essential for photoreceptor morphogenesis in *Drosophila*. *Development* 130, 4363-4372.

Napier, A., Yuan, A., Cole, G.J., 1999. Characterization of the chicken *transitin* gene reveals a strong relationship to the *nestin* intermediate filament class. *J Mol Neurosci* 12, 11-22.

Nichane, M., de Croze, N., Ren, X., Souopgui, J., Monsoro-Burq, A.H., Bellefroid, E.J., 2008. *Hairy2*-*Id3* interactions play an essential role in *Xenopus* neural crest progenitor specification. *Dev Biol* 322, 355-367.

Nishimura, T., Honda, H., Takeichi, M., 2012. Planar cell polarity links axes of spatial dynamics in neural-tube closure. *Cell* 149, 1084-1097.

Nishimura, T., Takeichi, M., 2008. Shroom3-mediated recruitment of Rho kinases to the apical cell junctions regulates epithelial and neuroepithelial planar remodeling. *Development* 135, 1493-1502.

Norris, F.C., Wong, M.D., Greene, N.D., Scambler, P.J., Weaver, T., Weninger, W.J., Mohun, T.J., Henkelman, R.M., Lythgoe, M.F., 2013. A coming of age: advanced imaging technologies for characterising the developing mouse. *Trends Genet* 29, 700-711.

Omori, Y., Malicki, J., 2006. *oko meduzy* and related crumbs genes are determinants of apical cell features in the vertebrate embryo. *Curr Biol* 16, 945-957.

Ornitz, D.M., Yayon, A., Flanagan, J.G., Svahn, C.M., Levi, E., Leder, P., 1992. Heparin is required for cell-free binding of basic fibroblast growth factor to a soluble receptor and for mitogenesis in whole cells. *Mol Cell Biol* 12, 240-247.

Osumi, N., Shinohara, H., Numayama-Tsuruta, K., Maekawa, M., 2008. Concise review: Pax6 transcription factor contributes to both embryonic and adult neurogenesis as a multifunctional regulator. *Stem Cells* 26, 1663-1672.

Pakan, J.M., McDermott, K.W., 2014. A method to investigate radial glia cell behavior using two-photon time-lapse microscopy in an ex vivo model of spinal cord development. *Front Neuroanat* 8, 22.

Pan, Q., Shai, O., Lee, L.J., Frey, B.J., Blencowe, B.J., 2008, Deep surveying of alternative splicing complexity in the human transcriptome by high-throughput sequencing *Nat. Genet.*, 40pp. 1413–1415

Peretto, P., Bonfanti, L., 2015. Adult neurogenesis 20 years later: physiological function vs. brain repair. *Front Neurosci* 9, 71.

Peterson, F.C., Penkert, R.R., Volkman, B.F., Prehoda, K.E., 2004. Cdc42 regulates the Par-6 PDZ domain through an allosteric CRIB-PDZ transition. *Mol Cell* 13, 665-676.

Petit, A., Sanders, A.D., Kennedy, T.E., Tetzlaff, W., Glattfelder, K.J., Dalley, R.A., Puchalski, R.B., Jones, A.R., Roskams, A.J., 2011. Adult spinal cord radial glia display a unique progenitor phenotype. *PLoS One* 6, e24538.

Pevny, L., Placzek, M., 2005. SOX genes and neural progenitor identity. *Curr Opin Neurobiol* 15, 7-13.

Pevny, L.H., Sockanathan, S., Placzek, M., Lovell-Badge, R., 1998. A role for SOX1 in neural determination. *Development* 125, 1967-1978.

Piliszek, A., Kwon, G.S., Hadjantonakis, A.K., 2011. Ex utero culture and live imaging of mouse embryos. *Methods Mol Biol* 770, 243-257.

- Pituello, F., Medevielle, F., Foulquier, F., Duprat, A.M., 1999. Activation of Pax6 depends on somitogenesis in the chick embryo cervical spinal cord. *Development* 126, 587-596.
- Pituello, F., Yamada, G., Gruss, P., 1995. Activin A inhibits Pax-6 expression and perturbs cell differentiation in the developing spinal cord in vitro. *Proc Natl Acad Sci U S A* 92, 6952-6956.
- Pla, P., Moore, R., Morali, O.G., Grille, S., Martinozzi, S., Delmas, V., Larue, L., 2001. Cadherins in neural crest cell development and transformation. *J Cell Physiol* 189, 121-132.
- Poluch, S., Juliano, S.L., 2007. A normal radial glial scaffold is necessary for migration of interneurons during neocortical development. *Glia* 55, 822-830.
- Prieto-Godino, L., Rytz, R., Bargeton, B., Abuin, L., Arguello, J., Dal Peraro, M., and Benton, R., (2016) Olfactory receptor pseudo-pseudogenes *Nature* 539, 93–97
- Ramahi, J.S., Solecki, D.J., 2014. The PAR polarity complex and cerebellar granule neuron migration. *Adv Exp Med Biol* 800, 113-131.
- Rashbass, P., Skaer, H., 2000. Cell polarity: Nailing Crumbs to the scaffold. *Curr Biol* 10, R234-236.
- Redies C, Takeichi M (1993) Expression of N-cadherin mRNA during development of the mouse brain. *Dev Dyn* 197:26–39.
- Renaud, O., Herbomel, P., Kissa, K., 2011. Studying cell behavior in whole zebrafish embryos by confocal live imaging: application to hematopoietic stem cells. *Nat Protoc* 6, 1897-1904.
- Rex, M., Orme, A., Uwanogho, D., Tointon, K., Wigmore, P.M., Sharpe, P.T., Scotting, P.J., 1997. Dynamic expression of chicken Sox2 and Sox3 genes in ectoderm induced to form neural tissue. *Dev Dyn* 209, 323-332.
- Richard, M., Roepman, R., Aartsen, W.M., van Rossum, A.G., den Hollander, A.I., Knust, E., Wijnholds, J., Cremers, F.P., 2006. Towards understanding CRUMBS function in retinal dystrophies. *Hum Mol Genet* 15 Spec No 2, R235-243.
- Roh, M.H., Fan, S., Liu, C.J., Margolis, B., 2003. The Crumbs3-Pals1 complex participates in the establishment of polarity in mammalian epithelial cells. *J Cell Sci* 116, 2895-2906.
- Roignot, J., Peng, X., Mostov, K., 2013. Polarity in mammalian epithelial morphogenesis. *Cold Spring Harb Perspect Biol* 5.

- Rowitch, D.H., 2004. Glial specification in the vertebrate neural tube. *Nat Rev Neurosci* 5, 409-419.
- Rowitch, D.H., Kriegstein, A.R., 2010. Developmental genetics of vertebrate glial-cell specification. *Nature* 468, 214-222.
- Royer, C., Lu, X., 2011. Epithelial cell polarity: a major gatekeeper against cancer? *Cell Death Differ* 18, 1470-1477.
- Sabourin, J.C., Ackema, K.B., Ohayon, D., Guichet, P.O., Perrin, F.E., Garces, A., Ripoll, C., Charite, J., Simonneau, L., Kettenmann, H., Zine, A., Privat, A., Valmier, J., Pattyn, A., Hugnot, J.P., 2009. A mesenchymal-like ZEB1(+) niche harbors dorsal radial glial fibrillary acidic protein-positive stem cells in the spinal cord. *Stem Cells* 27, 2722-2733.
- Sadler, T.W., Greenberg, D., Coughlin, P., Lessard, J.L., 1982. Actin distribution patterns in the mouse neural tube during neurulation. *Science* 215, 172-174.
- Sander, M., Paydar, S., Ericson, J., Briscoe, J., Berber, E., German, M., Jessell, T.M., Rubenstein, J.L., 2000. Ventral neural patterning by Nkx homeobox genes: Nkx6.1 controls somatic motor neuron and ventral interneuron fates. *Genes Dev* 14, 2134-2139.
- Sauka-Spengler, T., Bronner-Fraser, M., 2008. A gene regulatory network orchestrates neural crest formation. *Nat Rev Mol Cell Biol* 9, 557-568.
- Sauvageot, C.M., Stiles, C.D., 2002. Molecular mechanisms controlling cortical gliogenesis. *Curr Opin Neurobiol* 12, 244-249.
- Sawyer, J.M., Harrell, J.R., Shemer, G., Sullivan-Brown, J., Roh-Johnson, M., Goldstein, B., 2010. Apical constriction: a cell shape change that can drive morphogenesis. *Dev Biol* 341, 5-19.
- Schluter, M.A., Pfarr, C.S., Pieczynski, J., Whiteman, E.L., Hurd, T.W., Fan, S., Liu, C.J., Margolis, B., 2009. Trafficking of Crumbs3 during cytokinesis is crucial for lumen formation. *Mol Biol Cell* 20, 4652-4663.
- Schmidt, R., Strahle, U., Scholpp, S., 2013. Neurogenesis in zebrafish - from embryo to adult. *Neural Dev* 8, 3.
- Schwarz, M., Alvarez-Bolado, G., Dressler, G., Urbanek, P., Busslinger, M., Gruss, P., 1999. Pax2/5 and Pax6 subdivide the early neural tube into three domains. *Mech Dev* 82, 29-39.
- Seri, B., Garcia-Verdugo, J.M., Collado-Morente, L., McEwen, B.S., Alvarez-Buylla, A., 2004. Cell types, lineage, and architecture of the germinal zone in the adult dentate gyrus. *J Comp Neurol* 478, 359-378.

- Sevc, J., Daxnerova, Z., Miklosova, M., 2009. Role of radial glia in transformation of the primitive lumen to the central canal in the developing rat spinal cord. *Cell Mol Neurobiol* 29, 927-936.
- Shin, K., Fogg, V.C., Margolis, B., 2006. Tight junctions and cell polarity. *Annu Rev Cell Dev Biol* 22, 207-235.
- Sierralta, J., Mendoza, C., 2004. PDZ-containing proteins: alternative splicing as a source of functional diversity. *Brain Res Brain Res Rev* 47, 105-115.
- Simoës-Costa, M., Bronner, M.E., 2013. Insights into neural crest development and evolution from genomic analysis. *Genome Res* 23, 1069-1080.
- Simoës-Costa, M., Bronner, M.E., 2015. Establishing neural crest identity: a gene regulatory recipe. *Development* 142, 242-257.
- Singh, S., Solecki, D.J., 2015. Polarity transitions during neurogenesis and germinal zone exit in the developing central nervous system. *Front Cell Neurosci* 9, 62.
- Slavotinek, A., Kaylor, J., Pierce, H., Cahr, M., DeWard, S.J., Schneidman-Duhovny, D., Alsadah, A., Salem, F., Schmajuk, G., Mehta, L., 2015. CRB2 mutations produce a phenotype resembling congenital nephrosis, Finnish type, with cerebral ventriculomegaly and raised alpha-fetoprotein. *Am J Hum Genet* 96, 162-169.
- Smedley, M.J., Stanisstreet, M., 1986. Calcium and neurulation in mammalian embryos. II. Effects of cytoskeletal inhibitors and calcium antagonists on the neural folds of rat embryos. *J Embryol Exp Morphol* 93, 167-178.
- Snow, D.M., Steindler, D.A., Silver, J., 1990. Molecular and cellular characterization of the glial roof plate of the spinal cord and optic tectum: a possible role for a proteoglycan in the development of an axon barrier. *Dev Biol* 138, 359-376.
- Sotillos, S., Diaz-Meco, M.T., Caminero, E., Moscat, J., Campuzano, S., 2004. DaPKC-dependent phosphorylation of Crumbs is required for epithelial cell polarity in *Drosophila*. *J Cell Biol* 166, 549-557.
- Spassky, N., Merkle, F.T., Flames, N., Tramontin, A.D., Garcia-Verdugo, J.M., Alvarez-Buylla, A., 2005. Adult ependymal cells are postmitotic and are derived from radial glial cells during embryogenesis. *J Neurosci* 25, 10-18.
- Spear, P.C., Erickson, C.A., 2012. Interkinetic nuclear migration: a mysterious process in search of a function. *Dev Growth Differ* 54, 306-316.
- St Johnston, D., Sanson, B., 2011. Epithelial polarity and morphogenesis. *Curr Opin Cell Biol* 23, 540-546.

- Stenudd, M., Sabelstrom, H., Frisen, J., 2015. Role of endogenous neural stem cells in spinal cord injury and repair. *JAMA Neurol* 72, 235-237.
- Straight, S.W., Pieczynski, J.N., Whiteman, E.L., Liu, C.J., Margolis, B., 2006. Mammalian lin-7 stabilizes polarity protein complexes. *J Biol Chem* 281, 37738-37747.
- Streit, A., Berliner, A.J., Papanayotou, C., Sirulnik, A., Stern, C.D., 2000. Initiation of neural induction by FGF signalling before gastrulation. *Nature* 406, 74-78.
- Sturrock, R.R., 1981. An electron microscopic study of the development of the ependyma of the central canal of the mouse spinal cord. *J Anat* 132, 119-136.
- Sun, T.Q., Lu, B., Feng, J.J., Reinhard, C., Jan, Y.N., Fantl, W.J., Williams, L.T., 2001. PAR-1 is a Dishevelled-associated kinase and a positive regulator of Wnt signalling. *Nat Cell Biol* 3, 628-636.
- Tabuse, Y., Izumi, Y., Piano, F., Kempfues, K.J., Miwa, J., Ohno, S., 1998. Atypical protein kinase C cooperates with PAR-3 to establish embryonic polarity in *Caenorhabditis elegans*. *Development* 125, 3607-3614.
- Tepass, U., 1996. Crumbs, a component of the apical membrane, is required for zonula adherens formation in primary epithelia of *Drosophila*. *Dev Biol* 177, 217-225.
- Tepass, U., 2012. The apical polarity protein network in *Drosophila* epithelial cells: regulation of polarity, junctions, morphogenesis, cell growth, and survival. *Annu Rev Cell Dev Biol* 28, 655-685.
- Tepass, U., Theres, C., Knust, E., 1990. crumbs encodes an EGF-like protein expressed on apical membranes of *Drosophila* epithelial cells and required for organization of epithelia. *Cell* 61, 787-799.
- Torkko, J.M., Manninen, A., Schuck, S., Simons, K., 2008. Depletion of apical transport proteins perturbs epithelial cyst formation and ciliogenesis. *J Cell Sci* 121, 1193-1203.
- Tubby, K.C., Norval, D., Price, S.R., 2013. Chicken embryo spinal cord slice culture protocol. *J Vis Exp*.
- Uchikawa, M., Yoshida, M., Iwafuchi-Doi, M., Matsuda, K., Ishida, Y., Takemoto, T., Kondoh, H., 2011. B1 and B2 Sox gene expression during neural plate development in chicken and mouse embryos: universal versus species-dependent features. *Dev Growth Differ* 53, 761-771.
- van den Hurk, J.A., Rashbass, P., Roepman, R., Davis, J., Voeselek, K.E., Arends, M.L., Zonneveld, M.N., van Roekel, M.H., Cameron, K., Rohrschneider, K., Heckenlively, J.R., Koenekoop, R.K., Hoyng, C.B., Cremers, F.P., den Hollander, A.I., 2005. Characterization



of the Crumbs homolog 2 (CRB2) gene and analysis of its role in retinitis pigmentosa and Leber congenital amaurosis. *Mol Vis* 11, 263-273.

Varelas, X., Samavarchi-Tehrani, P., Narimatsu, M., Weiss, A., Cockburn, K., Larsen, B.G., Rossant, J., Wrana, J.L., 2010. The Crumbs complex couples cell density sensing to Hippo-dependent control of the TGF-beta-SMAD pathway. *Dev Cell* 19, 831-844.

Vesque, C., Ellis, S., Lee, A., Szabo, M., Thomas, P., Beddington, R., Placzek, M., 2000. Development of chick axial mesoderm: specification of prechordal mesoderm by anterior endoderm-derived TGFbeta family signalling. *Development* 127, 2795-2809.

Vorhagen, S., Niessen, C.M., 2014. Mammalian aPKC/Par polarity complex mediated regulation of epithelial division orientation and cell fate. *Exp Cell Res* 328, 296-302.

Wang, H., Chia, W., 2005. *Drosophila* neural progenitor polarity and asymmetric division. *Biol Cell* 97, 63-74.

Wang, H.R., Zhang, Y., Ozdamar, B., Ogunjimi, A.A., Alexandrova, E., Thomsen, G.H., Wrana, J.L., 2003. Regulation of cell polarity and protrusion formation by targeting RhoA for degradation. *Science* 302, 1775-1779.

Wang, E.T., Sandberg, R., Luo, S., Khrebtkova, I., Zhang, L., Mayr, C., Kingsmore, S.F., Schroth, G.P., Burge, C.B., (2008) Alternative isoform regulation in human tissue transcriptomes. *Nature*, 456 pp. 470–476

Wang, Q., Margolis, B., 2007. Apical junctional complexes and cell polarity. *Kidney Int* 72, 1448-1458.

Wang, T.W., Stromberg, G.P., Whitney, J.T., Brower, N.W., Klymkowsky, M.W., Parent, J.M., 2006. Sox3 expression identifies neural progenitors in persistent neonatal and adult mouse forebrain germinative zones. *J Comp Neurol* 497, 88-100.

Watanabe, T., Miyatani, S., Katoh, I., Kobayashi, S., Ikawa, Y., 2004. Expression of a novel secretory form (Crb1s) of mouse Crumbs homologue Crb1 in skin development. *Biochem Biophys Res Commun* 313, 263-270.

Whalley, K., Gogel, S., Lange, S., Ferretti, P., 2009. Changes in progenitor populations and ongoing neurogenesis in the regenerating chick spinal cord. *Dev Biol* 332, 234-245.

Wilson, L., Maden, M., 2005. The mechanisms of dorsoventral patterning in the vertebrate neural tube. *Dev Biol* 282, 1-13.

Wilson, L.J., Myat, A., Sharma, A., Maden, M., Wingate, R.J., 2007. Retinoic acid is a potential dorsalising signal in the late embryonic chick hindbrain. *BMC Dev Biol* 7, 138.

Wodarz, A., Grawe, F., Knust, E., 1993. CRUMBS is involved in the control of apical protein targeting during *Drosophila* epithelial development. *Mech Dev* 44, 175-187.

Wodarz, A., Nathke, I., 2007. Cell polarity in development and cancer. *Nat Cell Biol* 9, 1016-1024.

Wodarz, A., Ramrath, A., Grimm, A., Knust, E., 2000. *Drosophila* atypical protein kinase C associates with Bazooka and controls polarity of epithelia and neuroblasts. *J Cell Biol* 150, 1361-1374.

Xiao, Z., Patrakka, J., Nukui, M., Chi, L., Niu, D., Betsholtz, C., Pikkarainen, T., Vainio, S., Tryggvason, K., 2011. Deficiency in Crumbs homolog 2 (Crb2) affects gastrulation and results in embryonic lethality in mice. *Dev Dyn* 240, 2646-2656.

Yamanaka, T., Horikoshi, Y., Sugiyama, Y., Ishiyama, C., Suzuki, A., Hirose, T., Iwamatsu, A., Shinohara, A., Ohno, S., 2003. Mammalian Lgl forms a protein complex with PAR-6 and aPKC independently of PAR-3 to regulate epithelial cell polarity. *Curr Biol* 13, 734-743.

Yamashita, Y.M., Yuan, H., Cheng, J., Hunt, A.J., 2010. Polarity in stem cell division: asymmetric stem cell division in tissue homeostasis. *Cold Spring Harb Perspect Biol* 2, a001313.

Yu, K., McGlynn, S., Matise, M.P., 2013. Floor plate-derived sonic hedgehog regulates glial and ependymal cell fates in the developing spinal cord. *Development* 140, 1594-1604.

Zhang, X., Huang, C.T., Chen, J., Pankratz, M.T., Xi, J., Li, J., Yang, Y., Lavaute, T.M., Li, X.J., Ayala, M., Bondarenko, G.I., Du, Z.W., Jin, Y., Golos, T.G., Zhang, S.C., 2010. Pax6 is a human neuroectoderm cell fate determinant. *Cell Stem Cell* 7, 90-100.

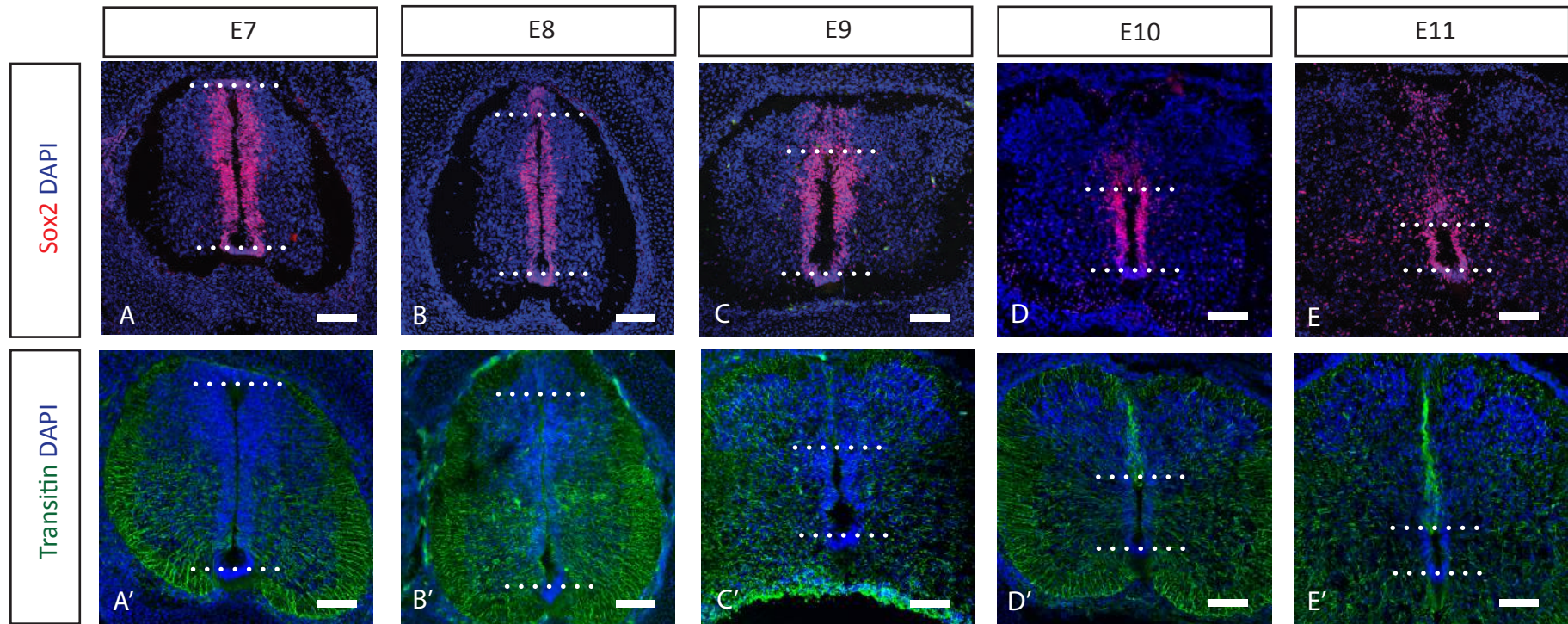
Zieger, M., Ahnelt, P.K., Uhrin, P., 2014. CX3CL1 (fractalkine) protein expression in normal and degenerating mouse retina: in vivo studies. *PLoS One* 9, e106562.

Zou, J., Wang, X., Wei, X., 2012. Crb apical polarity proteins maintain zebrafish retinal cone mosaics via intercellular binding of their extracellular domains. *Dev Cell* 22, 1261-1274.

# **Appendix**

## **Supplementary Information**

## Chick Transitin and Sox2



**A.F1** Chick expression of Sox2/Transitin between E8 and E11 mirrors that of mouse Sox2/Nestin between E13 and E16. As in mouse, dorsal radial glia stretch from the roof to the lumen plate as obliteration occurs. Sox2 cells are found dorsal to the obliterated lumen, closely associated with transitin RG processes.

## Dorsally moving cell

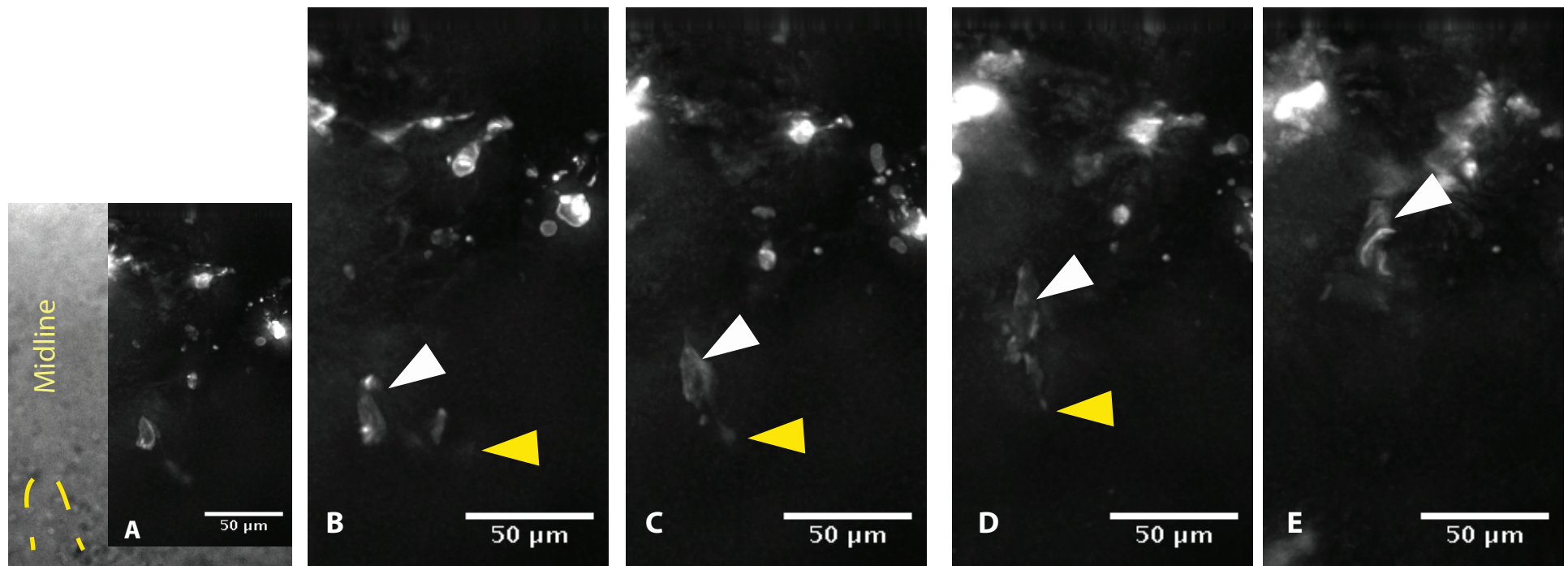


**Figure A.F2** Brightfield image of neural tube shown in (A), the lumen is outlined in a dashed yellow line, and the midline marked in text. A cell moves its cell body dorsally (white arrowhead) drawing its process behind it (white arrowhead). (Dorsally moving cell Movie, 2550 minutes).

## Laterally detaching cells

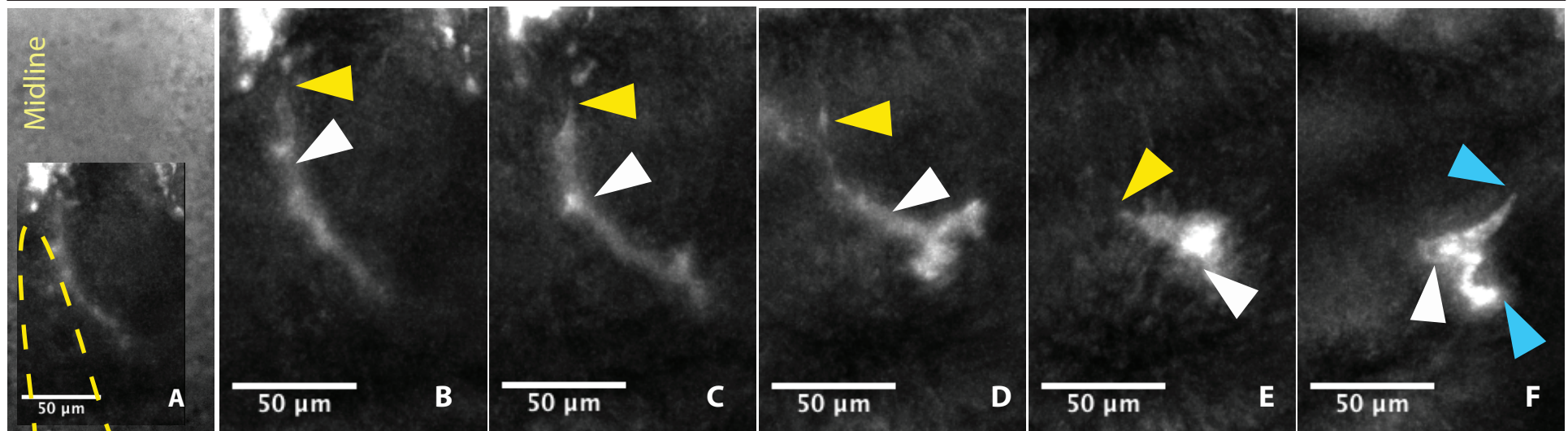


**Figure A.F3** Brightfield image of neural tube shown in (A), the lumen is outlined in a dashed yellow line, and the midline marked in text. A cell detaches from the lumen, draws a process in behind it (yellow arrowhead), then begins to extend two processes (Blue arrowhead). The white arrowhead indicates the approximate location of the cell body. (Laterally Detaching Cell Movie).

**Appendix Table 1:** GENSAT database interrogation

**Markers noted below have interesting expression around the midline or ventricular zone/ependymal zone**

**DML** dorsal midline, **VML** ventral midline, **DH** dorsal horn, **DCC** dorsal central canal (**bold** denotes strong expression); **ISH** – *in situ* Hybridisation, **GFP** – transgenically labelled tissue.

Marker	Type	E15	P7
<b>Abdh3</b> abhydrolase domain containing 3	ISH	Weak/Absent	<b>DF</b> <b>DCC</b>
<b>Abdh5</b> abhydrolase domain containing 5	ISH GFP	<b>DCC LCC</b>	<b>DML DCC LCC</b> <b>DCC LCC</b>
<b>Anxa2</b> annexin A2	ISH/ GFP	<b>DML VML DF</b>	DML VML DF <b>CC DF DH</b> (GFP only) (ISH only)
<b>Btg1</b> B cell translocation gene 1, anti-proliferative	ISH	Weak/Absent	<b>DCC</b> <b>CC</b>
<b>Bend5</b> BEN domain containing 5	ISH	Weak/ Absent	DML <b>DCC</b>
<b>Card6</b> Caspase recruitment domain family, member 6	ISH GFP	<b>DML</b> <b>VML</b>	<b>CC</b> <b>VML</b> Weak/Absent (ISH) (GFP)
<b>Cd63</b> CD63 Antigen	ISH	<b>Weak/Absent</b>	<b>DML</b> <b>VML</b> <b>CC VML</b> LCC
<b>Cx3cl1</b> chemokine (C-X3-C motif) ligand 1	ISH	<b>DML VML DH</b>	<b>DML VML</b> <b>DCC</b>
<b>Dcdc2a</b> doublecortin domain containing 2a	ISH	<b>CC</b>	<b>DML VML CC</b> <b>DML VML CC</b>
<b>Plxnb2</b> Plexin B2	ISH GFP	<b>CC</b> <b>VML</b>	<b>DML VML CC</b> <b>CC</b> (DML?)
<b>Zic2</b> zinc finger protein of the cerebellum 2	GFP	<b>DML DH</b>	<b>DML VML</b> <b>DML DH VH</b>
<b>Pus10</b> pseudouridylate synthase 10	ISH /	<b>DML VF DF</b>	<b>VCC VML</b> <b>VCC VML</b>

	GFP				
<b>Gdf10 (BMP3b) growth differentiation factor 10</b>	ISH/ GFP	<b>DML / DF</b>	DH (ISH only)	<b>DML</b>	
<b>Pla2g7 phospholipase A2, group VII</b>	ISH GFP	<b>DM VH DML LAT WINGS</b>	DML		Weak/Absent
<b>Sertm1 serine rich and transmembrane domain containing 1</b>	ISH	<b>DM DF</b>	DCC LCC	<b>DCC</b>	
<b>Tppp3 tubulin polymerization-promoting protein family member 3</b>	ISH/ GFP	<b>VML CC</b>	<b>CC VML DML</b>		CC VML DML
<b>BMP1 Bone Morphogenic Protein1</b>	ISH/ GFP	DML VML	DML VML	<b>VML</b>	
<b>Crip2 cysteine rich protein 2</b>	ISH	<b>DML DH VML</b>	<b>CC CML VML DF</b>		CC DML VML
<b>Gja1 (connexin43) gap junction protein alpha 1</b>	GFP ISH	Weak/Absent	<b>DML VML</b>	<b>DCC</b>	<b>DCC</b>
<b>Grin2c glutamate receptor, ionotropic, NMDA2C (epsilon 3)</b>	ISH GFP	<b>DML</b>	<b>DML</b>		Weak/Absent
<b>Thbs2 thrombospondin 2</b>	ISH	<b>DML DCC</b>	<b>DML DCC</b>	<b>DML DCC</b>	
<b>Syt13 synaptotagmin XIII</b>	ISH GFP	<b>DF VF</b>	<b>DF VF</b>	<b>CC</b>	
<b>Slitrk4 SLIT and NTRK-like family, member 4</b>	ISH	Weak/ Absent	<b>DML DF</b>		Weak/ Absent
<b>Sertm1 serine rich and transmembrane domain containing 1</b>	ISH	<b>DF</b>	Weak/ Absent	<b>DCC</b>	
<b>Sox4 SRY (sex determining region Y)-box 4</b>	iSH	Weak/ Absent	Weak/ Absent	<b>CC Scattered</b>	
<b>Sox9 SRY (sex determining region Y)-box 9</b>	ISH GFP	<b>CC (GFP)</b>	Weak/ Absent (ISH)	<b>CC (ISH)</b>	
<b>Pgrmc1 progesterone receptor membrane component 1</b>	ISH	<b>CC</b>	Weak/Absent		Weak/Absent
<b>Phox2b paired-like homeobox 2b</b>	ISH	DML (weak)	DML		



<b>Mgl1 monoglyceride lipase</b>	ISH GFP	<b>DML DCC</b>	<b>DML DCC</b>	<b>DML, Dorsal to CC/Vent to DF</b>
<b>Rps7 ribosomal protein S7</b>	ISH	<b>DML</b>	<b>Weak/ Absent</b>	<b>Weak/ Absent</b>
<b>Mdk Midkine</b>	ISH GFP	<b>DML DCC</b>	<b>DML DCC</b>	<b>DML</b>
<b>Id3 inhibitor of DNA binding 3</b>	ISH GFP	<b>DML DCC</b>	<b>VML</b> <b>Weak absent</b> <b>ISH</b>	<b>CC</b>
<b>Acvr1c (Alk-7) Activin A receptor, type IC</b>	ISH	<b>DF LF VF</b>	<b>Dorsal to CC/Vent to DF</b>	<b>CC?</b>